Composition and Function of Filamentous Influenza Virions

Jack Christopher Hirst
BA

Submitted in fulfilment of the requirements for the degree of Doctor of Philosophy

School of Infection, Immunity and Inflammation
College of Medical, Veterinary and Life Sciences
University of Glasgow

April 2021

Abstract

Influenza is a common and widespread disease caused by influenza viruses. It causes approximately half a million deaths globally each year, and poses the constant risk of a novel pandemic strain emerging with a much higher mortality rate than seasonal influenza viruses. Reducing the burden of influenza depends on effective vaccines and antiviral drugs, and the rational design of these depends on a thorough understanding of the basic biology of influenza viruses. While influenza viruses have been intensely studied, several aspects of their biology have been neglected. Notably, most laboratory-adapted strains of influenza virus produce virions with a predominantly spherical morphology, but clinical isolates produce virions ranging from spheres with diameters of ~100 nm to filaments with lengths that can exceed 30,000 nm. Passage experiments suggest this pleiomorphy is adaptive, but it has been the focus of very little research and so its role is unknown. Furthermore, methods with which to examine filamentous virions are lacking, meaning this area of influenza biology is both understudied and requires extensive methods development. To solve these problems, I developed a range of tools with which to analyse filamentous influenza virions. These included an adaptable, semi-automated analysis pipeline using confocal microscopy to assess the concentration and lengths of filamentous virions in a sample; a set of validated procedures that can be used to handle filamentous virions without damaging them; and a robust method to enrich samples in filamentous or non-filamentous virions. Using these methods, I examined how the proteome of influenza virions varied with their morphology using mass spectrometry and found that all viral proteins except haemagglutinin and matrix protein were depleted in filamentous virions relative to their size. This suggested that filamentous virions may be less robustly infectious than non-filamentous virions, and may have different levels of glycoprotein activity. Using functional assays, I found that non-filamentous virions were indeed enriched in fully infectious particles compared to filamentous virions, and that the HA activity relative to NA activity of filamentous virions was much higher than that of non-filamentous virions. However, this difference in glycoprotein activity did not affect inhibition by mucus. These characterisations of the composition and function of filamentous influenza virions, and the tools used to perform them, provide a solid foundation to elucidate the role of, and potential pharmaceutical interventions exploiting, these complex particles in influenza virus infections.

Contents

List of Tables

List of Figures

Acknowledgements

Thanks, first and foremost, to my supervisor, Dr Ed Hutchinson. In a world often described as cut-throat, I was privileged to work with someone who works so hard at creating an open, collaborative, and supportive research environment. I'm especially grateful for the support offered during the times when I was struggling personally, and I don't think I could give any future students better advice than "work in Ed's lab". I am also grateful for the extensive suggestions on ways to improve this thesis (occasional howls of despair at another page of red ink notwithstanding) and can say I have checked every figure to ensure I have not used two slightly different shades of black.

My labmates deserve equal credit for making the Hutchinson Lab such a pleasant place to work in, so many thanks to Drs Elizabeth Sloan, Pippa Harvey, Seema Jasim, Léa Meyer, and not-Drs-quite-yet Anna Sims and Jake MacCleod. I relied heavily on your support throughout my PhD, but this last year in particular would have been an utter nightmare without such lovely colleagues and friends. Thank you also to the many interns, undergrads, and Master's students whose degree structures I still don't understand, and particular thanks to Amy Burke for her diligent microscopy work during her project. I hope you can forgive me for all the particle counting.

Thank you to my collaborators on this project, particularly Svenja Hester for her support with mass spectrometry and for not laughing too hard when it transpired I'd misjudged the trypsin concentration by three orders of magnitude. While our collaboration was disrupted by the pandemic, I'd also like to thank nearly-a-Dr Andrew McMahon and Dr Nicole Robb for their super-cool super-resolution microscopy. Thanks also to future-Dr Joanna Wojtus for giving me the option to send so many emails beginning "Can I steal some of your mucus again?" and to everyone else who lent me reagents.

Thank you to the rest of my supervisory team, Professors Sheila Graham, Pablo Murcia, and David Bhella, for your helpful feedback and frequent reminders that I did actually need to produce a thesis at the end of all this. There's too many people who offered me technical support to name, but special thanks to Drs Matt Turnbull and Rute Maria Pinto, who helped me with a whole bunch of influenza problems and let me steal some pretty images for the thesis; Dr Colin Loney, for invaluable support with the light microscopes (and excellent sportsmanship during a tense finish in the fantasy football); Drs James Streetley and

Swetha Vijayakrishnan for invaluable support with the electron microscopes; and Dr Marion McElwee, for helping me with basically everything else. My work was also entirely dependent on the various logistics, washroom, administration, and cleaning teams at the CVR and so many thanks to everyone who made up these teams. Thank you also to the wider CVR community, and indeed, wider virology community, for all your helpful questions and feedback at presentations and conferences.

Thank you also to the Medical Research Council for funding me during this project. Continued solvency certainly made life easier.

Lots of of my friends have been mentioned in their capacity as colleagues already, but many thanks to the rest of them. I've had so many pleasant drunken conferences and Friday night Phoenix Bars that I'm not sure where to draw the line here, but thanks to Ste(ph/v)en Bryden, Natalia Cameron Ruiz, Victor Iliev, Betty Lau, Meredith Stewart, Douglas Stewart (unrelated) (I think), Elena Sugrue, Arthur Wickenhagen, and Gauthier Lieber for various quizzes, sports, games, discussions about who'd get eaten first if we were snowed in, and all that good stuff that makes life fun. Particular mention goes to Jamie Royle for fixing a microscopy issue I'd been struggling with for months in about thirty seconds, for making up the other half of the second best table football team of 2019 (Stryker Grove), and for successfully inferring the title "Adagio for Strings" purely from my rendition of it during a pub quiz. As I made Sam Stokes put me in his acknowledgements, I guess he also deserves a mention here. Beyond virology, I would also like to thank Susie Guinee, Tom Finney, Michael Free, Anna Hands, and Matt Harris for keeping me sane during lockdown. You'll never read this, but hey ho.

And thank you to Angela Taylor, Ian Hirst, Matt Hirst, Chris Taylor, Andrew Severn, Maureen Dunn, Chris and Margaret Hirst, and all the further bits of family who quickly get too numerous to list. Love and support are good and all, but I'm also grateful for how interested everyone pretended to be when I came home one Christmas with a micrograph of filaments and insisted on showing it to everyone.

At the time of writing, it's been a full year since the first covid restrictions were introduced in the UK, and my ability to see everyone on this list has varied from limited to nonexistent. I hope it's not too long before I can see you all in real life and say thank you properly.

Finally I would like to thank and remember my grandad, Ernie Dunn, and my friend, Sarah Wayman, who passed away during my time in Glasgow. I miss you both very much.

Author’s Declaration

This work was completed at the University of Glasgow between October 2016 and April 2021 and has not been submitted for another degree. All work presented in this thesis was obtained by the author’s own efforts, unless otherwise stated.

All experimental work in this thesis was generated by Jack Hirst under the supervision of Dr Edward Hutchinson at the MRC-University of Glasgow Centre for Virus Research.

Liquid chromatography and tandem mass spectrometry was performed by Svenja Hester at the Target Discovery Institute, University of Oxford.

Mucus from human bronchial epithelial cell cultures was prepared by Joanna Wojtus at the MRC-Unversity of Glasgow, Centre for Virus Research.

Publications

Publications arising from this thesis

Hirst, J.C., Hutchinson, E.C., 2019. Single-particle measurements of filamentous influenza virions reveal damage induced by freezing. J Gen Virol 100, 1631–1640. https://doi.org/10.1099/jgv.0.001330

Publications obtained from personal contribution to other studies

Bottermann, M., Foss, S., Tienen, L.M. van, Vaysburd, M., Cruickshank, J., O'Connell, K., Clark, J., Mayes, K., Higginson, K., Hirst, J.C., McAdam, M.B., Slodkowicz, G., Hutchinson, E., Kozik, P., Andersen, J.T., James, L.C., 2018. TRIM21 mediates antibody inhibition of adenovirus-based gene delivery and vaccination. PNAS 115, 10440–10445. https://doi.org/10.1073/pnas.1806314115

Abbreviations

Table 1: List of abbreviations.

Abbreviation	Definition
CAA	Chloroacetamide
CI	Confidence Interval
csv	Comma Separated Values
czi	Carl Zeiss Image
ddH_2O	Double-Distilled H_2O
DIP	Defective-Interfering Particle
DTT	Dithiothreitol
FCS	Foetal Calf Serum
FIP	Fully-Infectious Particle
HA	Haemagglutinin
HEF	Haemagglutinin-Esterase-Fusion protein
IAV	Influenza A Virus
IBV	Influenza B Virus
ICV	Influenza C Virus
IDV	Influenza D Virus
M1	Matrix protein
M2	Membrane protein
MDCK	Madin-Darby Canine Kidney
MOI	Multiplicity Of Infection
N.S	Not Significant
NA	Neuraminidase
NEP	Nuclear export protein
NS1	Non-structural protein 1
NTC	Buffer containing NaCl, Tris-HCl, and $CaCL_2$

Abbreviation	Definition
P3	Polymerase 3
PA	Polymerase Acidic
PB1	Polymerase Basic 1
PB2	Polymerase Basic 2
PBS	Phosphate-Buffered Saline
PBST	PBS containing Tween-20
pcv	Packed Cell Volume
PFU	Plaque-Forming Unit
PR8	Influenza A/Puerto Rico/8/34 (H1N1)
PTM	Post-Translational Modification
RdRP	RNA-dependent RNA Polymerase
RNA	Ribonucleic Acid
RNP	Ribonucleoprotein
S.D.	Standard Deviation
S.E.	Standard Error
SDS	Sodium Dodecyl Sulfate
SEM	Scanning Electron Microscopy
SIP	Semi-Infectious Particle
TCEP	Tris(2-carboxyethyl)phosphine)
TEAB	Tetraethylammonium Bromide
TEM	Transmission Electron Microscopy
TPCK	L-(tosylamido-2-phenyl) ethyl chloromethyl ketone
Udorn	Influenza A/Udorn/307/72 (H3N2)
WSN	Influenza A/WSN/33 (H1N1)

Chapter 1

Introduction

1.1 Influenza virus

1.1.1 An overview of influenza

Influenza is a common disease caused by influenza viruses. The main animal reservoir of influenza viruses is wild birds, but influenza is also widespread in humans and domesticated mammals such as pigs, horses, and dogs. Influenza viruses consist of four genera, named A, B, C, and D (abbreviated to IAV, IBV, ICV, and IDV). Of these, IAV, IBV, and ICV all infect humans, with IAV and IBV causing most human epidemics (Krammer et al., 2018).

1.1.2 Influenza symptoms

In humans, influenza viruses typically infect the upper respiratory tract. These infections can be asymptomatic, but often lead to symptoms including cough, sore throat, fever, runny nose, headache, muscle pain and fatigue. More severe cases can infect the lower respiratory tract and lead to severe pneumonia, either caused by influenza virus directly or via a secondary bacterial infection. In some cases, influenza infections can spread to, or otherwise stress, other systems, leading to cardiac or neurological complications. Those who are very young, very old, pregnant, immunocompromised, or suffering from other health conditions face a much higher risk of severe influenza symptoms. When there are no complications, influenza infections patients usually resolve within a fortnight (Krammer et al., 2018).

1.1.3 Influenza prevalence and burden

Influenza viruses circulate year-round, but in temperate climates cases are most common in winter. Influenza caused by these circulating endemic viruses is therefore usually referred to as seasonal influenza, though this is somewhat misleading as influenza is not seasonal in the tropics. Many illnesses cause influenza-like symptoms, and the amount of data gathered on influenza cases varies by nation, so it is difficult to estimate the global prevalence of human influenza. Better estimates exist for individual nations. For example, between 3 and 15% of US citizens are estimated to suffer from influenza each year, though these data are only available for symptomatic infections and ~33% of influenza cases are asymptomatic (CDC, 2020).

Seasonal influenza virus imposes a substantial economic and healthcare burden on society. For example, endemic human influenza is estimated to cost the USA $11.2 billion a year, both through direct medical costs and indirect factors such as the loss of productive working hours (Putri et al., 2018). Furthermore, the human cost of influenza is severe; approximately half a million global deaths are associated with influenza every year (Iuliano et al., 2018). Only ~0.001% cases of influenza are fatal (Wong et al., 2013), so the high number of annual deaths is correlated with a huge level of morbidity.

While the seasonal burden of influenza is already substantial, the risk of a far greater influenza burden is always present. Novel zoonotic strains of influenza A virus repeatedly emerge with the potential to cause pandemics. Five influenza pandemics have occurred since 1917 (Bean et al., 2013), with the most severe being the 1918 pandemic that killed as many as 100 million people (Spinney, 2017). A future influenza pandemic is a near certainty, which could be severe enough to dwarf the death toll of seasonal influenza. Consequently, it is vital to develop interventions to reduce the harm caused by influenza virus.

1.1.4 Reducing the burden of influenza

Reducing the burden of a virus is a multidisciplinary problem, requiring coordinated efforts combining politics and logistics as well as medicine and basic science. The ongoing SARS-CoV-2 pandemic is a useful case study of how the interplay of these factors affects control of a novel disease. For the first several months of the pandemic, non-pharmaceutical control measures such as travel restrictions, social distancing, hygiene, and face masks were the only option to prevent widespread infections and deaths. These reduced the spread of SARS-CoV-2 and even eliminated it in some countries (Health Protection Scotland, 2021). While not the primary aim of these measures, they also substantially reduced the incidence of colds and influenza (Iacobucci, 2020). However, these methods carried a significant cost of their own: the IMF estimates a combined $28 trillion of lost global economic output due to the pandemic and associated control measures (IMF, 2020). Furthermore, control mea-

sures led to excess deaths through factors such as people avoiding seeking care for other illness due to fear or the perception they should stay at home (ONS, 2020) . The severity of this impact means such measures cannot be maintained indefinitely, and ultimately their aim is to control the virus for long enough to develop and deploy pharmaceutical countermeasures. Preventing the ongoing harm from viral epidemics, including influenza, therefore ultimately depends on effective pharmaceutical interventions.

1.1.5 Pharmaceutical options for controlling influenza

Influenza therapies can be grouped into two categories: antiviral drugs and vaccines. Antivirals target influenza virus proteins to disrupt specific points of the replication cycle (see below), with key licensed drugs including: favipiravir, targeting PB1 (Furuta et al., 2013); baloxavir marboxil, targeting PA (Omoto et al., 2018); amantidine, targeting M2 (Jackson et al., 1963); and inhibitors of NA such as oseltamivir (Okoli et al., 2014). While useful, there is a constant risk of influenza viruses evolving resistance to these drugs and indeed this has led to the obsolescence of the adamantane class of drugs such as amantidine. NA inhibitors, the most widely used class of drugs (CDC, 2020) are also most effective when administered early in infection, but this requires rapid referral and diagnosis of the patient which is not always easy to achieve.

Because antivirals are not always effective, preventing infections via vaccination is the preferred method to control influenza. However, vaccination has its own limitations. The high mutation rate of influenza virus leads to a constant variation in its antigens (known as antigenic drift), resulting in frequent vaccine escape mutants, and necessitating annual updates to the four strains (H1N1 and H3N2 subtypes of IAV, Victoria and Yamagata lineages of IBV) recommended for inclusion in vaccines (WHO 2021). This means that even vaccinated individuals are unlikely to be fully immune to circulating influenza strains, and fully preventing the spread of influenza virus would require prohibitively expensive global mass vaccination campaigns every year. Furthermore, to allow time for vaccine manufacture and distribution, these annual updates depend on an ability to predict which strains of influenza virus will be circulating six months in advance. The difficulty of this task makes it even harder to match influenza vaccines to circulating strains, and similar logistical issues will delay any response to a novel pandemic virus (Houser & Subbarao, 2015).

The current limitations of drugs and vaccines mean that improved options are essential to reduce future harm from influenza virus. Rational design of improved pharmaceutical interventions depends on understanding the basic biology of influenza virus.

1.2 The biology of influenza virus

1.2.1 Introduction to the influenza virus replication cycle

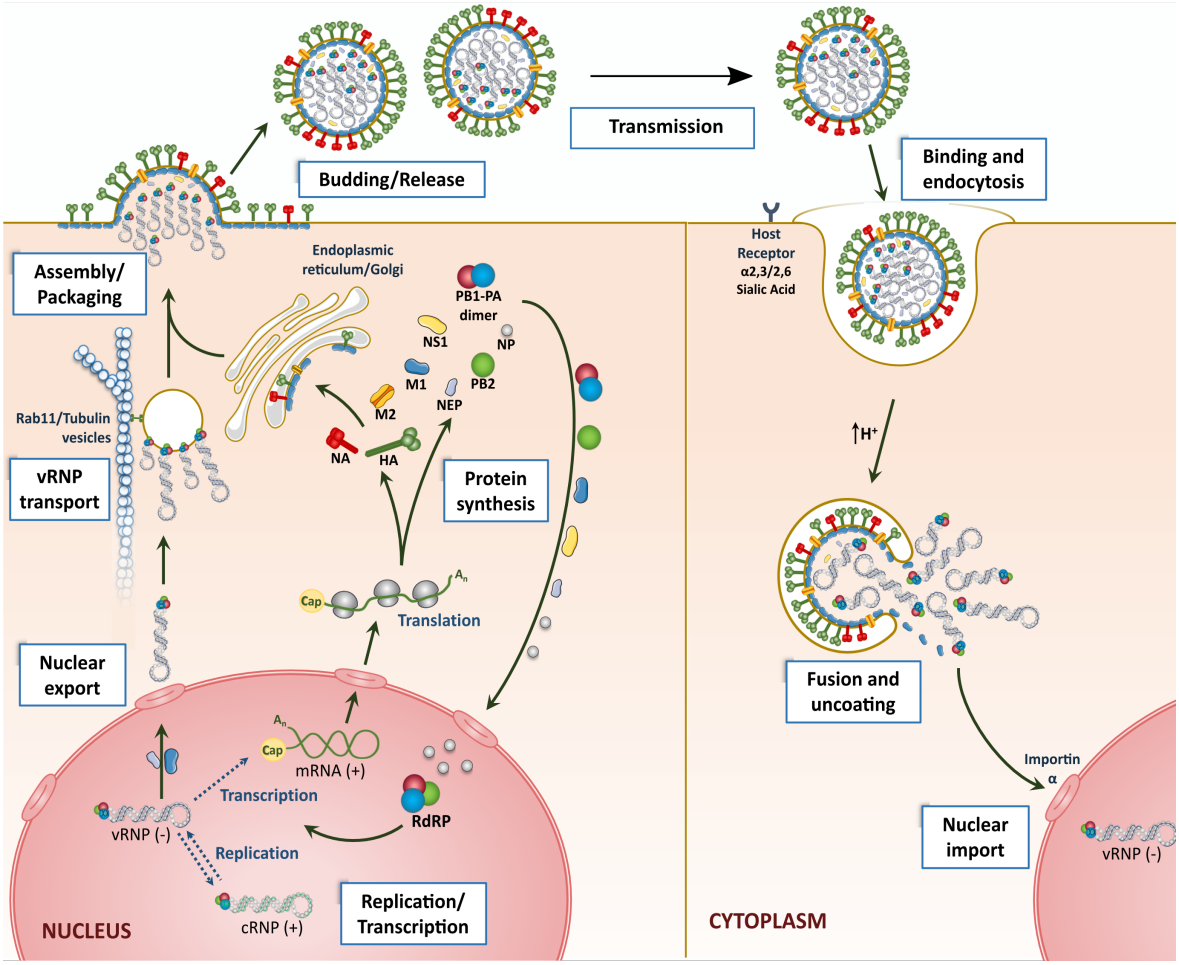

Figure 1.1: A simplified influenza virus replication cycle.

Adapted from (Pinto, 2019). References to relevant section of the main text in brackets. The minimal replicative unit of influenza virus consists of a set of RNPs (Section 1.2.3.1). These synthesise mRNA for protein expression, and cRNA to serve as a template for genome replication (Section 1.2.3.2). Viral proteins are synthesised by the host translation machinery (Section 1.2.3.3). Some transit to the nucleus to form new RNPs which then transit to the plasma membrane and some transit to the plasma membrane directly (Section 1.2.4.3). Virions assemble at the plasma membrane and bud from it (Section 1.2.4.4) before transmitting to a new cell (Sections 1.2.4.6 and 1.2.4.6). At the new cell, virions bind sialic acids to trigger entry, primarily by clathrin-mediated endocytosis, and RNPs are released into the cytoplasm as the endosome acidifies (Section 1.2.4.7). The RNPs are imported into the nucleus and the cycle begins again.

Despite being intensely studied, many aspects of the basic biology of influenza virus replication are poorly understood. One of these poorly understood areas is how the morphology of influenza virions impacts the biology of the virus, and this area forms the focus of this thesis. When considering the available information on virion morphology, it is useful to

first describe a simplified "canonical" replication cycle of influenza virus (Figure 1.1), before considering how the different steps of this cycle influence and are influenced by virion morphology.

1.2.2 The components of influenza virus

Influenza virus components can be grouped into three sets. The first set is those that can transcribe and replicate the genome, and thus produce all the viral components. This set can be described as the minimal replicative unit. The second set comprises proteins that modulate the host cell to facilitate transcription and replication, and the third set comprises proteins that transport the minimal replicative unit to a new host.

Influenza virus transcription and genome replication takes place in the nucleus of the host cell, and so a reasonable point to begin the replication cycle is when the full minimal replicative unit is present in the host cell. The cycle can be considered complete when a new minimal replicative unit has been delivered to the nucleus of a new host cell.

1.2.3 Replicating the minimal replicative unit

1.2.3.1 Composition of the minimal replicative unit

Influenza virus has an RNA genome of approximately 13.5 kb, encoding ten canonical proteins and several accessory proteins derived from non-canonical translation. The genomic RNA is referred to as vRNA, to distinguish it from messenger RNA (mRNA) and complementary RNA (cRNA). The genome comprises eight (IAV, IBV) or seven (ICV, IDV) segments, and at least one copy of each segment is necessary to produce fully infectious progeny (Krammer et al., 2018).

The influenza virus genome is negative sense, so viral protein synthesis and genome replication requires positive sense RNA to be synthesised from the vRNA template. Host cells lack a suitable RNA-dependent RNA polymerase (RdRP), so this process depends on a viral RdRP. The influenza virus RdRP is a heterotrimer comprising the proteins polymerase basic 1 and 2 (PB1 and PB2) and polymerase acidic (PA, in IAV and IBV) or polymerase 3 (P3, ICV and IDV) (Fodor, 2013). Transcription of mRNA occurs *in cis* and so each genome segment must be associated with its own RdRP (Hutchinson & Fodor, 2013).

The RdRP of influenza virus works most efficiently when vRNA is held in a suitable conformation through binding a basic groove on the viral nucleoprotein (NP). Each NP molecule associates with approximately 24 bases of the vRNA, and oligomerises into a double helix structure (though one which lacks cross-strand RNA interactions) which is capped with the RdRP (Ye et al., 2010). This structure is known as the ribonucleoprotein (RNP) and is

sufficient to transcribe mRNA from its constituent gene segment (Hutchinson & Fodor, 2013). This means the RNPs both contain the template for new genomes and are capable of inducing the synthesis of the proteins required for genome replication. A full set of RNPs therefore comprises the minimal replicative unit for an influenza virus.

1.2.3.2 Synthesis of RNA

Influenza virus replication requires synthesis of viral proteins and replication of the viral genome. Both processes require the synthesis of positive sense RNA: truncated, capped, and polyadenylated copies to act as mRNA for protein expression, and full-length copies to act as a cRNA template for vRNA synthesis.

Protein synthesis requires mRNA to be protected from degradation, exported from the nucleus, and recognised by host translation machinery. This is achieved in host mRNAs through the relevant machinery recognising a methylated 5′ guanosine cap (Carmody & Wente, 2009). The influenza virus RdRP does not encode capping capabilities, instead, transcription begins by PB2 binding the 5′ cap structure of host mRNA and PA or P3 cleaving the mRNA ~12 bases downstream of the cap. The capped RNA fragment acts as a primer for transcription, with PB1 providing the polymerase activity. This results in the synthesis of capped viral mRNA while also inhibiting the translation of host proteins which would divert resources from virion production or initiate immune responses (te Velthuis & Fodor, 2016).

Unlike mRNA transcription, cRNA synthesis depends on two RdRPs, which form a dimer stabilised by the host protein ANP32A/B (Fan et al., 2019; Carrique et al., 2020). This template is copied again to produce vRNA, which is co-transcriptionally encapsidated by free NP (Ye et al., 2012). As this process depends on newly synthesised viral proteins, the early stages of replication are dominated by mRNA transcription and the later stages by cRNA transcription.

1.2.3.3 Translation of viral proteins

Viral proteins are synthesised by the host translational machinery in the same manner as host proteins. Newly synthesised RdRP subunits and NP contain nuclear localisation signals, which are recognised by host importins to transport them into the nucleus (Hutchinson & Fodor, 2012). This provides the components necessary for genome replication and RNP assembly as described above, and so allows synthesis of new copies of the minimal replicative unit.

1.2.4 Transporting the minimal replicative unit to a new nucleus

1.2.4.1 The virion

While an infected cell can replicate the viral genome many times, eventually its resources will be depleted, or the cell will be destroyed by the immune response (see Section 1.2.4.8 below). Long term propagation of the viral genome, therefore, requires moving the minimal replicative unit to a new host cell and, eventually, a new host organism. This presents the virus with several challenges. First, at least one copy of each segment must make it into each new host cell, which is more efficient if the genome segments are delivered together. Second, the minimal replicative unit must be protected from environmental damage for long enough to make it to the new host. Third, the minimal replicative unit needs to cross barriers such as host cell membranes and the mucus layer coating the respiratory epithelium. These challenges are met by encasing the minimal replicative unit in a secure container lined with proteins that enable it to navigate these barriers: the virion. Influenza virions are highly heterogeneous but share common features, so while an "idealised" virion is described here, it is important to note that specific features such as the copy number of viral proteins, the organisation of the capsid structure, and the number of vRNPs packaged vary widely (Jones et al., 2020).

1.2.4.2 Composition of the influenza virion

Influenza virions are typically depicted as spherical. They are enveloped by a host-derived membrane studded with glycoproteins, haemagglutinin (HA) and neuraminidase (NA) in IAV and IBV and haemagglutinin-esterase-fusion protein (HEF) in ICV and IDV, and an ion channel, membrane protein (M2). These proteins, together with the envelope, are necessary for transmission and entry into new cells (the functional significance of these proteins is discussed below). Beneath the envelope is the viral capsid, comprised of repeating units of matrix protein (M1). Even though IAV virions are often spherical, the capsid structure is a loose helix rather than the icosahedron seen in many spherical viruses. The RNPs are packaged beneath the M1 layer (Krammer et al., 2018). Together, these components make up the "canonical" structure of the virion. Despite its name, the immune antagonist, non-structural protein 1 (NS1), is also packaged, although the abundance varies and it is unclear whether packaged NS1 impacts infectivity (Hutchinson et al., 2014). Virions also contain a diverse array of host-derived proteins (Hutchinson et al., 2014), but it is unknown whether these affect transmission.

1.2.4.3 Accumulating virion components at the budding site

To allow virion assembly, each of these components must be delivered to the budding site at the apical plasma membrane and organised in a manner that means there is a sufficient local concentration of components to form a complete virion.

HA and NA are trafficked to the apical plasma membrane after synthesis where they are concentrated in lipid rafts: regions of the cell that concentrate proteins to create specialised microdomains (Rossman & Lamb, 2011; Sato et al., 2019). M2 also traffics to the apical membrane but is excluded from lipid rafts, instead accumulating at their boundaries (Hutchinson & Fodor, 2013).

To reach the plasma membrane, RNPs must first cross the nuclear membrane. This process uses M1 as an adaptor protein, which contains a nuclear import signal and, after it has been imported into the nucleus, binds NP. M1 is in turn bound by nuclear export protein (NEP), a viral protein which contains nuclear export sequences that are recognised by the exportin Crm1 (Huang et al., 2013). After export, RNPs are trafficked to the membrane by Rab11+ membranes, initially believed to be recycling endosomes, but now thought to be modified endoplasmic reticulum and irregular vesicles that only form during infection (Martin et al., 2017). At the membrane, M1 associates with the cytoplasmic tails of HA, NA, and M2 and thus connects all the major structural components of the virion (Hutchinson & Fodor, 2013).

Influenza virus transmission between hosts is believed to occur at a low multiplicity of infection, and so is only possibly if some virions package a full complement of RNPs and can therefore initiate an infection alone (Hutchinson et al., 2010). The proportion of these fully infectious particles in the total virion population is higher than would be predicted if RNPs were packaged randomly (Enami et al., 1991; Nakajima & Sugiura, 1977), and *cis*-acting sequences have been identified which mediate segment specific packaging (Fujii et al., 2003, 2005; Ozawa et al., 2007, 2009), suggesting that RNPs are packaged as a regulated complex in a segment specific manner. Mutating the packaging signals on a given segment can also affect packaging of the remaining segments (Marsh et al., 2008; Hutchinson et al., 2008). The relationships between segments identified by mutagenesis are too complex to support a straightforward “daisy chain” model of assembly (where segments are added sequentially to a growing chain). However, the data may be compatible with a “master segment” model (where segments assemble around a single core segment) but further research is necessary to confirm this (Hutchinson et al., 2010). While the exact mechanism remains unknown, it is known that these inter-segment interactions begin during trafficking to the budding site (Chou et al., 2013).

1.2.4.4 Virion budding

To leave the cell, the budding virion must deform the plasma membrane into the shape of the virion and cut it. The mechanisms underpinning this process are poorly understood. Expression of HA, NA, and M2 alone can drive the budding of virus-like particles (Chen et al., 2007; Lai et al., 2010; Chlanda et al., 2015), and M1 polymerisation alone can drive membrane deformation (Saletti et al., 2017), but budding is far more efficient when HA, NA, M2, and M1 are co-expressed. Membrane scission is mediated by M2 (Rossman et al., 2010), though viable mutants lacking M2 have been reported (Cheung et al., 2005) so it is possible that scission can mediated by multiple mechanisms.

1.2.4.5 Virion transmission between host cells

After budding, virions need a mechanism to avoid immediately reinfecting their cell of origin. Influenza virions enter cells via receptor-mediated mechanisms including clathrin-mediated endocytosis and macropinocytosis (Rossman et al., 2012), which are triggered by HA binding sialic acids at the cell membrane. While the mechanisms to prevent re-entry into the cell of origin are still poorly understood, it seems that NA activity at the cell surface removes sialic acids from infected cell membranes and thus limits reinfection (Huang et al., 2008).

Having escaped its cell of origin, a virion must travel to a new target cell. Micrographs of respiratory tracts infected with multiple fluorescent influenza viruses show localised areas expressing the same fluorophores (Fukuyama et al., 2015), suggesting most infected cells produce virions which infect their immediate neighbours. The transit to a new cell is poorly understood. Part of it likely involves virions being carried within the flow of the mucus layer that coats epithelial cells. Another part involves “surfing” across sialylated surfaces, where HA-activity binds and releases sialic acids, and NA-activity cleaves them, preventing the virion from visiting the same region twice. This results in motility via a Brownian ratchet mechanism (Sakai et al., 2017). This would allow virions to move to new cells and search membranes for suitably dense clusters of receptors to trigger entry (Sieben et al., 2020).

These localised infections create many more copies of the minimal replicative unit, but ultimately the host will either mount an effective immune response or die. Either way, the virus will be eradicated. For an influenza virus to persist in the long term, therefore, it must transmit to a new host organism.

1.2.4.6 Virion transmission between host organisms

Moving to a new host organism presents influenza virions with many more challenges than moving within one. First, virions must penetrate the dense mucus layer coating epithelial cells. Mucus contains many sialylated proteins that act as decoy receptors for HA and must be cleaved by NA to allow traversal (Zanin et al., 2015). This means the balance between HA and NA activity is vital, as getting the balance wrong could lead to virions being permanently trapped by decoy receptors, or unable to bind entry receptors once the barriers have been crossed. Second, virions must escape their current host. Here, mucus acts as a help rather than a hindrance: droplets of mucus are shed into the airway and exhaled, and virions are carried with them (Zanin et al., 2015). Third, virions must enter a new host. This can occur through direct inhalation of droplets, but more commonly they contaminate surfaces and are inadvertently transferred to a new host airway via touch (Krammer et al., 2018). Fourth, the virion must again cross the mucus barrier, again relying on the balance of HA and NA activity. When considering the entire transmission route, it is noteworthy that virions must traverse the same barriers in opposite directions depending on whether it is entering or leaving a host. It is unclear how this is achieved, though possibly it is simply through producing virions in such abundance that all possible routes and directions are explored.

1.2.4.7 Entry and unpacking

After surmounting the many challenges to travel to a new cell surface, the RNPs are still separated from the nuclear interior by four barriers: the virion capsid, the virion envelope, the cell membrane, and the nuclear membrane. Virions initially cross the cell plasma membrane via HA binding to sialic acids at the cell surface and triggering tyrosine kinase signalling to induce cargo-uptake mechanisms, predominantly clathrin-mediated endocytosis (Rossman et al., 2012). This allows the virion to enter the cell, but, because endocytosis leaves its cargo in a membrane-bound late endosome, the RNPs still face the same number of topological barriers to reach the nuclear interior. Escape from the endosome occurs due to endosomal acidification and concurrent influx of potassium ions, which dissociate the RNPs from M1 and induce a conformational shift in HA, exposing a fusion domain which inserts into the endosome membrane. This induces fusion between the endosome membrane and the virion envelope and releases the RNPs into the cytoplasm (Skehel & Wiley, 2000). To cross the nuclear membrane, the RNPs first diffuse to it, then their nuclear localisation signals are recognised by importins and so the RNPs enter the nucleus of a new host cell (Martin & Helenius, 1991). At this stage, the entire minimal replicative unit has been transferred to a new nucleus, and the viral replication cycle begins again.

1.2.4.8 Evasion of immunity

An unchecked influenza virus infection would ultimately be fatal, so the host does not remain passive during viral replication. Instead, the host mounts an immune response to control the virus. In a naïve host, this initially takes the form of the innate immune response, triggered by the detection of pathogen-associated molecular patterns such as double-stranded or uncapped RNA. These signals are transduced into synthesis of antiviral proteins, most notably interferons, which can induce apoptosis in the infected cell and create an antiviral state in the surrounding cells (Randall & Goodbourn, 2008). Influenza virus has no mechanism to suppress an ongoing interferon response, so instead delays its onset by expressing interferon antagonists, primarily NS1. NS1 cannot indefinitely prevent the host organism from mounting an interferon response (some influenza virions lack the NS segment and markers of cell damage can be detected by uninfected cells), but NS1 can delay it for long enough for new influenza virions to assemble and spread to a new host (Hale et al., 2008).

Influenza virus infections are usually resolved by the innate immune system but hosts also mount an adaptive immune response against infections. A novel antibody response will typically peak 1-3 weeks after infection (Janeway et al., 2001), which is usually after the initial influenza virus infection is resolved. However, it results in the production of antibodies and memory lymphocytes that will prevent reinfection from the same strain of virus. These antibodies are most commonly directed against HA and NA, but these proteins rapidly acquire mutations over replication cycles that result in weakened antibody binding. This means a host can be reinfected by a very similar virus strain, so long as the glycoproteins have acquired enough mutations to render the existing antibody response ineffective (Krammer et al., 2018).

1.2.4.9 Conclusion to the influenza virus replication cycle

A simplified replication cycle such as this leaves out many poorly understood areas of influenza virology. These include such proposed mechanisms of direct cell-cell spread via tunnelling nanotubules (Kumar et al., 2017), and the different physiological barriers present in faeco-oral transmission in wild birds compared to respiratory transmission in mammals. In addition, even within the well-studied areas described, a great deal of complexity and heterogeneity is present. For example, the virion proteome varies depending on the cell of origin (Hutchinson et al., 2014), and virions can package incomplete genomes or even no genome, leading to highly varied consequences for the infected cells (Brooke, 2017). Heterogeneity is most clearly visible in the strikingly varied morphology of influenza virions, ranging from the commonly depicted spheres to filaments that can be over 300 times larger. This pleiomorphy was observed in the first micrographs to accurately identify the IAV virion (Figure 1.2) (Taylor et al., 1943), and has since been seen across an enormous range of influenza strains (Figure 1.3), but the significance of pleiomorphy in infection re-

mains unknown.

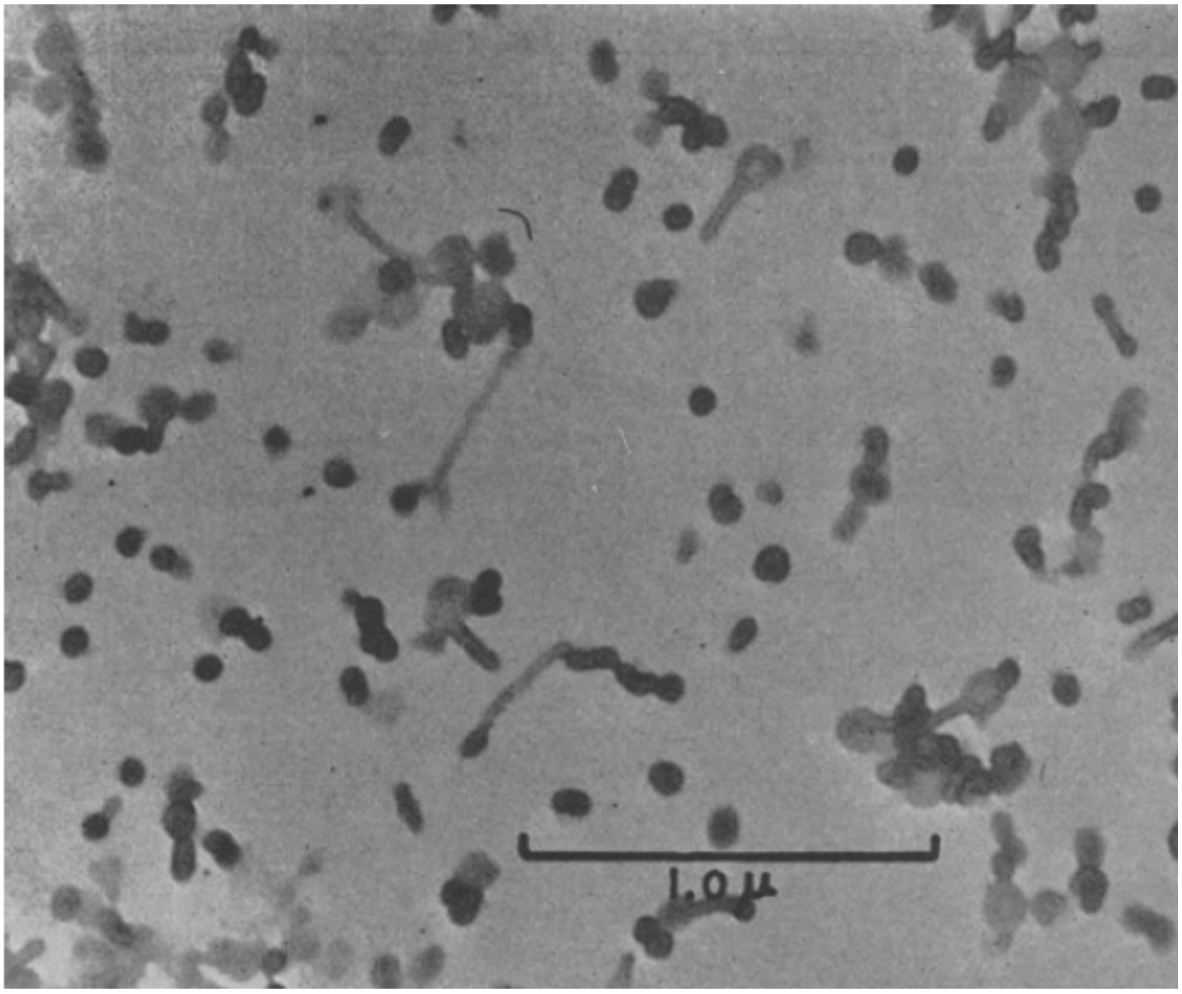

Figure 1.2: Influenza virus pleiomorphy was first seen in 1943.
Micrograph of chorio-allantoic fluid from an embyronated chicken egg infected with influenza/A/Puerto Rico/8/1934 (H1N1). 30,000x magnification, stain unspecified. Reproduced from Taylor et al. (1943).

a

A/California/07/2009

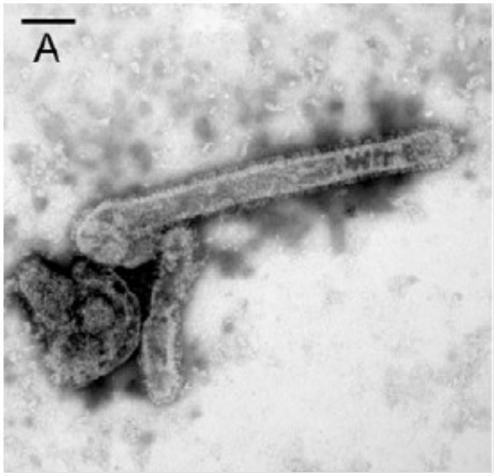

b

A/canine/Florida/43/2004

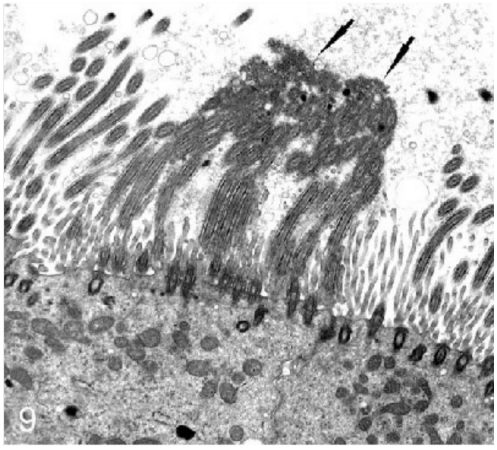

c

A/mallard duck/England/7277/06

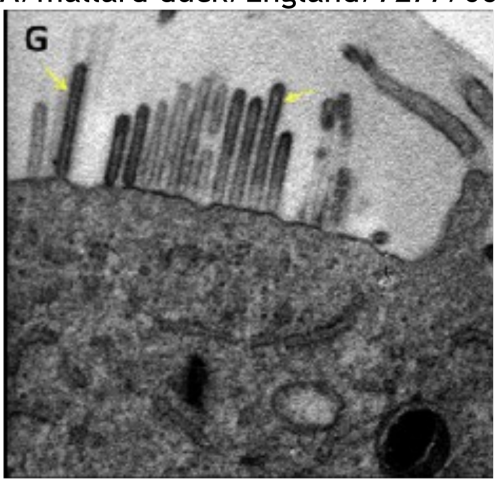

d

A/equine/Prague/56

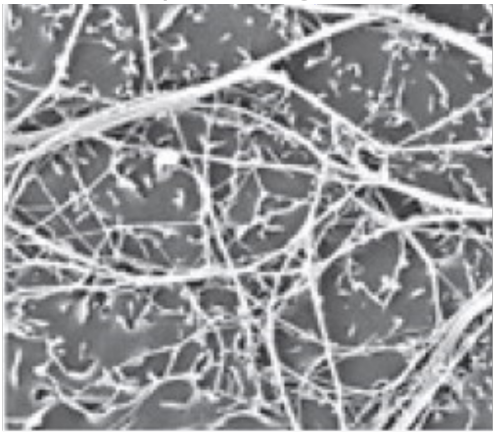

e

B/Lee

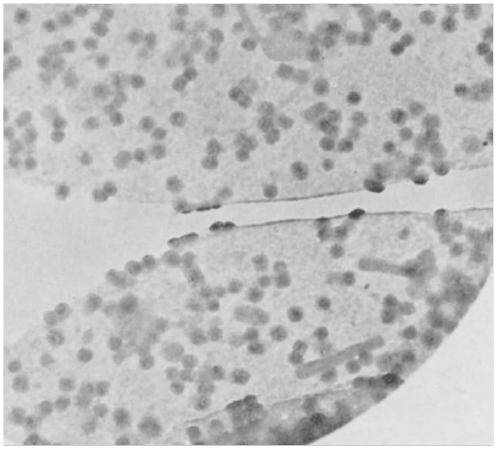

f

C/Ann Arbor/1/50

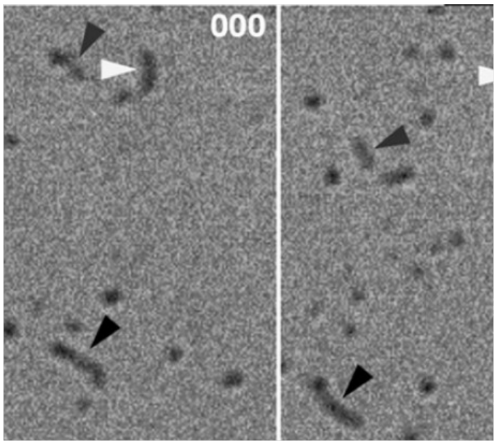

g

Saliva sample, 1968 pandemic

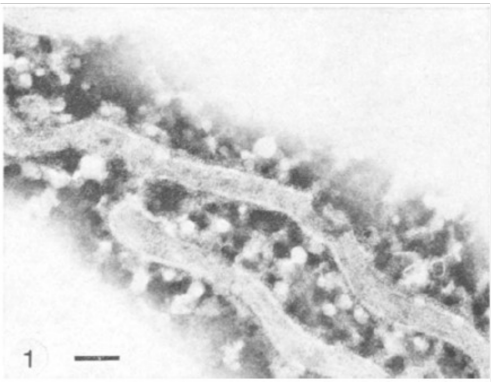

h

Lung autopsy, 2009 pandemic

Figure 1.3: Influenza virion pleiomorphy is widespread

Micrographs of filamentous influenza virions from a variety of strains.
(a) Recombinant 2009 H1N1 pandemic influenza grown in embyronated chicken eggs. Stained with methylamine tungstate and imaged with TEM, scale bar 100 nm (Lakdawala et al., 2011).
(b) Bronchus of racing greyhound five days after infection with A/canine/Florida/43/2004 virus. Stained with lead citrate and uranyl acetate and imaged with TEM (Castleman et al., 2010).
(c) Duck embryonic fibroblasts 7 h after infection with influenza A/mallard duck-/England/7277/06 (H2N3). Stained with 2% phosphotungstic acid and imaged with TEM (Al-Mubarak et al., 2015).
(d) MDCK cells 14 h after infection with influenza A/equine/Prague/56 (H7N7). Coated with AuPd and imaged with SEM (Elton et al., 2013).
(e) Influenza B/Lee adsorbed to avian erythrocytes. Stain unspecified, imaged by TEM (Dawson & Elford, 1949).
(f) Influenza C/Anna Arbor/1/50 adsorbed to bovine mucin. Imaged with surface reflection interference contrast microscopy (Sakai et al., 2017).
(g) Saliva sample from patient infected with 1968 pandemic influenza. Stained with 1% PTA (Bienz & Löffler, 1969).
(h) Lung autopsy from patient who died while infected with 2009 pandemic influenza virus. Stained with 4% uranyl acetate and lead citrate and imaged with TEM (Kataoka et al., 2019).

1.3 Influenza virus morphology

1.3.1 Overview of influenza virion morphology

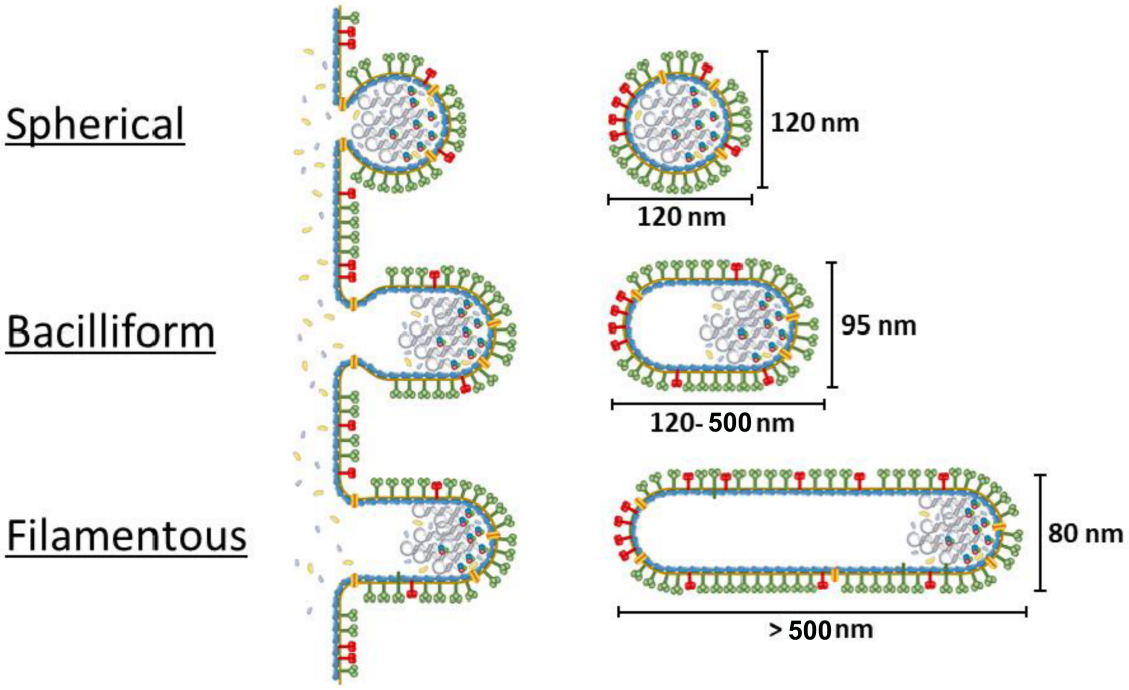

Figure 1.4: Influenza virions can be grouped into three classes. Adapted from Pinto (2019).

Influenza virions can be broadly categorised into three groups: spheres (diameters of ~120 nm, including glycoproteins), bacilli (diameters ~100 nm, lengths ~200 - 500 nm) and filaments (diameters of ~100 nm, lengths vary but can exceed 30,000 nm) (Vijayakrishnan et al., 2013) (Figure 1.4). The boundaries between these groups are somewhat arbitrary and not well defined, and pleiomorphy is visible within each group (Vijayakrishnan et al., 2013). Furthermore, the differences between the smaller spherical and bacilliform virions have not yet been studied beyond their initial identification. To aid in making comparisons, here I group all virions with lengths below 500 nm in the category of "non-filamentous virions", with all the longer virions grouped as "filamentous virions". This grouping loses some of the nuanced variation within the groups, but is conceptually useful when comparing studies with varying levels of virion characterisation.

Here it is also worth noting that "filament" and "filamentous virions" are sometimes used interchangeably (e.g. Hirst & Hutchinson (2019)). However, influenza virus-infected cells can produce filamentous structures that lack ordered matrices and often resemble long ellipses rather than rods (Figure 1.5). The term "filaments" encompasses these disordered structures as well as filamentous virions. To avoid confusion, I use the term "filament" exclusively to refer to the shape, and "filamentous virion" to refer to the virions.

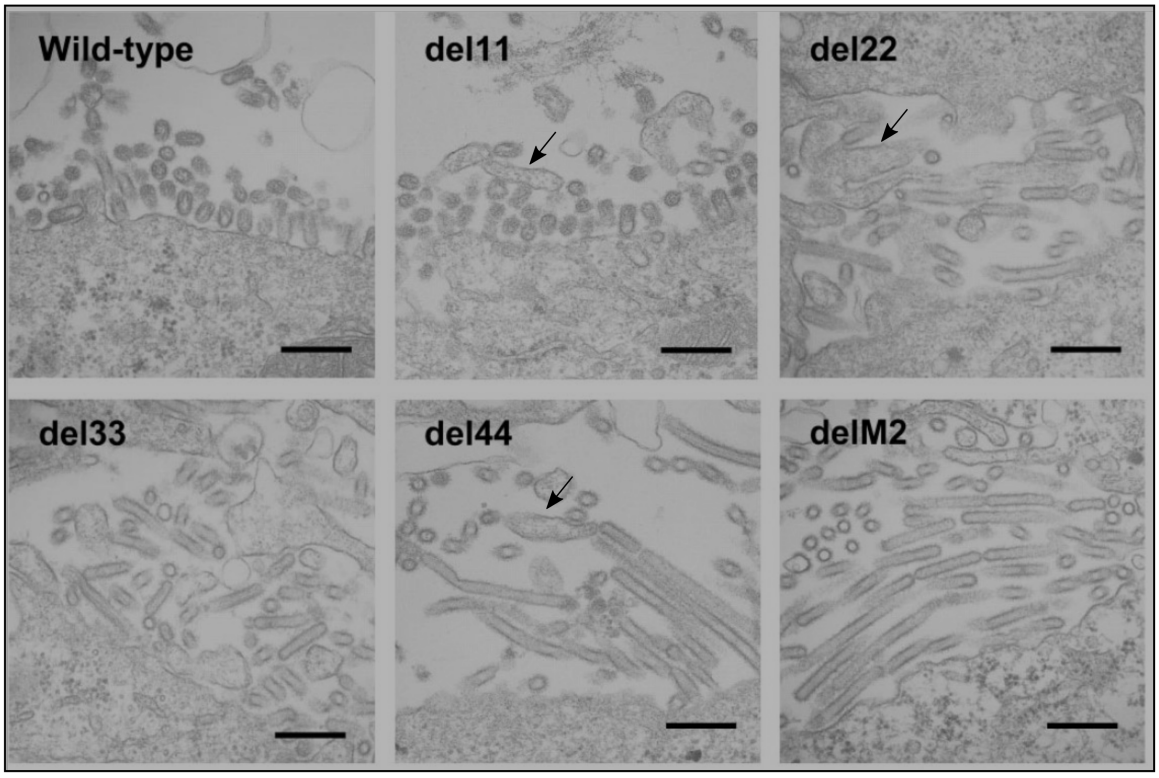

Figure 1.5: Influenza can produce filamentous structures that are not virions. A series of mutations in the cytoplasmic tail of M2 of influenza A/WSN/33(H1N1). Arrows indicate particles with filamentous shapes that lack ordered capsid structures and have inconsistent diameters. Filamentous virions are visible alongside, with densely stained capsids and consistent diameters. Scale bar 500nm, stained with 1% uranyl acetate. Reproduced from Iwatsuki-Horimoto et al. (2006).

1.3.2 Why it is thought that influenza virions can be filamentous

Despite controversy over whether filamentous structures seen in early electron microscopy studies were virions or artefacts of sample preparation (Angulo et al., 1950; Angulo, 1951), filamentous virions have been observed many times (reviewed in Dadonaite et al. (2016)). Identifying virions with electron microscopy is easiest when observing a highly concentrated sample (discussed by Seladi-Schulman et al. (2014)), and so almost all these studies have analysed virions grown in cell or tissue culture to generate a high yield of virus. This means that there has been long-standing uncertainty about whether filamentous virions are actually present in natural human infections. However, electron micrographs of lung autopsies from patients who died in the 2009 influenza pandemic clearly show filamentous virions in the lung (Figure 1.3h) (Nakajima et al., 2010) and internalised within alveolar macrophages (Kataoka et al., 2019), and filamentous virions were observed in throat washings from a patient infected during the 1968 pandemic (Bienz & Löffler, 1969) (though the latter study was published in a German language journal and seems to have been largely overlooked). Taken together, these studies suggest that filamentous virions do exist in natural infections of influenza virus, though it has not yet been possible to determine their frequency relative to non-filamentous virions.

1.3.3 Why it is thought that virion pleiomorphy is adaptive

1.3.3.1 Introduction

The mere presence of pleiomorphy is not enough to demonstrate that it is adaptive. Pleiomorphy could be a spandrel: a by-product of another adaptive mutation rather than adaptive in its own right (Gould & Lewontin, 1979). It could be neutral, conferring neither significant advantages nor disadvantages to virus strains. It could even be maladaptive, and pleiomorphic viruses could be trapped on suboptimal fitness peaks, where a series of mutations that would both reduce pleiomorphy and increase fitness cannot arise as the early steps in the series would render the virions non-functional (Rodrigues & Shakhnovich, 2019).

If pleiomorphy is indeed adaptive, antiviral therapies could in principle be designed to target it. If pleiomorphy is not adaptive, time and resources could be wasted on trying to understand its function, detracting from more fruitful research avenues. It is therefore vital to determine whether pleiomorphy is adaptive in influenza viruses. In asking this, we should begin by summing up the available evidence.

1.3.3.2 Other virions form filamentous virions

Filamentous virion formation is widespread among viruses, which could be interpreted as meaning this shape confers some advantage. Some viruses, such as ebolavirus (Bharat et al., 2012), tobacco mosaic virus (Klug, 1999) or bacteriophage M13 (Rakonjac et al., 2011), are exclusively filamentous. Here, filamentous virion formation is an inevitable consequence of the capsid structure: capsid subunits assemble directly around a central strand of nucleic acid, so the virion morphology is dictated by the shape of the genome. This also means pleiomorphy in these viruses is entirely dependent on genome size: polyploid virions are longer, while virions packaging genomes containing deletions are shorter. It is impossible to test whether filamentous virion formation is adaptive in these viruses as no spherical variants can exist. Consequently, conclusions about the role of filamentous virion structure in exclusively filamentous viruses cannot be generalised to the far more varied structures seen in influenza viruses.

Better evidence comes from viruses that can produce both filamentous and non-filamentous virions, particularly respiratory viruses such as respiratory syncytial virus (Bächi & Howe, 1973), human metapneumovirus (El Najjar et al., 2016), parainfluenza virus type 2 (Yao & Compans, 2000) and mumps virus (Duc-Nguyen & Rosenblum, 1967). These viruses share a tissue tropism and transmission route with influenza viruses and therefore face similar barriers to transmission, so it is plausible that their pleiomorphy is an adaptation to overcome these barriers. However, without experimental data assessing the fitness of different morphologies, pleiomorphy being a spandrel, neutral, or maladaptive in these viruses is just as possible as it is in influenza viruses. It is therefore difficult to suggest that pleiomorphy is being selected for in these viruses.

Taken together, the widespread formation of filamentous virions among many types of virus is suggestive that pleiomorphy is adaptive in certain scenarios. However, without experimental evidence, the mere presence of pleiomorphy is not sufficient to rule out the alternative hypotheses to pleiomorphy being adaptive.

1.3.3.3 Filamentous virions use more resources

It has been suggested that the sheer size of filamentous virions demonstrates their formation is adaptive, based on the assumption that they require more resources to produce than non-filamentous virions. Their formation would therefore be selected against if the fitness benefits did not outweigh those costs (Li et al., 2021). This idea is difficult to test experimentally, but an estimate of the energy budget of influenza virus suggests that protein synthesis is the most energetically expensive stage of the replication cycle (Mahmoudabadi et al., 2017), which supports the idea that it is less efficient to build a large virion if a smaller virion is equally infectious. However, given that most influenza virions are not

fully infectious (Brooke et al., 2013), it seems unlikely that resource efficiency is a significant factor in viral fitness. It is possible that the rate of virion production could impact viral fitness, as there is limited time after an infected cell begins producing virions before the cell dies, but it is possible to produce infectious virions at a similar rate in cell culture regardless of morphology (Seladi-Schulman et al., 2013). Therefore, there is no reason to believe that the metabolic costs of producing influenza virions strongly impacts viral fitness, and so the mere presence of filamentous virions, even if they require additional resources to produce, is not enough to infer that their formation is adaptive.

1.3.3.4 Passage histories suggest filamentous virions have a role *in vivo*

The strongest current evidence that influenza virus pleiomorphy is adaptive in infection comes from passage experiments. These initially took the form of natural experiments or serendipitous observations, noting that laboratory-adapted strains of influenza typically produced fewer filamentous virions than recent clinical isolates (Chu et al., 1949). This process is even visible across the chronology of the literature: with some exceptions, influenza A/Puerto Rico/8 (PR8) is commonly described as spherical in early studies (Taylor et al., 1943; Mosley & Wyckoff, 1946; Murphy et al., 1950) but is considered nearly exclusively spherical in later years (Chu et al., 1949; Werner & Schlesinger, 1954; Kilbourne & Murphy, 1960). These observations were tested formally by Burnet and Lind, who passaged pleiomorphic isolates in chicken eggs and saw that filamentous virion formation was reduced unless the experiments were performed at a limiting dilution (Burnet & Lind, 1957). More recently, Seladi-Schulman et al. demonstrated that serial passage of the clinical strain A/Georgia/M5081/2012 (H1N1) in chicken eggs caused a loss of pleiomorphy, but this was not observed with the contemporaneous strain, A/Netherlands/602/2009 (H1N1) (Seladi-Schulman et al., 2013). They also showed that serial intranasal passage of PR8 in guinea pigs led to a gain of pleiomorphy. Several point mutations in this pleiomorphic virus were sufficient to confer a more pleiomorphic phenotype on PR8. However, all but one of these mutations were attenuating in both eggs and guinea pigs, and the remaining mutation could not alone confer the capacity for contact transmission among guinea pigs on PR8 (Seladi-Schulman et al., 2013). Taken together, these findings support some link between pleiomorphy and adaptation, but it is more complex than pleiomorphy simply being adaptive in natural infections and maladaptive in the laboratory.

1.3.3.5 Conclusion

Taken together, despite decades of observation, there is little strong evidence that could help us examine the claim that influenza virus pleiomorphy is adaptive. Arguments for pleiomorphy being adaptive that stem from the mere existence of filamentous virions cannot be used to form robust conclusions. Experiments involving serial passage do suggest

that pleiomorphy is at least associated with fitness in some cases, but the relationship appears to be complex, and this type of experiment cannot examine whether pleiomorphy is adaptive or a spandrel. Ultimately, these top-down approaches to understand the role of pleiomorphy seem unlikely to provide firm conclusions. Instead, I propose that it would be better to use a bottom-up approach – first understanding how morphological variation leads to functional variation, and then building hypotheses that can be tested in the context of viral fitness in natural infections. To review the current understanding of how morphology affects function, I now return to the influenza virus replication cycle and discuss the differences that are known to correlate with viral morphology at each stage.

1.3.4 Morphology and the influenza replication cycle

1.3.4.1 Replication of the minimal infectious unit

Virion morphology is unlikely to directly affect the replication of RNPs, as it occurs after the capsid of the infecting virion has been disassembled but before the assembly of new virions. It is possible that differences at this stage could lead to differences in virion assembly and thus morphology, for example by altering the concentration of available RNPs, but no studies have yet addressed this.

1.3.4.2 Assembly

Variation in virion composition Differences in virion assembly will be reflected in differences in virion composition. Therefore, it useful to begin by comparing the composition of filamentous and non-filamentous virions. As well as the obvious difference in size and shape, many such compositional differences have been identified. Early suggestions that filamentous virions were multigenomic (Ada & Perry, 1958; Smirnov et al., 1991) were refuted by recent cryo-EM studies showing that filamentous virions contain at most one copy of the genome and often no genome at all (Calder et al., 2010; Vijayakrishnan et al., 2013; Halldorsson et al., 2021). This is reflected by western blot data showing a higher M1:NP ratio in samples containing more filamentous virions (Iwatsuki-Horimoto et al., 2006; Kordyukova et al., 2020; Liu et al., 2002; Roberts et al., 2013), though one study reported no difference (Seladi-Schulman et al., 2014). At least for IAV, the relative abundance of HA and NA also varies: M1:HA is constant regardless of morphology (Iwatsuki-Horimoto et al., 2006; Roberts et al., 1998; Seladi-Schulman et al., 2014), but M1:NA and HA:NA appears to be higher in filamentous virions (Chlanda et al., 2015; Vahey & Fletcher, 2019b,a). However, filament-producing mutants have been reported with no difference in HA:NA (Seladi-Schulman et al., 2014) and the available NA data is based on observing micrographs rather than directly quantifying protein abundance. M2 is also assumed to be proportionally less abundant in filamentous virions, although this is inferred

from observing that M2 clusters predominantly at the tips of filamentous virions rather than from a direct quantitative comparison with non-filamentous virions (Kolpe et al., 2019). These differences in proportion are often accompanied by a difference in organisation, with NA and M2 both reported to be more abundant at one or both poles of the filament (Calder et al., 2010; Chlanda et al., 2015; Kolpe et al., 2019; Vahey & Fletcher, 2019b) whereas HA is either much less polarised (Vahey & Fletcher, 2019a) or unpolarised (Calder et al., 2010; Kolpe et al., 2019). As well as viral proteins, influenza virions contain an array of host-derived proteins (Hutchinson et al., 2014), which may also vary with morphology, but this has not yet been addressed experimentally. Taken together, the evidence showing how composition varies with morphology is often limited and there are no detailed proteomic analyses comparing virions of different morphologies. Furthermore, these studies rarely investigate variation within morphological groups as well as between them, and the recent finding that HA, NA, M2 abundance per virion can vary across three orders of magnitude (Vahey & Fletcher, 2019b) suggests the relationship between morphology and composition is more complex than is currently understood. It also remains unclear which of these variations are consequences of pleiomorphy, and which, if any, are drivers of it.

All differences in virion composition must be driven by differences in assembly. Influenza virion assembly remains poorly understood, and there is currently no consensus on the mechanism by which assembly leads to pleiomorphy. However, many factors affecting morphology have been identified, and these can be used to infer where differences in assembly occur.

Viral genetics Early recombination studies identified a role for viral genetics in determining morphology (Burnet & Lind, 1957; Kilbourne & Murphy, 1960), and later reverse genetics approaches identified mutations in the M segment as having the biggest impact (Bourmakina & García-Sastre, 2003; Burleigh et al., 2005; Elleman & Barclay, 2004; Iwatsuki-Horimoto et al., 2006; Muraki et al., 2004; Roberts et al., 1998). These mutations can occur in both M1 and M2, and the distinct roles of these proteins in virion assembly suggest there are multiple mechanisms by which assembly affects morphology.

M1 Despite the plethora of studies identifying mutations in M1 that affect morphology, very few have investigated the mechanism by which this effect occurs. Liu et al. (2002) suggest the strength of association between M1 and RNPs could affect morphology, with the M1 from the predominantly spherical PR8 showing greater binding strength with RNPs than the pleiomorphic influenza A/Nanchang/933/95 (H3N2). However, these viral strains differ in many ways, and so it is not possible to be confident that the differences in morphology is directly linked to the difference in RNP binding. A similar idea was suggested by Burleigh et al. (2005), who found that mutations affecting a putative RNP binding domain in M1 both reduced M1-RNP binding and affected morphology, though most of these

mutants produced filaments which lacked organised M1 capsid structures rather than virions. However, one pleiomorphic mutant was identified with both a reduced binding strength between M1 and RNPs and a regular M1 helix. These data are supported by electron microscopy studies demonstrating that filamentous virions often lack genomes entirely, though comparisons between filamentous and non-filamentous virions of the same strain have not been reported (Vijayakrishnan et al., 2013; Halldorsson et al., 2021). Together, these studies suggest there may be a link between M1-RNP binding and filamentous virion assembly, but neither conclusively demonstrates this.

An alternate idea that has often been suggested is that mutations affecting M1-M1 interactions affect morphology, and so the variations may arise from differences in M1 polymerisation. Calder et al. (2010) suggest regularity of the M1 helix may play a role in morphology, with Udorn having both a more ordered helix and much longer filaments than influenza A/X-31 (H3N2), though the many other differences between these strains were not accounted for. The positions of mutations that affect morphology in M1 may also suggest an effect on polymerisation: a series of mutations affecting only the positive face of M1 restored filamentous virion formation to a predominantly spherical mutant strain, though the data presented could also be interpreted as these mutations simply restoring all virion budding to a defective mutant (Liu et al., 2017). Similarly, a point mutation in M1 has been identified in multiple studies (Campbell et al., 2014a; Elleman & Barclay, 2004; Roberts et al., 1998) which occurs in a alpha-helix of M1 that is likely solvent-exposed and could affect polymerisation.

Taken together, mutations in M1 appear to be able to affect assembly by affecting the strength of interaction between M1 and other major structural virion components, including other M1 monomers. However, no studies have demonstrated how such changes affect polymerisation, nor do they explain why these mutations lead to a pleiomorphic phenotype rather than an exclusively filamentous one. M1 therefore strongly influences assembly, but it is unclear how.

M2 As well as M1, mutations in M2 have repeatedly been linked to virion morphology (Beale et al., 2014; Bourmakina & García-Sastre, 2003; Elleman & Barclay, 2004; Iwatsuki-Horimoto et al., 2006; Roberts et al., 2013; Rossman et al., 2010), and antibodies directed against M2 can prevent filamentous virion formation (Roberts et al., 1998). These mutations do not appear to affect the ion channel activity of M2, and treating cells with amantadine to block the ion channel activity does not cause a reduction in filamentous virion production (Rossman et al., 2010). This suggests that it is not M2's ion channel activity that affects morphology, but rather its role in budding. This could be due to M2 stabilising the budding site for long enough to allow extended M1 polymerisation (Rossman & Lamb, 2011), though this is challenging to reconcile with the finding that M2 deletion can increase the number of filamentous virions formed (Iwatsuki-Horimoto et al., 2006). An alternate model is that filamentous virions could be produced as a "failed" budding

event, where the virion keeps growing because M2 does not induce scission. However, neither mechanism yet explains why the same M2 protein can produce both filamentous and non-filamentous virions, nor why filamentous virions eventually bud rather than just grow indefinitely.

HA and NA While most mutations affecting morphology have been linked to the M segment, some studies have suggested a role for HA and NA in morphology (Campbell et al., 2014a,b; Chlanda et al., 2015; Jin et al., 1994; Lakdawala et al., 2011; Mitnaul et al., 1996; Smirnov et al., 1991; Li et al., 2021). However, these studies either create recombinant strains where entire gene segments differ and so it is difficult to identify the specific factor causing the difference in morphology (Campbell et al., 2014a,b; Lakdawala et al., 2011; Smirnov et al., 1991), or identify mutations that lead to filamentous structures that lack an ordered M1 capsid (Chlanda et al., 2015; Jin et al., 1994; Mitnaul et al., 1996). It is therefore currently impossible to state that these proteins affect morphology directly. For example, many apparent changes in morphology may be due to both proteins being involved in recruiting M1 to the budding site, with M1 actually causing the morphological differences. It is noteworthy, however, that recombination experiments which create various combinations of the M, HA, and NA segments from a pleiomorphic or predominantly spherical virus strain yield strains with a broad range of morphological phenotypes where there is no obvious link between the genotype and morphology (Smirnov et al., 1991; Campbell et al., 2014a). This suggests that it may be too simplistic to claim a given mutation affects morphology in a given way. Instead, it seems more likely that the effect of a mutation on virion assembly depends on the genetic background into which it is introduced.

Cell polarity Viral factors have most commonly been linked to differences in morphology, but several studies also suggest the state of the host cell is also important. It has been suggested that cell polarisation state affects virion morphology, with more stably polarised cells more readily forming filamentous virions (Roberts & Compans, 1998). However, more recent studies have shown reliable filamentous virion formation even in poorly polarised cells (Chlanda et al., 2017) and chicken and duck embryonic fibroblasts yield virions of differing morphologies, despite a presumably comparable polarisation state (Al-Mubarak et al., 2015). Furthermore, when infected with the avian viral strain A/mallard duck/England/7277/06 (H3N2), highly polarised MDCK cells did not produce filamentous virions but unstably polarised duck embryonic fibroblasts did (Al-Mubarak et al., 2015). This suggests that the link between cell polarisation and virion morphology is complicated, or potentially just the product of an insufficiently broad sample of cell and virus types.

Microfilaments and lipids A potential link between virion morphology and cell polarity comes from cellular factors that are linked to both. Polarised actin microfilaments are essential to maintain polarity, and disrupting these with jasplakinolide led to a loss in

filamentous virion formation without affecting infectious titre or total protein synthesis (Simpson-Holley et al., 2002). The authors of this study noted that HA appeared to colocalise with cortical actin, and HA, NP and M1 distributions were also disrupted by jasplakinolide, suggesting that actin is necessary to arrange viral proteins in such a way to allow filamentous virion assembly. This may be due to actin organising lipid rafts, as disrupting these lipid rafts with methyl-β-cyclodextrin reduces filamentous virion formation and can partially collapse those that have already formed (Rossman et al., 2010; Simpson-Holley et al., 2002). This suggests lipid rafts are major structural components of filamentous virions and it is necessary to concentrate them to allow filamentous virion assembly. This model of an interplay between viral proteins, host cytoskeleton, and host lipids is supported by findings that mutations in putative cholesterol binding regions in M1 affect morphology (Tsfasman et al., 2015), and differences in lipid composition could explain why filamentous virions appear to form more readily at microvilli than the plasma membrane (Kolesnikova et al., 2013). However, this model of protein organisation affecting virion assembly is still incomplete. Non-filamentous virions also bud from lipid rafts, so it is unclear why methyl-β-cyclodextrin treatment would only affect filamentous virions. Furthermore, the key evidence supporting a role for protein organisation in virion morphology is mostly correlative, with actin or lipid disruption disrupting both protein organisation and morphology, but with a mechanistic link between them untested. As with cell polarity, it also appears that the effect of disrupting actin on virion morphology depends on which cell and virus are being tested, with a strong effect visible with Udorn and MDCK cells, but no effect visible with influenza A/mallard duck/England/7277/06 (H2N3) in duck embryonic fibroblasts (Al-Mubarak et al., 2015). Therefore, while the cytoskeleton can play a role in modulating virion morphology, it is not necessary in all cases.

Other host factors In addition to the differences discussed above, factors affecting morphology have been identified that are difficult to analyse due to a lack of related studies elsewhere in the literature. An LC3-interacting domain in M2 (Beale et al., 2014), Rab11-FIP3 (Bruce et al., 2010), and incubation temperature (Burleigh et al., 2005) have all been linked to morphology. However, none of these studies directly calculate the proportion of filamentous and non-filamentous virions in different conditions, making it hard to draw firm conclusions about the strength of the effects, and all focus on mechanisms that have otherwise not been explored in the context of virion morphology so there are no studies to compare them with. Therefore, while these factors may affect assembly, it is not yet possible to determine how.

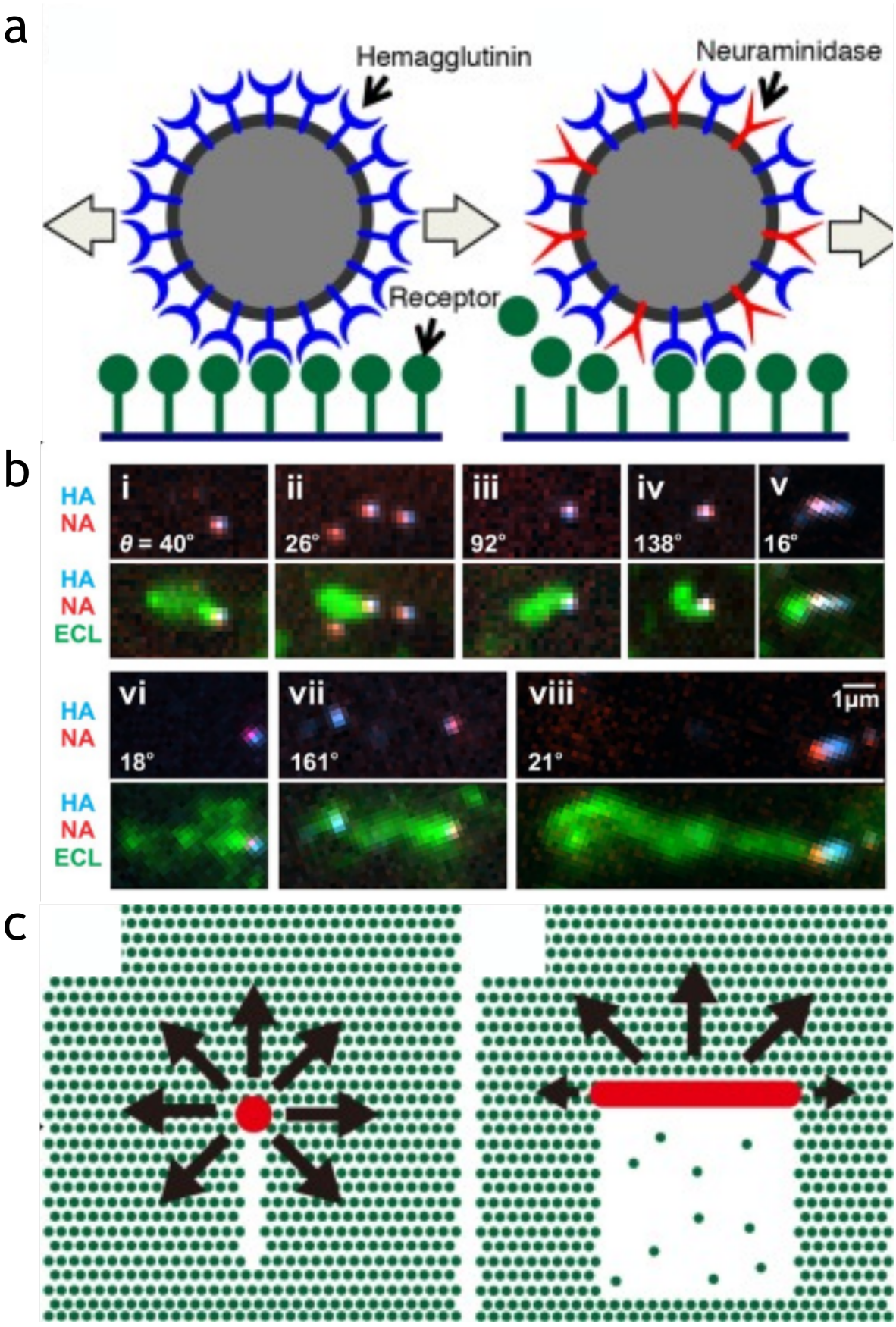
a
Hemagglutinin
Neuraminidase
Receptor
b
HA
NA
i
θ = 40°
ii
26°
iii
92°
iv
138°
v
16°
HA
NA
ECL
vi
18°
vii
161°
viii
21°
1μm
c

Figure 1.6: Two models explaining directed motion of filamentous virions

(a) A model for motility of influenza virions. Virions move across a sialylated surface by a Brownian ratchet mechanism, where HA activity continuously binds and releases sialic acids and NA activity permanently cleaves them. The virion therefore cannot bind the same location twice. Image reproduced from Sakai et al. (2017). (b) A model for directed movement of filamentous influenza A virions suggested by Vahey & Fletcher (2019a). Virions move across sialylated surfaces via the Brownian ratchet, leaving a wake of cleaved sialic acids (indicated by the green ECL stain). In this model, unpolarised distributions of HA and NA, such as that seen on non-filamentous virions, results in a random walk pattern. However, filamentous virions can have polarised HA and NA distributions, leading to preferential binding of sialic acids at one pole and preferential cleaving of sialic acids at the opposite pole. This results in filamentous virions preferentially moving perpendicular to their short axis. Image reproduced from Vahey & Fletcher (2019a). (c) A model for directed motion of filamentous influenza C virions suggested by Sakai et al. (2017). Non-filamentous virions can readily change directions and so move in a random walk pattern. Filamentous virions cannot easily turn due to the wide swathe of cleaved sialic acids behind them, and so preferentially move perpendicular to their long axis. Image reproduced from Sakai et al. (2017).

1.3.4.3 Transmission

Few studies have attempted to directly address differences between filamentous and non-filamentous virions in transmission, possibly because this requires complex experimental systems to replicate the environments in which transmission takes place. It has been suggested that filamentous influenza virions are an adaptation to traverse mucus, a major barrier to infection in the airway (Roberts et al., 1998). Sialylated mucin residues act as decoy receptors and bind HA and must be cleaved by NA to allow transmission. Therefore, the balance of HA:NA activity is vital to evading mucus inhibition, and the variation in HA:NA abundance with morphology discussed above may favour one type of virion when navigating this environment. This idea is supported by a recent study showing that polarised distribution of HA and NA on virion membranes allows filamentous virions to move directionally, parallel to their long axes, across sialylated surfaces via a Brownian ratchet mechanism (Figure 1.6a). Spherical virions or filamentous virions with no polarisation could only move in a random walk pattern (Vahey & Fletcher, 2019a). A similar process was observed for influenza C virions, though theses cannot have polarised receptor binding and destroying activity as both processes are mediated by the same protein. Furthermore, the filamentous virions move perpendicular to their long axes rather than their short axes (Figure 1.6b) (Sakai et al., 2017). It is challenging to reconcile these studies, as the two mechanisms of motion described are mutually exclusive. Furthermore, neither study measures infection, so there is not currently enough evidence to determine whether these differences in motility are indeed an adaptation to evade mucus.

More broadly, it has been suggested that pleiomorphy enables influenza virus to rapidly respond to an unpredictable environment, increasing the chance at least one virion will be able to navigate all the barriers blocking transmission (Vahey & Fletcher, 2019b). While provocative, this was only tested experimentally with NA inhibitors, which do not occur naturally and so cannot have driven the widespread pleiomorphy seen in influenza virus prior to the discovery of NA inhibitors in the 1960s (Edmond et al., 1966). Further research, focusing on naturally occurring barriers to transmission is therefore necessary to confirm this hypothesis.

1.3.4.4 Entry and unpacking

The upper bound for the diameter of clathrin-coated vesicles is approximately 100nm, meaning filamentous virions are far too large to enter cells via this pathway. Instead, filamentous virions are solely dependent on macropinocytosis for entry (Rossman et al., 2012). Non-filamentous virions can use either pathway, but clathrin-mediated endocytosis is much more common (Rossman et al., 2012). It is unclear whether this leads to any functional differences in infection, although macropinocytosis can lead to several virions being internalised simultaneously which could mean cells infected with filamentous virions are more

likely to be co-infected than cells infected by non-filamentous virions.

1.3.4.5 Evasion of immunity

As influenza virus's primary immunosuppression mechanism is expression of NS1, this stage of infection is largely independent of virions and so it is unlikely to be affected by morphological differences. It is perhaps possible that virions with different morphologies package different immunomodulatory proteins such as NS1 that affect immunity, but components directly delivered by IAV virions have not been shown to cause immunosuppression and there is not yet a detailed proteomic comparison of filamentous and non-filamentous virions with which to infer such a difference.

While differences in NS1 activity seem unlikely, it is possible that filamentous virions are more resistant to antibody neutralisation than non-filamentous virions. The much greater abundance of HA on filamentous virions increases the likelihood that some region of the virion contains enough functional HA proteins to form a fusion pore, even if a high proportion of HAs are neutralised by an antibody (Li et al., 2021). However, it has also been reported that haemagglutination inhibition titres are similar in mutants with different morphologies (Seladi-Schulman et al., 2014). Any resistance to antibody neutralisation is only likely to be adaptive in specific cases. It is unlikely to improve viral fitness when infecting a naïve host, as typical influenza virus infections usually resolve before a novel antibody response can be mounted. If a host organism has strong pre-existing immunity, in the form of well-matched antibodies or memory lymphocytes, it is unlikely that even the improved resistance of filamentous virions will be able to surmount it (if this were not the case, vaccination would not work). If a host has partial immunity, perhaps from being infected or vaccinated by a related strain of influenza virus, then a virion with a high tolerance to antibody neutralisation may be more likely to initiate infections than those that do not. However, filamentous virions often lack genomes (Vijayakrishnan et al., 2013; Halldorsson et al., 2021) and their formation is selected for during passage in immunologically naïve guinea pigs (Seladi-Schulman et al., 2013). If filamentous virions do confer a fitness advantage due to their superior antibody resistance, therefore, it cannot fully explain the pleiomorphy seen in influenza virus.

1.4 Challenges in interpreting the literature

1.4.1 Introduction

The survey of the literature above demonstrates that filamentous influenza virions are poorly understood and poorly characterised. This is surprising, given that the filamentous

influenza virions were first imaged in 1943 (Taylor et al., 1943) and recognised as clinically relevant in 1949 (Chu et al., 1949). However, several issues affect the subsequent literature describing filamentous influenza virions that have so far prevented a clear understanding of influenza virus pleiomorphy.

1.4.2 Few studies have examined influenza virus morphology

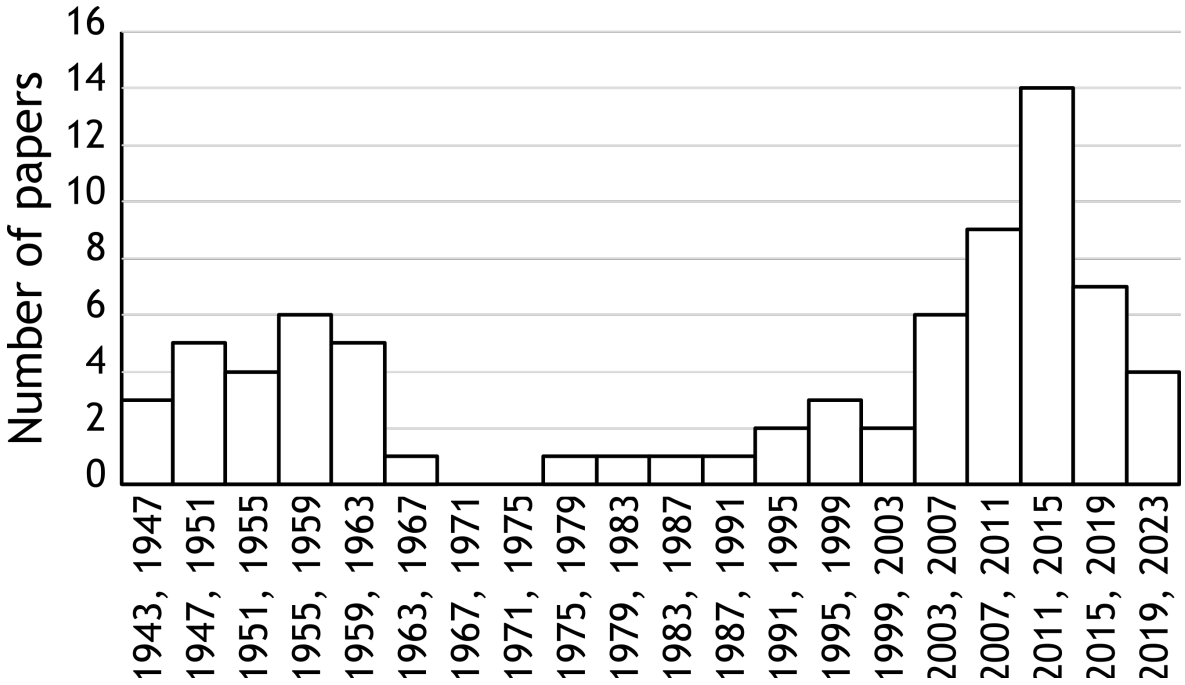

Figure 1.7: Influenza morphology research occurred in two waves.
Journal articles pertinent to influenza virus morphology were first identified through searching "filamentous influenza virus" and "influenza virus filaments" on PubMed. Articles which did not focus on morphology (e.g. those examining actin filaments rather than virion filaments) were removed manually. Further papers, not returned by the PubMed search, were identified by following the citations of the papers after an exhaustive reading of this curated list.

The biggest problem with understanding filamentous influenza virions is simply a lack of studies focusing on them. As of 25th March 2021, PubMed returns 80,034 papers when searching "influenza virus" but only 120 for "filamentous influenza virus" and 206 for "influenza virus filaments". Many of these latter studies focus on phenomena such as filamentous actin rather than virion morphology, so I removed these from my literature survey. Many of the remaining articles contained references to relevant studies that were not returned by the PubMed searches, and so these were identified and included by manual searches. This left me with a survey of 76 studies which provide useful information pertaining to influenza virion morphology. Many of these papers were published several decades ago, and are limited by outdated methods or an outdated understanding of influenza virology (for example, the first to reference the eight IAV RNPs by name is Smirnov et al. (1991), published after a third of the papers in this survey). It is unclear why so few studies

have focused on morphology. A histogram of papers published over time shows that filamentous influenza virus research occurs in two waves, the first from ~1943 to 1960, and the second from ~1995 to the present day (Figure 1.7). It is unclear why research into influenza virus pleiomorphy essentially halted in the 1960s, and was even unclear to those researchers working in this "interim" period (Cox et al., 1980). (Though it should be noted that several studies which reference filamentous influenza virions were published in the Soviet Union during this period, but these have been excluded as they are difficult to access and are only available in Russian (Klimenko et al., 1968; Makhov et al., 1989; Kuznetsova et al., 1990)). It is possible this chronological distribution of studies reflects the complexity of pleiomorphy, and the need for a deep understanding of the basic virology of influenza virus and advanced tools such as reverse genetics before anything beyond the basics could be approached. It could also be due to an increasing dependence on predominantly spherical laboratory strains of influenza virus such as PR8 and WSN during the latter half of the 20th century, though both of these strains have been popular throughout the timespan covered by this literature review (PR8 was isolated in 1934 and WSN in 1933, discussed in Hutchinson & Yamauchi (2018)). Whatever the cause, many findings about influenza morphology have not been reproduced, and in some cases the most relevant citation for a claim is based on outdated virus strains or methods (see Section 1.4.6 for a case study) and so cannot be easily compared to modern studies.

1.4.3 Samples of filamentous and non-filamentous virions are often poorly matched

As well as the difficulty in comparing different studies, it is also challenging to find suitable models for comparison within a study. Determining the properties of filamentous virions requires some way of generating a sample enriched for filamentous virions and one enriched for non-filamentous virions, but the methods available for this are limited.

One approach is to use naturally occurring strains with different morphologies as models, for example, comparing PR8 with a recent clinical isolate (Liu et al., 2002), but this sort of experiment cannot differentiate between the effects of the many variations between strains.

A second method is to compare closely related strains which contain mutations that affect morphology. Variants of PR8, WSN and Udorn have commonly been used for this (Bourmakina & García-Sastre, 2003; Bruce et al., 2010; Iwatsuki-Horimoto et al., 2006; Roberts et al., 1998; Seladi-Schulman et al., 2013; Sieczkarski & Whittaker, 2005; Tsfasman et al., 2015). While this significantly reduces the potential confounding variables in an experiment, until the underlying mechanism explaining the morphological changes is determined, it is impossible to be confident that these mutations do not also affect some other aspect of the virus. It is also possible that a change in morphology alone is not enough to confer a fitness advantage by itself, and that compensatory mutations are needed elsewhere in the

genome for the advantages of pleiomorphy to become apparent. For example, it has recently been reported that a “hinge” domain in HEF is necessary to allow it to conform to the different membrane curvatures of filamentous and non-filamentous influenza C virions (Halldorsson et al., 2021). Mutations in M1 that change virion morphology may therefore need to be accompanied by mutations in this “hinge” domain to produce correctly structured virions. Effects such as this could explain why infectivity is reduced when mutations increase filamentous virion production (Bialas et al., 2012; Seladi-Schulman et al., 2013) but also when they reduce filamentous virion production (Roberts et al., 2013) – the effect may be caused by a deviation from the norm of that strain rather than by an inherent property of a given morphology.

A third approach is to compare filamentous and non-filamentous virions from within the same initial population through purifying virions by morphology to allow bulk population analyses (Ada et al., 1958; Donald & Isaacs, 1958; Li et al., 2021; Roberts et al., 1998; Sieczkarski & Whittaker, 2005; Smirnov et al., 1991) (Discussed in greater detail in Chapter 5). This approach produces genetically identical but morphologically distinct samples, but, as all progeny virions will be pleiomorphic, it cannot be used for experiments requiring multiple cycles of infection. It is also liable to problems caused by incomplete purification: density gradient purification alone has produced samples ~70% comprised of filamentous virions (Smirnov et al., 1991), whereas a combination of density gradient purification and introducing a mutation to favour filamentous virion formation produced a sample ~92% comprised of filamentous virions (Sieczkarski & Whittaker, 2005). Non-filamentous virions will therefore still be contributing to the overall properties of these enriched populations, and so if a characteristic is present in non-filamentous virions but absent from filamentous virions, it may inaccurately appear as if both possess it. Furthermore, current purification methods are challenging to reproduce reliably (as noted by Kordyukova et al. (2020)), and so this cannot yet be considered a standard tool in influenza virus pleiomorphy research.

A fourth approach is to use microscopy to assess individual virions within a pleiomorphic stock (Calder et al., 2010; Sakai et al., 2017; Vahey & Fletcher, 2019b,a; Vijayakrishnan et al., 2013). This shares an advantage with purification methods, as all virions tested will be from the same initial stock and so will be isogenic. However, existing microscopy methods are limited: electron microscopy analyses of composition can be challenging to interpret as it is not easy to identify low-abundance proteins or those which lack distinctive shapes, and existing fluorescence microscopy methods to analyse filamentous influenza virion composition depend on a mutant virus which is labelled with bespoke reagents (Vahey & Fletcher, 2019b,a) and is thus hard to reproduce (discussed in greater depth in Chapter 5).

Taken together, the existing literature contains many studies that are difficult to interpret reliably due to poor matching of samples. Generating better matched samples is theoretically

possible, but currently limited due to a lack of understanding about mutations that influence morphology and technical limitations in separating virions from the same initial stock.

1.4.4 Artefactual damage may have affected characterisation of virions

Generating high quality samples is made harder still by the frequent observation that filamentous virions often seem to be damaged or otherwise removed from samples during standard laboratory handling (Donald & Isaacs, 1958; Elleman & Barclay, 2004; Kordyukova et al., 2020; Mitnaul et al., 1996; Morgan et al., 1956; Roberts et al., 1998; Valentine & Isaacs, 1957; Vijayakrishnan et al., 2013). This apparent fragility could mean researchers assumed that their samples contained more filamentous virions during experimental analysis than were present, leading to their contributions being underestimated. This artefactual damage is concerning, but has never been studied in detail and so its severity remains unclear.

1.4.5 Samples are often poorly characterised

Potential artefactual damage is a specific case of a broader problem: the samples being used in experiments are often poorly characterised, or characterised in a way that makes it difficult to compare studies. A particularly important case of this is that the proportion of filamentous virions in a sample is typically not calculated, and the distribution of virion lengths is rarely accounted for. This results in in the diverse array of influenza virion morphologies being reduced to a binary “more filamentous” or “less filamentous”, or “filamentous” vs “spherical”. This has some conceptual advantages and it has often been technically necessary as assessing particle dimensions via electron microscopy is laborious. However, it results in a loss of nuance and can make it impossible to compare results, even within a single study. Cases where proportions of filaments have been quantified only highlight this problem: a sample containing ~3% filamentous virions was considered to be “filamentous” in one study (Smirnov et al., 1991), but, in another study, a sample containing ~9% filamentous virions was considered to be “spherical” (Sieczkarski & Whittaker, 2005).

1.4.6 A case study: difficulties in determining the infectivity of filamentous virions

The various issues affecting the filamentous virion literature can be clearly seen when trying to answer the ostensibly simple question: “Are filamentous virions as infectious as non-filamentous virions?”. This question is controversial: various studies support filamentous virions being more infectious (Ada et al., 1957; Ada & Perry, 1958; Ada et al., 1957;

Roberts et al., 1998; Smirnov et al., 1991; Valentine & Isaacs, 1957), equally infectious (Donald & Isaacs, 1958; Li et al., 2021; Seladi-Schulman et al., 2014), or less infectious (Burnet, 1956; Burnet & Lind, 1957) than non-filamentous virions. These differences seem largely to be due to methodological problems. Several of the cited conclusions are based on untested assumptions about artefactual loss of filamentous virions or estimated virion sizes (Ada et al., 1957; Ada & Perry, 1958; Ada et al., 1957; Roberts et al., 1998; Valentine & Isaacs, 1957). Two calculate infectivity by normalising to HA activity (Li et al., 2021; Seladi-Schulman et al., 2014), but this is not useful for assessing virion infectivity as HA abundance differs hugely between filamentous and non-filamentous virions (see Section 1.3.4.2). One does not measure infectivity of virions per particle but instead infers infectivity differences from UV-inactivation kinetics, which are difficult to interpret (Smirnov et al., 1991). This leaves only one robust comparison of particle to PFU ratio in filamentous and non-filamentous virions, Donald & Isaacs (1958), and it was performed using influenza A/Persian Gulf/2/52 (H1N1): a strain separated from modern clinical isolates by 69 years and 3 pandemics.

1.4.7 Conclusion to challenges in interpreting the literature

In conclusion, the difficulty in synthesising the literature to fully explain the role of influenza virus pleiomorphy stems from a lack of studies with robust and readily comparable methods. We can see that this is largely due to technical limitations, which constrain the ability of researchers to generate well-characterised, well-matched samples for analysis. This in turn prevents robust characterisation of many of the basic biological properties of filamentous influenza virions. Therefore, understanding pleiomorphy in influenza virus infections depends on developing new tools with which to analyse filamentous virions, and using these to perform the basic characterisations necessary to support more complex investigations into their role.

1.5 Aims of this thesis

The next four chapters of this thesis detail my work to resolve these methodological issues and perform basic characterisations of filamentous influenza virions. This work can be broken down into four key aims, each of which comprise one of the subsequent results chapters.

Aim 1: Develop a method to analyse the dimensions of individual filamentous virions in a sample and detect changes to their concentration.

Aim 2: Validate a set of standard laboratory handling techniques that can be used to manipulate filamentous virions without damaging them.

Aim 3: Perform a detailed comparison of the composition of filamentous and non-filamentous virions.

Aim 4: Use the compositional comparison to build and test hypotheses about the functional differences between filamentous and non-filamentous virions.

Through developing these tools and robustly determining the basic properties of filamentous virions, I aimed to build a solid foundation to explore their roles *in vivo*. This understanding would improve our understanding of the complex replication cycle of influenza virus, and potentially present new therapeutic targets to reduce the harm it causes.

Chapter 2

Materials and Methods

2.1 Materials

2.1.1 General Reagents

Table 2.1: List of general reagents.

Reagent	Supplier
Coomassie Brilliant Blue	Bio-Rad
Glacial Acetic Acid	VWR Chemicals
Formvar Carbon-Coated Copper Grids	Agar Scientific
Phosphotungstic Acid (PTA)	Agar Scientific
Chicken Red Blood Cells	TCS Biosciences
PageRuler Prestained Protein Ladder 10 – 180 kDa	ThermoFisher Scientific
Triethylammonium bicarbonate (TEAB)	ThermoFisher Scientific
Prolong Diamond Antifade Mountant	ThermoFisher Scientific

2.1.2 Cell culture reagents

Table 2.2: List of reagents used in cell culture.

Reagent	Supplier
Dulbecco's Modified Eagle's Medium (DMEM)	Gibco
Foetal Calf Serum (FCS)	Gibco
TrypLE Express	Gibco
Dulbecco's Phosphate Buffered Saline (PBS)	Gibco
TPCK-treated Trypsin	Sigma
Low-melting point agarose	Sigma

2.1.3 Viruses

Table 2.3: List of virus strains.

Strain	Source
Influenza A/Udorn 307/1972 (H3N2) (Udorn)	Prof. David Bhella (MRC-University of Glasgow Centre for Virus Research)
Influenza A/WSN/1933 (H1N1) (WSN)	Prof. Ervin Fodor (University of Oxford)

2.1.4 Cell Lines

Table 2.4: List of cell lines.

Cell line	Culture Medium	Source
Madin-Darby Canine Kidney (MDCK)	DMEM with 10% FCS	Prof. Ervin Fodor (University of Oxford)

2.1.5 Antibodies

Table 2.5: List of primary antibodies.

Antigen	Species	Clonality	Working concentration	Source
Haemagglutinin (H3)	Mouse	Monoclonal	1:2000	Dr Steven Warton (National Institute of Health Research)
Nucleoprotein	Rabbit	Polyclonal	1:500	Prof. Paul Digard (Roslin Institute)
Matrix 1	Rabbit	Polyclonal	1:500	Prof. Paul Digard (Roslin Institute)

Table 2.6: List of secondary antibodies.

Antibody	Species	Target species	Working concentration	Supplier
Alexa-Fluor 555	Goat	Mouse	1:5000	ThermoFisher Scientific
Alexa-Fluor 555	Goat	Rabbit	1:5000	ThermoFisher Scientific
Alexa-Fluor 488	Goat	Mouse	1:5000	ThermoFisher Scientific
Alexa-Fluor 488	Goat	Rabbit	1:5000	ThermoFisher Scientific
DyLight 700	Donkey	Rabbit	1:5000	ThermoFisher Scientific
Dylight 800	Donkey	Rabbit	1:5000	ThermoFisher Scientific

2.2 Methods

2.2.1 Cell culture

2.2.1.1 Maintaining cells

MDCK cells were maintained in culture medium at 37 °C and 5% CO_2 in T150 tissue culture flasks (Corning). When cells reached confluency, they were passaged by rinsing in 1x PBS, trypsinising with ~5 ml TrypLE Express for ~20 min, and resuspending one-twentieth of the cells in growth medium and transferring them to a new flask. The properties of the cells did not appear to vary even after extensive passage, so cell lines were typically maintained until work was interrupted for extended periods (e.g. major holidays).

2.2.1.2 Long-term cell storage

Additional aliquots of 10^6 MDCKs were stored long term in liquid nitrogen. To store cells, they were trypsinised as above, then pelleted at 600 *g* for 5 min at room temperature. Cells were resuspended in FCS containing 10% DMSO, before being transferred to 2 ml cryovials (Alpha Laboratories). To freeze aliquots, vials were placed in a polyethylene container (”Mr Frosty”, Merck) that was filled with isopropyl alcohol and incubated at -70 °C, then transferred to liquid nitrogen storage ~1 day later. To retrieve a cell line, aliquots were thawed by placing the cryovial in a 37 °C waterbath, then immediately diluted in ~20 ml culture medium. DMSO was removed by pelleting the cells at 600 *g* for 5 min at room temperature, discarding the supernatant, and resuspending the cells in culture medium.

2.2.2 Virus propagation and purification

All virus handling took place in a microbiological safety cabinet at biosafety containment level 2.

2.2.2.1 Virus propagation

Standard yield propagation An inoculum was prepared containing serum-free DMEM, 1 µg/ml TPCK-treated trypsin and virus at an MOI of 0.3–1 when generating virus for direct analysis, or an MOI of 0.001 when passaging virus to amplify stocks. Culture medium was removed from confluent MDCKs and the cells rinsed twice in 1x PBS. The inoculum was added to the MDCKs, which were then incubated at 37 °C for 1 h with occasional rocking. The inoculum was removed, and the MDCKs incubated in the presence of serum-free DMEM supplemented with 1 µg/ml TPCK-treated trypsin for 24 h when generating virus for direct analysis, or 48 – 72 h when passaging virus to amplify stocks. Virus-containing medium was removed from the MDCKs and clarified by centrifuging at 1800 *g* for 5 min.

High yield propagation When highly concentrated virus was needed for proteomic or electron microscopy analysis, virus was prepared in 2 L roller bottles (Corning) seeded with MDCKs to be confluent at the time of infection and supplemented with 50 ml CO_2. Cells were infected with virus at an MOI of 0.001 in 40 ml serum-free DMEM supplemented with TPCK-treated trypsin and incubated for 72 – 96 h. Virus-containing medium was collected and clarified by centrifuging twice at 1800 *g* for 5 min and discarding the pellet.

2.2.2.2 Purification by density gradient

Table 2.7: Density gradient buffers.

Buffer	Components (diluted in ddH_2O unless otherwise stated)
1 x NTC	1 M NaCl; 0.2 M Tris-HCl pH 7.4; 50 mM $CaCl_2$
x% iodixanol	$(\frac{x}{60} \times 100)$ % OptiPrep, diluted in 1 x NTC

Haemadsorption purification Erythrocytes (final pcv 1%) were washed by two cycles of pelleting at 1250 *g* and resuspending in chilled 1x PBS. Clarified virion samples were mixed with erythrocytes and adsorbed by incubating samples at 4 °C for 30 min, inverting every few minutes to prevent clumping of erythrocytes. Cells were pelleted at 1250 *g* for 10 min, rinsed by resuspending in chilled 1x PBS, and then pelleted again at 1250 *g*. Virions were eluted by resuspending the pellets in prewarmed 1x PBS and incubating for 15 minutes at 37 °C. Cells were pelleted at 1250 *g* for 10 minutes, and the supernatant collected to yield the purified virions.

Concentrating samples Large-scale virion preparations were concentrated by overlaying the samples on a cushion of 10 % iodixanol and pelleting at 116,000 *g* for 90 minutes at 4 °C. Supernatant was carefully removed, and pellets resuspended in 100 µl 1x NTC.

Density gradient separation Eleven evenly spaced dividing lines were drawn on an ultracentrifuge tube (Beckman Coulter) to allow later fractionation. The tube was filled to just under halfway with 20 % iodixanol, then an equal volume of 30 % iodixanol was underlaid using a syringe and a cannula. The tube was capped, and mixed using a gradient maker at an inclination of 80 °, 20 rpm, 2 minutes. Samples were overlaid on the gradient and centrifuged in a Sorvall Discovery ultracentrifuge for 17 h at 21,000 *g* at 4 °C. The gradient was fractionated by puncturing the base of the tube with a 24 G needle and collecting the flowthrough in a 24-well plate, moving to a new well as the meniscus reached each of the dividing lines.

Determining sample density To determine the density of each fraction, density gradients were run in parallel with virus-infected samples, but using 1 x NTC instead of medium from virus-infected cells. After fractionation, the refractive index of each sample was determined with a Atago 3T refractometer and compared with a standard curve of samples of known iodixanol concentrations to determine their density.

2.2.3 Microscopy

2.2.3.1 Confocal microscopy

Where necessary, all reagents were diluted to working concentrations in 1x PBS unless otherwise stated.

Adhering filaments to coverslips 1.3 mm coverslips were placed in a 24-well plate and cleaned by soaking in 500 µl 70 % ethanol (diluted in ddH_2O) for 20 min, before washing twice with 1x PBS. Next, each coverslip was covered with 1 ml 1x PBS. Any wells which did not contain coverslips were also filled with 1 ml 1x PBS to ensure the plate was balanced. Virus samples were pipetted into their respective wells and the plate rocked briefly to mix them into the PBS. Virions were then centrifuged onto the coverslip at 1000 *g*, 4 °C for 30 min in a plate spinner. PBS was carefully removed, and 200 µl 4% formaldehyde added to each well for 15 min. Formaldehyde was then removed and samples were blocked in 1 ml 2% FCS for 1 h. To conserve the α-H3 antibody, coverslips were removed from the plate, inverted and floated on 40 µl drops of diluted antibody pipetted onto a sheet of a parafilm for 1 h. For other antibodies, coverslips were incubated in 200 µl of diluted antibody in the 24-well plate for 1 h. Coverslips were returned to the plate and washed three times in 2% FCS, before applying 200 µl of diluted secondary antibody and incubating for 30 min in the dark. Coverslips were then washed twice in 2% FCS, once in 1x PBS, then briefly immersed in ddH_2O before wicking off excess liquid with a paper towel and mounting on glass slides with 5 µl Prolong Diamond Antifade Mountant. Prepared slides were stored in the dark at room temperature.

Image acquisition Micrographs were collected using a Zeiss 710 confocal microscope, using the 63x oil immersion objective. For Chapters 3 and 4, twelve images were captured per coverslip; to increase throughput, this was reduced to nine images per coverslip in Chapters 5 and 6.

Image analysis Micrographs were analysed with a pipeline of custom scripts (See Appendix A. BatchFilamentAnalysis.ijm was used to count the filamentous objects in a micrograph and determine their lengths and the resulting individual CSV files were combined using CSVcombiner.py to allow further processing. The eccentricity of ellipses fitted to the filaments was assessed using EccentricityAnalysis.ijm, and spherical objects were counted using BatchSphereAnalysis.ijm. Most graphs were plotted using AllFilamentAnalysisPlots.py and the associated functions in FilamentAnalysisFunctions.py, while the major and minor axes of the fitted ellipses were plotted using Major-Minor_Axis_Plots.R.

2.2.3.2 Electron microscopy

Negative staining Formvar carbon-coated copper grids were made hydrophilic by treating in an Emitech K100X glow discharger for 30 s at 50 mA negative charge. 5 µl of sample was pipetted onto a clean sheet of parafilm, and a copper grid floated, carbon-side down, on the droplet for 90 s. The grid was washed by sequentially floating it on three droplets of ddH_2O, before floating it on 5 µl 1% PTA for 90 s. Excess PTA was wicked off using filter paper, and the grid was air-dried before viewing.

Image acquisition Transmission electron micrographs were acquired with a JEOL 1200 Transmission Electron Microscope and a Gatan Orius camera.

Particle counting To determine absolute virion counts, virus samples were mixed with suspended polystyrene latex spheres (TAAB, diameters 0.204 µm) to a final concentration of approximately 6.45 x 10^9 latex spheres per ml, then stained as described above. Virions and beads were counted manually using a JEOL 1200 Transmission Electron Microscope, generally at 25 K magnification so that virions could be distinguished by their fringe of glycoproteins. Every object on a square of the grid was counted, and the ratio of virions to beads calculated. This process was repeated until at least three squares had been counted, and the virion/bead ratio changed by less than 10% with the most recent square. Typically, 50-100 virions were counted per sample.

2.2.4 Virological assays

Where appropriate, all reagents were diluted to their working concentration in 1x PBS unless otherwise stated.

2.2.4.1 Plaque assay

Assay set-up Cells were seeded in 6- or 12-well plates at the densities indicated in Table 2.8, 24 h before performing the assay. To titrate the virus, samples were diluted in serum-free DMEM supplemented with 1 µg/ml TPCK-trypsin in a ten-fold dilution series, mixing thoroughly between each dilution. Medium was removed from the plated cells and the cells were washed twice in 1 x PBS before overlaying with the diluted virus samples. Plates were incubated at 37 °C for 1 h, rocking the plate every 15 min. The medium was then removed, and the wells overlaid with low-melt agarose diluted to a final concentration of 1% in serum-free DMEM, supplemented with 1 µg/ml TPCK-trypsin. Plates were incubated for 30 min at room temperature to allow the agarose to set, then inverted and incubated at 37 °C for 48 h.

Table 2.8: Plaque assay seeding densities.

Plate	MDCK seeding density (12-well plate)
6-well	1×10^6
12-well	5×10^5

Coomassie Staining Agarose was removed and the cells fixed and stained with Coomassie Blue Fixing Solution to facilitate plaque counting. The well with the highest number of clearly distinct plaques was used to calculate the plaque-forming units in the initial sample.

2.2.4.2 Semi-infectious particle assay

Plaque assay Plaque assays were performed as described above, but were incubated after applying the agarose overlay for 24 h rather than 48 h and immunostained rather than Coomassie stained.

Immunostaining Agarose was removed and cells were fixed in 2% formaldehyde for 15 min, before being permeabilised in 0.1% Triton X-100 for 8 min. Cells were blocked in 2% FCS for 1 h before staining with a primary antibody diluted in 2% FCS to the working concentrations listed in Table 2.5 for 1 h. Cells were washed three times in 2% FCS, then counter-stained with Alexa-Fluor 488 secondary antibody for 30 min in the dark. Cells were washed twice with 2% FCS, once with 1x PBS then stored in the dark at 4 °C until imaging.

Image analysis Plates were imaged using the Celigo Imaging Cytometer (Nexcelcom).

2.2.4.3 Mucus inhibition assay

Mucus generation Mucus samples were kindly prepared by Joanna Wojtus (MRC-University of Glasgow Centre for Virus Research) as a by-product of her own PhD project. Briefly, a human airway epithelial culture was generated from human airway epithelial cells of bronchial origin (Epithelix, Batch No. 02AB0793.01 – Male, 62, Hispanic). Cells were grown to confluency on 6.5 mm Transwell Plates with 0.4 µm Pore Inserts in Human Airway Epithelial Cell (hAEC) medium (Epithelix). Once confluent, medium was aspirated from the apical chamber and the medium in the basal chamber replaced by Pneumacult-ALI medium every two days. After two weeks to allow differentiation, mucus was removed from the epithelium twice a week by adding 200 µl 1X PBS and incubating for 30 min at 37 °C. Liquid was removed by gently pipetting up and down to dislodge the mucus and stored as 1 ml aliquots at -70 °C.

Assay set-up Mucus was initially diluted 2:3 in DMEM to generate enough working stock for plaque assays. Three, six-fold, dilution series of working mucus stock in serum-free DMEM were performed for each virus sample to be assessed. Three-fold dilution series of virus sample were performed in each of the mucus dilutions, plus a no mucus control. From here, plaque assays were performed as described above for standard plaque assays, but initially incubated for 30 min instead of 60 min.

2.2.4.4 Haemagglutination assay

Assay set-up 50 µl 1x PBS was added to wells 2-12 of a U-bottomed 96-well plate. Virus samples were diluted 1 in 10 in 1x PBS and 100 µl added to well 1 of the plate. Samples were serially diluted down the wells, pipetting 50 µl at a time and removing 50 µl from the final well to ensure even volumes. 50 µl 0.5% pcv chicken red blood cells were added to each well and incubated for approximately 30 min at room temperature. HA titre was calculated as the reciprocal of the last dilution to show full agglutination of red blood cells.

2.2.4.5 Neuraminidase assay

Assay set-up For each sample, a two-fold dilution series was prepared by mixing the sample with 1x PBS in a 96-well plate, for a total of five dilutions and one neat sample of 50 µl each. In parallel, a dilution series was prepared, beginning with 1 neuraminidase unit (NAU) of neuraminidase from *Clostridium perfringens* (Fisher Scientific). Neuraminidase activity was measured using an Amplex Red Neuraminidase Assay Kit (ThermoFisher Scientific) per the manufacturer's instructions, with samples being incubated with the reaction mix for 30 minutes and then the absorbance at 560 nm (A560) of each well was measured using a Pherastar FS microplate reader (BMG Labtech). The known concentrations of NAU from *Clostridium perfringens* were used to plot a standard A560 curve. For each sample, the A560 value that was most clearly within the linear range of the standard curve was selected, and the dilution of that sample was used to infer the NAU present in the undiluted sample.

2.2.5 Protein assessment

2.2.5.1 Western blot

Table 2.9: Western blot buffers.

Buffer	Components (diluted in ddH_2O unless otherwise stated)
1x Loading Dye	50mM Tris HCl pH 6.8; 0.4% SDS; 10% Glycerol; sufficient Bromophenol Blue; 0.02% DTT (added immediately before sample digest)
1x RunBlue Running Buffer	20 mM Tricine; 30 mM Tris; 0.5% SDS
1x Transfer Buffer	25 mM Tris; 192 mM Glycine; 20% methanol
PBST	0.001% TWEEN-20 (diluted in 1x PBS)
Blocking buffer	5% skimmed milk (diluted in PBST)

Preparing membranes Samples were denatured in 1x loading dye at 100 °C for 5 min, then incubated on ice for 2 min. Denatured samples were loaded onto a 10% RunBlue polyacrylamide gel in a Bio-Rad Mini-PROTEAN Tetra Vertical Electrophoresis Cell. 1 µl PageRuler Prestained Protein Ladder was added to a parallel well to aid in identifying proteins. Electrophoresis was carried out at 120 V for approximately 80 min, until the dye front reached the bottom of the gel. Protein was transferred to a nitrocellulose membrane using a Bio-Rad Mini Trans-Blot Electrophoretic Transfer Cell, submerged in 1x Transfer Buffer and run at 100 V for 60 min. Membranes were blocked in blocking buffer for 1 h at room temperature or overnight at 4 °C, then stained with primary antibodies at the concentrations listed in Table 2.5 diluted in blocking buffer. Membranes were washed three times in PBST, then incubated with secondary antibodies at the concentrations indicated in Table 2.6, diluted in blocking buffer. Membranes were washed twice in PBST, and once in ddH_2O before imaging.

Imaging Membranes were imaged using the Li-Cor Odyssey Clx. Band intensities were calculated using the Analysis tools in Image Studio Lite Ver 5.2.

2.2.5.2 Mass spectrometry

Table 2.10: Mass spectrometry buffers.

Buffer	Components (diluted in ddH_2O unless otherwise stated) All reagents MS grade and stored separately from other reagents
Urea Lysis Buffer	8 M Urea (Sigma); 100 mM TEAB (Thermo Scientific); 0.5% Sodium Deoxycholate (Sigma); 1x Mini Complete Protease Inhibitor (Sigma)
Urea Dilution Buffer	7.2 M Urea; 100 mM TEAB; 1x Mini Complete Protease Inhibitor (Sigma)
Loading Buffer	5% formic acid (Sigma); 5% DMSO (Sigma)

Sample digests Samples were denatured in Urea Lysis Buffer for 30 min at room temperature. Protein concentration was determined via Bradford Assay (see below), and samples diluted in Urea Dilution Buffer so that each sample contained 20 µg of protein and had the same volume. Samples were reduced with a final concentration on 10 mM TCEP for 30 min at room temperature, then alkylated with a final concentration of 50 mM C-AA for 30 min at room temperature in the dark. Samples were diluted to 6 M urea by adding 50 mM TEAB, then incubated with 0.5 µg LysC for 4 h at 37 °C. Samples were then diluted to 1.5 M urea by adding 50 mM TEAB, and 0.02 µg of trypsin was added to each before incubating overnight at 37 °C. Samples were then stored at -70 °C before being shipped on dry ice to the Target Discovery Institute, University of Oxford for mass spectrometry analysis.

Mass Spectrometry Liquid chromotography and tandem mass spectrometry was performed by Svenja Hester (Target Discovery Institute, University of Oxford) as described in Hutchinson et al. (2014). Briefly, peptides were harvested by spinning them through a 10 kDa filter, and the flow-through retained. Further peptides were washed off the filter with 0.1% formic acid and retained. Remaining peptides were washed off the filter with 0.1% formic acid in 50% acetonitrite and retained. The flow-through from each of the preceding steps was pooled, and samples were dried in a vacuum centrifuge.

Samples were reconstituted in loading buffer and added to a V-bottom 96-well plate. The plate was loaded into a Dionex UltiMate 3000 autosampler and samples were injected. Peptides were desalted on-line by a trap column, separated on an analytical C18 reversed-phase capillary column (flow rate, 200 nL/min; gradient, 7–30% (v/v) mobile phase B over 60 min; column temperature, 45 °C) and analysed by an Q Exactive Hybrid Quadrupole-Orbitrap Mass Spectrometer.

Data analysis. To determine protein abundances, data were analysed using MaxQuant, using the Udorn proteome and a modified *Canis familiaris* proteome (all ubiquitinated proteins were removed except ubiquitin itself) obtained from UniProt. To identify PTMs, data were analysed using PEAKS, using the same proteomes.

Bradford Assay A two-fold dilution series of BSA (New England Biolabs) was prepared in 1x PBS, ranging from 1 mg/ml to 0.0625 mg/ml. 10 µl of each sample and 10 µl of each BSA dilution was pipetted in duplicate into a 96-well plate. Bio-Rad Protein Assay Dye Reagent was diluted 1:4 in ddH_2O and filtered three times through 0.22 µm syringe filters to remove impurities. 200 µl of dye solution was added to each well of the plate and mixed, then incubated for five minutes. Absorbance at 595 nm was measured using a Pherastar FS microplate reader (BMG Labtech), and the BSA dilution series used to plot a standard curve from which the sample protein concentrations could be interpolated.

Chapter 3

Measuring the concentration and lengths of filamentous virions

3.1 Introduction

3.1.1 The criteria for assessing filamentous virions

I aimed to characterise the stability, composition, and function of filamentous influenza virions, which all depended on a method to efficiently assess virion morphology. This method would allow me to confirm that filamentous virions were present and undamaged in a sample, increasing my confidence that they are contributing to the functional and compositional characteristics of a given virion population. To achieve this, the method I would use to assess filamentous virion populations had to meet the following four criteria:

1. The method must detect unconcentrated filamentous virions that have been released from cells, in a manner that enables their concentration and physical dimensions to be measured.

   This criterion is necessary as experiments characterising filamentous virions require confirmation that filamentous virions are indeed present. The method must be able to detect unconcentrated virions, as it was unclear whether procedures to concentrate virions, such as ultracentrifugation, would cause damage. The virions must have been released from cells, I aimed to characterise the properties of the virions themselves in future work and this would not have been possible in samples containing large amounts of host cell material. The method must also be able to measure the lengths of filamentous virions, as these vary enormously both within and between strains (Dadonaite et al., 2016) and this variation should be accounted for when assessing their properties.

2. Analysing samples must be resource- and time-efficient.

   I aimed to use this method as routine early step when characterising virions. If it were laborious or expensive enough to become a rate-limiting step, it would limit the range of characterisations that could be performed. An efficient method is also more likely to be adopted by other researchers, which would make it easier to compare different studies.

3. The method must be reproducible.

   As this method will primarily be used to ensure consistency between experiments, it must itself be consistent to be useful.

4. The method must detect changes in the characteristics of filamentous virion samples.

   It is possible that a characterisation pipeline could contain steps which become saturated or bottlenecked, so the measured concentration of a sample may not reflect the true concentration. As this could lead to misleading results, it is necessary to show that the method I use to measure virion concentration can accurately detect changes to that concentration.

These four criteria could only be met by a method to assess the physical dimensions of filamentous virions. The relationship between the functional properties of influenza virions and their physical dimensions is unknown, so the physical dimensions had to be measured directly rather than inferred from a sample's functional properties. The most straightforward method to achieve this, which is therefore likely to be the most efficient, is directly assessing the virions through microscopy.

3.1.2 The suitability of electron microscopy

The most popular method to assess the dimensions of filamentous virions has been electron microscopy: most commonly using positive staining (Chu et al., 1949; Donald & Isaacs, 1954b; Morgan et al., 1956) or negative staining (Archetti, 1955; Horne et al., 1960; Roberts et al., 2013), but with recent studies employing cryo-electron microscopy (Calder et al., 2010; Vijayakrishnan et al., 2013; Peukes et al., 2020). Electron microscopy can readily image filamentous virions, but typically requires a concentrated sample (noted in Seladi-Schulman et al. (2014)), and so it does not meet the first criterion for a suitable analysis method. Even if this issue could be avoided, it has been noted that longer filamentous virions are visible when virions are adsorbed to red blood cell ghosts than when adsorbed directly to electron microscopy grids (Donald & Isaacs, 1954b), suggesting this method could bias against longer virions and give an inaccurate representation of the population. Electron microscopy also requires specialised expertise and equipment that are not widely available, and so does not meet the second criterion. Together, these issues suggested that electron microscopy would not be suitable for the type of analysis I required to measure the concentrations and lengths of filamentous virions.

3.1.3 The suitability of fluorescence microscopy

Electron microscopy is usually favoured for directly imaging influenza virions, as the typical spherical virion diameter of 100 nm is below the resolution limit for conventional fluorescence microscopy of ~300 nm (Wilson, 2016). However, filamentous influenza virions are usually defined as having lengths greater than 500 nm and frequently reach several microns in length (Dadonaite et al., 2016), and so can be resolved by light microscopy. Fluorescence microscopy may therefore be a suitable method to characterise filamentous virion populations.

While most fluorescence microscopy approaches have been used to analyse cell-associated virions, recently Vahey & Fletcher (2019b) demonstrated that confocal microscopy can be used to reproducibly visualise, and assess the dimensions of, filamentous virions that have been adsorbed onto a coverslip. The study demonstrated how the size of influenza virions varied under different growth conditions, and therefore that this method could detect changes to a virion population. Together, these findings showed how this approach could meet criteria 1, 3, and 4 from the list above. However, this study used an extensively modified virus and labelled the virions with bespoke reagents, making it difficult to reproduce. This meant this method would have to be adapted to meet the second criterion.

While a fluorescence microscopy method meeting all four criteria for influenza virions had yet to be demonstrated, a similar method for visualising filamentous respiratory syncytial virions has been described (Alonas et al., 2016). As with Vahey and Fletcher, this method adsorbed filamentous virions to a coverslip, but used an unmodified form of the virus and labelled it with an antibody. This makes the method cheaper and more efficient, and so capable of fulfilling the four criteria necessary to analyse filamentous virions. However, this approach had not been applied to filamentous influenza virions and lacked options for high-throughput analysis.

3.1.4 Conclusion

Taken together, past studies indicated that an analysis pipeline based on fluorescent confocal microscopy could be suitable for quickly and easily counting, and measuring the lengths of, filamentous virions. Here, I describe such a method and test it against each of the necessary criteria to demonstrate its suitability for further investigations into the stability, composition, and functional properties of filamentous influenza virions.

3.2 Results

3.2.1 Visualising filamentous virions

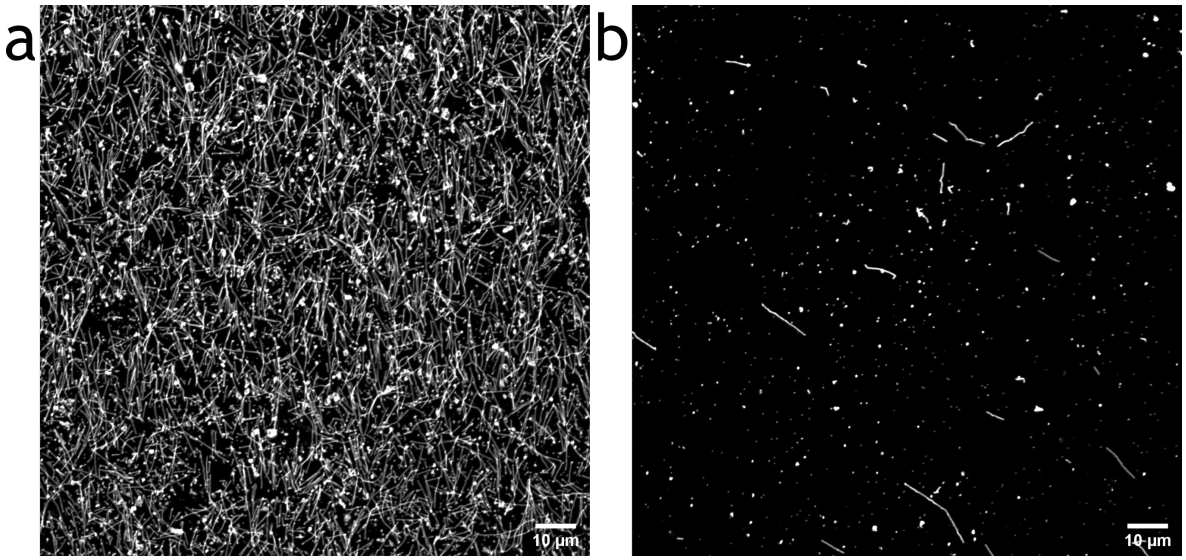

Figure 3.1: Filamentous influenza virions can be imaged by fluorescence microscopy. Filamentous influenza virions were obtained by collecting supernatant from MDCK cells infected with influenza A/Udorn/307/72 (H3N2) for 24 h, which were then adsorbed to glass coverslips. (a) To identify filamentous virions, coverslips were immunostained for haemagglutinin and images were collected by confocal microscopy (63x magnification, scale bar 10 µm). (b) To distinguish individual filamentous virions, samples were prepared as in (a) but diluted 100-fold before analysis.

To produce a sample of filamentous virions to visualise, I infected Madin-Darby Canine Kidney (MDCK) cells with influenza A/Udorn/307/72 (H3N2) (Udorn) at an MOI of 1 for 24 hours. Udorn is laboratory-adapted and easy to handle and has retained a pleiomorphic phenotype (Roberts et al., 1998), making it ideal for this study.

To image the virions, I first overlaid samples onto glass coverslips in a 24-well plate and centrifuged the virions onto the coverslip using a plate spinner (adapting a protocol described by Alonas et al. (2016)) for respiratory syncytial virus). While similar procedures generally treat the coverslip to enhance its adhesive properties, filamentous influenza virions have been described to stick readily to glass (Burnet & Lind, 1957) and so I assumed this step was unnecessary. Adsorbed virions were fixed with 4% formaldehyde, labelled with an anti-haemagglutinin (HA) primary antibody, then a fluorescently tagged secondary antibody, and imaged on a confocal microscope. In this way, all material which contained HA (hereafter HA+ material) was made visible, and elongated filamentous particles could clearly be seen (Figure 3.1). While it is possible that some HA+ cell debris had the same elongated shape as a filamentous virion, I assumed that this was unlikely as this shape is presumably energetically unfavourable without some kind of underlying scaffold. Even with an unconcentrated sample, the micrograph contained too many virions for them to

be easily distinguished (Figure 3.1a), but a diluted sample clearly delineated the virions (Figure 3.1b). Subsequent infectivity titrations (see section 4.2.6) with similarly prepared samples suggested that the infectious titre for these samples was between 10^4 and 10^7, suggesting that the preparation did not yield an unusually high concentration of virions. Confocal microscopy, therefore, does not share the same requirement as electron microscopy for highly concentrated samples.

By taking account of the acquisition settings of the microscope, the length of the particles in pixels could be converted into a length in micrometres. This means that the length of filamentous virions can be determined crudely by comparing them with a scale bar, or more efficiently and accurately by using the "Measure" or "Ridge Detection" tools in FIJI (Schindelin et al., 2012; Wagner et al., 2017). This means that this method can measure the lengths of filamentous virions as well as simply visualising them.

As well as filamentous virions, small, apparently circular particles were visible in the micrographs (Figure 3.1b). The resolution limit in these micrographs appeared to be ~400 nm (the filamentous virions had apparent widths of 400 nm, despite past electron microscopy data suggesting they should have widths of ~80 nm (Calder et al., 2010; Vijayakrishnan et al., 2013)). This meant the shape of any objects smaller than 400 nm in both axes could not be resolved and it was not possible to determine which were HA+ cell debris, and which were non-filamentous virions. However, it is reasonable to assume that at least some of these particles were virions, and so imaging influenza virion populations in this manner can at least give an indication of the abundance of the non-filamentous virions.

This method to visualise filamentous virions in this way has limitations. As noted above, the length of the long axis of filaments exceeds the ~400 nm resolution limit of the microscope but the length of the short axis does not. To be confident a particle was a filamentous virion, I excluded particles where the axial ratio was lower than 3, as particles below this limit could more easily be large pieces of amorphous cell debris. Consequently, any filamentous virions shorter than ~1.5 μm would not be detected by this method. While the definition of a filamentous virion is somewhat arbitrary, previous studies usually defined their minimum length at ~300 – 500 nm (Dadonaite et al., 2016), so the subclass of filamentous virions between 500 nm and 1.5 μm would not be detected by this method. A similar problem affects the analysis of non-filamentous virions, all of which are smaller than the resolution limit of the microscope and so it cannot be easily determined which small particles are virions. It is still possible to estimate the abundance of non-filamentous virions by assuming that the proportion of cell debris is equivalent in every sample, and so the abundance of small, spherical objects will directly scale with the abundance of non-filamentous virions. This allows comparisons to be made between similarly prepared samples, but can only be treated as suggestive. Analysing virions with confocal microscopy also means that absolute virion concentrations cannot be calculated. Absolute concentrations can be calculated using electron microscopy, by mixing the virion with a known concentration of mark-

ers and comparing the ratio of virions to markers to infer the virion concentration. It is not known if a marker exists that adheres to glass similarly to filamentous influenza virions, so calculating absolute concentrations of filamentous virions with confocal microscopy is not yet possible. Similarly, it is not clear whether all virions adhere to glass with equal efficiency, which could lead to a skewed assessment of their properties if, for example, adhesion varies with length. These issues affect all quantitative analysis by microscopy to some degree, and they can be circumvented by making reasonable assumptions about the samples. It can be assumed that undetectable filamentous virions have similar properties to the shortest detectable filamentous virions, and any systematic errors in measuring concentration can be mitigated by performing experiments based on relative, rather than absolute, measurements.

Taken together, this result demonstrates that this method can detect unconcentrated, free filamentous virions in a manner that enables their concentration and lengths to be measured. Therefore, this method meets the first of the four necessary criteria.

3.2.2 Automated micrograph analysis

The speed and reproducibility of an analysis pipeline can be substantially improved by automating it. HA is specifically labelled in the micrographs generated by this method, so micrograph analysis is easily automatable as any elongated object visible can be assumed to be a filamentous virion. Furthermore, labelling in these micrographs is only necessary to show the location and the dimensions of the virions and so the intensity of the labelling does not have to be preserved during data analysis. This means the micrographs can be converted to binary images, which are simple to assess and analyse computationally.

To automate analysis of the micrographs, I wrote an ImageJ macro to implement the Ridge Detection algorithm (Wagner et al., 2017), which detects all curvilinear structures in an image and allows their dimensions to be extracted (Figure 3.2a). This macro automatically moves through all micrographs in a folder as follows:

```
\\BatchFilamentAnalysis.ijm
   ...
   //The micrograph, in the form of a czi file, is opened
   open(input + File.separator + file);

   //The micrograph is thresholded to yield a binary image, which is
      necessary for the subsequent particle removal step
   setAutoThreshold("Default dark");
   run("Convert to Mask");

   //Circular particles are removed to reduce the risk of ring-shaped debris
      being classed as a filament
```

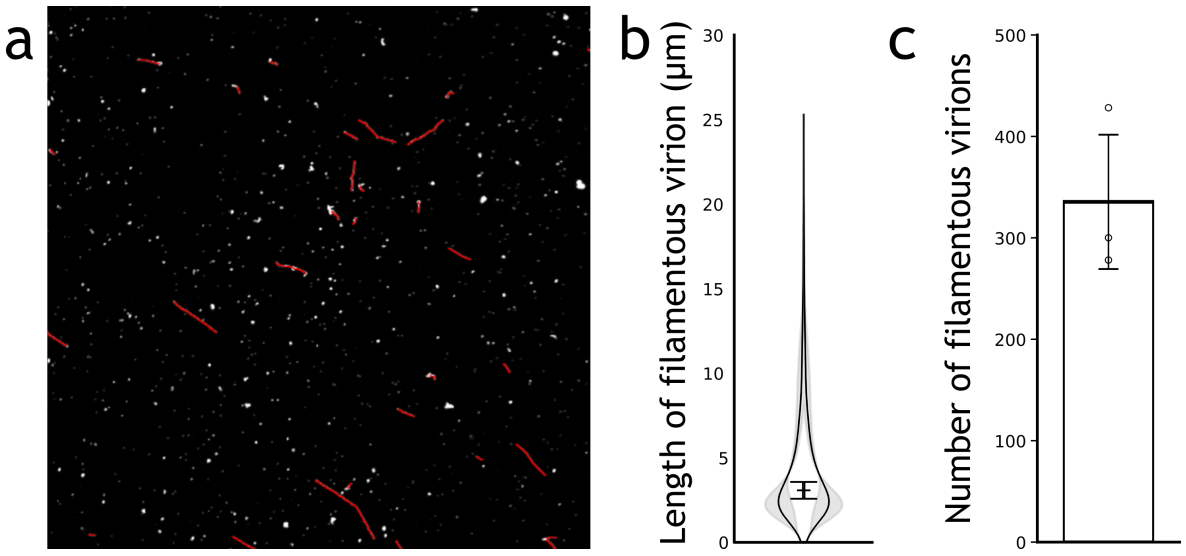

Figure 3.2: Filamentous virions concentration and length can be extracted automatically. Filamentous influenza virions were obtained by collecting supernatant from MDCK cells infected with influenza A/Udorn/307/72 (H3N2) for 24 h, which were then adsorbed to glass coverslips. To identify filamentous virions, coverslips were immunostained for haemagglutinin and images were collected by confocal microscopy (63x magnification). (a) A Ridge Detection algorithm was used to identify and measure filaments, highlighted in red. (b) A frequency distribution of filament length was calculated for an example sample. The violin plot indicates the mean frequency distribution, with the 95% CI of the distribution shaded in grey. The median filamentous virion length was also calculated for each repeat, with the mean and s.d. of these median lengths across different experiments indicated by a line and whiskers (three independent experiments). The number of filamentous virions was calculated for an example sample. Column indicates mean, whiskers indicate s.d. (three independent experiments).

```
run("Colors...", "foreground=black background=black selection=yellow");
run("Particle Remover", " circularity=0.50-1.00 include");

//The Ridge Detection algorithm is used to detect all curvilinear
    structures in the micrograph, which can be assumed to be filamentous
    virions. Algorithm parameters were determined empirically
run("Set Scale...", "distance=4.6267 known=0.45 pixel=1 unit=micron");
run("Ridge Detection", "line_width=5 high_contrast=230 low_contrast=87
    extend_line displayresults method_for_overlap_resolution=NONE sigma=2
    lower_threshold=3.06 upper_threshold=7.99 minimum_line_length=15
    maximum=0");

//The Ridge Detection output is saved as a csv file
selectWindow("Summary");
saveAs("Results", input + File.separator + getCleanTitle(file) + ".csv");
...
```

This produces a csv file for each field of view. I combined the csv files for each field of view per coverslip using a custom Python script (CSVCombiner.py). I then used a further custom Python script (FilamentAnalysisPlots.py) to generate summary graphs for each sample. These scripts generate violin plots, showing the distribution of filament lengths within a population and its 95% confidence interval for any number of repeats (Figure 3.2b), and bar charts, showing the number of filamentous virions detected in each sample (Figure 3.2c). This process takes a few seconds per micrograph, so, once the micrographs are captured, an entire experiment can be analysed in minutes. Furthermore, any changes to the analysis pipeline can be retroactively applied to an entire project in minutes, allowing a flexible approach to investigating filamentous virions which can be adapted in response to new findings.

Analysing samples in this way increases throughput and reduces the impact of human bias, but it is not infallible. Aberrant structures such as dirt or clumps of filamentous virions can be misinterpreted by the algorithm. While these issues vary, typically they result in the algorithm reporting many tiny filamentous virions. These problems are clearly visible to the human eye when analysing micrographs and can be solved by manually inspecting micrographs if the algorithm suggests a very unusual virion population. This issue does slow down throughput, but these problems rarely affected more than one or two fields of view per experiment, so the overall workload is still well below that of performing the entire analysis manually.

In conclusion, automation using open-source software means the data analysis stage of the pipeline is rapid, cheap, and inherently reproducible, meaning it clearly meets the four criteria I require to analyse filamentous virion populations.

3.2.3 Accounting for the uneven distributions of virions

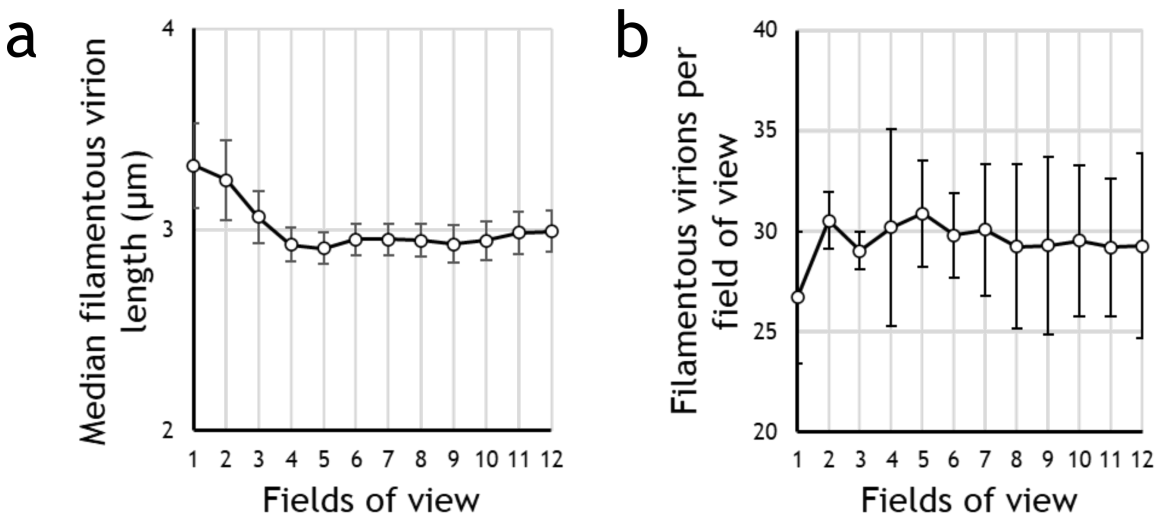

Figure 3.3: Six fields of view per micrograph are necessary for consistent results. Filamentous influenza virions were obtained by collecting supernatant from MDCK cells infected with influenza A/Udorn/307/72 (H3N2) for 24 h, which were then adsorbed to glass coverslips. To identify filamentous virions, coverslips were immunostained for haemagglutinin and images were collected by confocal microscopy. A Ridge Detection algorithm was used to identify and measure filaments. (a) Median filament length was calculated using increasing numbers of fields of view from the same micrograph. Points show mean, whiskers show s.d. (three independent experiments). (b) The number of filamentous virions per field of view was calculated using increasing numbers of fields of view from the same micrograph. Points show mean, whiskers show s.d. (three independent experiments).

While taking micrographs, I noted the distribution of virions across the coverslip was not always even. This suggested that multiple fields of view would be necessary to generate a robust representation of the filamentous virion population. It was therefore necessary to calculate the minimum number of micrographs that ensured the measured population was representative.

To do this, I first generated twelve micrographs per coverslip for three identically prepared samples. I analysed the concentration and median length of the filamentous virions, first using only one field of view, then repeating the analysis eleven times with a further field of view added each time. For both concentration (Figure 3.3a) and median filamentous virion length (Figure 3.3b), the measured value appeared to stabilise after approximately six fields of view, suggesting this was the minimum necessary to acquire consistent measurements.

While the analysis appeared stable after six fields of view were captured, it seemed plausible that experiments using less concentrated samples could require more images to reach a representative threshold. To mitigate this problem, all subsequent experiments used at least nine fields of view per coverslip.

In conclusion, these data further demonstrated that the data acquisition stage of the analysis pipeline gives reliable results without requiring an impractical number of micrographs. This method therefore meets the second required criterion: to be resource efficient.

3.2.4 The reproducibility of sample preparation

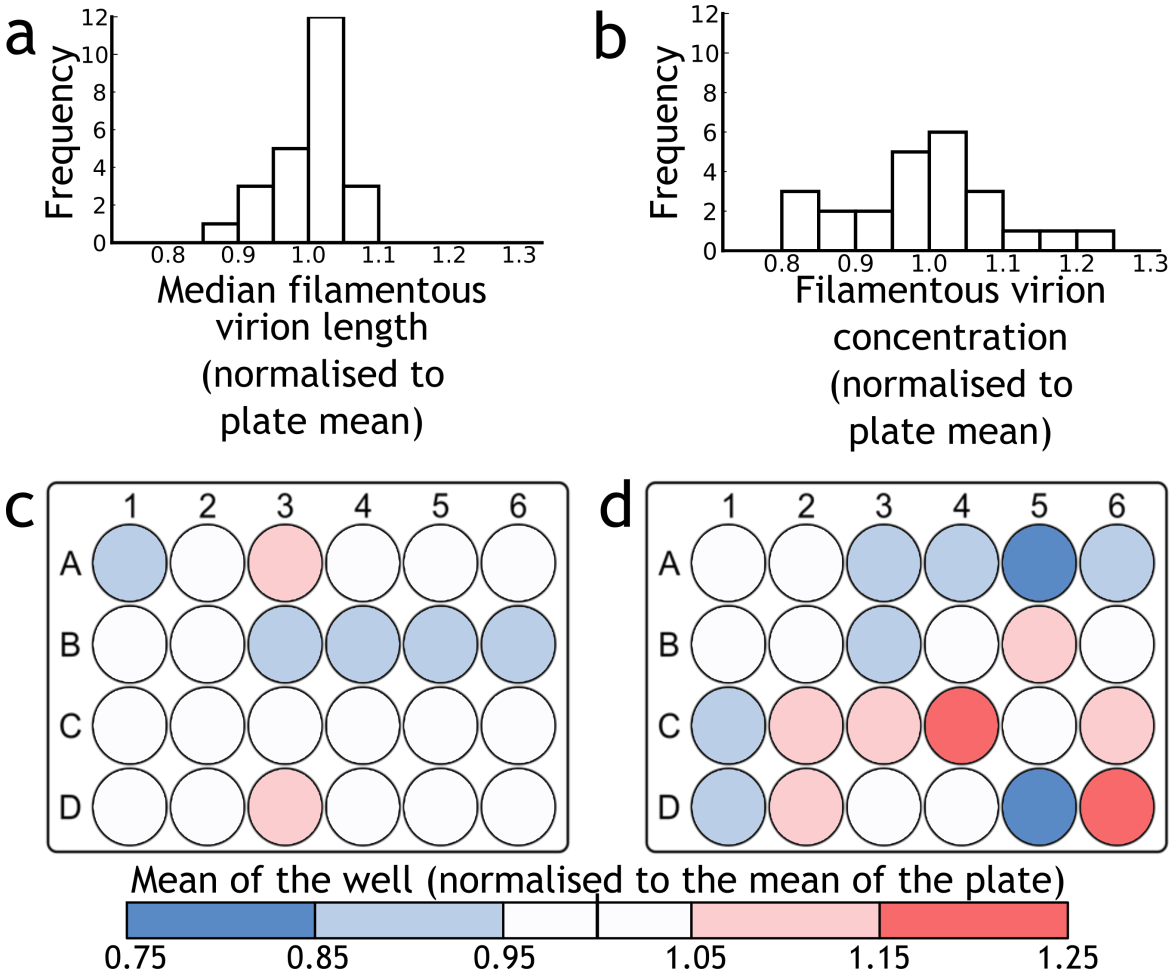

Figure 3.4: The confocal analysis pipeline gives reproducible results.

To assess the reproducibility of the analysis pipeline, populations of filamentous virions from the same preparation were divided into each well of 24-well plates. Measurements of length and concentration were taken from each well, and the mean for each of the 24 positions in the plate was calculated and then normalised to the total (three independent experiments). Mean values for each position are shown of (a) median filament length within a well and (b) filament concentration per well. (c, d) To assess whether the position of the sample within the 24-well plate affected the analysis, the data from (a) and (b) were plotted relative to their positions in the plate, for (c) median lengths and (d) concentration. Red wells indicate values above the plate mean, and blue wells indicate values below the plate mean, with shading intensity correlating with the degree of divergence.

Having demonstrated that the data acquisition and analysis stages of the pipeline could give reliable results, I then needed to ensure that the process of preparing coverslips did not introduce random variation that would skew the final analysis. There are many steps in cov-

erslip preparation that could unpredictably alter the virion population, such as changing buffers with enough force to dislodge virions from the coverslip or through uneven centrifugal forces affecting filament adsorption depending on their position in the plate spinner.

To ensure reproducibility of the sample preparation process, I prepared 24 coverslips from the same sample of virions (one for each well of the 24-well plate) and analysed the concentration and median length of the filamentous virions as described above. I performed three independent repeats of this experiment. To assess the variance in filamentous virion concentration, I calculated the mean concentration of the three repeats for each well, and expressed the mean for each well as a proportion of the mean for the whole plate. The standard deviation for wells from the overall plate mean was 0.05 (Figure 3.4a). To assess the variance in filamentous virion length, for each well I calculated the mean of the median filamentous virion lengths from each of the three repeats. For each well, I expressed this mean as a proportion of the mean for the whole plate. The standard deviation for wells from the overall plate mean was 0.1 (Figure 3.4b).

These results suggested that sample preparation does not introduce much variability into the final analysis, though changes smaller than 10% in the concentration or median length of filaments might be challenging to detect. Furthermore, the variation in concentration and median length of each sample bore no relation to the position of the sample within the 24-well plate used when centrifuging samples onto coverslips (Figure 3.4c and d), suggesting the analysis pipeline is free from artefacts such as edge effects.

These data, when combined with the findings on the reliability of data analysis and acquisition, showed that the entire analysis pipeline gives reproducible results, meeting the third criterion for filamentous virion population analysis.

3.2.5 The dynamic range of the analysis pipeline

Having shown the analysis pipeline gave reproducible results, it was then necessary to ensure it could quantify changes in virion concentration. I therefore tested whether it could detect predictable alterations to a filamentous virion population.

To alter the filamentous virion concentration, I diluted a sample of Udorn by 50% and 75% in 1x PBS. I then measured the concentration and median lengths of the filamentous virions as previously described. The measured change in virion concentration closely matched the predicted change (Figure 3.5a), suggesting the analysis pipeline could both accurately and reliably detect changes in concentration over at least a fourfold range. There is no reason to expect dilution to affect virion length, and indeed the distribution of filamentous virion lengths for all samples was equivalent (Figure 3.5b).

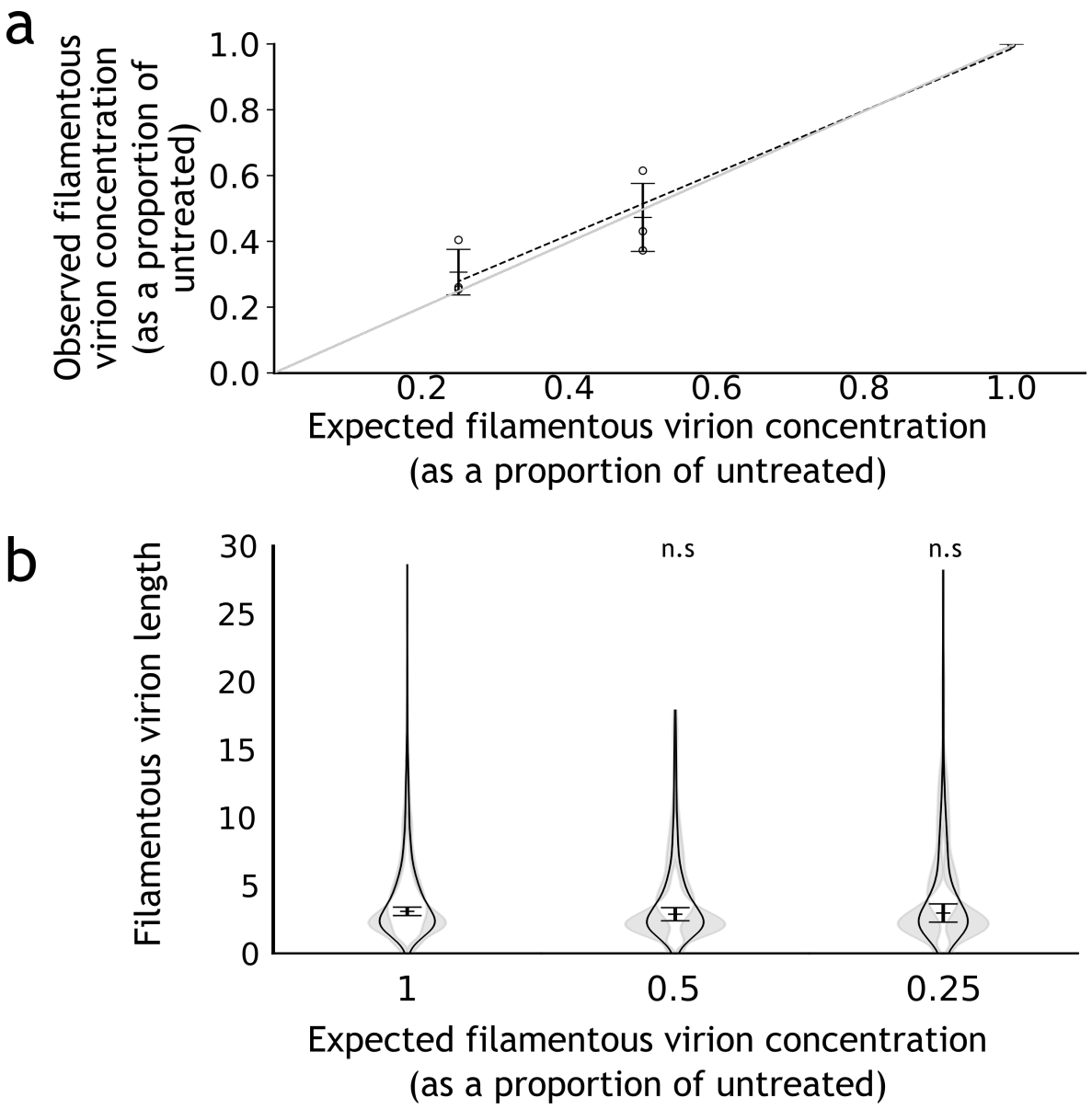

Figure 3.5: Changes in concentration can be detected over at least a fourfold range. To assess sensitivity, filamentous virions were diluted in PBS prior to analysis. (a) Means and s.d. of filamentous virion concentration are shown of 3 experiments, normalised to undiluted. Concentrations were compared to undiluted with two-tailed single-sample t-tests, * $p < 0.05$, ** $p < 0.01$. A polynomial trend line was fitted by the least squares method. Light grey guideline indicates expected values exactly matching measured values. (b) Frequency distributions of filament lengths were calculated for each sample. Violin plots indicate the mean frequency distribution, with the 95% CI shaded in grey. The median filament length was also calculated for each repeat; the means and s.d. of these median positions are indicated by lines and whiskers (three independent experiments). Population medians were compared to the undiluted sample with two-tailed Student's t-tests; n.s $p > 0.05$.

While it was possible to deliberately alter virion concentration, it was not possible to predictably alter filamentous virion lengths to test the analysis pipeline. This may be feasible by using a filter of a known pore size, but it was not obvious what the predicted result should be. For example, long filamentous virions may be able to pass through a small pore while coiled, and so if these particles were detected it would be unclear if the analysis pipeline was failing or if filters were unable to change the distribution of filamentous virion lengths. I could not therefore exclude the possibility that this analysis pipeline does not detect changes in filamentous virion length, though there was also no evidence suggesting this problem was likely to occur.

In conclusion, it is not possible to state definitively whether the analysis pipeline can detect changes in filamentous virion length, but it can accurately detect at least fourfold changes in filamentous virion concentration. As detecting changes in concentration was my main concern for this criterion, the pipeline therefore meets the fourth criterion for establishing a suitable method to analyse filamentous virion populations.

3.3 Discussion

3.3.1 Assessing virion populations with a confocal analysis pipeline

Taken together, my results indicate that this confocal analysis pipeline meets the four criteria I deemed necessary for characterising filamentous virions prior to investigating their stability, composition, and function. Using well-characterised samples in this way will make the experiments much more robust, and allow them to be readily comparable to studies from other researchers. The pipeline is resource-efficient to the extent that it will rarely be rate-limiting, meaning experimental design will not have to be compromised to accommodate the extra workload of validating the samples. The pipeline does, however, have some limitations and these must be considered when choosing which experimental questions it can be used to answer.

3.3.2 The analysis pipeline is suitable for studies of filamentous virion stability

Testing the stability of filamentous virions during laboratory handling procedures involves analysing a sample before and after a procedure and measuring the difference. The confocal analysis pipeline is well suited to this task, as all measurements will be normalised to an untreated standard, and so calculating absolute virion concentrations is unnecessary. However, the pipeline does depend on filamentous virions sticking to the glass coverslip,

and so experimental conditions that alter the adhesive properties of virions will be indistinguishable from those that destroy them. It is difficult to see how mechanical handling techniques, such as liquid transfer or vortexing, could affect virion adhesion, but it could be affected by chemical alterations, such as those that affect pH. Consequently, an alternate method would have to be found in the case of studying chemical alterations to virions, but the confocal analysis pipeline is well-suited to test common physical stressors to filamentous virion populations.

3.3.3 The analysis pipeline is suitable for studies of filamentous virion composition and function

Comparing filamentous and non-filamentous virion composition can be performed based on two underlying principles: assessing individual virions (e.g. by microscopy) or assessing bulk populations (e.g. by western blot). The confocal analysis pipeline can be used to support both approaches.

Assessing bulk populations requires a method to enrich samples for filamentous or non-filamentous virions. While such methods have been described (e.g. Roberts et al. (1998); Smirnov et al. (1991)), they are challenging to replicate (noted in Kordyukova et al. (2020)) and often use ultracentrifugation with sucrose gradients which could cause osmotic damage (Smirnov et al., 1991). A new method of enrichment is therefore necessary to assess the composition of bulk populations. Methods development is typically an iterative process, and will require many virion population analyses to determine how effectively a sample has been enriched. This would have been extremely time-consuming with electron microscopy, but the confocal analysis pipeline makes it possible to move through these iterations quickly. The enrichment method would still need to be verified using electron microscopy, as confocal microscopy cannot reliably measure the concentration of non-filamentous virions, but this could take place after performing the optimisation and would therefore be much less time-consuming. Bulk population analysis may also be challenging to interpret, as the size of filamentous virions means they will have a higher absolute protein content than non-filamentous virions. Using the confocal analysis pipeline to describe the lengths of filamentous virions in a population makes it possible to normalise bulk population measurements by size differences, and so to infer composition on a per virion level. Therefore, the analysis pipeline will support research into filamentous virion composition by facilitating methods to enrich samples by morphology and account for size differences.

As previously discussed, the only widespread method at present to analyse the proteome of individual virions is microscopy (see Section 1.4.3). The confocal analysis pipeline uses HA immunolabelling to detect filamentous virions, but it is also a simple form of compositional analysis. It could therefore be possible to detect the presence and abundance of other proteins using antibody labelling, although so little is known about the composition

of filamentous virions it may be difficult to validate this approach due to a lack of positive controls. In this way, the confocal analysis pipeline can support compositional analysis by allowing direct analysis of individual virions.

As with studying composition, studying filamentous virion function would be facilitated by developing methods to enrich a sample for a given virion morphology. As such, the confocal analysis pipeline supports assessment of filamentous virion function for the same reasons as described for assessing filamentous virion composition.

3.3.4 Conclusion

In conclusion, the confocal analysis pipeline I have described in this chapter will allow the study of the stability, composition, and function of filamentous virions. This method does have limitations, and these must be carefully considered when choosing which experimental questions it is best suited to answer. However, this quick, easy, and reproducible method makes answering these questions possible, and greatly strengthens confidence in the results, avoiding the many pitfalls that prevent comparisons between different studies into the characteristics of filamentous virions.

Chapter 4

Stability of filamentous virions during laboratory handling

4.1 Introduction

Hypothesis-driven experiments depend on controlling as many variables as possible, which in turn depends on using well-characterised samples. If the sample is altered in unpredictable ways after characterisation, then the necessary degree of control can be lost. We can often avoid deliberately altering samples, but some manipulation is required for every experiment and this could inadvertently cause alterations. When studying filamentous influenza virions, the biggest concern about such inadvertent alterations is that virions could be damaged by basic laboratory handling techniques.

Microscopy studies into influenza virus morphology contain frequent observations that filamentous virions appear to break down during laboratory handling, particularly after ultracentrifugation (Donald & Isaacs, 1958; Elleman & Barclay, 2004; Kordyukova et al., 2020; Mitnaul et al., 1996; Morgan et al., 1956; Roberts et al., 1998; Valentine & Isaacs, 1957; Vijayakrishnan et al., 2013), but this has never been directly investigated. Unpredictable virion damage could affect experiments if, for example, the damage caused a loss of infectivity. Any such damage would be a problem, but research into morphology would be specifically impacted if damage disproportionately affects virions of a particular shape. The past reports of virion damage generally refer to damage to filamentous virions, and none mention damage specific to non-filamentous virions. It is most likely, therefore, that any damage incurred from laboratory handling would disproportionately affect filamentous virions. This could, for example, be due to filamentous shapes being less energetically stable than spheres, and so more susceptible to shear forces and other issues incurred during handling. It could also be due to filamentous virions being larger than non-filamentous virions, so there are more components to break. Regardless of the mechanism, damage that disproportionately affected filamentous virions could have led to researchers underestimat-

ing the contribution of these virions to the properties of a virion population. It is therefore vital to determine whether this damage occurs.

Addressing the issue of filamentous virion stability during laboratory handling first requires identifying the most commonly-used manipulations when studying filamentous virions. Basic analyses of filamentous virions require five generic manipulations:

1. A means to separate filamentous virions from cellular debris. Debris can clog liquid handling apparatus, and its presence makes it difficult to determine whether a characteristic of a sample is due to virions or to debris. For example, when using the confocal analysis pipeline described in Chapter 3, HA+ cellular debris could be mistaken for virions.
2. A means to move filamentous virions around. As virions will be analysed in suspension, this method will be based on liquid transfer.
3. A means to mix samples containing filamentous virions. This ensures virions are evenly distributed throughout a sample.
4. A means to disaggregate clumps of filamentous virions. This is necessary as aggregated virions may have different properties to individual virions. For example, clumped semi-infectious virions could complement each other and allow a productive infection from a co-infected cell, whereas none of the virions would initiate a productive infection alone (Brooke, 2017).
5. A means to store filamentous virions. This would make analyses of virion properties more efficient, as otherwise virions would have to be prepared fresh at the start of each experiment. Aliquotting and storing a large preparation of virions also allows functionally equivalent samples to be used in multiple experiments, making it easier to standardise experimental inputs.

To determine the stability of filamentous virions during laboratory handling, in this chapter I examine the effects of a set of common laboratory handling techniques on filamentous virions. Using the confocal analysis pipeline outlined in the previous chapter, I assessed how these handling techniques alter the concentration and length of filamentous virions.

4.2 Results

4.2.1 Separating virions from cell debris

Cell debris is commonly removed by centrifugation at a low relative force. This causes cell debris larger than microvesicles to pellet, whereas the smaller and less dense virions

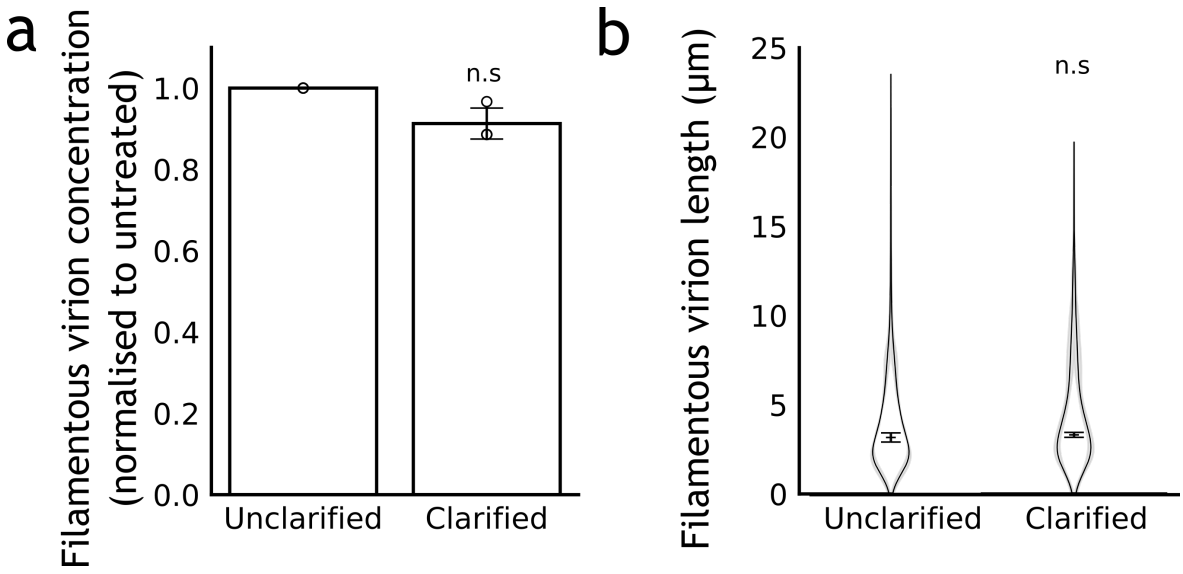

Figure 4.1: Filamentous virions are not damaged by clarification.

Filamentous influenza virions were obtained by collecting supernatant from MDCK cells infected with influenza A/Udorn/307/72 (H3N2) for 24 h. To determine the impact of clarification by low-speed centrifugation on filamentous virions, one sample was centrifuged at 1800 *g* for 5 min. (a) Concentration and (b) length distributions of filamentous virions were calculated with the confocal analysis pipeline described in Chapter 3 (three independent experiments). Concentration data are normalised to the untreated sample and the means and s.d. are shown; comparisons to untreated were made by two-tailed single-sample t-test: n.s $p > 0.05$. Filamentous virion length distributions are shown as frequency distributions (mean, with 95% CI in grey) and distributions of the median filamentous virion length (mean indicated as a line, s.d. as whiskers). Population medians were compared to the untreated sample by two-tailed Student's t-tests: n.s $p > 0.05$.

remain in the supernatant (see Chapter 5 for a detailed discussion of the underlying principles of clarification by centrifugation). However, filamentous virions are larger than non-filamentous virions and their relative densities are unknown. It is therefore plausible that clarifying samples in this manner would remove filamentous virions as well as cell debris. However, if samples were left unclarified, HA+ cell debris could be mistaken for virions by the confocal analysis pipeline, leading to the concentration of filamentous virions being overestimated.

To test if clarification by centrifugation selectively depleted filamentous virions, I analysed 1 ml samples of Udorn before and after 5 minutes of centrifugation at 1800 g. This sample was too small to generate a visible pellet, but comparably treated 40 ml samples (as used in Chapter 5) showed a clear pellet at the base of the tube. There was no difference between the median length of filamentous virions before and after this treatment (Figure 4.1a, $p > 0.05$), or of their concentration (Figure 4.1b, $p > 0.05$), suggesting clarification by centrifugation under these conditions caused no damage. However, I still considered it plausible that irregular HA+ cell debris could arise unpredictably in future experiments and be detected by the confocal analysis pipeline. All subsequent experiments therefore used clarified samples.

4.2.2 Liquid transfer

Liquid transfer is almost unavoidable in microbiology, but rapidly pushing liquid through a pipette tip or needle with a narrow bore creates shear forces that can damage the biological material being transferred (Wiegmann et al., 2017; Xie et al., 2007). To test if pipetting damaged filamentous virions, I repeatedly pipetted 1 ml samples of Udorn 0, 5, 10, or 30 times. I used a Starlab 1000 µl pipette tip, resting the tip just above the base of the microfuge tube which contained the sample, and used a metronome to ensure a consistent pipetting rate of 30 pipette actions per minute. No single treatment resulted in a significant reduction in either concentration (Figure 4.2a, $p > 0.05$) or filamentous virion length (Figure 4.2b, $p > 0.05$) compared to 0 pipette actions, though the number of pipetting actions was slightly negatively correlated with concentration. As the median virion length was unaffected, this suggested extensive pipetting was removing filamentous virions from the sample, rather than fragmenting them. However, this correlation was weak, and the damage could be considered negligible unless performing an unusually large number of pipette actions.

4.2.3 Mixing samples

While pipetting can be used to mix samples, vortexing is often more efficient and convenient. Like pipetting, vortexing subjects samples to shear forces that could cause damage

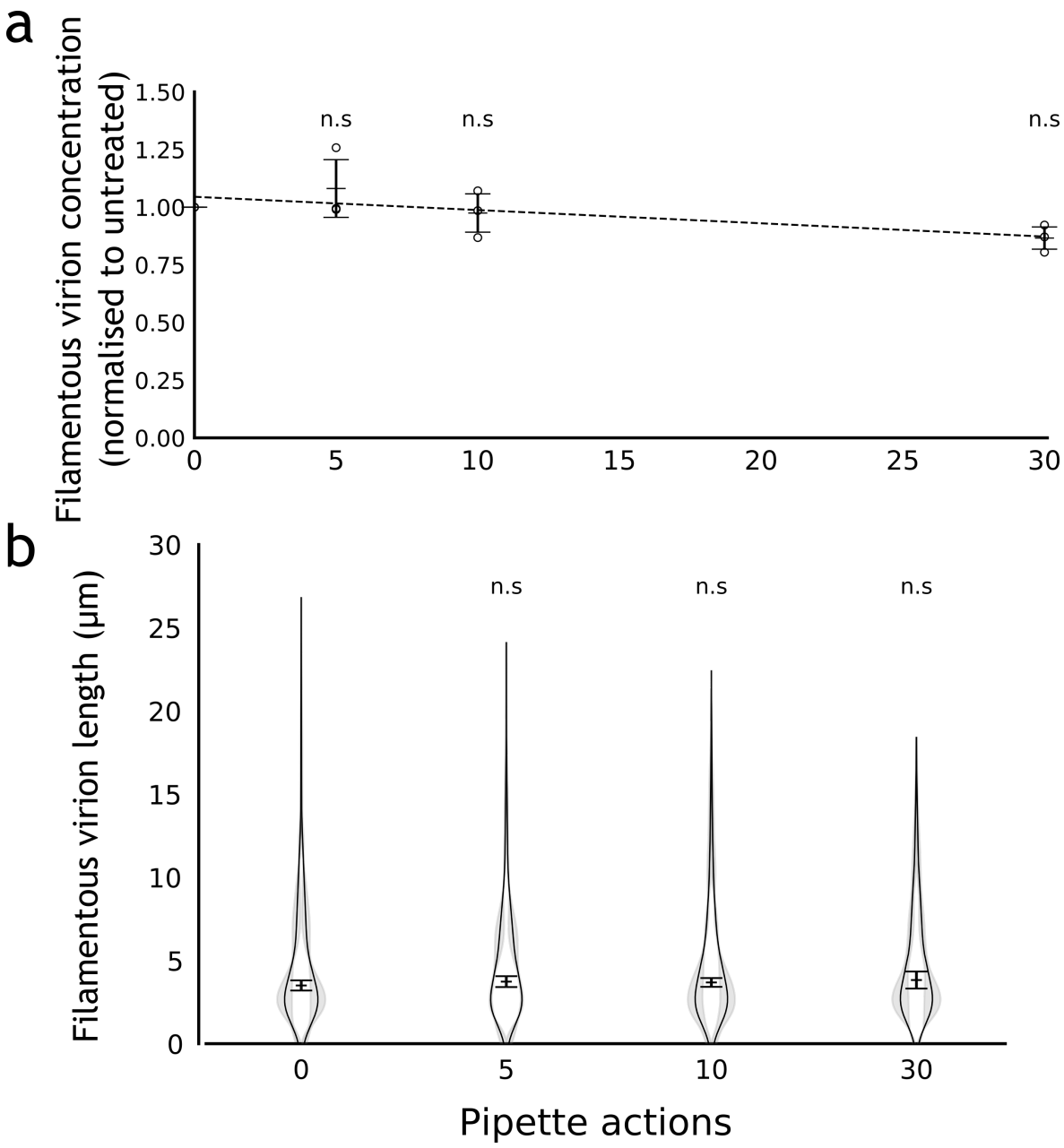

Figure 4.2: Filamentous virions are not damaged by pipetting.

Filamentous influenza virions were obtained by collecting supernatant from MDCK cells infected with influenza A/Udorn/307/72 (H3N2) for 24 h. To determine the impact of pipetting on filamentous virions, samples were subjected to increasing levels of pipetting. (a) Concentration and (b) length distributions of filamentous virions were calculated with the confocal analysis pipeline described in Chapter 3 (three independent experiments). The polynomial trend line was fitted by the least squares method. Concentration data are normalised to the untreated sample and the means and s.d. are shown; comparisons to untreated were made by two-tailed single-sample t-tests: n.s $p > 0.05$. Filamentous virion length distributions are shown as frequency distributions (mean, with 95% CI in grey) and distributions of the median filamentous virion length (mean indicated as a line, s.d. as whiskers). Population medians were compared to the untreated sample by two-tailed Student's t-tests: n.s $p > 0.05$.

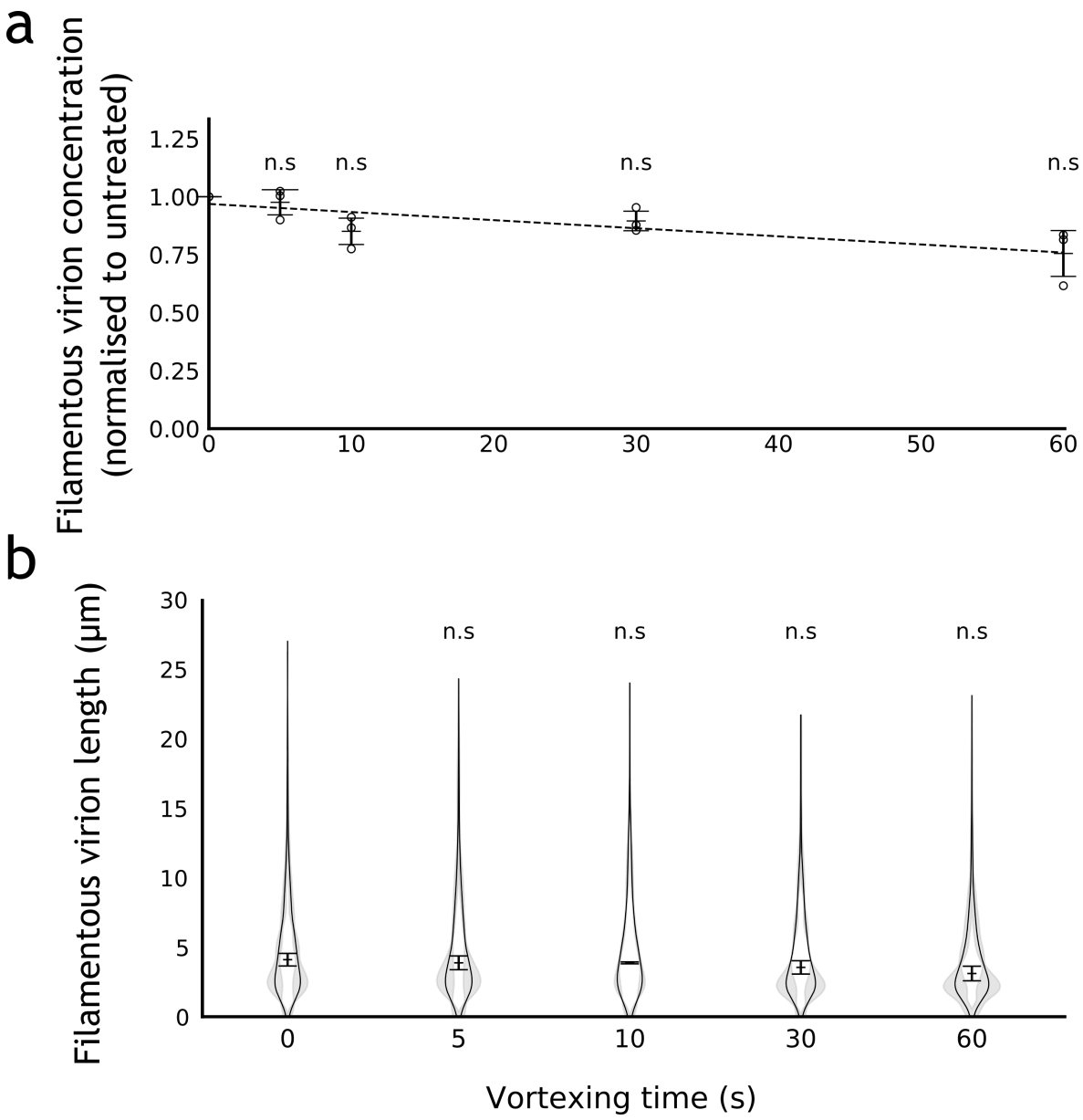

Figure 4.3: Filamentous virions are not damaged by vortexing.

Filamentous influenza virions were obtained by collecting supernatant from MDCK cells infected with influenza A/Udorn/307/72 (H3N2) for 24 h. To determine the impact of vortexing on filamentous virions, samples were subjected to increasing levels of vortexing. (a) Concentration and (b) length distributions of filamentous virions were calculated with the confocal analysis pipeline described in Chapter 3 (three independent experiments). The polynomial trend lines was fitted by the least squares method. Concentration data are normalised to the untreated sample and the means and s.d. are shown; comparisons to untreated were made by two-tailed single-sample t-tests: n.s $p > 0.05$. Filamentous virion length distributions are shown as frequency distributions (mean, with 95% CI in grey) and distributions of the median filamentous virion length (mean indicated as a line, s.d. as whiskers). Population medians were compared to the untreated sample by two-tailed Student's t-tests: n.s $p > 0.05$.

(Kheradvar & Pedrizzetti, 2012). To assess the impact of vortexing, I subjected 1 ml samples of Udorn to 0, 1, 5, 10, 30, and 60 seconds of vortexing at 2500 rpm using a Starlab Vortexer. No duration of vortexing substantially reduced the concentration of filamentous virions when compared to untreated (Figure 4.3a, $p > 0.05$). Vortexing did, however, appear to be slightly negatively correlated with concentration and it is possible an unusually high degree of vortexing would have shown a substantial reduction. There was however, no indication than vortexing affected the length of filamentous virions (Figure 4.3b, $p > 0.05$). This suggested that shear forces from vortexing may damage filaments but this is unlikely using standard protocols. Vortexing at speeds below 2500 rpm creates weaker shear forces than vortexing at 2500 rpm (Kheradvar & Pedrizzetti, 2012), so it is reasonable to assume that these would not cause more damage. I therefore concluded that mixing samples by vortexing at speeds of up to 2500 rpm, for times of up to 60 seconds, does not damage filamentous virions and is suitable for use in experiments.

4.2.4 Disaggregating virions

Aggregates of particles are commonly disaggregated via sonication: the use of sound energy to agitate samples, which is achieved by forming bubbles that release heat and liquid jets when they implode (Forde et al., 2014). This is useful for disrupting aggregates of virions (Sharp, 1965; Müller, 1976), but risks damaging the sample. For this reason, low-frequency sonication is often used in electron microscopy to disrupt clumps of virions, whereas high-frequency sonication has been deliberately used to rupture influenza virion membranes (Donald & Isaacs, 1958). To test the impact of low-frequency sonication on filamentous virions, I subjected 1 ml samples of Udorn in 1.5 ml microfuge tubes to 0, 1, 5, 10, 30, and 60 seconds of sonication at 50 kHz in a Guyson Kerry KC2 Ultrasonic Bath. I found no reduction in filamentous virion concentration (Figure 4.4a, $p > 0.05$), though 10 seconds of sonication appeared to increase the filamentous virion concentration ($p < 0.01$). This is likely to be an outlier, as no statistically significant effect was seen at 30 or 60 seconds, though it is plausible that disaggregating clumps of virions would increase the concentration of individual virions. Median length was unaffected by sonication (Figure 4.4b, $p > 0.05$). Together, these data suggest that sonication at this frequency does not cause damage. Sonication at frequencies below 50 kHz delivers less energy to the virions (Forde et al., 2014), so it is reasonable to assume that not cause more damage than sonication at 50 kHz. I therefore concluded that disaggregating virions using sonication at frequencies of up to 50 kHz, for times of up to 60 seconds, does not damage filamentous virions and is suitable for use in experiments.

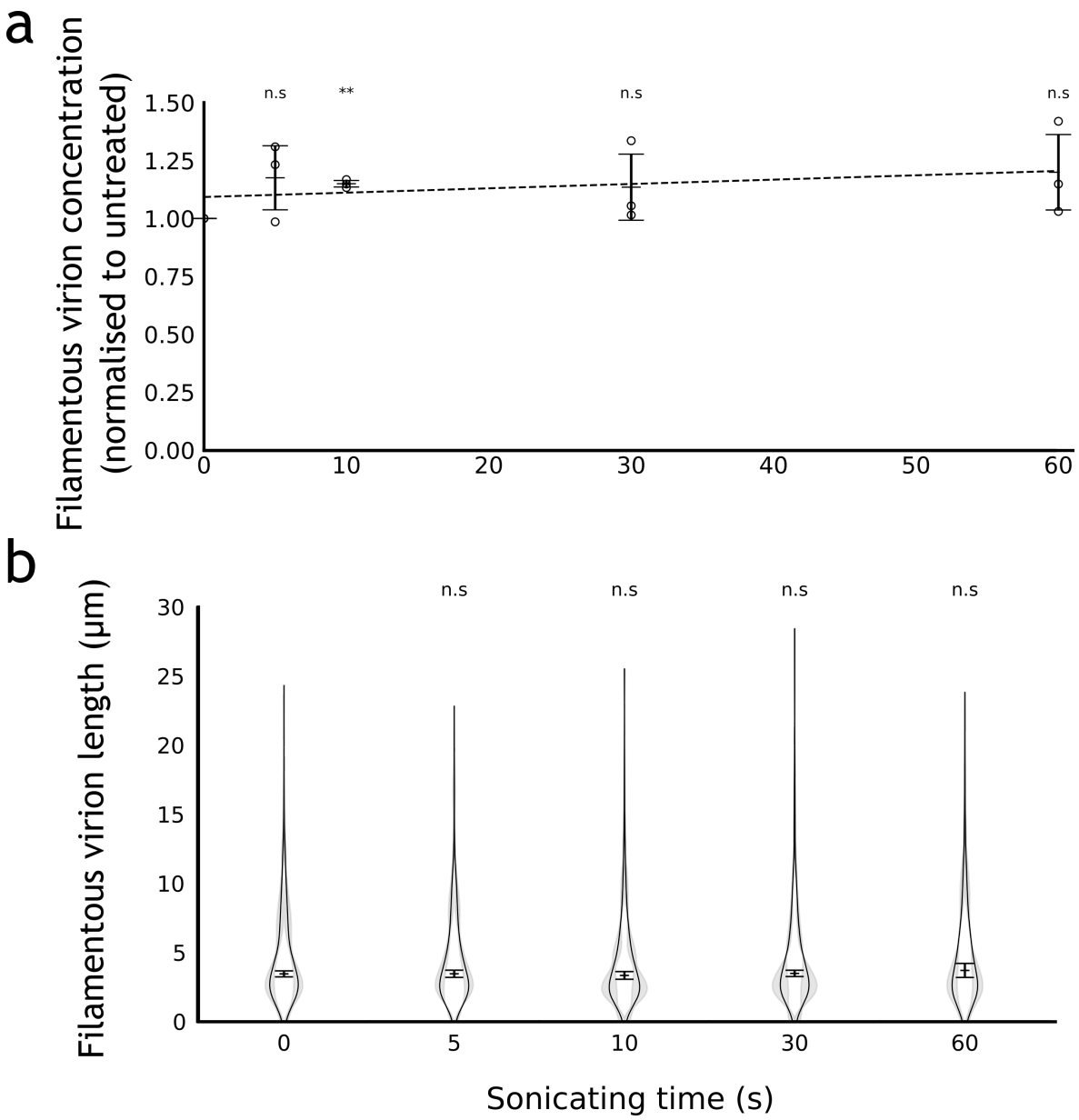

Figure 4.4: Filamentous virions are not damaged by sonication.

Filamentous influenza virions were obtained by collecting supernatant from MDCK cells infected with influenza A/Udorn/307/72 (H3N2) for 24 h. To determine the impact of sonicating on filamentous virions, samples were subjected to increasing levels of sonicating. (a) Concentration and (b) length distributions of filamentous virions were calculated with the confocal analysis pipeline described in Chapter 3 (three independent experiments). The polynomial trend line was fitted by the least squares method. Concentration data are normalised to the untreated sample and the means and s.d. are shown; comparisons to untreated were made by two-tailed single-sample t-test: n.s $p > 0.05$, ** $p < 0.01$. Filamentous virion length distributions are shown as frequency distributions (mean, with 95% CI in grey) and distributions of the median filamentous virion length (mean indicated as a line, s.d. as whiskers). Population medians were compared to the untreated sample by two-tailed Student's t-tests: n.s $p > 0.05$.

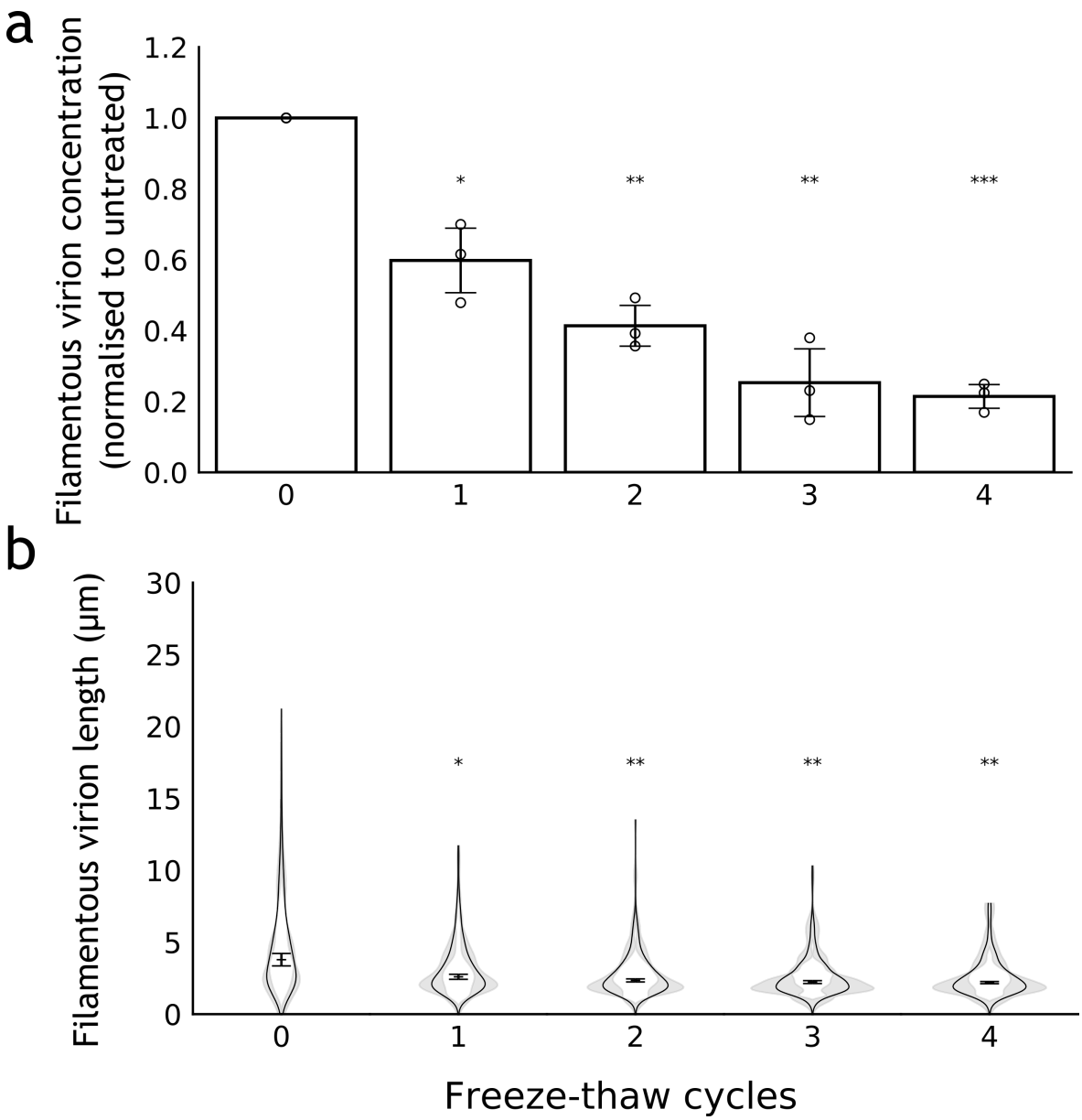

Figure 4.5: Filamentous virions are damaged by freezing.

Filamentous influenza virions were obtained by collecting supernatant from MDCK cells infected with influenza A/Udorn/307/72 (H3N2) for 24 h. To determine the impact of pipetting on filamentous virions, samples were subjected to repeated freeze-thaw samples. One sample was stored at 5 °C in the dark during the experiment as a control. (a) Concentration and (b) length distributions of filamentous virions were calculated with the confocal analysis pipeline described in Chapter 3 (three independent experiments). Concentration data are normalised to the untreated sample and the means and s.d. are shown; comparisons to untreated were made by two-tailed single-sample t-test: * $p < 0.05$, ** $p < 0.01$, *** $p < 0.001$. Filamentous virion length distributions are shown as frequency distributions (mean, with 95% CI in grey) and distributions of the median filamentous virion length (mean indicated as a line, s.d. as whiskers). Population medians were compared to the untreated sample by two-tailed Student's t-tests: * $p < 0.05$, ** $p < 0.01$, *** $p < 0.001$.

4.2.5 Storing virions

Influenza virus is commonly stored at sub -70 °C temperatures, to allow long-term storage without loss of infectivity and to allow characterisation of an entire batch of samples by analysing a single aliquot (Eisfeld et al., 2014). However, freezing is known to reduce the infectious titre of influenza virus (Greiff et al., 1954; Eisfeld et al., 2014), likely due to localised pH changes that occur during freezing and thawing (Van Den Berg, 1966) or from ice crystals puncturing virion membranes (Greiff et al., 1954). To test the impact of freezing on filamentous virion integrity, I subjected Udorn samples to repeated freeze-thaw cycles. A cycle consisted of placing a 1 ml aliquot in a 1.5 ml microfuge tube (Greiner) in a consistent position in a polypropylene cryobox (VWR) towards the centre of a C760 Innova − 70 °C freezer (New England Biolabs) for 1 h, before thawing in a 37 °C waterbath for ~2 min. A control sample was incubated at 5 °C for the duration of the experiment, and protected from light to remove the risk of UV radiation damage. I found that even a single freeze-thaw cycle substantially reduced the concentration ($p < 0.05$) of a filamentous virion population, an effect which was compounded with repeated cycles (Figure 4.5a). Furthermore, the median length of filamentous virions was reduced by 1.2 μm after a single cycle ($p < 0.05$), though it remained unchanged for subsequent cycles (Figure 4.5b). This indicated that routine freezing methods cause significant damage to filamentous virions, which could skew analyses of their properties.

Even though freezing destroyed many filamentous virions, I reasoned that the surviving virions may have still been suitable for analysis. If true, this would mean that freezing damage could be accounted for by reassessing the samples with the confocal analysis pipeline after they are thawed, and so the convenience of freezing would not have to be sacrificed. However, while analysing these micrographs, I noticed that filamentous virions that had been frozen were often distorted (Figure 4.6a), which could indicate damage to the capsid. To quantify the distortion, I altered the image analysis script described in Chapter 3 to fit an ellipse to each filamentous virion and calculate the eccentricity (i.e. length of the major axis divided by the length of the minor axis) of this ellipse. Elongated filaments without distortions have a long, narrow fitted ellipse and so a very high eccentricity. Distorted virions, which curl back on themselves, have a wider fitted ellipse and so a lower eccentricity. This analysis showed a substantial reduction in the eccentricity of fitted ellipses in the frozen sample compared to the unfrozen (Figure 4.6b and c, $p < 0.001$). This indicated that all filamentous virions in the sample were being damaged even if they were not removed. I therefore concluded that no filamentous virions that were frozen in this manner could be suitable for further analysis.

As the freezing changed the physical appearance of filamentous virions, I wondered whether this would also affect the functional properties of virions in the stock. I therefore used plaque assays to determine the infectious titre of frozen and unfrozen samples and found that freezing led to a drop in infectivity of approximately 25% (Figure 4.7a, $p < 0.05$).

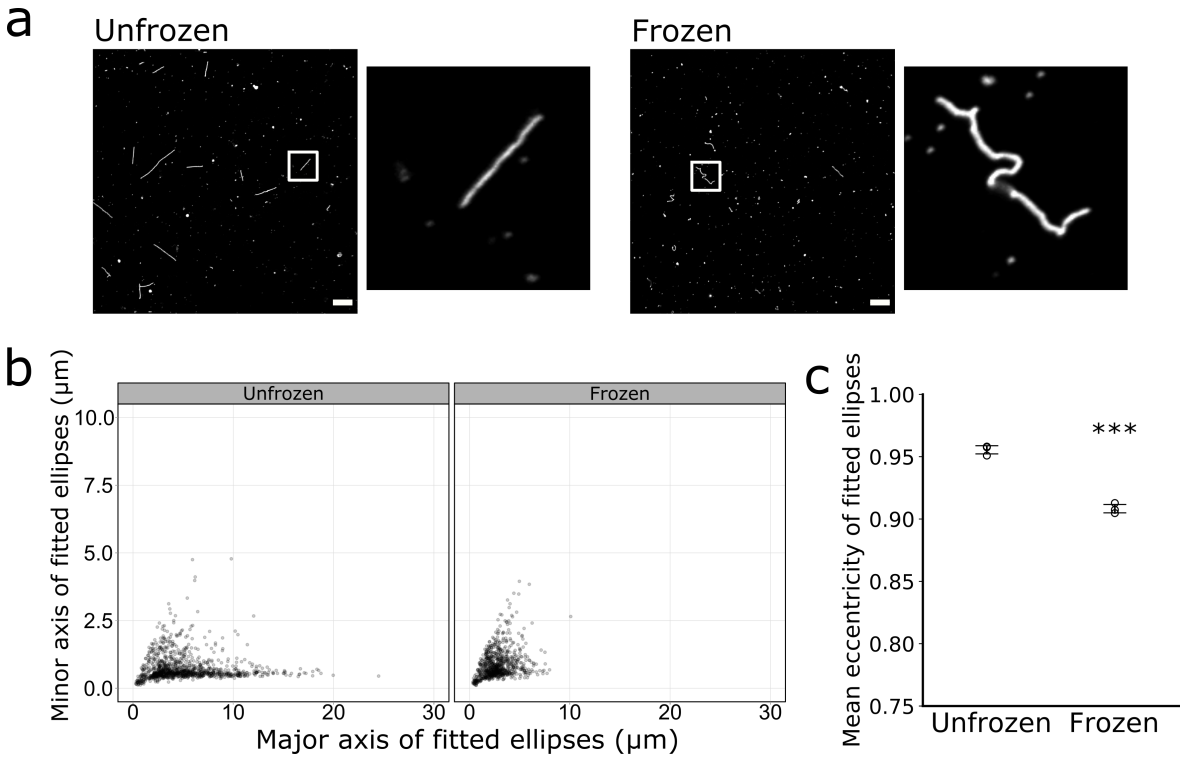

Figure 4.6: Filamentous virions are distorted by freezing.

To assess the level of distortion caused by freezing, the micrographs for the unfrozen and the single freeze-thaw cycle from Figure 4.5 were re-examined. (a) Representative confocal micrographs of unfrozen and freeze-thawed samples, with HA immunostained and with insets magnifying an individual filamentous virion (images acquired at 63x magnification, scale bar 10 µm). (b) Measurements of individual filamentous virions from unfrozen samples and samples that had undergone a single freeze-thaw cycle, combining data from 3 separate experiments. Ellipses were fitted to each filamentous virion, and the major and minor axes of the ellipses are plotted. (c) The major and minor axes from (b) were used to calculate the eccentricity of the fitted ellipses. Mean eccentricities for each repeat are shown (three independent experiments, mean indicated by a line, s.d. as whiskers). Conditions were compared by two-tailed Student's t-test: *** $p < 0.001$.

While it was not possible to determine the relative contributions of filamentous and non-filamentous virions to infectivity, this finding highlights that routine freezing both damages virions and changes the functional properties of the sample.

These findings depend on two key assumptions. First, that virions stored at 4 ˚C do not degrade over the course of four hours, as these samples were used as negative controls in the above experiments. Subsequent experiments on virion stability over time (see Section 4.2.5 below) suggest that this assumption is well-founded. Second, that freezing does not leave virions intact, but undetectable by the confocal analysis pipeline. Freezing creates localised pH changes (Van Den Berg, 1966), and, while these would be reversed upon thawing, there is a chance they could permanently alter virions. For example, pH changes could cause conformational changes in HA (Singanayagam et al., 2019) that affect reduce the adhesive properties of the virions to the coverslip or reduce the affinity of the HA antibody. There is, however, no evidence yet suggesting that this problem occurs.

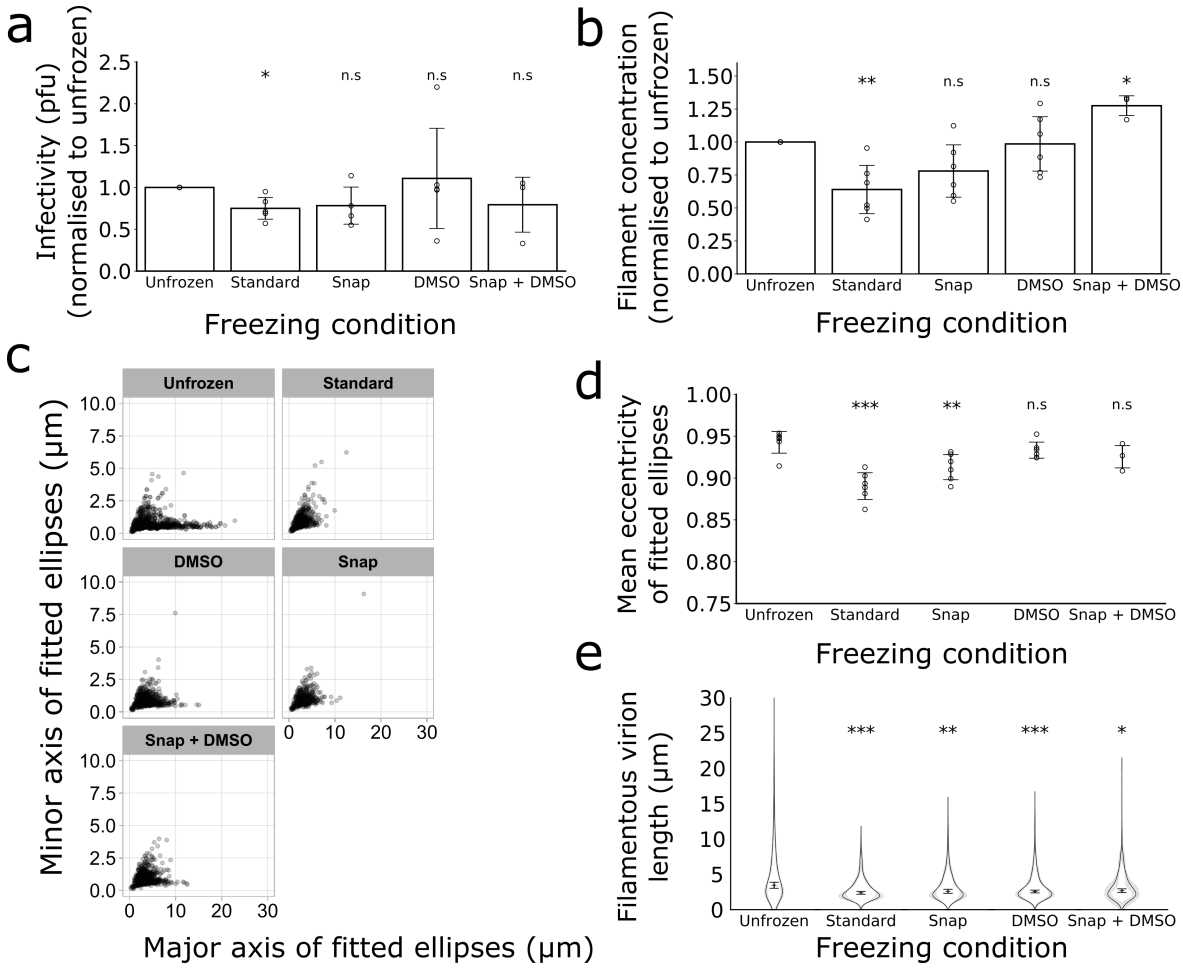

Figure 4.7: Alternative freezing methods cause less filamentous virion damage.

Filamentous influenza virions were obtained by collecting supernatant from MDCK cells infected with influenza A/Udorn/307/72 (H3N2) for 24 h. To determine the effects of different freezing methods on filamentous virions, samples were incubated at 5 ˚C (Unfrozen); frozen by placement in a - 70 ˚C freezer (Slow); frozen by placement in dry ice and ethanol, before being transferred to a - 70 ˚C freezer (Snap); made up to a final concentration of 10 % DMSO and frozen by placement in a - 70 ˚C freezer (DMSO); made up to a final concentration of 10 % DMSO and frozen by placement in dry ice and ethanol, before being transferred to a - 70 ˚C freezer (Snap + DMSO). All conditions that did not include DMSO were diluted in 1x PBS to ensure consistent levels of dilution. After 1 h, all samples were placed in a 37 ˚C waterbath for 2 min to thaw. (a) Infectious titres were measured by plaque assay in MDCK cells and normalised to 0 h; means and s.d. are shown (three independent experiments), with comparisons to 0 h by two-tailed single-sample t-test: n.s. $p > 0.05$, * $p < 0.05$, ** $p < 0.01$, *** $p < 0.001$. (b) Filamentous virion concentrations were calculated using the confocal analysis pipeline from Chapter 3 and normalised to unfrozen. Means and s.d. of 3 independent repeats are shown, with comparisons to unfrozen by two-tailed one-sample t-test: * $p < 0.05$, ** $p < 0.01$. (c) Individual filamentous virion dimensions based on fitted ellipses, combining data from the experimental repeats described in (b). (d) Eccentricity of the fitted ellipses, calculated from the major and mi-

nor axes from (c). Mean eccentricities for each repeat are shown (repeats as (b), mean indicated by a line, s.d. as whiskers). Time points were compared to 0 h by two-tailed Student's t-tests: n.s $p > 0.05$, ** $p < 0.01$, *** $p < 0.001$. (e) Frequency distributions of filamentous virion lengths were calculated using the confocal analysis pipeline from Chapter 3 (mean, with the 95% CI shaded in grey) as well as the position of the median filamentous virion length (mean and s.d.). Population medians were compared to unfrozen with two-tailed Student's t-tests: * $p < 0.05$, ** $p < 0.01$, *** $p < 0.001$ (six independent experiments, except Snap + DMSO which shows three independent experiments).

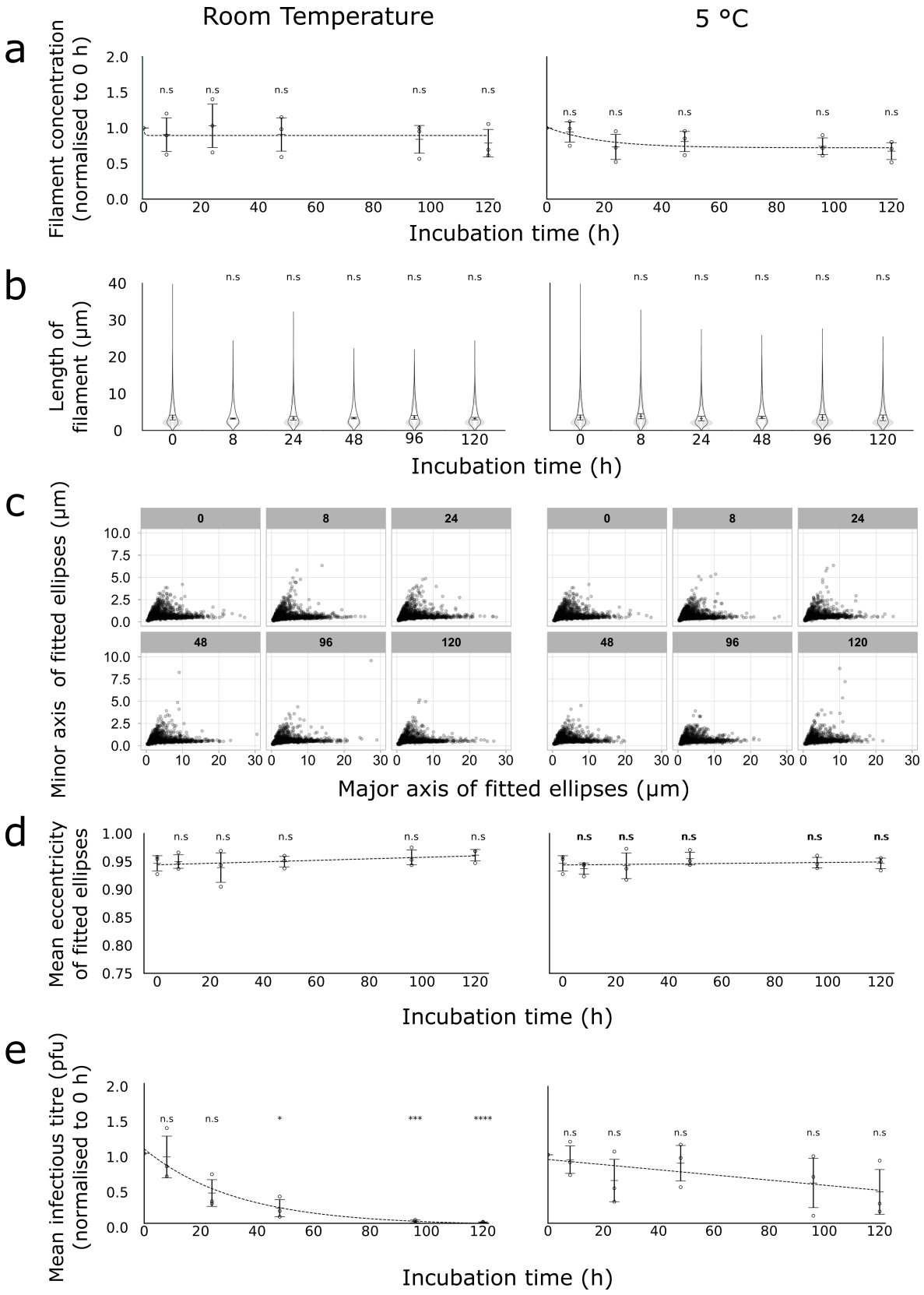

Figure 4.8: Filamentous virion structure is stable over time, but infectivity declines.

Filamentous influenza virions were obtained by collecting supernatant from MDCK cells infected with influenza A/Udorn/307/72 (H3N2) for 24 h. To determine the stability of filamentous virions at different temperatures, samples were incubated in the dark at 5 °C (left-hand panels) or room temperature (right-hand panels) for up to 5 days. Trend lines show exponential decay curves fitted by the least squares method.

(a) Filamentous virion concentrations at different time points, normalised to 0 h. Means and s.d. of 3 repeats are shown, with comparisons to unfrozen by two-tailed one-sample t-test: n.s $p < 0.05$. (b) Filamentous virion length distributions were calculated by the confocal analysis pipeline described in Chapter 3, shown as frequency distributions (mean, with 95% CI in grey) and distributions of the median filamentous virion length (mean position indicated as a line, s.d. as whiskers). Population medians were compared to 0 h sample by two-tailed Student's t-tests: n.s $p > 0.05$. (c) Dimensions of individual filamentous virions following incubation, combining data from 3 separate experiments. Ellipses were fitted to each filamentous virion, and the major and minor axes of the ellipses are plotted. Subtitles of each graph in grey boxes indicate the hours of incubation before analysis. (d) The major and minor axes from (c) were used to calculate the eccentricity of the fitted ellipses. Mean eccentricities for each repeat are shown, ($n = 3$, mean indicated by a line, s.d. as whiskers). Time points were compared to 0 h by two-tailed Student's t-tests: n.s $p > 0.05$. (e) Infectious titres were measured by plaque assay in MDCK cells and normalised to 0 h; means and s.d. are shown ($n = 3$), with comparisons to 0 h by two-tailed single-sample t-test: n.s. $p > 0.05$, * $p < 0.05$, ** $p < 0.01$, *** $p < 0.001$.

4.2.6 Mitigating freezing damage

Despite the damage it can cause, freezing is necessary for many studies to be practicable and so I investigated whether the damage it causes could be mitigated. Research into storing eukaryotic cells has identified snap freezing (Kon et al., 2016) or adding a cryoprotectant like DMSO (McGann & Walterson, 1987) as methods to reduce the formation of ice crystals, and, thereby, damage. I aimed to investigate whether these methods could protect filamentous virions during freeze-thaw cycles (the freezing protocol described above is referred to in this section as "slow freezing" to distinguish it from "snap freezing" using dry ice and ethanol). I compared unfrozen samples, slow frozen samples, snap frozen samples, samples slow frozen in 10% DMSO, and samples snap frozen in 10% DMSO (Figure 4.7). Snap frozen samples showed no loss in filamentous virion concentration ($p > 0.05$) or infectivity ($p > 0.05$), but still showed a reduction in median length ($p < 0.01$) and eccentricity of fitted ellipses ($p > 0.01$), indicating that longer filamentous virions were still removed and the remaining filamentous virions were still damaged. Samples frozen in 10% DMSO showed no reduction in concentration, infectivity, or eccentricity of fitted ellipses ($p > 0.05$), but still showed a reduction in median length ($p < 0.001$), suggesting that longer filamentous virions were removed, but the remaining virions did not suffer damage. Samples which were snap frozen in 10% DMSO showed similar results to those that were slow frozen in DMSO. Taken together, these results suggest that snap freezing and incorporating 10% DMSO could negate the impact of freezing on concentration and virion distortion, but could not prevent the reduction in median filamentous virion length of 1 μm.

As there seemed to be no way to freeze filamentous virions without damaging them, I asked whether virions could be stored without freezing. For most experiments, this would require a method to maintain filamentous virions for several days without incurring damage. It was unknown how stable filamentous virions were at 5 °C, or even room temperature and so I incubated samples at these two temperatures for five days. I found that at both temperatures, filamentous virion populations showed no reduction in concentration (Figure 4.8a, $p > 0.05$), median length (Figure 4.8b, $p > 0.05$), or eccentricity of fitted ellipses (Figure 4.8c and d, $p > 0.05$) for at least five days. However, the samples stored at 5 °C showed a steady decline in infectivity to 50% of the initial infectious titre after five days, and the samples stored at room temperature showed a sharp decline to 50% of the initial infectious titre after one day (Figure 4.8e). These results suggested that the functional properties of filamentous virions incubated in liquid media could change over time, but their structures remain intact for at least five days.

4.3 Discussion

4.3.1 Summary

By measuring the impact of standard laboratory manipulations on filamentous virions, I established a set of validated procedures for handling them. Standard methods for clarifying samples, transferring liquids, mixing samples, and disaggregating virions caused no substantial damage to filamentous virions. However, long-term storage by freezing caused substantial damage to filamentous virion populations, and should therefore be avoided whenever experiments are dependent on undamaged samples. This limitation is inconvenient, but being aware of it makes it possible to design robust and interpretable experiments to characterise the composition and function of filamentous virions.

4.3.2 Limitations of the experimental design

Assessing basic laboratory handling techniques itself depends on some degree of laboratory handling. For example, the confocal analysis pipeline requires every sample to be pipetted at least once to apply it to the coverslip. However, as repeated pipetting and vortexing caused negligible damage to virions, I considered it reasonable that the minor amount of manipulation necessary to perform the experiments was unlikely to cause substantial damage. Similarly, I tested laboratory manipulations individually, but many experimental work flows will use them in combination. These combinations could have synergistic effects that cause more damage than any manipulation alone. As I saw no theoretical basis for this synergistic damage, I considered it reasonable to assume it would not occur in future. It would, however, be worth using the analysis pipeline to assess specific work flows if experiments with many handling steps yielded unusual results.

4.3.3 Enriching virions by morphology

As described in the previous chapter (see Section 3.3.3) investigating how composition and function varies with morphology would depend on developing a new method to separate filamentous from non-filamentous virions. As this method would be novel, it would be unknown whether it caused virion damage. The findings described in this chapter demonstrated the efficiency with which the confocal analysis pipeline can be used to test virion stability, making it possible to quickly determine whether a novel purification method yields samples suitable for analysis.

4.3.4 Assessing the composition of bulk populations

Virion composition can be assessed by generating a sample that is highly enriched for the virions of interest and then measuring the properties of the entire sample. Methods based on this principle to assess composition, such as western blot or mass spectrometry, denature the sample in the process. It therefore does not matter if virion structures are damaged after generating these samples, and so it would be suitable to store these samples frozen and analyse their composition when convenient.

4.3.5 Functional analyses of filamentous virions

As with their composition, the functional properties of virions can be measured by measuring the bulk properties of a sample highly enriched in the virions of interest. However, unlike composition, assays to measure functional properties depend on avoiding virion damage after the enriched sample has been generated. For example, the distribution of HA and NA proteins along the virion has been reported to impact their activity (Vahey & Fletcher, 2019a), and this distribution could be disrupted if the virion is damaged. Samples for functional analysis, therefore, cannot be stored for long periods after they are generated, and so functional analyses must take place as soon as possible after sample enrichment.

This requirement to use samples as soon as possible makes it hard to titrate viruses to standardise experimental inputs. For example, a standard influenza virus plaque assay takes two to three days to complete (Gaush & Smith, 1968), by which point some functional properties of the sample may have changed. Unless an experiment can be designed around a much faster titration, such as an HA assay, interpreting functional analyses will require some means to normalise the data after it has been collected. For example, relative activity of two proteins could be examined rather than the absolute activity of a single protein.

4.3.6 Assessing the composition of individual virions

As an alternative to analysing an entire virion population at once, the composition of individual virions could be analysed using microscopy. This approach is less dependent on maintaining the concentration of virions, so long as enough remain to collect a representative sample. However, as with functional studies, the virions which are analysed must be undamaged in order to collect useful data. It is therefore preferable to use unfrozen samples for this type of analysis, and therefore the analysis should be performed as soon as possible after generating the sample.

4.3.7 Conclusion

Most common laboratory handling techniques have little or no effect on filamentous virions, but freezing causes severe damage. While this damage can be mitigated, the most reliable analyses of filamentous virion properties require the use of unfrozen samples. These findings thereby identify precautions that must be taken when designing clearly interpretable experiments to study the properties of filamentous virions. They therefore lay the necessary foundation for a robust characterisation of the composition and function of filamentous influenza virions.

Chapter 5

Compositional comparison of filamentous and non-filamentous virions

5.1 Introduction

Virion composition is likely to vary with morphology

Characterising the compositional differences between filamentous and non-filamentous virions should give insight into corresponding differences in assembly and function. Potential compositional differences can be grouped into four categories. First, the absolute copy number of some proteins may differ. It is intuitively obvious that there will be at least some differences of this kind due to the size difference between filamentous and non-filamentous virions. Second, the relative abundance of proteins may differ between the virion types (as previously suggested by Iwatsuki-Horimoto et al. (2006); Kordyukova et al. (2020); Liu et al. (2002); Roberts et al. (2013, 1998); Seladi-Schulman et al. (2014); Chlanda et al. (2015); Vahey & Fletcher (2019a,b)). Third, the nature and site-occupancy of post-translational modifications of proteins may differ. Fourth, the lipid composition of virions may vary with morphology. As with the formation of filamentous virions themselves, the presence of any of these variations alone would not demonstrate that they are adaptive. However, identifying them would be invaluable for forming hypotheses to drive further investigation of the role of filamentous virions.

5.1.1 Assessing composition with microscopy

A key tool in the analysis of filamentous virion composition has been microscopy. Cryo-electron tomography has revealed the structure of the M1 capsid in filamentous virions (Calder et al., 2010; Vijayakrishnan et al., 2013; Peukes et al., 2020) and the proportion of

filamentous virions which contain genomes (Vijayakrishnan et al., 2013). However, this approach can only give details about abundant and readily identifiable proteins. An alternate method is confocal microscopy, which is more amenable to antibody labelling than electron microscopy and the stark contrast between fluorophore and background on fluorescence micrographs make them more suitable for automated image analysis. Though light microscopy, even super-resolution microscopy, is still lower resolution than cryo-electron tomography, the advantages it offers for labelling make it easier to investigate proteins which are less recognisable or abundant than major structural proteins such as M1 or HA. Assessing composition with confocal microscopy does, however, depend on highly specific labels and the relevant reagents may not exist for every protein of interest. Furthermore, protein abundance does not necessarily scale in a linear fashion with fluorescence intensity when using antibody labelling (Verdaasdonk et al., 2014), making abundance hard to quantify. Finally, the researcher must select which labels are used, and so the proteins to be examined have to be selected in advance. Microscopy approaches are therefore powerful when assessing virion composition but have limitations which make them less suitable for comprehensively assessing virion composition. Instead, it may be best to use microscopy to provide localisation data to support broader compositional analyses.

5.1.2 Assessing composition with western blot or mass spectrometry

Bulk population analyses involve assessing the properties of large populations of virions. They can provide enough data to investigate less abundant proteins or modifications, but do not capture the localisation data provided by microscopy. This style of approach includes methods which require antibody labelling, such as western blotting. It also includes label-free methods, such as mass spectrometry, which enables the simultaneous analysis of hundreds of proteins and so can detect differences without the researcher needing to select the proteins of interest in advance.

A bulk population analysis to measure how composition varies with morphology requires a method to prepare samples enriched in either filamentous or non-filamentous virions. This can be achieved by mutating a virus to alter its morphology (Elleman & Barclay, 2004; Roberts et al., 1998; Sieczkarski & Whittaker, 2005), but mutations of this sort could affect composition through other means and so this method is unsuitable for assessing how composition varies with morphology. This problem can be avoided by physically separating filamentous and non-filamentous virions from the same initial sample. While such separations have been reported several times (Roberts et al., 1998; Liu et al., 2002; Sieczkarski & Whittaker, 2005; Smirnov et al., 1991; Ada et al., 1958), they are challenging to replicate (discussed in Kordyukova et al. (2020)). Furthermore, this separation has often been performed with sucrose density gradients, but these are not isosmotic with influenza virions and this could damage or distort them (Smirnov et al., 1991; Sugita et al., 2011). Adopting

a bulk population approach to characterising compositional differences therefore requires the development of an efficient and reproducible method to separate filamentous and non-filamentous virions.

5.1.3 Conclusion

To date, several methods have been used to assess how influenza virion composition varies with morphology, but each has their own strengths and limitations and our understanding of this area is still limited. Here, after describing a preliminary analysis based on microscopy, I will demonstrate an efficient and robust method to enrich virions by morphology, and use it perform a comprehensive comparison of the proteomes of filamentous and non-filamentous virions using mass spectrometry.

5.2 Results I: Assessing composition with microscopy

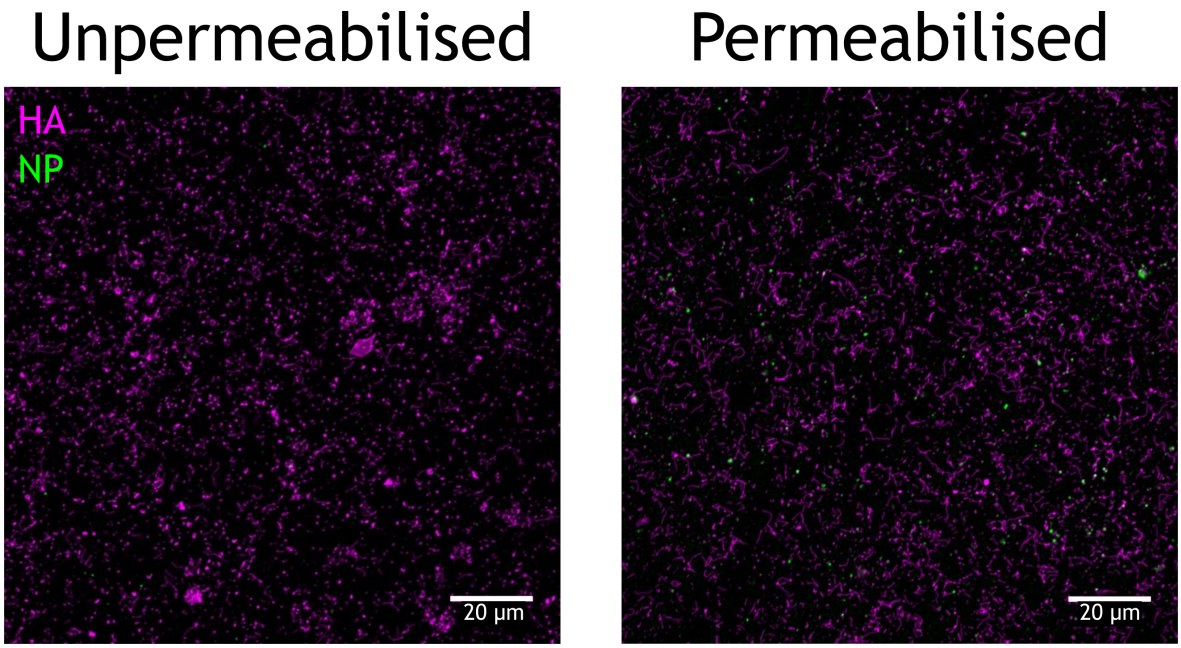

Figure 5.1: Effect of permeabilisation on NP staining in filamentous virions. Filamentous influenza virions were obtained by collecting supernatant from MDCK cells infected with A/Udorn/307/72 (H3N2) for 24 h, which was stored at -70 ˚C until use. Virions were centrifuged onto glass coverslips and fixed in 4% formaldehyde. One sample was permeabilised in 0.1 % Triton X-100 and the other was untreated. Haemagglutinin (HA) was immunostained to identify virions and nucleoprotein (NP) was immunostained to identify RNPs. Images were collected by confocal microscopy, 63x magnification.

While I used the confocal microscopy pipeline from Chapter 3 to measure the concentration and lengths of filamentous virions, the principles underlying it could also be used to assess protein localisation.

As a proof of principle, I aimed to examine the localisation of NP within filamentous virions, as detailed cryo-electron microscopy could be used for comparison (Vijayakrishnan et al., 2013). As a preliminary experiment, I adsorbed virions to coverslips and immunostained HA as described in Chapter 3, this time immunostaining NP in parallel. To control for non-specific binding, I stained both permeabilised and unpermeabilised samples, as all NP in the sample ought to be contained beneath the membrane of a virion or a microvesicle. As this experiment was only intended as a proof of concept, frozen samples were used.

More NP puncta were visible in the permeabilised sample than the unpermeabilised (Figure 5.1), suggesting it may be possible to use this approach to examine virion composition. However, I was unable to quantify the NP puncta, as this process required thresholding the image to distinguish signal from noise. Even slight adjustments to the thresholding intensity could change the apparent number of NP puncta by orders of magnitude, and, because they lacked distinctive shapes and sizes, it was impossible to determine the appropriate thresholding intensity. I concluded that microscopy was not suitable for my analysis of virion composition. Instead, I focused on a bulk population approach.

5.3 Results II: Clarifying samples and enriching them by morphology

Comparing the proteomes of filamentous and non-filamentous virions requires a method to separate them, or at least strongly enrich a sample by morphology. Without further purification, these samples will also contain cellular detritus which will also contribute to the overall composition of the sample. Analysing the virion proteome would therefore be considerably easier if, before enrichment, as much cellular debris as possible could be removed from the sample.

5.3.1 Removing cellular debris

Virions can be separated from cell debris by haemadsorption purification, a technique based on the principle that only HA+ material will bind red blood cells, and only NA+ material will elute from those cells (Francis and Salk, 1942). This method has recently been used to clarify samples for mass spectrometry (Hutchinson et al., 2014): it removes debris from infected cells and the chicken proteins it introduces into the sample can be identified by their unique protein sequences and filtered out of the results. However, these studies used predominantly spherical strains of influenza virus and it was unclear whether this method would be suitable for use with filamentous virions.

I performed a pilot experiment to test the impact of haemadsorption purification on filamentous virions. I incubated a sample of Udorn with chilled chicken red blood cells to al-

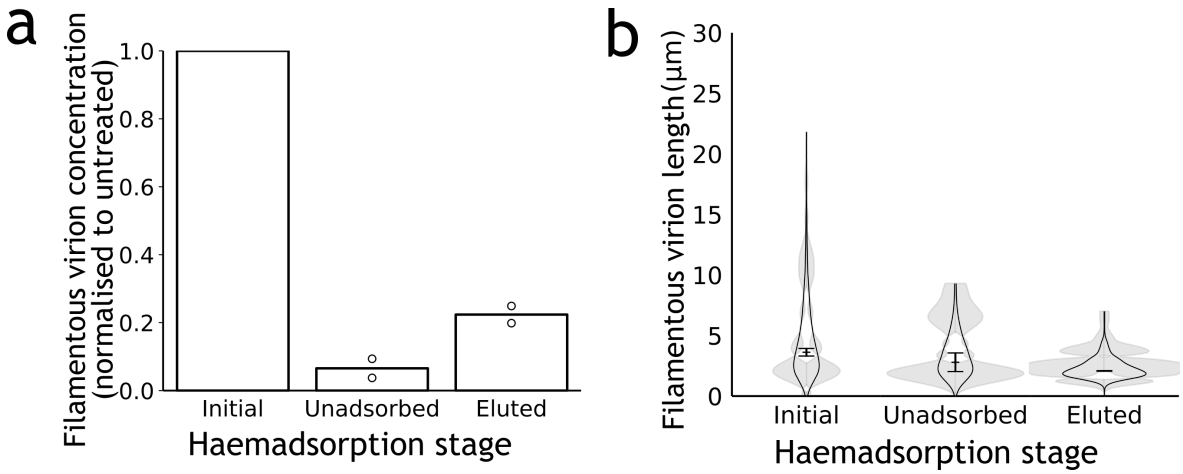

Figure 5.2: Haemadsorption purification alters the distribution of lengths of filamentous virions.

Filamentous virions were obtained by collecting supernatant from MDCK cells infected with influenza A/Udorn/307/72 (H3N2) for 24 hours. Samples were clarified, then mixed with chilled 0.5% chicken red blood cells and incubated at 4 ˚C for 30 minutes. Red blood cells were pelleted at 1250 *g*, washed, resuspended in prewarmed 1x PBS and incubated at 37 ˚C for 15 minutes before cells were again pelleted at 1250 g and discarded. “Initial” sample was taken from the initial population of virions, “Unadsorbed” sample was taken from the supernatant after the first pellet step, “Eluted” sample was taken from the supernatant after the final pellet step. Concentration and lengths of filamentous virions were measured using the confocal analysis pipeline described in Chapter 3. The number of filamentous virions were calculated for each sample. Column indicates mean, whiskers indicate range (two independent experiments). (b) A frequency distribution of filament length was calculated for each sample. The violin plot indicates the mean frequency distribution, with the 95% CI shaded in grey. The median filamentous virion length was also calculated for each repeat, with the mean and range of these median lengths indicated by a line and whiskers (two independent experiments).

low HA-mediated adsorption, then pelleted the cells and discarded the supernatant. I then resuspended and warmed the cells to allow NA-mediated elution, before pelleting the cells again and retaining the supernatant. The remaining material should therefore be both HA+ and NA+. At each step, I assessed the concentration and length distributions of the filamentous virions in the supernatant.

I found that nearly 90% of filamentous virions adsorbed to the red blood cells in the initial step, but only 20% of the initial population successfully eluted from the red blood cells (Figure 5.2a). Furthermore, the eluted filamentous virions were substantially shorter than the virions in the initial sample, with a median length of 2.1 µm (Figure 5.2b) compared to an initial median length of 3.6 µm. This suggested the longer virions were less able to elute. As it was unclear whether longer filamentous virions had different compositions to the shorter filamentous virions, haemadsorption therefore altered the virion population in an unpredictable way, so any analysis of their composition could be skewed. Therefore, I decided to preserve the virion population by not including a haemadsorption step in subsequent experiments, noting that this would be at the cost of leaving cell debris in the samples.

5.3.2 Separating virions with size filters

The biochemical differences between filamentous and non-filamentous virions are unknown, so any method to separate them must depend on their physical properties. As the size difference between the types of virion is so large, I reasoned that passing virions through a size filter could provide a quick method to separate virions by morphology. Morphology enrichment by filtration has been described (Donald & Isaacs, 1954a), so it was a feasible approach. However, when I passed unconcentrated samples through a 0.22 µm centrifuge filter, the filter became blocked and very little material was able to pass through. While it may have been possible to optimise this method to avoid this issue (for example, using a cross-flow concentrator, (“Crossflow cassette systems”, 2016)) , I reasoned that it would likely be even more severe when using the highly concentrated samples necessary for mass spectrometry, and so I decided to explore alternative approaches.

5.3.3 Separating virions with density gradients

Almost all attempts to separate filamentous and non-filamentous virions have been based on centrifugation. The velocity of a spherical particle undergoing centrifugation can be described by the equation:

$$\frac{dr}{dt} = \frac{2r_p^2(\rho_p - \rho_m)\omega^2 r}{9\eta} \tag{5.1}$$

where $\frac{dr}{dt}$ is the velocity of the particle, r_p is the radius of the particle, $(\rho_p - \rho_m)$ is the buoyancy caused by the different in density between the particle and the medium, ω is the angular momentum, r is the radial distance of the particle from the axis of rotation, and η is the viscosity of the medium.

This equation assumes the particles are spherical, but non-spherical particles have a higher frictional coefficient than spherical particles which increases drag and reduces velocity. This can be accounted for by modifying the equation thus:

$$\frac{dr}{dt} = \frac{2r_p^2(\rho_p - \rho_m)\omega^2 r}{9\eta(f/f_0)} \tag{5.2}$$

where f is the frictional coefficient of the particle and f_0 is the frictional coefficient of a sphere (Rickwood, 1984).

Equation 5.2 suggests it should be possible to separate filamentous and non-filamentous virions based on their different velocities during centrifugation, as filamentous virions are much larger and so r_p is greater, though this will be counteracted to some extent as filamentous virions are far less spherical than non-filaments, and so (f/f_0) will also be greater. This is complicated, however, by suggestions that filamentous and non-filamentous have different densities (Smirnov et al., 1991), meaning that ρ_p may also vary and could further counteract differences in velocity caused by size.

One way in which this difference could be exploited is differential pelleting, based on the principle that the largest particles will move fastest through the medium during centrifugation and so will preferentially pellet at the base of the tube (this principle also underlies the clarification by centrifugation described in Chapter 4). However, the force necessary to pellet the largest particles at the top of the tube will often be sufficient to pellet the smaller particles near the base of the tube, leading to co-sedimentation of different particle types. It is therefore difficult to achieve a totally pure population of large particles, though purity can be improved by using repeated centrifugation cycles (Rickwood, 1984). This approach has been used by Ada et al. (1958), working with an initial sample of the Ryan strain which was ~20% comprised of filamentous virions, to produce one sample ~50% comprised of filamentous virions and another ~98% comprised of non-filamentous virions. Near identical results were obtained 74 years later by Li et al. (2021), using a variant of Udorn, yielding one sample 47.2% comprised of filamentous virions and another 94.9% comprised of non-filamentous virions.

An alternative method, that avoids the problem of co-sedimentation, is rate-zonal centrifugation. In this method, a sample is layered on top of a density gradient before centrifugation. Larger particles move through the gradient faster than smaller particles, so, if the centrifuge is stopped before any particles reach the bottom of the tube, particles will aggregate in layers throughout the gradient based on their size. In this procedure, the density

gradient is used to limit convection currents that may disrupt the layers of particles, and to encourage tighter layering by slowing particles that migrate further through the gradient (Rickwood, 1984). This style of separation was used by Roberts et al. (1998), and electron microscopy evidence suggested it was effective, though detailed particle counts were not reported. Their method was used by subsequent studies (Liu et al., 2002; Sieczkarski & Whittaker, 2005), with Sieczarski and Whittaker reporting a sample 92% comprised of filamentous virions, and one 8% comprised of non-filamentous virions (though they began with an unusually filamentous mutant of Udorn, which was 28% comprised of filamentous virions).

A third centrifugation approach is to separate particles on the basis of density rather than size, a process known as isopycnic centrifugation. As with rate-zonal centrifugation, this involves layering a sample on top of density gradient. However, this time, the lower regions of the gradient are denser than any particle contained in the sample and the centrifuge is run for much longer, so that each particle has time to migrate to its equilibrium position. In this manner, the particle velocity, and therefore particle size, is irrelevant (Rickwood, 1984). This technique has been used by Smirnov et al. (1991) to create a sample ~68% comprised of filamentous virions, and one which was 98.8% comprised of non-filamentous virions.

Of the three methods, differential pelleting seemed the least appropriate for generating samples to analyse composition, as it generated the samples with the lowest enrichment for filamentous virions. Repeated pelleting would also likely leave large cell debris mixed with the filamentous virions that would be absent from the non-filamentous virions, skewing the compositional analysis. Rate-zonal centrifugation seemed like it could be effective, but Smirnov et al. (1991) reported difficulties with this method and anecdotal evidence suggests this method is hard to replicate. I therefore decided to attempt separation using isopycnic centrifugation, which seemed likely to yield samples with high proportions of filamentous virions, without the issues associated with the other two methods.

Effective isopycnic separation would be easiest if the density gradient closely matched the distribution of virion densities for Udorn, as this would give them the most space to spread out. Comparative densities of filamentous and non-filamentous had not been described for Udorn, so it was not immediately possible to rationally design a density gradient. Furthermore, it has been suggested that ultracentrifugation can deform spherical influenza virions (Sugita et al., 2011) but its impact on filamentous virions is unknown. Enriching by morphology with isopycnic centrifugation therefore required first determining the range of densities of Udorn virions, then testing the method to see whether it could separate virions by morphology, and finally testing the method to determine whether separation yields virions in a state suitable for analysis.

5.3.3.1 Determining virion density

As a starting point for assessing virion density, I used a density gradient previously used to clarify samples for mass spectrometry (Hutchinson et al. (2014), though this study effectively used rate-zonal centrifugation due to a short centrifugation time). This gradient was made with iodixanol rather than sucrose, as iodixanol is isosmotic with influenza virions and so less likely to cause damage (Hill et al., 1994). I prepared a highly concentrated stock of Udorn by infecting confluent MDCK cells in 800 cm^2 roller bottles at an MOI of 0.001, incubating for 96 hours, and then concentrating the culture medium by ultracentrifugation for 90 min at 4 °C at 116,000 *g*.

I overlaid this sample on a 10-35% iodixanol gradient and ran it at 210,000 *g* overnight to allow the sample time to equilibrate. This yielded a gradient containing a clear white band, which past data show contains the bulk of the non-filamentous virions (Hutchinson et al., 2014) (Figure 5.3a). However, from observing the gradient with the naked eye, it was not obvious where the filamentous virions were located.

To locate the filamentous virions, I split the gradient into fractions by puncturing the base of the ultracentrifuge tube and collecting the flow-through into separate containers. I assessed each fraction with the confocal analysis pipeline described in Chapter 3. To calculate the density of the virions, I ran a parallel gradient containing no virions and assessed the density of each fraction by refractometry (Figure 5.3a). I then repeated this with a range of different density gradients (10-35% iodixanol, 15-30% iodixanol, 20-30% iodixanol) and calculated the abundance of filamentous virions and their density in each fraction. A plot of this data showed that filamentous virions had a density range of 1.1 - 1.2 g/ml, with most between 1.12 and 1.23 g/ml (Figure 5.3b).

Estimating the density distribution of the non-filamentous virions was more difficult, as they were both mixed in with the filamentous virions and hard to detect reliably with the confocal analysis pipeline. However, I reasoned that if I performed similar experiments using the almost exclusively non-filamentous WSN strain, then I would be able to determine the virion distribution by measuring the distribution of M1 within the gradient by western blot. These experiments showed the distribution of WSN virions peaked at approximately 1.14 g/ml (Figure 5.4), slightly denser than the filamentous Udorn virions. While the non-filamentous virions of Udorn may have different properties to those of WSN, I reasoned they were likely to be similar enough to use this value as a starting point for attempting virion separation. I therefore concluded that a 1.1 – 1.2 g/ml gradient, equivalent to 20% - 30% iodixanol, was likely to cover the full range of Udorn virion densities, and so was a sensible range to begin attempting virion separation.

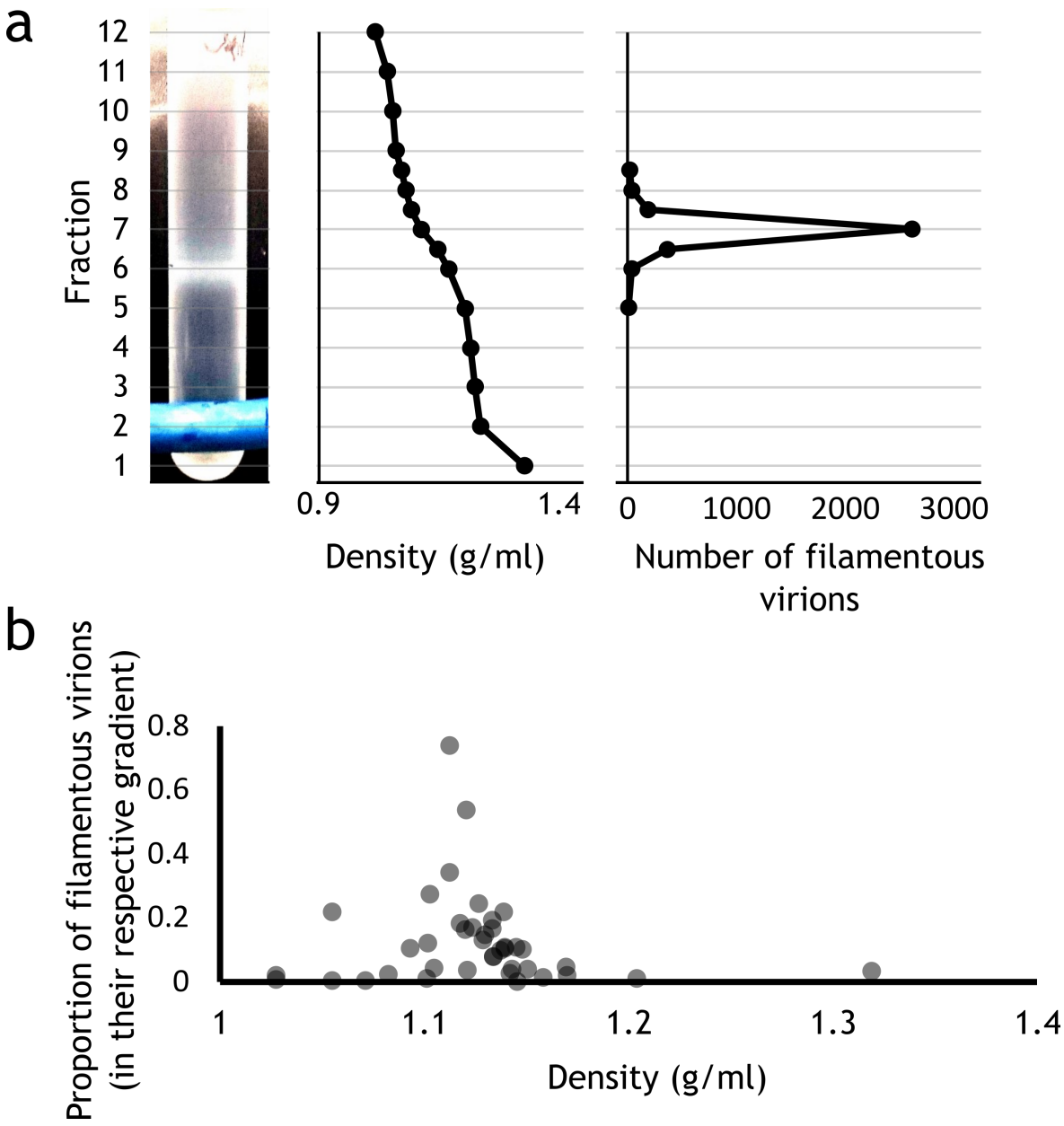

Figure 5.3: The density of range of filamentous virions.

Filamentous virions were obtained from the supernatant of MDCK cells that had been infected with influenza A/Udorn/307/72 (H3N2) for 96 hours, and concentrated by ultracentrifugation. (a) Virions were purified with a 10-35% iodixanol gradient overnight by ultracentrifugation at 4 °C at 21,000 *g*. A past study suggests the thick white band approximately halfway down the tube comprises non-filamentous virions (Hutchinson et al., 2014). A mock-infected control sample was separated on a 10-35% iodixanol gradients and split into fractions by puncturing the base of the tube and collecting the flowthrough in separate containers. The density of each fraction was calculated by refractometry. In parallel, the virus-infected sample was split into fractions and the number of virions was determined using the confocal analysis pipeline described in Chapter 3. (b) The process described in (a) was repeated with various gradients (10-35%, 15-30%, 20-30% iodixanol). Data from the three experiments were pooled, and the proportion of filamentous virions in each fraction was plotted against the density of the parallel fraction.

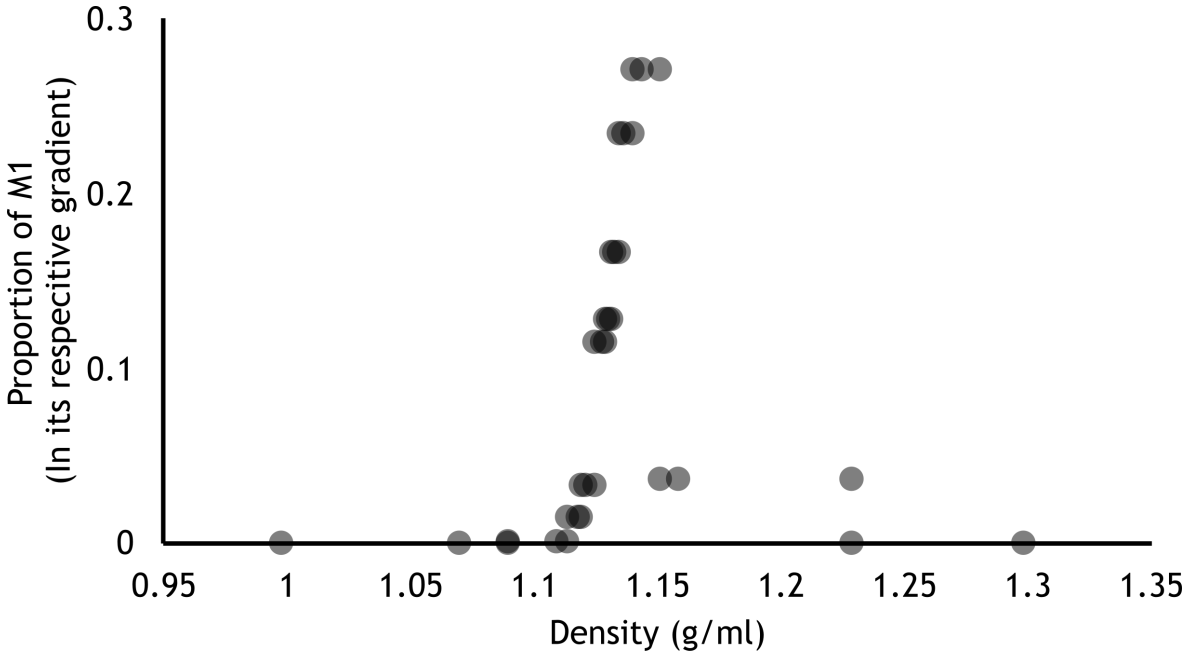

Figure 5.4: Density range of non-filamentous WSN virions.

Non-filamentous virions were obtained from the supernatant of MDCK cells that had been infected with influenza A/WSN/1933 (H1N1) for 96 hours, and concentrated by ultracentrifugation. Virions were purified with a 20-30% iodixanol gradient overnight by ultracentrifugation at 4 °C at 210,000 *g* and the sample was split into fractions by puncturing the base of the tube and collecting the flowthrough in separate containers. M1 abundance for each fraction was determined by western blot, and the density of each fraction was calculated by purifying a mock-infected sample in parallel and measuring the refractive index of each fraction with refractometry. Graph shows pooled data from three independent experiments.

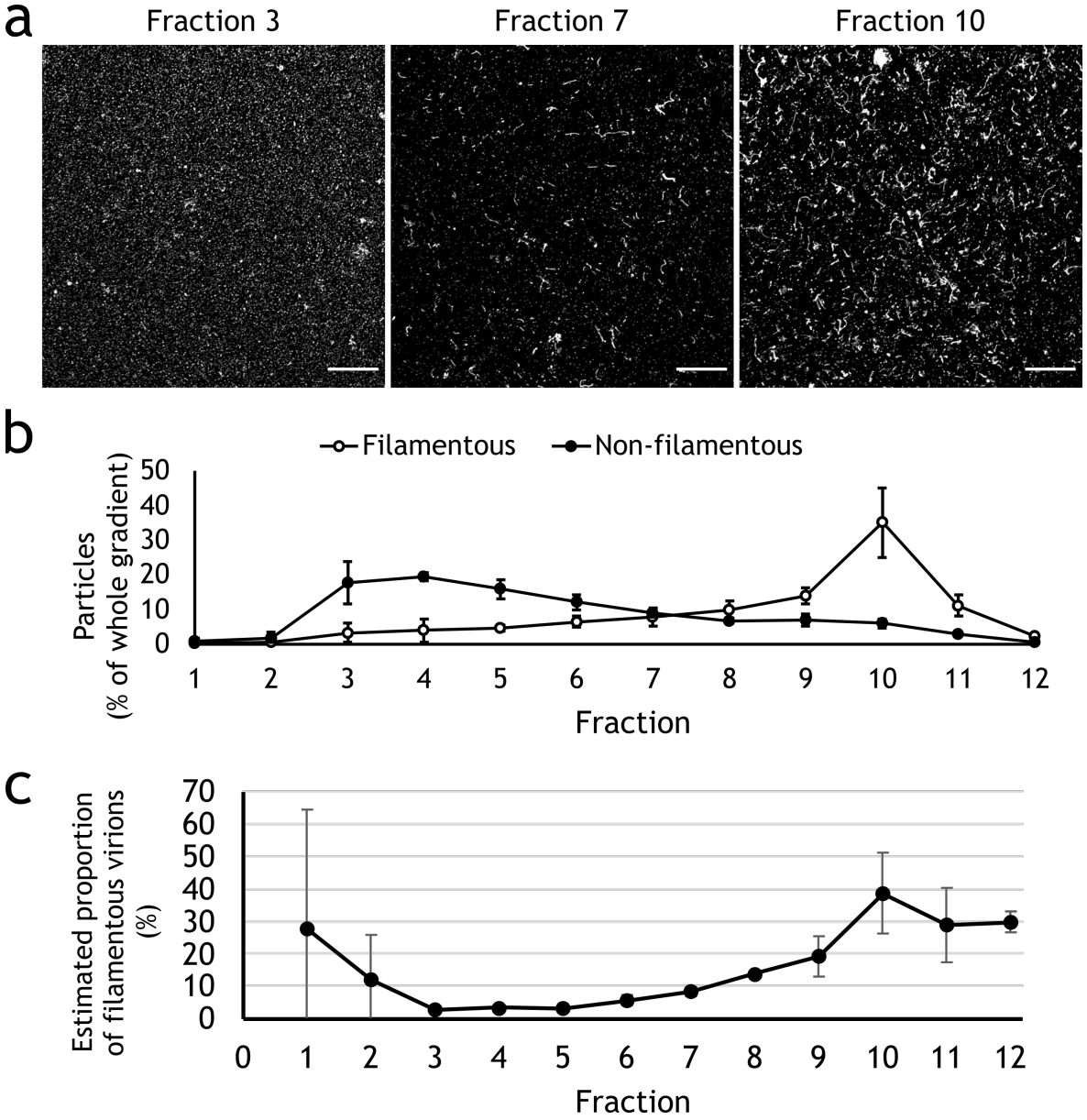

Figure 5.5: Isopycnic centrifugation can separate filamentous and non-filamentous virions.

Filamentous virions were obtained from the supernatant of MDCK cells that had been infected with influenza A/Udorn/307/72 (H3N2) for 96 hours, and concentrated by ultracentrifugation. Virions were purified with a 20-30% iodixanol gradient overnight by ultracentrifugation at 4 °C at 210,000 *g* and split into 12 fractions by puncturing the base of the tube and collecting the flowthrough in separate containers. (a) Samples from each fraction were centrifuged onto coverslips, and haemagglutinin was immunostained to identify virions. Images were captured at 63x magnification by confocal microscopy, scale bar 10 μm. (b) Filamentous virions were quantified using the analysis pipeline described in Chapter 3. Non-filamentous virions were detected by using Analyse Particles to count particles with empirically determined parameters of a circularity > 0.9 and an area between 0.03 and 0.1 μm^2 (implemented with the custom ImageJ Macro BatchSphereAnalysis.ijm). Values for each fraction were expressed as a proportion of the total particles of that morphology counted in the gradient. Points indicate the mean abundance measured in each fraction, whiskers indicate s.d. (three independent experiments, except for Fraction 3 where one coverslip was unusable due to a technical problem). (c) The data described in (b) were used to plot the abundance of filamentous virions as a proportion of all virions detected in each fraction.

5.3.3.2 Enriching samples by morphology

To test how well this gradient design could separate filamentous and non-filamentous virions, I separated a highly concentrated Udorn sample over the gradient and assessed each fraction with confocal microscopy (Figure 5.5a). During this process, I noticed that the number of small circular particles, some of which should be non-filamentous virions, in each fraction varied considerably. While it was not possible to determine which of these were virions and which were HA+ cell debris, I reasoned that the concentration of these particles was likely to correlate with the concentration of non-filamentous virions. Measuring the concentration of these particles, therefore, would allow me to infer the location of the non-filamentous particles in the gradient. From these micrographs, I observed that the distribution of filamentous and non-filamentous particles varied throughout the gradient, with filamentous virions peaking at Fraction 10 (in the less dense region of the gradient) and non-filamentous virions peaking at Fraction 3 (in the more dense region of the gradient) (Figure 5.5b). The estimated proportion of filamentous virions was 39% in Fraction 10 and 3% in Fraction 3 (Figure 5.5c), though these are likely to be underestimates assuming that many of the apparent non-filamentous virions are in fact cell debris.

To verify the effectiveness of the separation, I analysed Fractions 3, 7, and 11 using negative strain transmission electron microscopy (Figure 5.6a). By counting particles manually, I observed that estimates of the filamentous virion proportion made by confocal microscopy were slightly above that of electron microscopy for Fraction 3, but were almost half that of electron microscopy in Fractions 7 and 11 (Figure 5.6b). I was unable to acquire similar data for the fraction most enriched in filamentous virions, Fraction 10, due to time constraints. However, assuming a similar relationship between the proportion of filamentous virions estimated by confocal and negative strain electron microscopy as in Fraction 11, this suggested that Fraction 10 was ~75% comprised of filamentous virions.

Finally, I measured the infectious titre of each fraction by plaque assay. I found that most of the infectivity in the gradient was concentrated in the denser regions of the gradient, which contained few filamentous virions (Figure 5.7). The presence of infectious material demonstrates that this region of the gradient is enriched in non-filamentous virions, and so this finding supports the microscopy findings suggesting that virions are being separated by morphology.

Having calculated the proportion of the number of filamentous virions in each sample, it was then possible to infer the proportion of biomass in each fraction contributed by filamentous virions. The mean filamentous virion length in Fractions 3 and 10 was ~1.8 μm. This was likely to be a slight overestimate due to the presence of filamentous virions below the resolution limit of the microscope. The smallest filamentous virions detected were ~1.4 μm. Using the measured values of filamentous virion length as upper and lower bounds, and assuming non-filamentous virions have lengths of ~100 nm (Vijayakrishnan et al.,

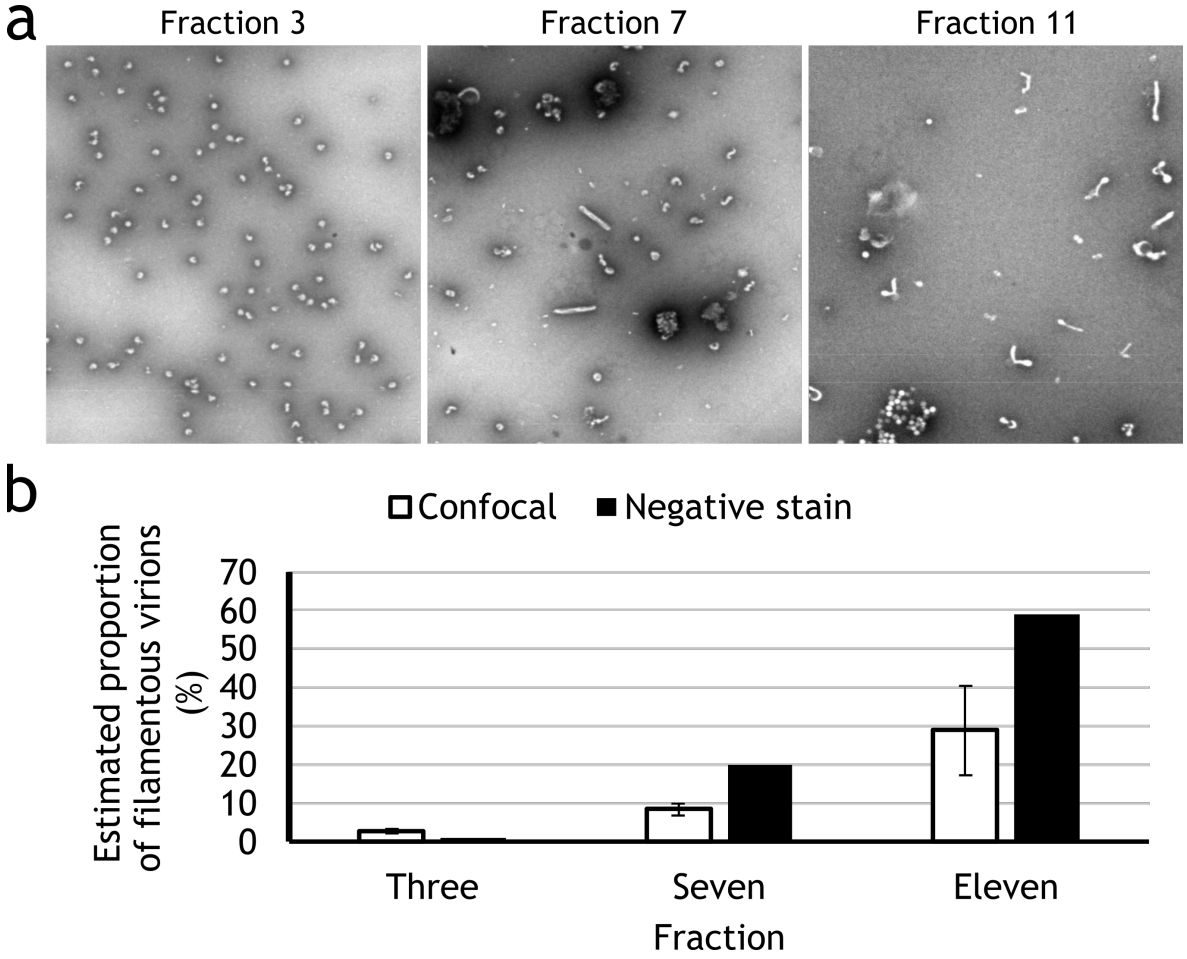

Figure 5.6: Negative stain electron microscopy confirms separation by isopycnic centrifugation.

Samples of filamentous virions were prepared as described in Figure 5.5. (a) To validate the apparent separation indicated by confocal microscopy, Samples were stained with 1% PTA and imaged on a JEOL 1200 transmission electron microscope. Magnification 20,000x. (b) The proportion of filamentous virions in fractions 3, 7, and 11 was determined by manual particle counting using the electron microscope (one independent experiment). Graph shows these values compared with the values determined by confocal microscopy in Figure 5.5c.

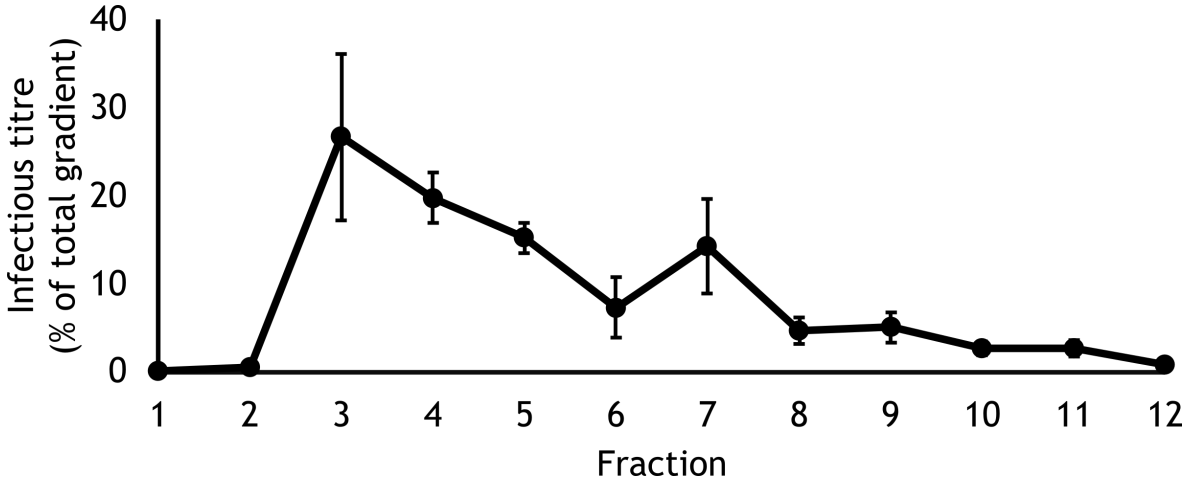

Figure 5.7: Distribution of infectivity in the density gradient.
To determine the distribution of infectivity in the density gradient following enrichment by morphology, the infectious titres of the samples generated in Figure 5.5 were measured by plaque assay. Points indicate mean infectious titre, normalised to the titre of the whole gradient, and whiskers indicate s.d. (three independent experiments).

2013), it can be assumed that filamentous virions are between 14 and 18x more massive than the non-filamentous virions in these samples. By combining these values with the proportional abundance of filamentous virions, using the estimates from confocal microscopy and negative stain microscopy as upper and lower bounds, a reasonable range for the proportion of the biomass contributed by the filamentous virions can be estimated. The proportion of the biomass contributed by filamentous virions was therefore 12–35% of Fraction 3, 54–82% of Fraction 7, and 90–98% of Fraction 10 (Figure 5.8). Even when selecting the most extreme of these values, it is reasonable to assume that the composition of Fraction 10 of this gradient will largely reflect the composition of filamentous virions, and the composition of Fraction 3 will largely reflect the composition of non-filamentous virions. Furthermore, the morphology contributing most of the biomass to these two fractions would also be the most abundant type of morphology as measured by particle count. Conversely, the biomass of Fraction 7 would be dominated by filamentous virions, but the particle abundance would be dominated by non-filamentous virions.

It is also noteworthy that there may be variation in composition within the two groups of virions, such that the filamentous virions in Fraction 10 and the non-filamentous virions in Fraction 3 may not be a representative sample. For the purposes of this study, I have assumed that the fraction with the most virions of either morphology is the most representative.

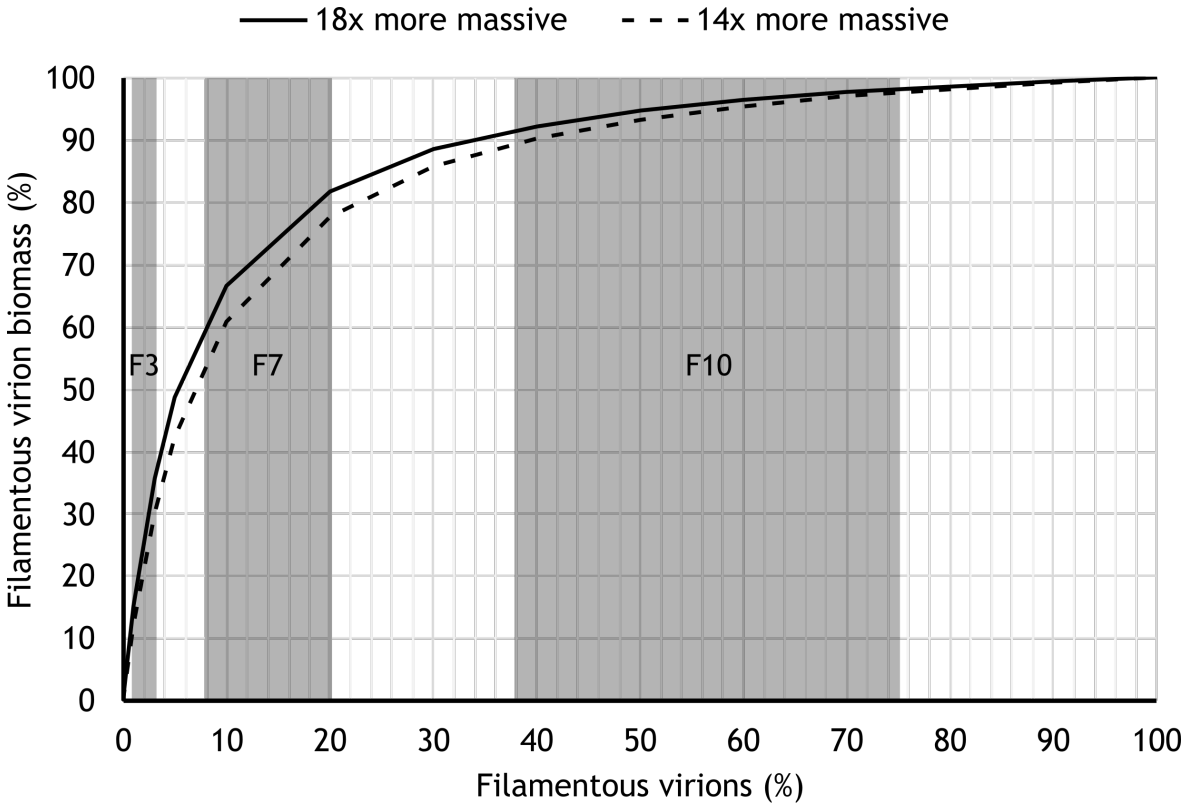

Figure 5.8: Estimating the biomass of filamentous virions in enriched samples. The estimated difference in mass between filamentous and non-filamentous virions was used to generate a curve showing how the percentage of biomass contributed by filamentous virions to a sample varied with the percentage of filamentous virions present. Non-filamentous virions were assumed to be 100 nm in length. The true mean filamentous virion length was assumed to be between 1400 nm (the minimum virion length detectable by the confocal analysis pipeline) and 1800 nm (the mean filamentous virion length measured from the samples in Figure 5.5). Shaded areas indicate the range estimated for the percentage of filamentous virions in Fractions 3, 7, and 10, using the confocal microscopy estimates and negative stain electron microscopy estimates from Figures 5.5 and 5.6 as upper and lower bounds.

5.3.3.3 Virion stability during enrichment

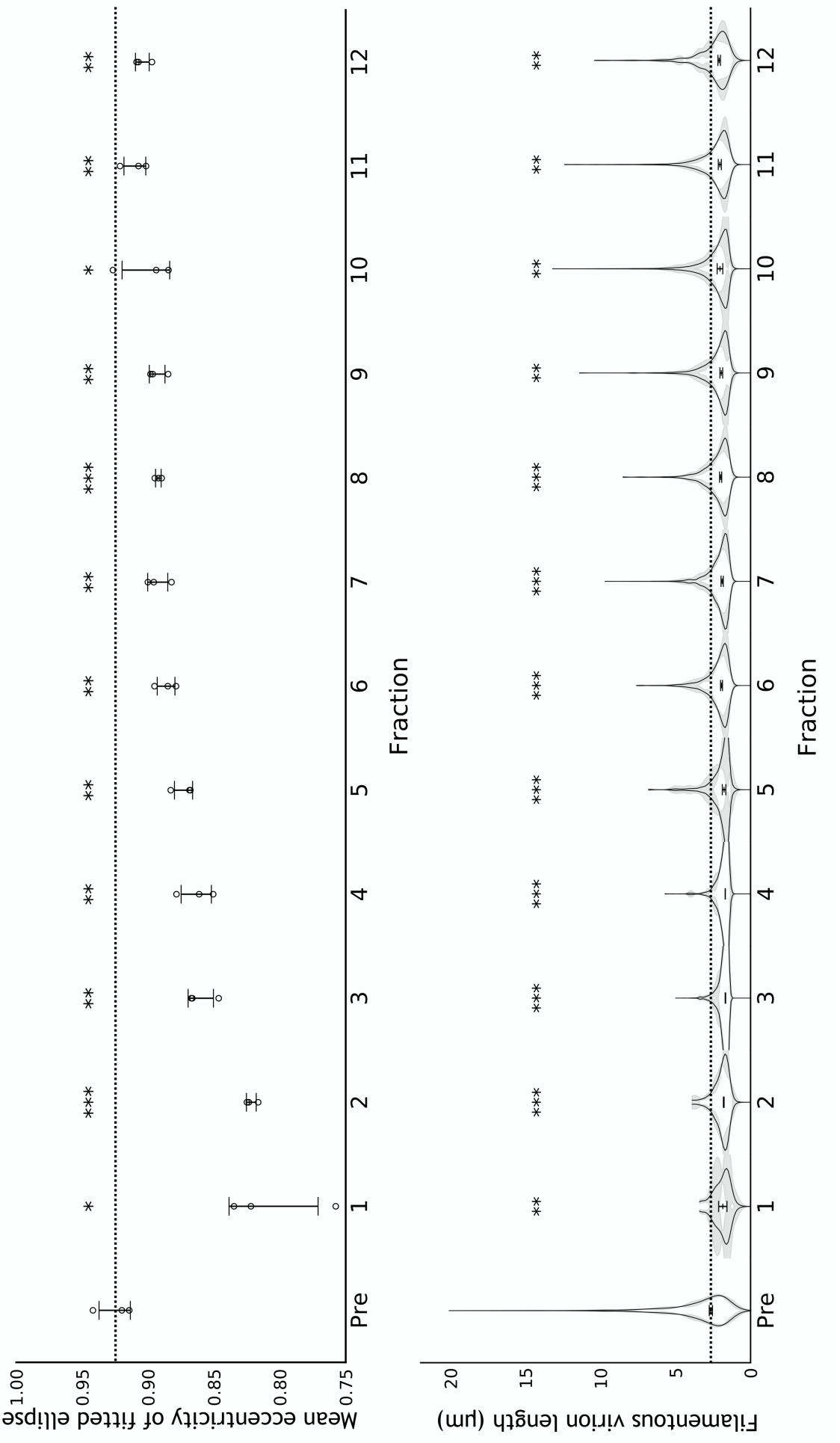

Figure 5.9: Enrichment can damage filamentous virions.

To determine whether the enrichment method damaged filamentous virions, the micrographs from Figure 5.5 were examined for signs of damage. (a) Ellipses were fitted to each filamentous virion, and the major and minor axes of these ellipses used to calculate the eccentricity. Mean eccentricities for each repeat are shown (three independent experiments, mean indicated by a line, s.d. as whiskers). Dashed line indicates the mean for unpurified samples (”Pre”). Comparisons to unpurified were made by two-tailed single-sample t-test: * $p < 0.05$, ** $p < 0.01$, *** $p < 0.001$. (b) Length distributions of filamentous virions were calculated with the confocal analysis pipeline described in Chapter 3. Distributions are shown as frequency distributions (mean, with 95% CI in grey) and distributions of the median filamentous virion length (mean position of the population median indicated as a line, s.d. of this as whiskers). The mean of the population medians for each fraction were compared to the untreated sample by two-tailed Student’s t-tests: ** $p < 0.01$, *** $p < 0.001$ (three independent experiments).

As detailed in Chapter 4, laboratory handling can cause inadvertent damage to filamentous virions. While ultracentrifugation has been reported to damage influenza virions (Sugita et al., 2011), no study has assessed the potential damage it causes to filamentous virions. As described in Chapter 4, apparent capsid damage was reflected by distortions to the filamentous virions, so I measured this by measuring the eccentricity of the fitted ellipses to the filamentous virions in each fraction. To test whether particular subclasses of filamentous virions were being removed during the purification I also measured the median length of the filamentous virions in each fraction of the gradient. I found that the eccentricity of the fitted ellipses was reduced throughout the gradient, though least severely in Fractions 10 and 11 ($p < 0.05$, Figure 5.9a). This distortion suggested filamentous virions were being damaged during purification. Similarly, the median length of the filamentous virions was reduced throughout the gradient and the population distributions of filaments skewed towards shorter lengths, so that no virions longer than 15 μm were detected ($p < 0.01$, Figure 5.9b). This suggested the longer virions were being destroyed or otherwise removed from the sample.

As the virions will in any case be denatured during proteomic analysis, any capsid damage would be unlikely to affect the analysis. However, the absence of longer filamentous virions could impact the results, if virions longer than 15 μm had substantial differences in their composition that those which are shorter. While it might therefore be beneficial to avoid this damage, I reasoned that the losses most likely occurred during the pelleting step of the protocol, as compressing virions onto the base of an ultracentrifuge tube is presumably more damaging that leaving them suspended in a density gradient. Omitting this step is not possible as compositional analyses require highly concentrated samples. I therefore concluded that this minor damage would be a limitation of this method, but it was required to produce concentrated samples separated by morphology. Overall, I concluded this method of enrichment would be suitable for compositional analysis.

5.4 Results III: Determining virion composition

5.4.1 Determining whether compositional differences can be detected

Before committing resources to mass spectrometry analysis, I wanted to verify that samples enriched for different virion morphologies had detectable differences in composition. Previous studies indicate that filamentous virions should have a much higher ratio of M1 to NP than non-filamentous virions (Iwatsuki-Horimoto et al., 2006; Liu et al., 2002; Roberts et al., 1998), as they are much larger but package at most one copy of the genome (Vijayakrishnan et al., 2013). I therefore predicted that the M1 to NP ratio would be much higher in the filamentous virion-enriched regions of the density gradient.

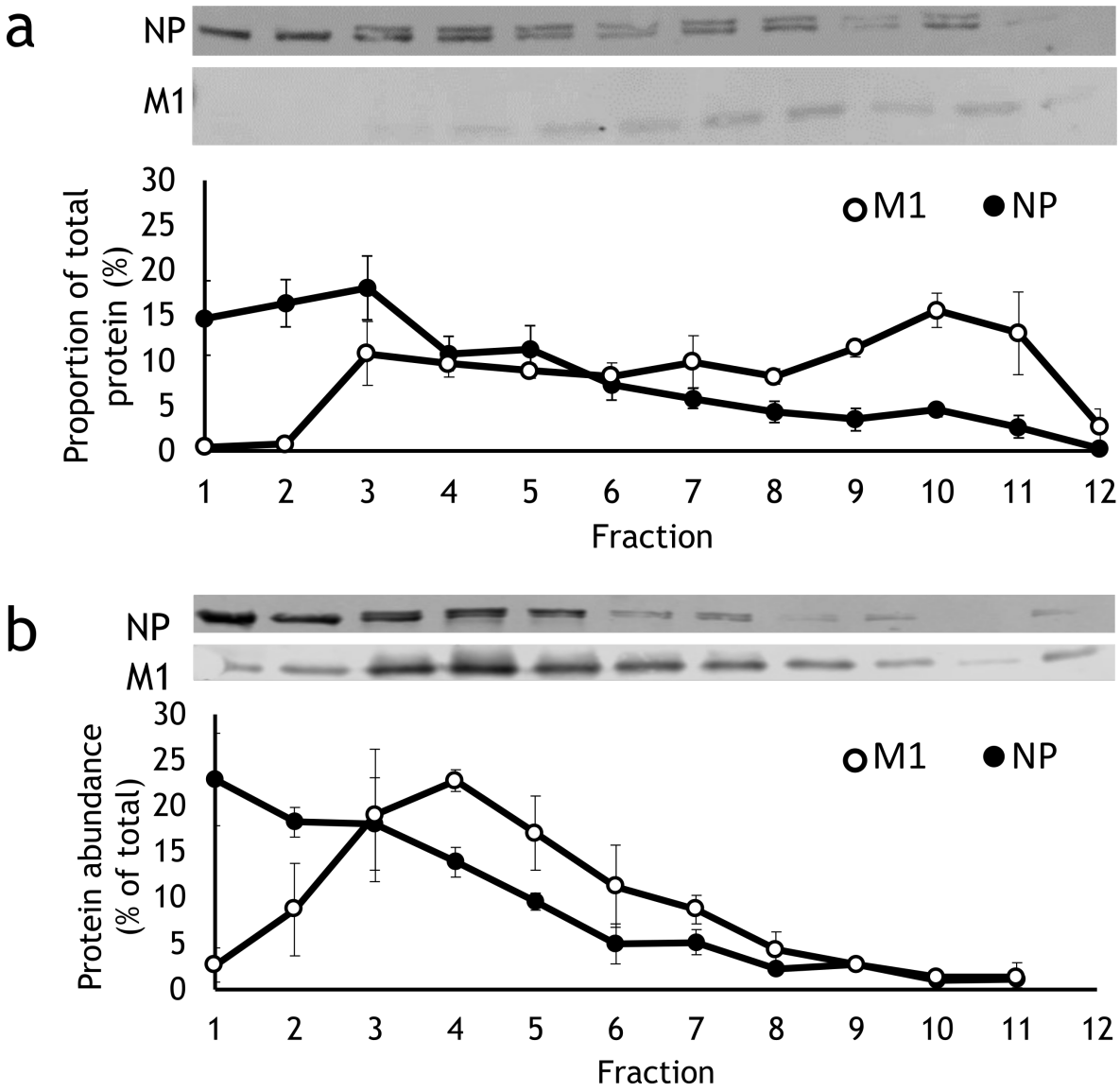

Figure 5.10: Samples enriched in morphology have detectable differences in composition. To determine whether the separation method could detect compositional differences in fractions enriched in a given morphology, virions were obtained from the supernatant of MDCK cells that had been infected with influenza A/WSN/1933 (H1N1) for 96 hours, and concentrated by ultracentrifugation. Virions were purified with a 20-30% iodixanol gradient overnight by ultracentrifugation at 4 °C at 210,000 *g* and the sample was split into fractions by puncturing the base of the tube and collecting the flowthrough in separate containers. Abundance of nucleoprotein (NP) and matrix 1 (M1) was measured by western blot for each fraction and normalised to the total signal across the whole gradient for (a) the pleiomorphic strain influenza A/Udorn/307/72 (H3N2) and (b) the predominantly spherical strain influenza A/WSN/1933 (H1N1). Points indicate mean, whiskers indicate s.d. (three independent experiments).

To assess the ratio of M1 and NP, I took the Udorn gradient fractions previously described and measured the abundance of these proteins by western blot. For comparison, I also measured M1 and NP from gradients prepared using the predominantly spherical virus strain, WSN. The ratio of M1 and NP varied throughout the gradient for Udorn, with the ratio of M1 to NP being much higher in the less dense fractions that were enriched in filamentous virions (Figure 5.10a). Conversely, I observed that M1 and NP abundance correlated closely throughout the gradient for WSN (Figure 5.10b), with the exception of Fractions 1 and 2 which are likely to be dominated by cell debris rather than virions (based on the confocal and infectivity analysis from the Udorn gradient, Figures 5.5 and 5.7). I concluded that virion composition does predictably vary with morphology, and so it was appropriate to proceed with the resource-intensive mass spectrometry analysis.

5.4.2 Measuring protein abundance with mass spectrometry

To analyse the full proteome of filamentous and non-filamentous virions, I sent samples of Fractions 3, 7, and 10 from the separation gradient to collaborators at the Target Discovery Institute in the University of Oxford for analysis by liquid chromatography and tandem mass spectrometry (LC-MS/MS) with a Q Exactive Mass Spectrometer. This analysis was then processed using MaxQuant.

As these samples had not undergone haemadsorption purification, there was likely to be cell debris in the samples whose composition might be mistaken for that of virions. To help identify the proteins introduced by cell debris, I also sent mock-infected samples for analysis along with the virus-infected samples. For each protein detected, I calculated the ratio of the protein abundance between Fractions 3, 7 and 10 (Figures 5.11, 5.12, 5.13). For each pair of fractions, if the ratio for the mock-infected samples was within tenfold of the ratio for virus-infected samples, the protein was removed from the analysis. This meant that the final analysis would not consider differences in protein abundance that could be readily explained by the presence of cell debris. This mitigation is only partial – it controls for debris shed by uninfected cells, but debris from infected cells will likely have a different abundance and composition and could contain viral proteins – but it does reduce the impact of cell debris when using samples that could not be purified by haemadsorption. The samples were also likely to contain contaminants introduced while preparing samples for mass spectrometry, including the trypsin used for sample digests and keratin from hair and skin flakes. These likely contaminants were removed from the analysis by filtering out the "common contaminants" list in MaxQuant.

Having controlled for debris, I then considered how to account for the different sizes of virion. As filamentous virions are much larger than non-filamentous, I considered it likely that they would typically package more of each protein. Furthermore, the largest filamentous virions detected in Fraction 10 were approximately ten times longer than the smallest

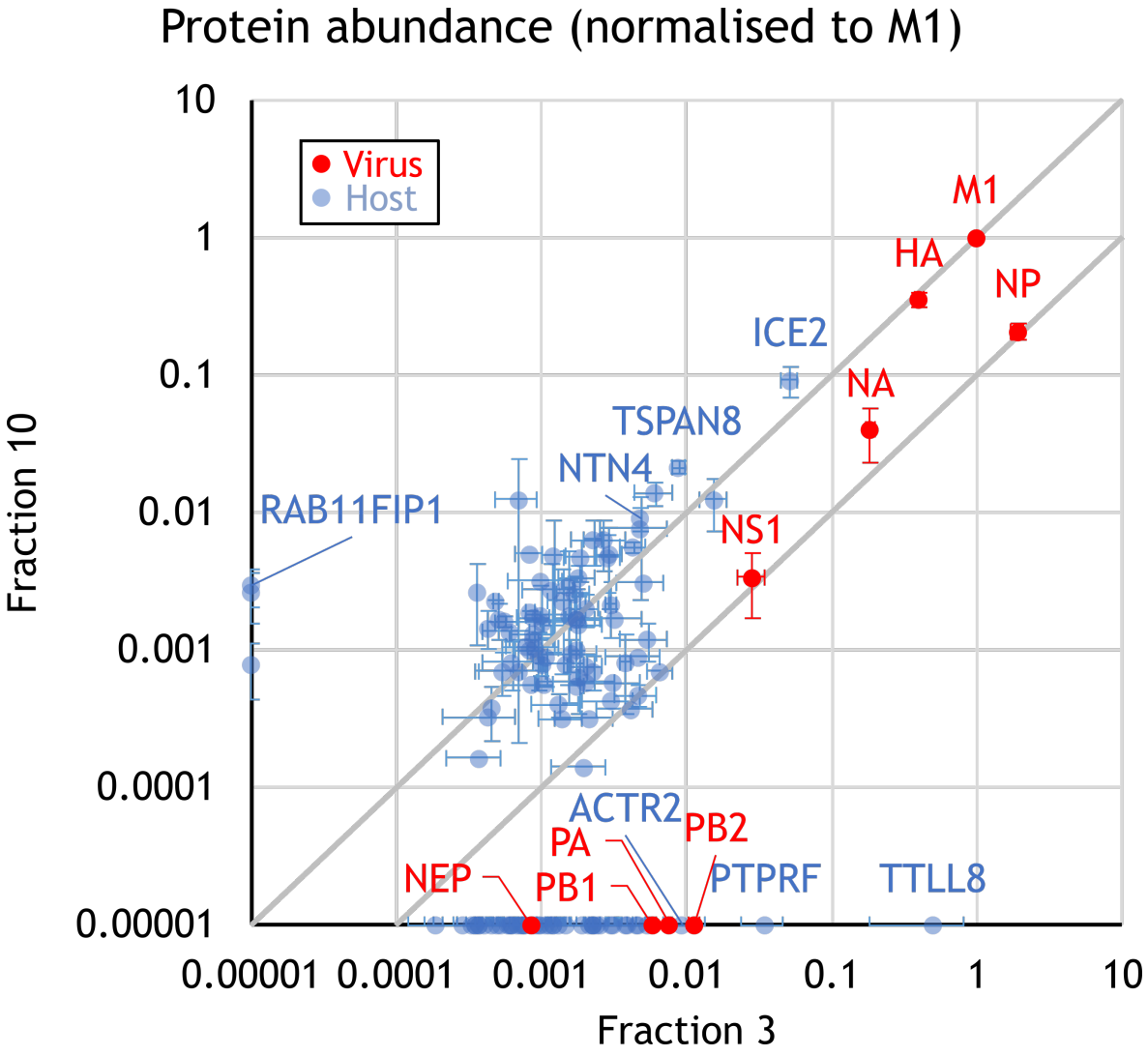

Figure 5.11: Mass spectrometry comparison of Fraction 3 and Fraction 10.

Virions were obtained from the supernatant of MDCK cells that had been infected with influenza A/WSN/1933 (H1N1) for 96 hours, and concentrated by ultracentrifugation. Virions were purified with a 20-30% iodixanol gradient overnight by ultracentrifugation at 4 °C at 210,000 *g* and the sample was split into fractions by puncturing the base of the tube and collecting the flowthrough in separate containers. Fractions 3 (predominantly non-filamentous) and 10 (predominately filamentous) were compared analysis by liquid chromatography and tandem mass spectrometry (LC-MS/MS) with a Q Exactive Mass Spectrometer. Proteins which were not detected in at least two of the three experimental repeats for at least one fraction were removed from the analysis. To account for cell debris, a parallel gradient was performed using a mock-infected sample and the ratio of the protein abundance between Fractions 3 and 10 was calculated. If this ratio for a given protein was within tenfold of the ratio calculated for the virus-infected samples, the protein was removed from the analysis. Points show mean protein abundance, normalised to M1, and whiskers show s.e. Proteins which were undetected in one fraction had their abundance set to the arbitrarily low value 0.00001 to allow them to be plotted on a log scale.

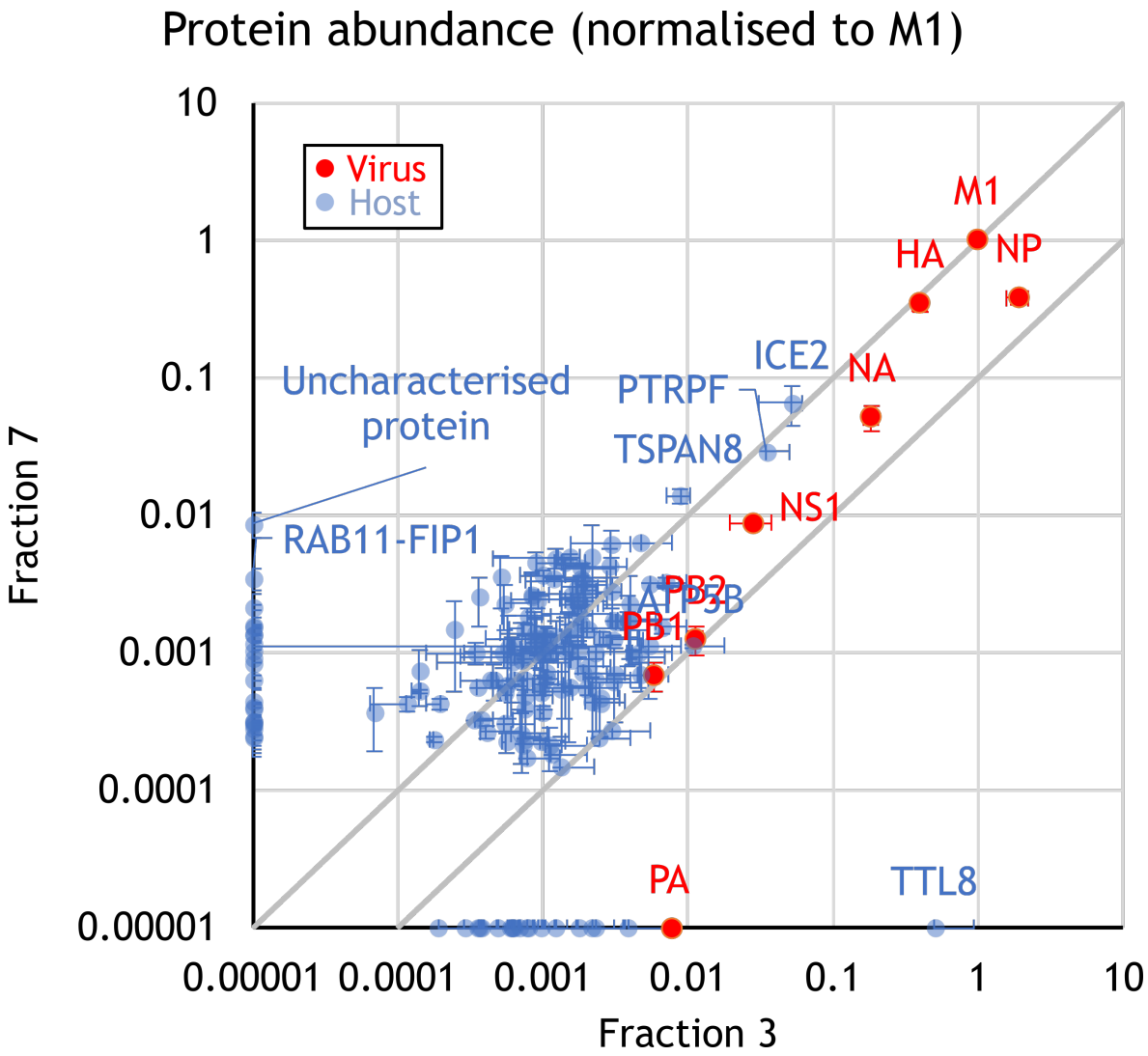

Figure 5.12: Mass spectrometry comparison of Fraction 3 and Fraction 7.
Samples were prepared and data were analysed as described for Figure 5.11, but comparing Fractions 3 and 7 instead of Fractions 3 and 10.

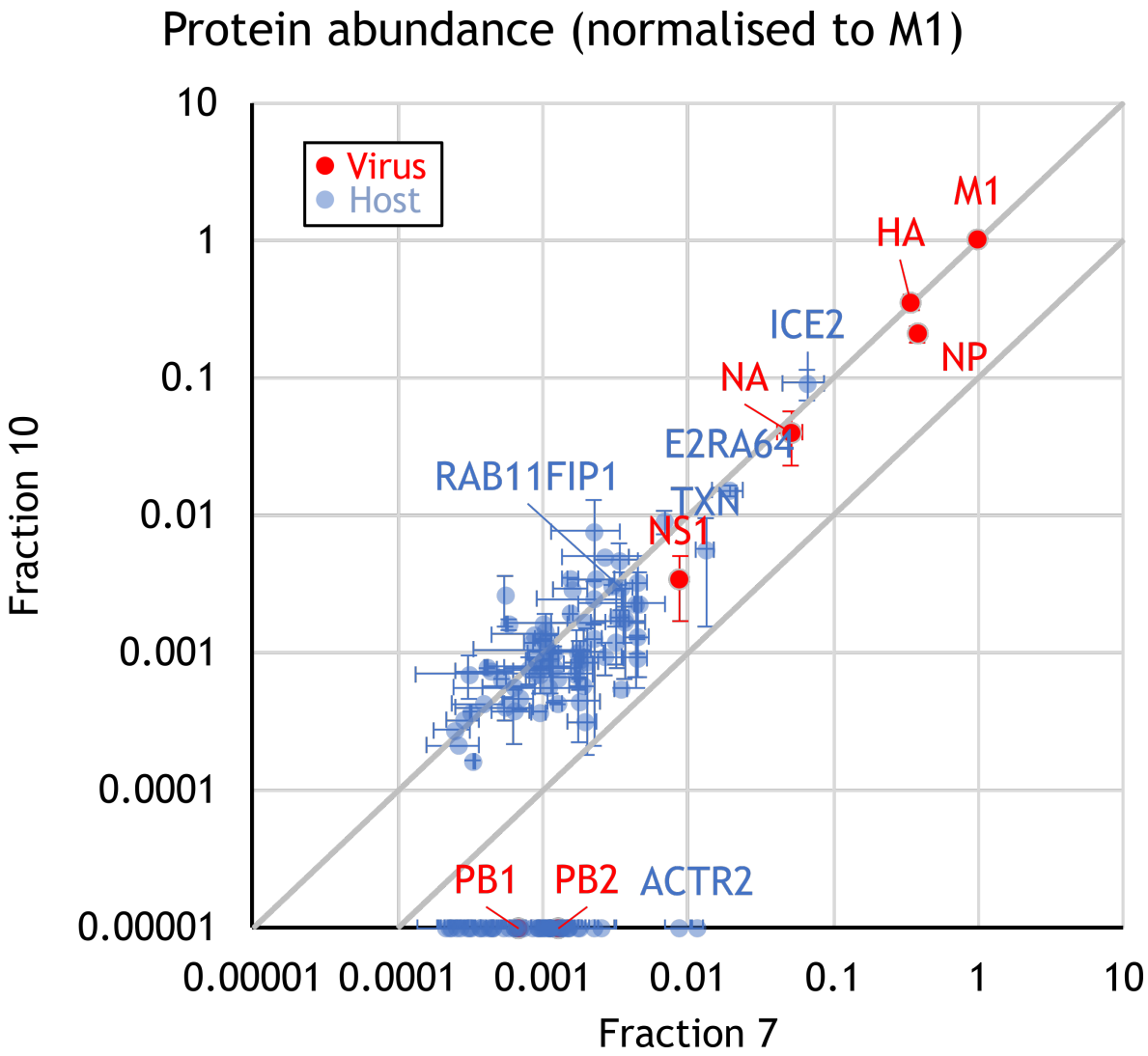

Figure 5.13: Mass spectrometry comparison of Fraction 7 and Fraction 10. Samples were prepared and data were analysed as described for Figure 5.11, but comparing Fractions 7 and 10 instead of Fractions 3 and 10.

(Figure 5.9b), so it would not be straightforward to determine a per virion copy number. Therefore the absolute abundance of proteins was unlikely to be of interest. Instead, when comparing filamentous and non-filamentous virions, it was of more interest to identify proteins whose relative abundance could not be explained simply by virion size. To assess this relative abundance, I normalised the abundance of each detected protein to M1, as M1 makes up the viral capsid and so is the most likely protein to scale directly with virion size.

After controlling for cell debris and virion size, I compared the protein composition of filamentous and non-filamentous virions. As I considered Fractions 3 and 10 to be the most representative of non-filamentous and filamentous virions respectively, most of the analysis focused on these two samples (Figure 5.11).

When considering host-derived proteins, only two were unique to Fraction 10, a small cluster were enriched in Fraction 3, but the great majority of were present at similar ratios regardless of virion morphology, Furthermore, almost all host-derived proteins were less abundant than the viral polymerase proteins (which had an abundance relative to M1 of ~0.001) in Fraction 3, which are the least abundant proteins that can be confidently predicted to be present in virions. These host-derived proteins are therefore unlikely to be highly abundant in virions. As polymerase proteins were not detected in Fraction 10, so a similar comparison cannot be made for this sample. The most abundant host-derived proteins, and the most abundant protein only identified in Fraction 10, are listed in Table 5.1.

Table 5.1: Abundant host-derived proteins present in Fractions 3 and 10.

Protein	Abundance in F3 (Relative to M1)	Abundance in F10 (Relative to M1)	Role
TTL8	0.496	Undetected	Tubulin modification
PTPRF	0.0347	Undetected	Signalling
ACTR2	0.009	Undetected	Actin regulation
ICE2	0.052	0.091	snRNA transcription
TSPAN8	0.009	0.021	Integrin binding
NTN4	0.005	0.009	Laminin-1 binding
RAB11FIP1	Undetected	0.003	Intracellular trafficking

Protein roles obtained from UniProt on the 27th March 2021.

Of these proteins, none have previously been linked to the functional properties of influenza virions. Rab11, and its binding proteins Rab11-FIP2 and Rab11-FIP3 are involved in trafficking NP to the plasma membrane and can influence morphology (de Castro Martin et al., 2017; Bruce et al., 2010), so it is plausible Rab11-FIP1 could affect viral morphology. However, these proteins regulate trafficking beneath the plasma membrane, so it is unclear how they would be incorporated into virions or how they could have any functional effects once there. For these reasons, and because the host-derived proteins were predomi-

nantly present in low abundance, I concluded they were unlikely to contribute to any functional differences between filamentous and non-filamentous virions.

Unlike host-derived proteins, the relative abundance of some viral protein clearly varied with morphology. HA abundance scaled directly with M1 abundance in all samples, but NA was reduced approximately fivefold in Fraction 10 compared to Fraction 3. This difference was still apparent when comparing Fractions 3 and 7, but absent when comparing Fractions 7 and 10. Assuming the biomass of Fractions 7 and 10 is dominated by filamentous virions and the biomass of Fraction 3 is dominated by non-filamentous virions, this is consistent with the relative abundance of HA and NA varying between filamentous and non-filamentous virions (Figure 5.8).

NP was reduced approximately tenfold in Fraction 10 when compared to Fraction 3. This difference was still apparent when comparing Fractions 3 and 7 but, unlike NA, NP abundance was still reduced in Fraction 10 compared to Fraction 7. The difference in the changes in NP and NA abundance may reflect Fraction 7 still containing more non-filamentous than filamentous virions, even though its biomass is dominated by the filamentous virions (Figure 5.8). As virions seem able to package, at most, one copy of the genome regardless of morphology (Vijayakrishnan et al., 2013; Halldorsson et al., 2021), it is reasonable to assume that NP abundance will be more strongly influenced by the number of virions rather than their mass, which would be consistent with these results. These data therefore suggest that NP is depleted in filamentous virions, but it is harder to determine whether this reflects differences in genome packaging or differences in virion size.

The polymerase subunits were not detected at all in Fraction 10, but they were only detected in low abundance in Fraction 3 and it is likely they are below the limit of reliable detection rather than completely absent. Indeed, PB2 and PB1 could be detected in Fraction 7, but were approximately tenfold less abundant than in Fraction 3 (Figure 5.12). It is therefore harder to draw conclusions about these proteins, but it seemed that their abundance scaled with NP, which is likely as they all form part of the RNP complexes.

NS1 was reduced fivefold in Fraction 10 compared to Fraction 3. This protein is not believed to be specifically packaged into virions (Hutchinson et al., 2014), and so it would be expected to scale with virion size like NA. However, unlike NA, NS1 was still depleted in Fraction 10 when compared to Fraction 7. NS1 is therefore depleted in filamentous virions, but it does not appear to scale directly with virion size.

Taken together, the data suggest all viral proteins except HA are depleted in filamentous virions relative to M1, though the mechanisms underlying this may vary between proteins that would be expected to scale with virion size (e.g. NA) and those that would not (e.g. NP).

This conclusion assumes that variation in composition is a direct consequence of variation in morphology. It is, however, possible that other factors that are indirectly associated with

morphology also have an effect. For example, the virions used here were grown over 96 hours and it is likely that the host cell proteome varies throughout infection. This variation could lead to compositional differences associated with morphology if virions of a different morphology were favoured at different times of infection. If this were the case the density gradient could effectively act as a time course, showing variation throughout a course of infection. Furthermore, microvesicles shed by infected cells contain viral proteins such as NP and NS1 (Hutchinson et al., 2014). If these microvesicles all had comparable densities to non-filamentous virions, they would aggregate at the same region of the density gradient and so their composition would be mistake for that of virions. This could explain why NS1 abundance does not appear to scale with virion size. Potential problems such as these mean that these findings are best treated as a foundation step and validated with further investigation.

5.4.3 Post-translational modifications

Having determined how the abundance of proteins varied with morphology, I then considered whether the post-translational modifications (PTMs) of those proteins also varied. To assess this, I took the mass spectrometry data from the previous section and filtered it to remove any protein that was not detected in at least two repeats in both Fraction 3 and Fraction 10. I then ran an analysis to detect PTMs in the remaining samples and compared the frequency of each modification of each protein. A total of 1819 sites across 208 proteins were considered. No clear pattern was observed: these data were very noisy, and no PTM of any protein stood out as varying with morphology more strongly than noise. Consequently, I could not conclude that PTMs vary with morphology.

5.5 Discussion

5.5.1 Summary

Here, I have shown that standard resolution confocal microscopy has limitations for assessing filamentous virion composition in detail, but is invaluable in the rational design of gradient purification methods to enrich samples for a given morphology. Mass spectrometry comparisons of these enriched samples suggested that most host-derived proteins and PTMs were either of a very low abundance or similar regardless of morphology, but all viral proteins expect HA are depleted in filamentous virions compared to non-filamentous virions.

5.5.2 Composition beyond the proteome

The work I have described here focuses purely on the proteome of virions, but factors such as the lipid content of virions or the glycosylation of proteins may also vary with morphology. Due to restrictions on time and access to the appropriate equipment and expertise, I was unable to assess these other aspects of composition during the course of this thesis, but I did use the procedures described above to provide samples to a collaborating group, which will be used in ongoing lipidomic and glycomic analysis.

5.5.3 Differences in composition may underpin differences in function

The relative depletion of most viral proteins in filamentous virions suggests possible effects on virion function. First, the depletion of NP and the polymerase relative to M1 may mean that filamentous virions are less infectious than non-filamentous virions. However, this apparent depletion may just be due to the much greater size of filamentous virions. For this to be true, the tenfold decrease in NP abundance would have to correlate with filamentous virions being, on average, ten times larger than non-filamentous virions. As discussed in Section 5.3.3.2, this is not far from my estimate that the filamentous virions in these samples are 14–18x larger than non-filamentous virions, but it is still below it. It is therefore a reasonable interpretation of these data that filamentous virions package less NP per virion than non-filamentous virions, consistent with single-particle observations of genome packaging in filamentous virions (Vijayakrishnan et al., 2013; Zhu et al., 2021; Vahey & Fletcher, 2019b). Second, the relative reduction in NA compared to HA suggests that the balance of activity between these two proteins varies with morphology. This, too, is consistent with single-particle observations of glycoprotein abundance (Calder et al., 2010; Vahey & Fletcher, 2019a,b). Indeed, the finding that larger filamentous virions do not spontaneously free themselves from adsorption to red blood cells (Figure 5.2) could be explained by filamentous virions having much more HA activity relative to NA activity. I therefore decided that my analysis of the functional differences between filamentous and non-filamentous virions would begin by investigating infectivity and glycoprotein activity.

As with analysing composition, analysing how virion function varies with morphology will depend on a method to separate filamentous and non-filamentous virions. I reasoned that the gradient purification method described here could enable functional comparisons of these types of virions. However, the damage that virions incur during this purification, while not affecting compositional analysis, could plausibly affect functional analysis. The methods developed in this chapter therefore provided a useful starting point for functional analysis, but needed to be adapted to avoid the problem of virion damage.

5.5.4 Conclusion

In conclusion, the methods developed in this chapter allowed the analysis of how virion composition varies with morphology. This in turn provided the necessary data to design a targeted study of how virion function varies with morphology. The technical issues associated with these compositional analyses mean they cannot be interpreted in isolation, and instead need to be validated by functional analysis. This integrative approach will help to overcome the drawbacks of any one method and place the characterisation of the roles of filamentous virions on a solid foundation.

Chapter 6

Functional comparison of filamentous and non-filamentous virions

6.1 Introduction

6.1.1 Investigating infectivity and glycoprotein activity

Function could vary with morphology in many ways. Here, I will focus on the two promising functional properties identified from the analysis of virion composition: infectivity and glycoprotein activity. By themselves, differences in these basic properties may not fully explain the role of filamentous virions – for example, if one virion morphology is more infectious than the other, then it raises the question of why influenza virus does not evolve to only produce virions of that morphology. However, understanding these basic properties of virions is a necessary first step before examining the more complex interactions between virions and their environment.

Many methods exist to examine infectivity and glycoprotein activity, but they need to be adapted due to the unique analytical problems caused by filamentous virions. The size difference between filamentous virions and non-filamentous virions must be considered, as some properties will likely scale with size, such as HA activity, whereas others will not, such as the number of cells a virion can infect. Care must be taken when comparing these two types of property. For example, comparing infectivity and HA activity could yield the seemingly interesting conclusion "filamentous virions have more HA activity per infectious unit than non-filamentous virions", but this would just reflect the trivial observation that "larger virions contain more proteins than smaller virions". Furthermore, the damage caused to virions by freezing constrains the use of many common methods of standardising experimental input, such as plaque titre or protein concentration, as these are typically performed after freezing several equivalent aliquots of a sample which can then be thawed for

use in separate assays. As inputs cannot be easily standardised, my analyses of virion function will measure multiple, related properties and examine the relationship between them rather than measuring the absolute value of just one.

6.1.2 Identifying an optimal system to assess virion function

Determining how functional properties vary with morphology requires a method to generate a predominantly filamentous sample and a predominantly non-filamentous sample. As discussed in the previous chapter, mutants that alter morphology are not suitable for this analysis, as the mutations may unpredictably affect other properties of the virion. Therefore, as with the compositional analysis, it is better to separate filamentous and non-filamentous virions from the same initial stock. However, functional analyses have additional requirements. First, functional properties do not necessarily scale with biomass, and so the non-filamentous virions present in samples enriched for filamentous virions cannot be considered negligible. For example, a filamentous virion may have twice the biomass of seven non-filamentous virions, but can only initiate $\frac{1}{7}th$ as many infections (assuming all the virions are fully infectious). Second, the non-filamentous virions present in both samples might have different properties which would be difficult to rule out experimentally. Third, once samples enriched for a particular morphology have infected cells, they will produce pleiomorphic progeny, so any experiments based on replication can only measure effects that occur during an initial viral replication cycle. Fourth, the damage caused by the purification methods described in the previous chapter may impact virion function, and so a less damaging purification method is necessary. These constraints must all be considered in order to design a protocol to enrich samples of virions for a functional analysis of different morphologies.

6.1.3 Conclusion

In this chapter, I describe a modified purification method that can produce samples suitable for functional analysis. Using these samples, I compared functional properties that were independent of absolute virion concentration and which did not require multi-cycle replication. To assess how infectivity varies with morphology, I compared how efficiently virions initiate productive infections. To assess how glycoprotein activity varies with morphology, I measured the HA and NA activity of virions and tested whether this variation is likely to affect the more physiologically relevant property of resisting mucus inhibition.

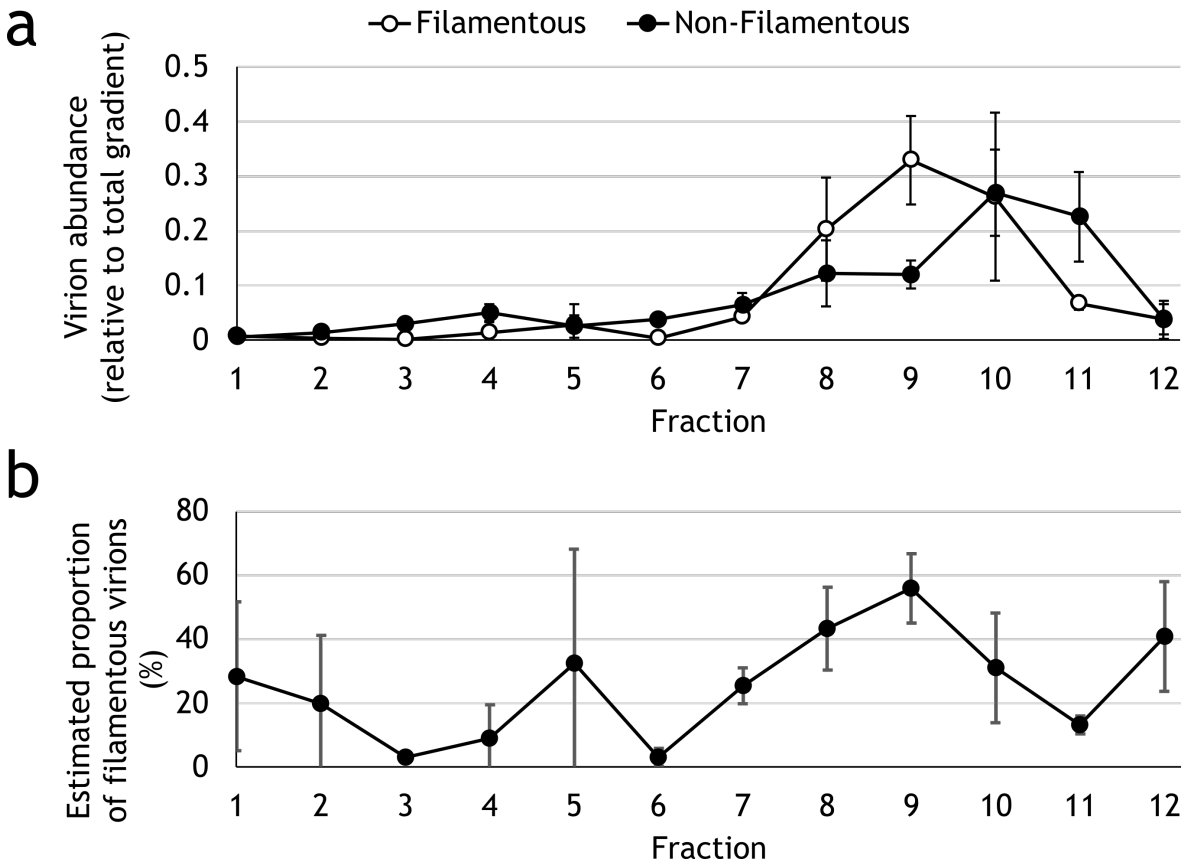

Figure 6.1: A low-yield gradient can enrich samples by morphology.

To determine whether the altered purification methodology could still enrich samples by morphology, virions were obtained by collecting supernatant from MDCK cells that had been infected with influenza A/Udorn/307/72 (H3N2) for 24 hours. Samples were clarified by centrifugation for 5 min at 1800 *g* at room temperature, then purified with a 20-30% iodixanol gradient overnight by ultracentrifugation at 4 °C at 210,000 *g* and the sample was split into 12 fractions by puncturing the base of the tube and collecting the flowthrough in separate containers. The abundance of filamentous virions was calculated using the analysis pipeline described in Chapter 3. Non-filamentous virions were detected by using Analyse Particles to count particles with empirically determined parameters of a circularity > 0.9 and an area between 0.03 and 0.1 μm^2 (implemented with the custom ImageJ Macro BatchSphereAnalysis.ijm). (a) Values for each fraction were expressed as a proportion of the total particles of that morphology counted in the gradient. Points indicate mean, whiskers indicate s.d. (three independent experiments). (b) The data described in (a) were used to plot the abundance of filamentous virions as a proportion of all virions detected in each fraction. Points indicate mean, whiskers indicate s.d. (three independent experiments).

6.2 Results I: Non-damaging virion enrichment

To develop a purification process that would minimise damage to virions, I modified the protocol described in the previous chapter. I reasoned that removing as many steps as possible from the protocol would minimise the opportunities for damage to occur. The previous protocol contained a pelleting step to generate high-concentration samples of virions, and I suspected that compressing virions against the base of an ultracentrifuge tube was the most likely step to cause damage. This step was previously necessary as the compositional analysis required high concentration samples, but most functional analyses do not. Therefore, instead of growing a high volume of virus over four days and concentrating it by ultracentrifugation, I prepared samples of virus grown for one day in a low volume of medium that could be applied to a density gradient directly. From that point I performed the protocol as previously described. To distinguish the two methods, I refer to the original method as “high-yield purification” and the updated method as “low-yield purification”.

Before checking whether low-yield purification reduced virion damage, it was first necessary to confirm that it could still enrich samples for different morphologies. To do this, I analysed the virions in each fraction of the gradient with the confocal analysis pipeline, collecting data both on the filamentous virions and the less robust data on non-filamentous virions (Figure 6.1a). The filamentous virions appeared to be distributed similarly in both high-yield and low-yield purification, though they peaked in Fraction 9 rather than Fraction 10 (likely because a higher volume of sample was added to the gradient, which will have diluted the upper fractions). However, the distribution of non-filamentous virions differed; in the low-yield purification there were substantially fewer detected, and their distribution was similar to that of the filamentous virions. Despite this difference, it appeared that the relative proportion of filamentous virions in each fraction still varied, with ~11% filamentous virions in Fraction 4 and ~56% in Fraction 9 (Figure 6.1b). As observed in the previous chapter, these are likely to be underestimates, though it was not possible to determine by how much as low-yield purification does not produce samples with a high enough concentration for electron microscopy. As the capacity of the confocal analysis pipeline to predict correlations with density and morphology had been validated in the previous chapter (Figure 5.6), I concluded that the confocal analysis pipeline results demonstrated that separation with a low-yield gradient had been successful.

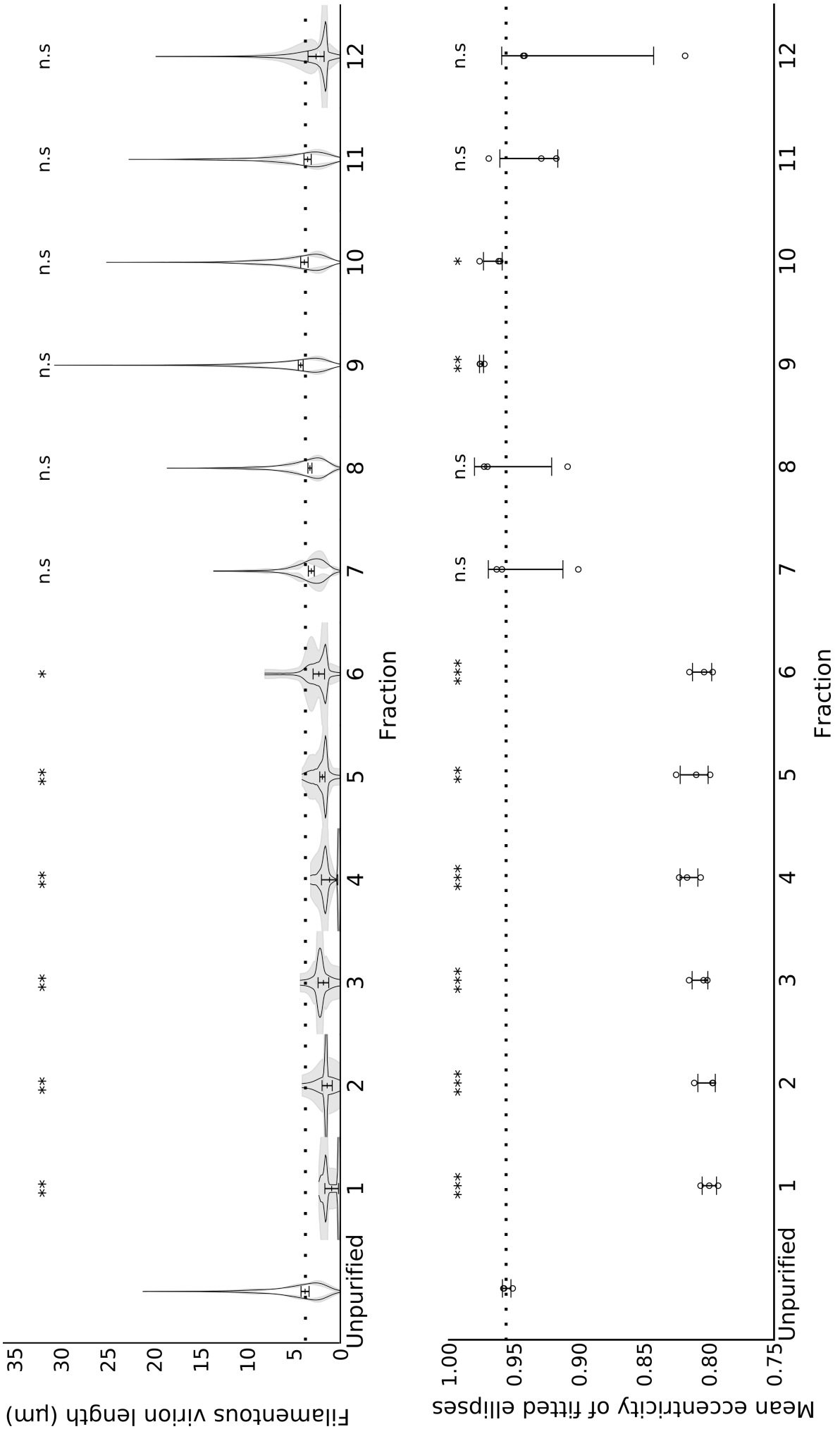
a
Filamentous virion length (µm)
0
5
10
15
20
25
30
35
Unpurified
1
2
3
4
5
6
7
8
9
10
11
12
Fraction
**
**
**
**
**
*
n.s
n.s
n.s
n.s
n.s
n.s
b
Mean eccentricity of fitted ellipses
0.75
0.80
0.85
0.90
0.95
1.00
Unpurified
1
2
3
4
5
6
7
8
9
10
11
12
Fraction
***
***
***
**
***
n.s
**
*
n.s
n.s
n.s
n.s

Figure 6.2: Omitting the pelleting step allows damage-free virion enrichment.

To determine whether the altered enrichment method damaged filamentous virions, the micrographs from Figure 6.1 were examined for signs of damage. (a) Length distributions of filamentous virions were calculated with the confocal analysis pipeline described in Chapter 3. Distributions are shown as frequency distributions (mean, with 95% CI in grey) and distributions of the median filamentous virion length (mean position of the population median indicated as a line, s.d. of this as whiskers). Dashed line indicates the mean for unpurified samples prepared separately but in an equivalent manner (”Unpurified”). The mean of the population medians for each fraction were compared to the unpurified sample by two-tailed Student’s t-tests: n.s $p > 0.05$, * $p < 0.05$, ** $p < 0.01$, *** $p < 0.001$ (three independent experiments). (b) Ellipses were fitted to each filamentous virion, and the major and minor axes of these ellipses used to calculate the eccentricity. Mean eccentricities for each repeat are shown (three independent experiments, mean indicated by a line, s.d. as whiskers). Dashed line indicates the mean for unpurified samples prepared separately but in an equivalent manner (”Unpurified”). Comparisons to unpurified were made by two-tailed single-sample t-test: n.s $p > 0.05$, * $p < 0.05$, ** $p < 0.01$.

To assess whether this method reduced damage to virions, I re-analysed the same micrographs and assessed the distribution of filamentous virions lengths and the eccentricities of their fitted ellipses. The median virion length was not substantially different between fractions 7 and 12 and an unpurified sample, suggesting longer virions were not removed during purification (Figure 6.2a, $p > 0.05$). Similarly, the eccentricities of the fitted ellipses were not substantially lower than unpurified in fractions 7 to 12 and were even slightly higher in fractions 9 and 10 (Figure 6.2b $p < 0.05$), which could be due to the reduced proportion of shorter particles in these two fractions. This suggested that filamentous virions were not being distorted and, together with the median length of the virions being maintained, suggested damage was not incurred during purification.

In conclusion, it appeared that the low-yield gradient could still enrich samples by virion morphology, though it was harder to be certain about the degree of enrichment than when using the high-yield gradient. I decided that this uncertainty was outweighed by the fact the process left the filamentous virions undamaged and presumably with their functional properties intact. Therefore, while caution would be needed if an assay suggested the samples were functionally identical (as this could mean the separation had not worked), I concluded that it was appropriate to use this protocol to look for differences in virion function.

6.3 Results II: Infectivity varies with morphology

6.3.1 Introduction

Before discussing how infectivity varies among virions, it is useful to clarify the relevant terminology. Here, “genome packaging” refers to the capacity of a virion to package any RNPs, even if the full set is not present. A defect in genome packaging would therefore lead to a virion completely lacking RNPs. “Genome bundling” refers to the capacity of a virion to package a full set of RNPs. Virions with defects in genome bundling would therefore contain some RNPs, but not the full set necessary to initiate an infection.

The first functional property I investigated was how infectivity varied with morphology. This was based on the finding that filamentous virions had approximately tenfold less NP than M1, which could suggest filamentous virions are less efficient at genome packaging or bundling. However, it is difficult to analyse the efficiency of genome packaging and bundling on a per virion basis. For example, when using microscopy (Vahey & Fletcher, 2019b; Vijayakrishnan et al., 2013; Zhu et al., 2021) the presence of RNPs does not necessarily indicate a complete genome is present, as some of the segments may be missing. When using bulk population analysis, finding that there is one gene segment present in a population per virion could mean all virions package that segment, or it could mean half of virions package two and half package none. Instead, I focused on whether the bulk differences I had observed in genome packaging in the previous chapter (based on abundance

of NP and the polymerase) affected the capacity of a population of virions to utilise those genomes.

6.3.2 The ratio of NP abundance to infectivity does not vary with morphology

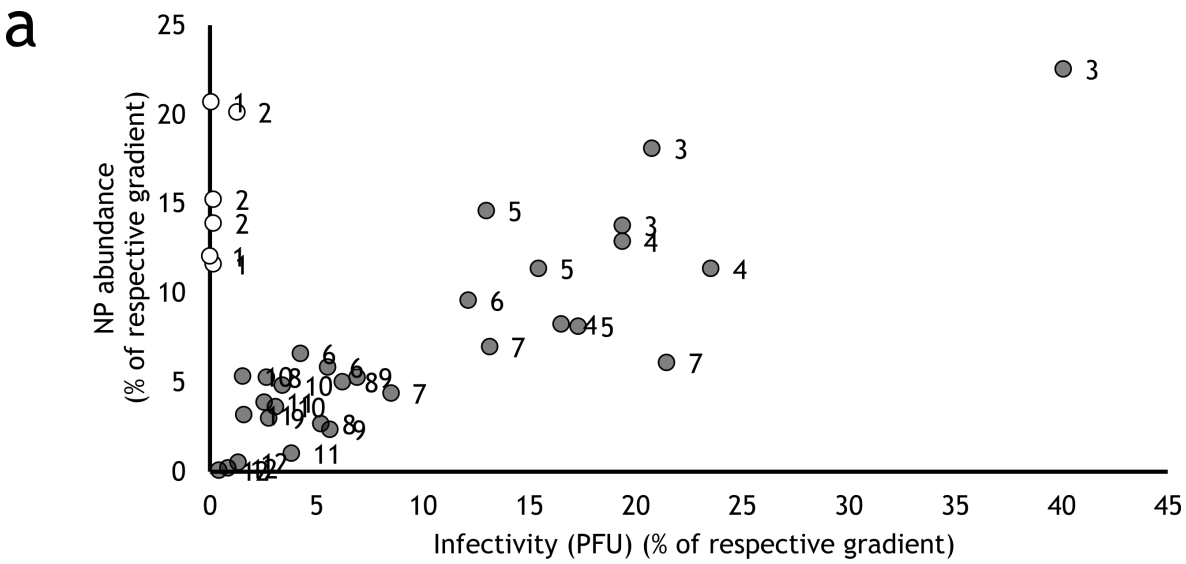

Figure 6.3: The ratio of NP abundance to infectivity does not vary with morphology
Virions were obtained from the supernatant of MDCK cells that had been infected with influenza A/Udorn/307/72 (H3N2) for 96 hours, and concentrated by ultracentrifugation. Virions were purified with a 20-30% iodixanol gradient overnight by ultracentrifugation at 4 °C at 210,000 *g* and split into 12 fractions by puncturing the base of the tube and collecting the flowthrough in separate containers. Abundance of nucleoprotein (NP) was measured by western blot for each fraction and normalised to the total signal across the whole gradient. Infectivity was calculated for each fraction by plaque assay, and normalised to the total infectious titre across the whole gradient. Graph shows pooled data from three independent experiments, with the numbers indicating the fraction number. White points indicate samples taken from fractions thought not to contain virions, based on the microscopy data from Figure 5.5 and western blot data from Figure 5.10.

If virions had defects in bundling, a higher proportion of RNPs would be present in virions that cannot initiate a full replication cycle. Therefore, the ratio of NP to PFUs would be higher in virions with bundling defects. The opposite phenomenon, of virions packaging multiple genomes, would yield a similar result but is inconsistent with electron microscopy data (Vijayakrishnan et al., 2013). To test this, I enriched samples for filamentous or non-filamentous virions by density gradient purification and measured the NP content by western blot and infectious titre by plaque assay. Despite the disadvantages of using high-yield purification to assess function, it was unavoidable in this case as the western blots needed a higher protein concentration than could be achieved by low-yield purification. I saw that the proportion of NP in a fraction was generally closely correlated with the infectious titre of that fraction (Figure 6.3). The exceptions were Fractions 1 and 2 which contained a very

high proportion of NP but almost no infectivity. As the confocal analysis did not detect virions in these samples, and the western blot analysis from the previous chapter detected minimal M1 in the bottom two fractions (Figure 5.10), I concluded that these were most likely dominated by cell debris rather than virions. Of the fractions that did contain virions, there was some variation in the ratio of NP content to infectivity. However, this variation did not correlate with morphology and was not highly reproducible between repeats. Overall, there was no evidence for a link between morphology and the efficiency with which a genome could initiate an infection.

As previously mentioned, the damage sustained by high-yield purification could have affected virion infectivity, which makes these data more difficult to interpret. Improvements in confocal microscopy of filamentous virions may make it possible to measure the NP content of fractions from low-yield purifications and compare that with infectivity. However, that is not currently viable with antibody labelling for the reasons discussed in the previous chapter, and alternative labelling strategies have only been successfully reported using an unusual reassortant virus (Vahey & Fletcher, 2019b) which may have unusual functional properties. It also worth noting that virions with defects in genome packaging, which appear to be common for filamentous virions (Vijayakrishnan et al., 2013; Zhu et al., 2021), would be undetectable in this assay. For these reasons, and due to the noise in the data mentioned above, it cannot be concluded there is no difference in genome packaging efficiency between filamentous and non-filamentous virions from these data. However, it is reasonable to assume that any large disparities between NP and infectivity would have been discernible, and so it is likely that any differences in genome bundling are relatively minor at the population level.

6.3.3 Filamentous virions are enriched in semi-infectious particles

As well as differences in the ratio of NP to infectivity, variation in genome bundling efficiency should manifest in variation in the ratio of semi-infectious particles (SIPs, virions which package some, but not all, functional RNPs) to fully infectious particles (FIPs, virions which package a full set of functional RNPs). I therefore measured this ratio in samples enriched for different virion morphologies.

To measure the abundance of semi-infectious particles. I adapted a previously described method (Brooke et al., 2013). I infected a monolayer of MDCK cells with a limiting dilution of Udorn and incubated it for 24 hours (under an agarose overlay to prevent virion diffusion), before fixing the cells and immunostaining NP. Any cell infected by a FIP would (by definition) have produced infectious progeny which could infect neighbouring cells, resulting in a cluster of cells expressing viral proteins. Any cell infected by a single SIP could (by definition) not produce infectious progeny and so only this initial cell would express viral proteins. At dilutions where foci of infection could be distinguished, the ratio of

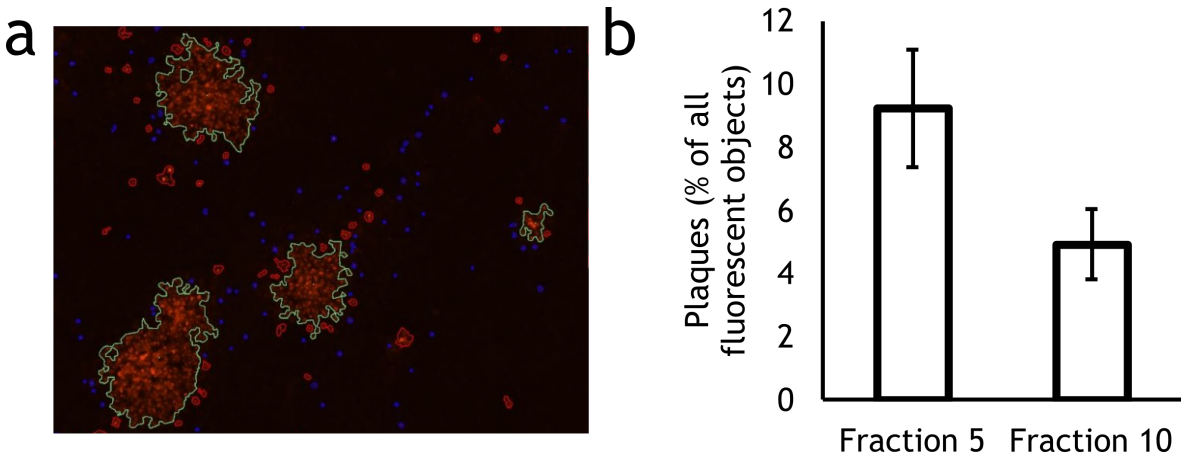

Figure 6.4: Filamentous virions are enriched in semi-infectious particles.
Virions were obtained by collecting supernatant from MDCK cells that had been infected with influenza A/Udorn/307/72 (H3N2) for 24 hours. Samples were clarified by centrifugation for 5 min at 1800 *g* at room temperature, then purified with a 20-30% iodixanol gradient overnight by ultracentrifugation at 4 °C at 210,000 *g* and the sample was split into 12 fractions by puncturing the base of the tube and collecting the flowthrough in separate containers. Fraction 5 (as a predominantly non-filamentous sample) and Fraction 10 (as a predominantly filamentous sample) were used to infect a confluent monolayer of MDCK cells for 24 hours. (a) This was then fixed and NP was immunostained (indicated in red) to identify infected cells. Fluorescent objects larger than 350 μm^2 but smaller than 3300 μm^2 were classified as cells and are highlighted in red and objects larger than 3300 μm^2 were classified as plaques and are highlighted in green. (b) The number of plaques was calculated as a proportion of the total fluorescent objects. Bars indicate mean proportion, whiskers indicate s.d. (three independent experiments). Means were compared using two-tailed Student's t-tests: * $p < 0.05$.

infectious particles to cells would be much less than one, and so the probability of complementary SIPs coinfecting a cell and producing infectious progeny would be extremely low. By using size-gating, I could compare the ratio of plaques to single cells in the monolayer (Figure 6.4a). As I only stained NP, this measurement will underestimate the concentration of SIPs in the initial sample, as FIPs necessarily express NP whereas SIPs can fail to express any combination of viral proteins, including NP (Brooke et al., 2013). However, the ratio of plaques to single cells calculated by staining NP will correlate with the ratio of FIPs to SIPs, provided any packaging defects affect all genome segments equally. Furthermore, as I was comparing the ratio in filamentous and non-filamentous virions in the same way, both samples would be equally affected by this issue. I observed that ~9% of the infectious particles in a sample enriched in non-filamentous virions were fully infectious, compared to ~5% of the infectious particles in a sample enriched in filamentous virions (Figure 6.4b). This suggests that filamentous virions are enriched in SIPs relative to non-filamentous virions, which is likely underpinned by differences in genome bundling.

It is unclear why this analysis suggested a difference in genome bundling but the comparison of NP abundance and infectivity did not. It is possible that the comparison of NP and infectivity was affected by virion damage, or the presence of unevenly distributed NP that was not virion associated (such as that packaged in microvesicles, Hutchinson et al. (2014)). These issues would not affect the analysis of FIPs and SIPs, so I considered this result to be more robust.

This interpretation of the data assumes that only morphology accounts for the different densities of influenza virions. However, as shown in the previous chapter, even a predominantly spherical virus such as WSN still produces virions with a broad range of densities (Figure 5.4). It is possible that this range could be influenced by genome packaging and bundling; for example, virions with fewer genome segments could be less dense. If this is the case, then the non-filamentous virions present in the samples enriched for filamentous virions may have different genome packaging and bundling efficiencies than their counterparts in samples enriched for non-filamentous virions. Controlling for this possibility requires a method to enrich virions that does not depend on density. As discussed in the previous chapter, this is challenging, but an improved method to separate virions by size, such as filtration or rate-zonal centrifugation, will make it possible to validate these measurements of the proportion of fully infectious particles.

6.3.4 Conclusion

These data suggest that filamentous virions are less likely to package complete genomes than non-filamentous virions, resulting in an apparently less efficient use of the resources of the host cell. In contradiction to some previous reports (Ada et al., 1957; Smirnov et al., 1991), the data do not support a model where filamentous virions are more robustly infec-

tious than non-filamentous. If the formation of filamentous virions is indeed adaptive, it therefore seemed likely that their advantages lay in functional properties other than infectivity.

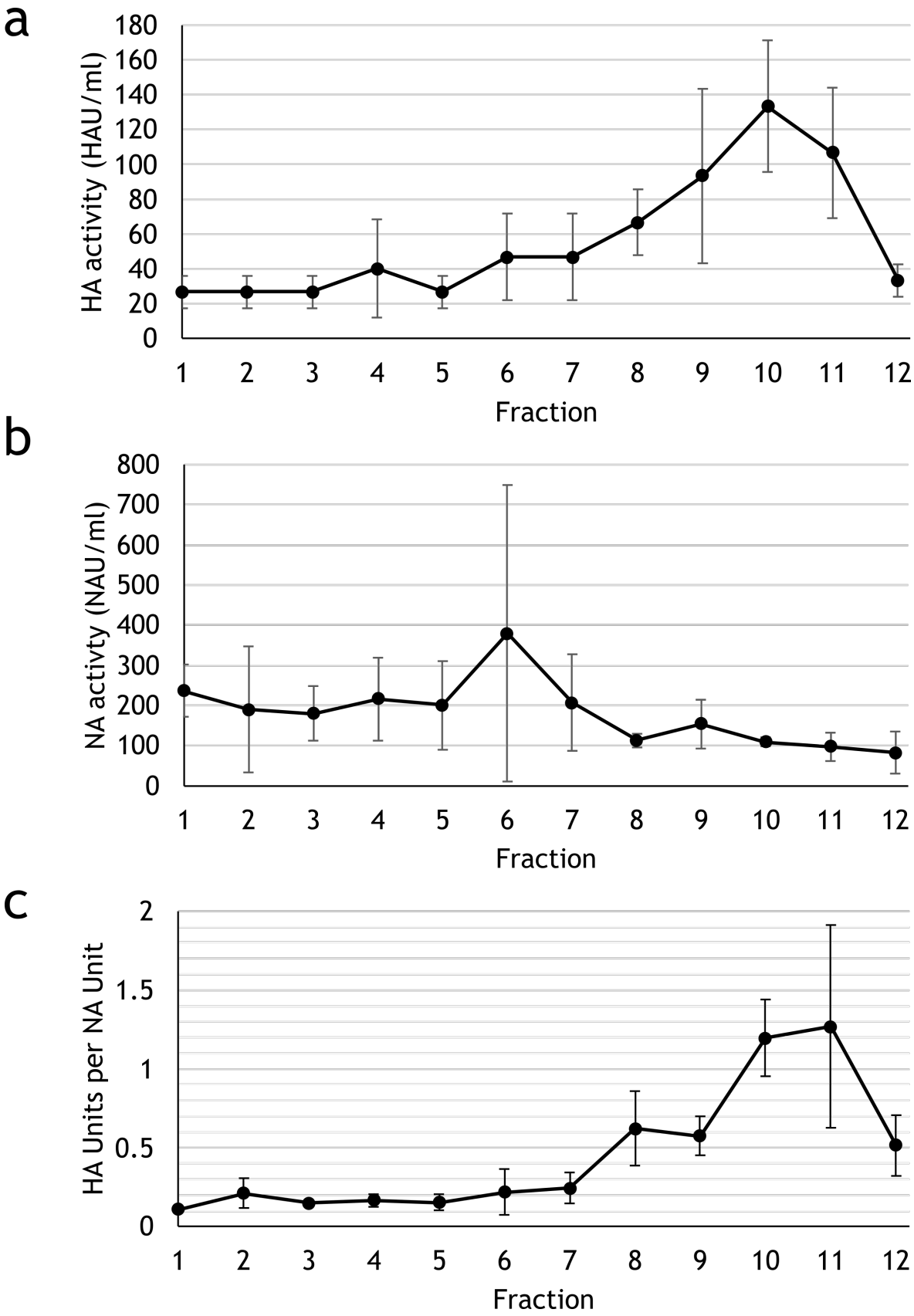

Figure 6.5: Filaments virions have more HA activity relative to NA activity.

Virions were obtained by collecting supernatant from MDCK cells that had been infected with influenza A/Udorn/307/72 (H3N2) for 24 hours. Samples were clarified by centrifugation for 5 min at 1800 *g* at room temperature, then purified with a 20-30% iodixanol gradient overnight by ultracentrifugation at 4 °C at 210,000 *g*. The

sample was split into fractions by puncturing the base of the tube and collecting the flowthrough in separate containers. (a) HA activity for each fraction was measured with an HA assay. Points indicate mean HAU/ml, whiskers indicate s.d. (three independent experiments). (b) NA activity for the same samples as (a) was calculated using an Amplex Red Assay. Points indicate mean NAU/ml, whiskers indicate s.d. (c) The data from (a) and (b) were combined to calculate the HAU/NAU for each fraction. Points indicate mean, whiskers indicate s.d.

6.4 Results III: Glycoprotein activity varies with virion morphology

6.4.1 Introduction

From the compositional analysis, I predicted that glycoprotein activity would vary with morphology. The ratio of HA to NA in filamentous virions is approximately fivefold higher than in non-filamentous virions, which suggests that filamentous virions should have a fivefold increase in HA activity relative to NA activity. If this activity difference exists, it could underpin functionally relevant differences *in vivo*, affecting processes such as navigating mucus and adhering to target cells.

6.4.2 The balance of HA and NA activity varies with morphology

To measure how the ratio of HA to NA activity varied with morphology, I first determined the HA titre of each fraction from a low-yield purification by HA assay using chicken red blood cells (Figure 6.5a). Using samples of the same fractions, I also determined the NA activity using an Amplex Red assay (Figure 6.5b). Combining these two titres gave the HA activity relative to NA activity for each fraction (Figure 6.5c). This value was highest in Fractions 10 and 11 (at 1.2 and 1.3 HAU/NAU respectively) and lowest in Fractions 1-7 (at 0.2 HAU/NAU). This meant there was an approximately sixfold change in the ratio of HA to NA activity between the fractions most enriched for filamentous virions and the fractions most enriched for non-filamentous virions. This was in close agreement with the predicted fivefold difference from the compositional comparison.

These findings confirmed that compositional differences between virions of different morphologies can lead to functional differences. They also suggest that the activity of individual glycoproteins is similar regardless of virion morphology, as the difference in functional effects is closely tied to their abundance. As well as validating the compositional analysis performed in the previous chapter, these findings also suggests that any viral processes that depend on the HA/NA balance could vary with morphology.

6.4.3 Virion morphology does not affect inhibition by mucus

The various mucins that comprise mucus are highly enriched in sialic acids, and so act as decoy receptors for HA. This inhibits virion spread (Zanin et al., 2016). Virions can traverse mucus because these decoy receptors are cleaved by NA, however, if the NA activity is too high relative to the HA activity, the virions will also be unable to bind entry receptors at the plasma membrane. The HA/NA balance therefore is vital for successfully evading

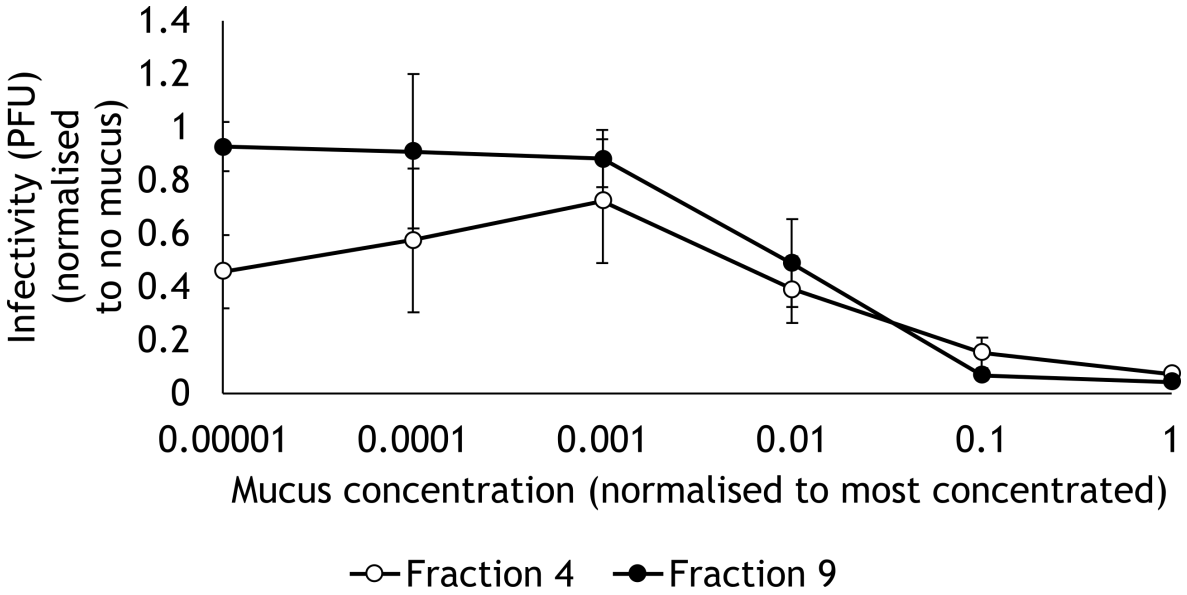

Figure 6.6: Virion morphology does affect inhibition by mucus

Virions were obtained by collecting supernatant from MDCK cells that had been infected with influenza A/Udorn/307/72 (H3N2) for 24 hours. Samples were clarified by centrifugation for 5 min at 1800 *g* at room temperature, then purified with a 20-30% iodixanol gradient overnight by ultracentrifugation at 4 °C at 210,000 *g* and the sample was split into 12 fractions by puncturing the base of the tube and collecting the flowthrough in separate containers. Mucus was harvested from human airway epithelial cells, which had been grown to confluency and differentiated over the previous four weeks. Plaque assays were performed using serial dilutions of mucus, where virus samples were diluted in mucus and incubated at 37 °C for 30 min, before the mucus was removed and cells overlaid with 2% agarose. Graph indicates mean infectivity for each mucus dilution, normalised to a no-mucus control, for the predominantly non-filamentous Fraction 4 and the predominantly filamentous Fraction 9.

mucus, and so the finding that this balance varies with morphology could mean resistance to mucus inhibition also varies with morphology.

The inhibitory effects of mucus vary depending on its constituent mucins. For example, strains of influenza that are inhibited by human mucus may not be inhibited by porcine mucus (Zanin et al., 2015). Furthermore, any individual mucin might not have the same inhibitory properties as the collection of mucins which make up mucus. To minimise these potential confounding effects, I wanted to use mucus as similar as possible to actual human mucus for the experiment. I therefore obtained mucus derived as a by-product from a differentiated primary human bronchial epithelium model, which was kindly donated by Joanna Wojtus (MRC-University of Glasgow Centre for Virus Research).

To measure the inhibitory effects of mucus on virions, I performed a modified plaque assay where the virus samples were diluted in mucus. I serially diluted the initial mucus samples and, with each dilution of mucus, made a dilution series of viruses, using samples enriched in filamentous or non-filamentous virions. These samples were overlaid on MDCK cells for 30 minutes to allow virions to adsorb to cells, then removed. The cells were overlaid with agarose, incubated for two days, and fixed and stained per a standard plaque assay. The plaques were then counted to determine the infectious titre (Figure 6.6). The concentration of mucus was negatively correlated with the infectivity of the samples, suggesting that the mucus could indeed prevent virions from infecting cells. However, the inhibitory effect of mucus was near identical for both filamentous and non-filamentous virions. Therefore, the fivefold difference in HA/NA activity associated with virion morphology does not lead to differences in susceptibility to mucus inhibition. This may be because fivefold is too small a difference to have a meaningful effect, or it may be that virions with the appropriate HA/NA balance to evade mucus are less able to stably bind entry receptors and vice versa, so the two effects cancel out. Regardless of the reason, the data do not support a model where pleiomorphy is an adaptation to evade mucus inhibition.

It should be noted here that the apparent decline in infectivity at dilution levels 0.00001 and 0.0001 relative to 0.001 for Fraction 4 (Figure 6.6) is difficult to explain. As samples are normalised to a control containing no mucus, infectivity would not be expected to decline as mucus was diluted out of the samples. This suggests there may have been a technical problem affecting the plaque assays, and so these data should be treated as preliminary.

These experiments assume that the reduction of infectivity seen was caused by mucins, and not by some other product present within the mucus. It would have been preferable to validate this by degrading the mucus with exogenous neuraminidase to see if this relieved the inhibition. Unfortunately, this was not possible due to time constraints. Despite this drawback, it is reasonable to assume that mucins were causing the inhibition as there is no other obvious candidate that could have caused it. Similarly, these conclusions assume that the mucus that could be removed from bronchial epithelial cells is a good representation of respiratory mucus at the natural site of infection. In reality, respiratory mucus com-

prises membrane-bound and secreted mucins (Bansil & Turner, 2018), and so the impact of any cell-associated mucins will have been missed as they cannot be removed. Mucus also comprises distinct layers *in vivo*, which vary in composition and density (Bansil & Turner, 2018), whereas the experiments described here used homogenised mucus across a range of concentrations. It would therefore be useful for future research to explore the role of mucins further by infecting a bronchial epithelial model directly.

6.4.4 Conclusion

Together, these data suggest that variations in HA and NA abundance in virions underpin functional differences in HA and NA activity. However, these functional differences did not lead to different susceptibilities to mucus inhibition. It may be the case that the variation in HA and NA bears no physiological relevance, perhaps due to the advantages and drawbacks cancelling each other out, or due to the range of activities seen simply not being broad enough to have a functional effect. It may also be the case that the balance of HA/NA activity is relevant elsewhere in the replication cycle. In future work it would be of interest to test these other areas, such as measuring the rate of virion uptake or the susceptibility of different virions to neutralising antibodies.

6.5 Discussion

In this chapter, I have shown how methods to enrich virion samples by morphology can be readily adapted to address questions about virion function. I applied compositional analysis of filamentous virions to make predictions about their function, and then used these methods to test those predictions. I found that differences in the M1, NP, HA, and NA protein levels in virions corresponded with filamentous virions being less robustly infectious than non-filamentous virions but possessing a higher ratio of HA/NA activity. The finding that morphology has no impact on susceptibility to mucus inhibition suggests that these differences detected *in vitro* may not simply map to physiological differences *in vivo*, possibly because these physiological effects are influenced by many factors, both host and viral, and cannot be explained simply by one. If this is the case, unpicking these complex combinations will depend on first identifying their constituent parts. The work described here therefore not only provides data characterising two functional properties of filaments, infectivity and glycoprotein activity, but also demonstrates a readily adjustable work flow for further studies of filament functions.

Chapter 7

Discussion

7.1 Summary of key findings

In Chapter 1, I introduced the following four aims for this project:

Aim 1: Develop a method to analyse the dimensions of individual filamentous virions in a sample and detect changes to their concentration.

Aim 2: Validate a set of standard laboratory handling techniques that can be used to manipulate filamentous virions without damaging them.

Aim 3: Perform a detailed comparison of the composition of filamentous and non-filamentous virions.

Aim 4: Use the compositional comparison to build and test hypotheses about the functional differences between filamentous and non-filamentous virions.

In the subsequent chapters I demonstrated how confocal microscopy can be used to quickly count and measure filamentous influenza virions. With this method, I demonstrated that most laboratory handling methods cause minimal damage, but freezing severely damages filamentous virions. I showed how filamentous and non-filamentous virions can be enriched by an adaptable and reproducible isopycnic centrifugation method, which allowed me to determine that, other than HA and (presumably) M1, viral proteins in filamentous virions are depleted relative to their size. This results in a reduction in their infectivity and an increase in their ratio of HA to NA activity, though filamentous virions were nonetheless as susceptible to mucus inhibition as non-filamentous virions.

Having therefore achieved my aims, and obtained these data on the basic characteristics of filamentous virions, here I return to the questions raised in Chapter 1 and discuss how my findings relate to outstanding questions about the biology of influenza viruses and broader questions about how to reduce the harm they cause.

7.2 Resolving methodological problems

7.2.1 Visualisation allows efficient sample characterisation

A common issue in influenza virus morphology research is that studies often lack detailed information about the size and concentration of filamentous virions, particularly when samples are not concentrated enough for electron microscopy. The confocal microscopy analysis pipeline I have described in Chapter 3 offers an efficient, readily adaptable solution to this problem. While it lacks some potentially useful features, notably the capacity to measure absolute virion concentrations, the method I describe here could be readily adapted by future researchers to characterise the samples they are using. Presenting these data alongside research into the biological properties of filamentous virions would make it much easier to compare studies from different researchers and could give insight into why these studies often disagree with each other.

7.2.2 Past characterisations of filamentous virions are likely to have been affected by virion damage

My finding that freezing causes severe damage to filamentous virions (Chapter 4) suggests that artefactual damage to virions during laboratory handling issue are likely to have affected past research, as many previous studies on isolated filamentous virions have either clearly used frozen samples (Ada et al., 1958; Donald & Isaacs, 1954a) or failed to state sample storage conditions (Campbell et al., 2014a,b; Rossman et al., 2010; Seladi-Schulman et al., 2014; Sakai et al., 2017; Sieczkarski & Whittaker, 2005; Vahey & Fletcher, 2019a,b). Similarly, the finding that high-yield density gradient purification can damage filamentous virions suggests that this could have affected many key studies of the properties of filaments (Donald & Isaacs, 1954a; Liu et al., 2002; Roberts et al., 1998; Sieczkarski & Whittaker, 2005; Smirnov et al., 1991), and particularly those that used differential centrifugation techniques featuring many ultracentrifugation cycles (Ada et al., 1958; Li et al., 2021). It is impossible to tell to what extent damage has skewed the results of any of these studies, but in the light of my results it is sensible to interpret their results with caution. This issue could be avoided in future research by characterising virion samples using the confocal microscopy pipeline, or a similar method, and validating the suitability of any handling methods using a work flow as described in Chapter 4.

7.2.3 An adaptable isopycnic centrifugation method facilitates future research into influenza virion morphology

Although the various studies cited in the previous section reported using ultracentrifugation to enrich virions by morphology, this process is widely considered difficult to reproduce and a standard enrichment method has not been established (discussed in Kordyukova et al. (2020)). My own data suggest this lack of reproducibility could be due to the properties of the virions varying depending on their growth conditions. In my hands, the distribution of non-filamentous virions was strikingly different between the low-yield and high-yield purification processes (Figures 5.5 and 6.1). This suggests that an established protocol for purifying filaments of one strain under particular conditions would not necessarily be applicable elsewhere, which may explain why most recent studies using ultracentrifugation use a near identical rate-zonal protocol with Udorn or Udorn variants (Roberts et al., 1998; Liu et al., 2002; Roberts et al., 1998; Sieczkarski & Whittaker, 2005) though a recent study used differential sedimentation instead (Li et al., 2021). The approach I have described in Chapter 5, using confocal microscopy to rapidly assess the distribution of virions in a density gradient and adjust it accordingly, should allow this issue to be avoided in future. It can be applied to any virus strain that can be fluorescently labelled, and therefore would allow a broader range of strains, grown in a broader range of conditions, to be studied.

7.2.4 Conclusion

Taken together, the methods I have described show how confocal microscopy validation can underpin a broad range of tools to analyse the properties of filamentous influenza virions. These methods would be readily adaptable to novel strains or methods and will make it possible to perform a range of basic characterisation processes that have not been previously possible.

7.3 The biology of filamentous virions

The tools I developed enabled me to characterise the composition and function of filamentous virions. These findings do still rely on certain assumptions (see Chapters 5 and 6 for detailed discussion), but these are quite conservative. Here I will discuss how the findings relate to the differences between filamentous and non-filamentous influenza virions during the replication cycle, as set out in Chapter 1.

7.3.1 Assembly

That filamentous virions are enriched in semi-infectious particles suggests that they are less likely to package a full complement of genome segments. It could be that they package the full complement and somehow acquire more defective segments, but it is difficult to suggest a mechanism by which this could occur and the possible reduced abundance of NP in filamentous virions better matches a model in which genome segments are entirely absent. This finding agrees with previous data suggesting filamentous virions often package no genome (Vijayakrishnan et al., 2013; Halldorsson et al., 2021) and suggestions that the strength of M1:NP binding correlates with morphology (Burleigh et al., 2005; Liu et al., 2002). It also provides further evidence against earlier suggestions that filamentous virions may be multigenomic or otherwise enriched in NP (Ada & Perry, 1958; Roberts et al., 1998; Smirnov et al., 1991). If true, however, it is not clear whether this alteration in genome packaging is a cause or a consequence of a filamentous morphology. It is possible, for example, that a full complement of RNPs in a nascent virion enhances scission and so virions lacking RNPs are more likely to keep growing into filaments. Conversely, it is possible that the tighter M1 helix in filamentous virions somehow reduces the capacity of M1 to bind NP, and so filamentous virions are less likely to package RNPs. Regardless of the mechanism, it is not clear how the reduced packaging efficiency could be directly adaptive.

The similarities between in the host-derived proteome of filamentous and non-filamentous virions described in Chapter 5 suggest that the budding sites of the two types of virion are very similar. This is unsurprising, as microscopy shows virions of different morphologies budding in close proximity (Morgan et al., 1956), but is provides some evidence against a model where differences in lipid raft composition affect the morphology of the virions assembling there.

While the presence of most of the proteins present in influenza virions does not vary with morphology, the differences in the abundance of these proteins suggests that some aspect of assembly does. If this were not the case, then filamentous virions could be viewed as "long spherical virions", but in that instance the relative abundance of viral proteins would be the same. Instead, the data presented here support a model of filamentous virions being like spherical virions at one pole, but with a long tail mostly comprised of M1 and HA. This agrees with previous findings that the viral components of filamentous virions are often polarised (Calder et al., 2010; Chlanda et al., 2015; Kolpe et al., 2019; Vahey & Fletcher, 2019b,a), though is hard to reconcile with the observation that NA can be concentrated on the opposite pole to the RNPS (Calder et al., 2010). This could arise if HA were the most abundant viral protein outside of the lipid raft where the viral proteins were initially concentrated. If scission was delayed after the first stages of assembly and M1 continued to oligomerise, then surrounding material would be non-specifically incorporated into the virion, leading to an imbalance in proportional protein abundance. If this is correct, then the relative abundance of viral proteins should scale with filamentous virion length.

It would therefore be interesting for future work to compare the proteomes of filamentous virions that had been enriched based on length, potentially by passing them through a series of filters with different pore sizes.

7.3.2 Transmission

The finding that HA and NA activities vary with morphology could underpin differences between filamentous and non-filamentous virions throughout the replication cycle. Filamentous virions having relatively more HA suggests that they should be more likely to become permanently entangled with mucins, in a similar process to that which prevents them eluting from red blood cells (Figure 5.2). It has been suggested that the distribution of HA and NA can matter as much as their abundance, and and one study has shown filamentous virions can have HA and NA activity which is polarised in such a way as to allow them to penetrate mucus (Vahey & Fletcher, 2019a). However, this study did not measure infectivity and so it was not clear whether this phenomenon increased viral fitness. My data suggest that variations in the activity of HA and NA do not confer any advantage when infecting cells in the presence of mucus. It may be that the two effects cancel out, where filamentous virions with appropriately polarised glycoproteins are better at penetrating mucus than non-filamentous virions, but filamentous virions with less polarised proteins are more likely to be trapped. It may also be due to filamentous virions often lacking genomes (Vijayakrishnan et al., 2013) or carrying incomplete genomes (see Chapter 6) – it does not matter if filamentous virions can better evade mucus if they cannot initiate a full infection once they have done so. It also seems unlikely that differential HA and NA activity will be the cause of the sole fitness advantage from forming filamentous virions, as influenza C virus (as do many other respiratory viruses, see Chapter 1) forms filamentous virions but uses only one protein to bind and destroy receptors.

7.3.3 Entry and unpacking

My characterisation of filamentous influenza virions suggests there may be some differences at the entry stage of the replication cycle. The effect of morphology on HA and NA activity may affect virion entry, as more HA activity should result in tighter binding of virions to cells and so improves the likelihood of triggering entry. Conversely, it may make the virion more likely to be trapped at a region of the cell where the receptor density is too low to initiate entry (Sieben et al., 2020). It would therefore be interesting to measure the uptake rate of filamentous and non-filamentous virions directly, perhaps by labelling virions with a lipophilic dye and using it to measure fusion as described by Banerjee et al. (2013).

The finding that filamentous virions are enriched in SIPs means that research into the varying contributions of FIPs, SIPs, and defective interfering particles (DIPs) (reviewed by

Brooke (2017)) may also be applicable to morphology. This includes the finding that SIPs are more prone to reassortment than FIPs - the same is presumably therefore likely to be true of filamentous virions relative to non-filamentous. The mechanism for this is unclear, but it could be enhanced due to variation in virion entry due to morphology. Filamentous virions depend on macropinocytosis for entry (Rossman et al., 2012), and the much larger vesicles involved means it is physically possible to internalise multiple virions simultaneously. It is therefore possible that cells infected by filamentous virions are more likely to be coinfected and also more likely to produce reassortant virions. It seems unlikely that this phenomenon would lead in itself to the selection of filament-forming mutations, but it could be that filamentous virions drive influenza virus genome diversity more than would be expected from their abundance alone.

7.4 The role of pleiomorphy in replication

After characterising the composition and some functions of filamentous virions, their role is arguably more elusive than before. If anything, filamentous virions are less infectious than non-filamentous virions, and the variation in their glycoprotein activity does not appear to be physiologically relevant, nor can it explain why influenza C viruses, which only express one type of glycoprotein, still form filamentous virions. Indeed, the simplest explanation which fits the available data as to why filamentous virions form is that they are caused by a failure of scission and not a regulated process. Despite this, evidence based on passage histories still suggests that pleiomorphy is somehow adaptive (Dadonaite et al., 2016).

It is possible that the difficulty in understanding the role of filamentous virions derives from the popularity of one laboratory-adapted strain, Udorn (Roberts et al., 1998; Roberts & Compans, 1998; Liu et al., 2002; Simpson-Holley et al., 2002; Bourmakina & García-Sastre, 2003; Elleman & Barclay, 2004; Burleigh et al., 2005; Sieczkarski & Whittaker, 2005; Speshock et al., 2007; Calder et al., 2010; Grantham et al., 2010; Elton et al., 2013; Roberts et al., 2013; Vijayakrishnan et al., 2013; Hirst & Hutchinson, 2019; Kolpe et al., 2019), or mutants and reassortants based on it (Roberts et al., 1998; Bourmakina & García-Sastre, 2003; Sieczkarski & Whittaker, 2005; Bruce et al., 2010; Beale et al., 2014; Vahey & Fletcher, 2019b,a) as a model strain. Udorn's popularity among researchers, including in the work presented in this thesis, is because it grows readily under laboratory conditions but still forms filamentous virions. However, this combination of properties is not typical of influenza virus strains and it may be that Udorn filamentous virions are not representative of influenza filamentous virions generally. Indeed, is noteworthy that although much of the biochemical characterisation of filamentous virions has been performed using Udorn, the passage experiments and observations which demonstrate that pleiomorphy is adaptive have been performed with other strains (Burnet & Lind, 1957; Chu et al., 1949; Seladi-Schulman et al., 2013). It would therefore be advantageous for future work to sample a

broader range of strains and to perform basic characterisations and passage experiments using the same strain. This approach is only viable if the methods used are efficient and widely accessible, and so the simple, adaptable methods described in this thesis will facilitate these future studies. Similarly, virion properties are generally characterised in artificial *in vitro* settings, but this does not necessarily correlate with physiological relevance. These *in vitro* characterisations are a prerequisite to identifying roles *in vivo*, but they should then be tested in more relevant models such as primary cultures and tissue explants. As these systems are more complex that *in vitro* models, removing confounding variables by thoroughly characterising virion samples before experiments is even more important. The methods described in this thesis allow this robust characterisation to be performed, and so will facilitate this move into more complex model systems.

Research into pleiomorphy may also be limited as it has often focused on the intrinsic properties of filamentous virions. However, mutations which lead to filamentous virion production may also change the properties of non-filamentous virions, and it may be that it is these other changes that are adaptive. This could be studied by taking genetically similar strains of influenza virus that have different morphologies and enriching them all for non-filamentous virions only. If these samples show significant functional differences, it could indicate that filamentous virion production is simply a side-effect of changes elsewhere, and is not itself adaptive.

It should also be noted that the natural reservoir of influenza virus is waterfowl, where the main route of transmission is faeco-oral rather than respiratory (Fleming, 2005). It is possible that pleiomorphy has a much greater effect on viral fitness via this transmission route and has only minor effects on respiratory transmission. It would therefore be useful for future research to examine the impact of pleiomorphy on faeco-oral transmission, such as stability in lake water or resistance to the pH changes in the digestive tract. If strong effects of morphology are seen here, it might even be that pleiomorphy has little direct impact on human transmission, though even then it may still present therapeutic targets.

7.5 Pharmaceutical options to control influenza

Even in the absence of a clearly defined role for pleiomorphy in infection, it may still be possible to target filamentous virions pharmaceutically. Most influenza virus vaccination strategies, and the neuraminidase inhibitor class of drugs, target glycoproteins. As the abundance and activity of IAV glycoproteins varies with virion morphology, this may affect response to treatments. Indeed, formation of filamentous virions has been linked to resistance to neutralising antibodies (Li et al., 2021) and oseltamivir (Vahey & Fletcher, 2019b). These therapeutic interventions have already been tested empirically against natural strains of diverse morphologies, but the morphology of the strains involved has not been accounted for. In the future, considering morphology may reveal ways to improve these in-

terventions, for example, by adjusting treatment regimens to target strains which favour a particular morphology, or potentially by finding methods to reduce the degree of filamentous virion formation in patients. Discovering such methods will depend on developing a thorough knowledge of the assembly mechanism of filamentous virions.

7.6 Reducing the burden of influenza

It is not currently possible to develop therapeutic measures to exploit pleiomorphy, but nor is it possible to dismiss it as irrelevant. To use our understanding of pleiomorphy to reduce the harm caused by influenza, we must first determine whether pleiomorphy is physiologically relevant, as otherwise research into it may drain resources which are better applied elsewhere. If it is determined to be relevant, further research will be necessary to determine how best to exploit this in therapeutic measures. In either case, efforts to reduce the harm caused by influenza will depend on a detailed understanding of influenza virus pleiomorphy. Given the difficulties this poses, this should begin with a detailed characterisation of the basic composition and function of filamentous influenza virions across a range of virus strains and in a variety of experimental systems. These basic characteristics can then be combined and used to build a progressively more complex and representative model of the role of pleiomorphy in infection. The methods and findings described in this thesis add to our understanding of the elusive properties of filamentous influenza viruses and provide a robust set of methods to expand it further.

Bibliography

2016. Crossflow cassette systems optimized for filtration. Filtration + Separation, **53**(3), 26–28.

Ada, G. L., & Perry, B. T. 1958. Properties of the nucleic acid of the Ryan strain of filamentous influenza virus. Journal of General Microbiology, **19**(1), 40–54.

Ada, G. L., Perry, Beverley T., & Edney, Margaret. 1957. Infectivity of Influenza Virus Filaments. Nature, **180**(4595), 1134–1134.

Ada, G. L., Perry, Beverley T., & Abbot, A. 1958. Biological and Physical Properties of the Ryan Strain of Filamentous Influenza Virus. Microbiology, **19**(1), 23–39.

Al-Mubarak, Firas, Daly, Janet, Christie, Denise, Fountain, Donna, & Dunham, Stephen P. 2015. Identification of morphological differences between avian influenza A viruses grown in chicken and duck cells. Virus Research, **199**(Mar.), 9–19.

Alonas, Eric, Vanover, Daryll, Blanchard, Emmeline, Zurla, Chiara, & Santangelo, Philip J. 2016. Imaging viral RNA using multiply labeled tetravalent RNA imaging probes in live cells. Methods, **98**(Apr.), 91–98.

Angulo, J. J. 1951. On the identity of the so-called filamentous forms of influenza and fowl pest viruses. Archiv Fur Die Gesamte Virusforschung, **4**(3), 199–206.

Angulo, J. J., Watson, J. H. L., & Olarte, J. 1950. Artifacts, with other nonspecific appearances resembling virus particles, and the so-called filamentous forms of influenza and fowl pest viruses in human skin tissue fluid examined with the electron microscope. Journal of Bacteriology, **60**(2), 129–138.

Archetti, I. 1955. Appearances associated with filamentous forms of influenza viruses. Archiv für die gesamte Virusforschung, **6**(1), 29–35.

Bächi, Thomas, & Howe, Calderon. 1973. Morphogenesis and Ultrastructure of Respiratory Syncytial Virus. Journal of Virology, **12**(5), 1173–1180.

Banerjee, Indranil, Yamauchi, Yohei, Helenius, Ari, & Horvath, Peter. 2013. High-Content Analysis of Sequential Events during the Early Phase of Influenza A Virus Infection. PLOS ONE, **8**(7), e68450. Publisher: Public Library of Science.

Bansil, Rama, & Turner, Bradley S. 2018. The biology of mucus: Composition, synthesis and organization. Advanced Drug Delivery Reviews, **124**(Jan.), 3–15.

Beale, Rupert, Wise, Helen, Stuart, Amanda, Ravenhill, Benjamin J., Digard, Paul, & Randow, Felix. 2014. A LC3-Interacting Motif in the Influenza A Virus M2 Protein Is Required to Subvert Autophagy and Maintain Virion Stability. Cell Host & Microbe, **15**(2), 239–247.

Bean, Andrew G. D., Baker, Michelle L., Stewart, Cameron R., Cowled, Christopher, Deffrasnes, Celine, Wang, Lin-Fa, & Lowenthal, John W. 2013. Studying immunity to zoonotic diseases in the natural host - keeping it real. Nature Reviews. Immunology, **13**(12), 851–861.

Bharat, Tanmay A. M., Noda, Takeshi, Riches, James D., Kraehling, Verena, Kolesnikova, Larissa, Becker, Stephan, Kawaoka, Yoshihiro, & Briggs, John A. G. 2012. Structural dissection of Ebola virus and its assembly determinants using cryo-electron tomography. Proceedings of the National Academy of Sciences, **109**(11), 4275–4280. Publisher: National Academy of Sciences Section: Biological Sciences.

Bialas, Kristy M., Desmet, Emily A., & Takimoto, Toru. 2012. Specific residues in the 2009 H1N1 swine-origin influenza matrix protein influence virion morphology and efficiency of viral spread in vitro. PloS One, **7**(11), e50595.

Bienz, K., & Löffler, H. 1969. Ein Beitrag zur Morphologie des Influenzavirus: Struktur des Influenza-A2-(«Hongkong»)-Virus. Experientia, **25**(9), 987–989.

Bourmakina, Svetlana V., & García-Sastre, Adolfo. 2003. Reverse genetics studies on the filamentous morphology of influenza A virus. The Journal of General Virology, **84**(Pt 3), 517–527.

Brooke, Christopher B. 2017. Population Diversity and Collective Interactions during Influenza Virus Infection. Journal of Virology, **91**(22).

Brooke, Christopher B., Ince, William L., Wrammert, Jens, Ahmed, Rafi, Wilson, Patrick C., Bennink, Jack R., & Yewdell, Jonathan W. 2013. Most Influenza A Virions Fail To Express at Least One Essential Viral Protein. Journal of Virology, **87**(6), 3155–3162.

Bruce, Emily A., Digard, Paul, & Stuart, Amanda D. 2010. The Rab11 Pathway Is Required for Influenza A Virus Budding and Filament Formation. Journal of Virology, **84**(12), 5848–5859.

Burleigh, Laura M., Calder, Lesley J., Skehel, John J., & Steinhauer, David A. 2005. Influenza a viruses with mutations in the m1 helix six domain display a wide variety of morphological phenotypes. Journal of Virology, **79**(2), 1262–1270.

Burnet, F. M. 1956. Filamentous Forms of Influenza Virus. Nature, **177**(4499), 130.

Burnet, F. M., & Lind, P. E. 1957. Studies on filamentary forms of influenza virus with special reference to the use of dark-ground-microscopy. Archiv Fur Die Gesamte Virusforschung, **7**(5), 413–428.

Calder, Lesley J., Wasilewski, Sebastian, Berriman, John A., & Rosenthal, Peter B. 2010. Structural organization of a filamentous influenza A virus. Proceedings of the National Academy of Sciences, **107**(23), 10685–10690.

Campbell, Patricia J., Danzy, Shamika, Kyriakis, Constantinos S., Deymier, Martin J., Lowen, Anice C., & Steel, John. 2014a. The M Segment of the 2009 Pandemic Influenza Virus Confers Increased Neuraminidase Activity, Filamentous Morphology, and Efficient Contact Transmissibility to A/Puerto Rico/8/1934-Based Reassortant Viruses. Journal of Virology, **88**(7), 3802–3814.

Campbell, Patricia J., Kyriakis, Constantinos S., Marshall, Nicolle, Suppiah, Suganthi, Seladi-Schulman, Jill, Danzy, Shamika, Lowen, Anice C., & Steel, John. 2014b. Residue 41 of the Eurasian Avian-Like Swine Influenza A Virus Matrix Protein Modulates Virion Filament Length and Efficiency of Contact Transmission. Journal of Virology, **88**(13), 7569–7577.

Carmody, Sean R., & Wente, Susan R. 2009. mRNA nuclear export at a glance. Journal of Cell Science, **122**(12), 1933–1937. Publisher: The Company of Biologists Ltd Section: Cell Science at a Glance.

Carrique, Loic, Fan, Haitian, Walker, Alexander P., Keown, Jeremy R., Sharps, Jane, Staller, Ecco, Barclay, Wendy S., Fodor, Ervin, & Grimes, Jonathan M. 2020. Host ANP32A mediates the assembly of the influenza virus replicase. Nature, **587**(7835), 638–643. Number: 7835 Publisher: Nature Publishing Group.

Castleman, W, L, Powe, J, R, Crawford, P, C, Gibbs, P, J, Dubovi, E, J, Donis, R, O, & Hanshaw, D. 2010. Canine H3N8 Influenza Virus Infection in Dogs and Mice. Veterinary Pathology.

CDC. 2020 (Oct.). Burden of Influenza. `https://www.cdc.gov/flu/about/burden/index.html`.

CDC. 2021 (Jan.). Influenza Antiviral Medications: Clinician Summary. `https://www.cdc.gov/flu/professionals/antivirals/summary-clinicians.htm`.

Chen, Benjamin J., Leser, George P., Morita, Eiji, & Lamb, Robert A. 2007. Influenza Virus Hemagglutinin and Neuraminidase, but Not the Matrix Protein, Are Required for Assembly and Budding of Plasmid-Derived Virus-Like Particles. Journal of Virology, **81**(13), 7111–7123.

Cheung, T. K. W., Guan, Y., Ng, S. S. F., Chen, H., Wong, C. H. K., Peiris, J. S. M., & Poon, L. L. M. 2005. Generation of recombinant influenza A virus without M2 ion-channel protein by introduction of a point mutation at the 5′ end of the viral intron. Journal of General Virology,, **86**(5), 1447–1454. Publisher: Microbiology Society,.

Chlanda, Petr, Schraidt, Oliver, Kummer, Susann, Riches, James, Oberwinkler, Heike, Prinz, Simone, Kräusslich, Hans-Georg, & Briggs, John A. G. 2015. Structural Analysis of the Roles of Influenza A Virus Membrane-Associated Proteins in Assembly and Morphology. Journal of Virology, **89**(17), 8957–8966.

Chlanda, Petr, Mekhedov, Elena, Waters, Hang, Sodt, Alexander, Schwartz, Cindi, Nair, Vinod, Blank, Paul S., & Zimmerberg, Joshua. 2017. Palmitoylation contributes to membrane curvature in Influenza A virus assembly and hemagglutinin-mediated membrane fusion. Journal of Virology, Aug.

Chou, Yi-ying, Heaton, Nicholas S., Gao, Qinshan, Palese, Peter, Singer, Robert, & Lionnet, Timothée. 2013. Colocalization of Different Influenza Viral RNA Segments in the Cytoplasm before Viral Budding as Shown by Single-molecule Sensitivity FISH Analysis. PLOS Pathogens, **9**(5), e1003358. Publisher: Public Library of Science.

Chu, C. M., Dawson, I. M., & Elford, W. J. 1949. Filamentous Forms Associated With Newly Isolated Influenza Virus. The Lancet, **253**(6554), 602–603.

Cox, J. C., Hampson, A. W., & Hamilton, R. C. 1980. An immunofluorescence study of influenza virus filament formation. Archives of Virology, **63**(3-4), 275–284.

Dadonaite, Bernadeta, Vijayakrishnan, Swetha, Fodor, Ervin, Bhella, David, & Hutchinson, Edward C. 2016. Filamentous influenza viruses. Journal of General Virology, **97**(8), 1755–1764.

Dawson, I. M., & Elford, W. J. 1949. The investigation of influenza and related viruses in the electron microscope, by a new technique. Journal of General Microbiology, **3**(2), 298–311.

de Castro Martin, Isabel Fernández, Fournier, Guillaume, Sachse, Martin, Pizarro-Cerda, Javier, Risco, Cristina, & Naffakh, Nadia. 2017. Influenza virus genome reaches the plasma membrane via a modified endoplasmic reticulum and Rab11-dependent vesicles. Nature Communications, **8**(1), 1396. Number: 1 Publisher: Nature Publishing Group.

Donald, H. B., & Isaacs, A. 1954a. Some properties of influenza virus filaments shown by electron microscopic particle counts. Journal of General Microbiology, **11**(2), 325–331.

Donald, Heather B., & Isaacs, A. 1954b. Counts of Influenza Virus Particles. Microbiology,, **10**(3), 457–464. Publisher: Microbiology Society,.

Donald, Heather B, & Isaacs, A. 1958. Microbiology Society Journals | Some Properties of Influenza Virus Filaments shown by Electron Microscopic Particle Counts. Journal of General Microbiology, **11**, 325–331.

Duc-Nguyen, Huu, & Rosenblum, Edith N. 1967. Immuno-Electron Microscopy of the Morphogenesis of Mumps Virus. Journal of Virology, **1**(2), 415–429.

Edmond, J. D., Johnston, R. G., Kidd, D., Rylance, H. J., & Sommerville, R. G. 1966. The Inhibition of Neuraminidase and Antiviral Action. British Journal of Pharmacology and Chemotherapy, **27**(2), 415–426. _eprint: https://bpspubs.onlinelibrary.wiley.com/doi/pdf/10.1111/j.1476-5381.1966.tb01673.x.

Eisfeld, Amie J., Neumann, Gabriele, & Kawaoka, Yoshihiro. 2014. Influenza A virus isolation, culture and identification. Nature Protocols, **9**(11), 2663–2681.

El Najjar, Farah, Nicolas Cifuentes-Munoz, Nicolas, Chen, Jing, Zhu, Haining, Bucholz, Ursula, J, Moncman, Carole, L, & Dutch, Rebecca, Ellis. 2016. Human metapneumovirus Induces Reorganization of the Actin Cytoskeleton for Direct Cell-to-Cell Spread. PLOS Pathogens.

Elleman, C. J., & Barclay, W. S. 2004. The M1 matrix protein controls the filamentous phenotype of influenza A virus. Virology, **321**(1), 144–153.

Elton, Debra, Bruce, Emily A., Bryant, Neil, Wise, Helen M., MacRae, Shona, Rash, Adam, Smith, Nikki, Turnbull, Matthew L., Medcalf, Liz, Daly, Janet M., & Digard, Paul. 2013. The genetics of virus particle shape in equine influenza A virus. Influenza and Other Respiratory Viruses, **7**(s4), 81–89.

Enami, M., Sharma, G., Benham, C., & Palese, P. 1991. An influenza virus containing nine different RNA segments. Virology, **185**(1), 291–298.

Fan, Haitian, Walker, Alexander P, Carrique, Loic, Keown, Jeremy R, Martin, Itziar Serna, Karia, Dimple, Sharps, Jane, Hengrung, Narin, Pardon, Els, Steyaert, Jan, Grimes, Jonathan M, & Fodor, Ervin. 2019. Influenza A virus RNA polymerase structures provide insights into viral genome replication. Nature, **573**(7773), 287–290.

Fleming, Douglas. 2005. Influenza pandemics and avian flu. BMJ : British Medical Journal, **331**(7524), 1066–1069.

Fodor, E. 2013. The RNA polymerase of influenza a virus: mechanisms of viral transcription and replication. Acta Virologica, **57**(2), 113–122.

Forde, Ciarán John, Meaney, Marie, Carrigan, John Bosco, Mills, Clive, Boland, Susan, & Hernon, Alan. 2014. Chapter 12 - Biobased Fats (Lipids) and Oils from Biomass as a Source of Bioenergy. Pages 185–201 of: Gupta, Vijai K., Tuohy, Maria G., Kubicek, Christian P., Saddler, Jack, & Xu, Feng (eds), Bioenergy Research: Advances and Applications. Amsterdam: Elsevier.

Fujii, Ken, Fujii, Yutaka, Noda, Takeshi, Muramoto, Yukiko, Watanabe, Tokiko, Takada, Ayato, Goto, Hideo, Horimoto, Taisuke, & Kawaoka, Yoshihiro. 2005. Importance of both the coding and the segment-specific noncoding regions of the influenza A virus NS segment for its efficient incorporation into virions. Journal of Virology, **79**(6), 3766–3774.

Fujii, Yutaka, Goto, Hideo, Watanabe, Tokiko, Yoshida, Tetsuya, & Kawaoka, Yoshihiro. 2003. Selective incorporation of influenza virus RNA segments into virions. Proceedings of the National Academy of Sciences of the United States of America, **100**(4), 2002–2007.

Fukuyama, Satoshi, Katsura, Hiroaki, Zhao, Dongming, Ozawa, Makoto, Ando, Tomomi, Shoemaker, Jason E., Ishikawa, Izumi, Yamada, Shinya, Neumann, Gabriele, Watanabe, Shinji, Kitano, Hiroaki, & Kawaoka, Yoshihiro. 2015. Multi-spectral fluorescent reporter influenza viruses (Color-flu) as powerful tools for in vivo studies. Nature Communications, **6**(Mar.), 6600.

Furuta, Yousuke, Gowen, Brian B., Takahashi, Kazumi, Shiraki, Kimiyasu, Smee, Donald F., & Barnard, Dale L. 2013. Favipiravir (T-705), a novel viral RNA polymerase inhibitor. Antiviral Research, **100**(2), 446–454.

Gaush, Charles R., & Smith, Thomas F. 1968. Replication and Plaque Assay of Influenza Virus in an Established Line of Canine Kidney Cells. Applied Microbiology, **16**(4), 588–594.

Gould, S. J., & Lewontin, R. C. 1979. The Spandrels of San Marco and the Panglossian Paradigm: A Critique of the Adaptationist Programme. Proceedings of the Royal Society of London. Series B, Biological Sciences, **205**(1161), 581–598.

Grantham, Michael L., Stewart, Shaun M., Lalime, Erin N., & Pekosz, Andrew. 2010. Tyrosines in the Influenza A Virus M2 Protein Cytoplasmic Tail Are Critical for Production of Infectious Virus Particles. Journal of Virology, **84**(17), 8765–8776.

Greiff, Donald, Blumenthal, Herman, Chiga, Masahiro, & Pinkerton, Henry. 1954. The Effects on Biological Materials of Freezing and Drying by Vacuum Sublimation: Ii. Effect on Influenza Virus. Journal of Experimental Medicine, **100**(1), 89–101.

Hale, Benjamin G., Randall, Richard E., Ortín, Juan, & Jackson, David. 2008. The multifunctional NS1 protein of influenza A viruses. Journal of General Virology,, **89**(10), 2359–2376. Publisher: Microbiology Society,.

Halldorsson, Steinar, Sader, Kasim, Turner, Jack, Calder, Lesley J., & Rosenthal, Peter B. 2021. In situ structure and organization of the influenza C virus surface glycoprotein. Nature Communications, **12**(1), 1694. Number: 1 Publisher: Nature Publishing Group.

Health-Protection-Scotland. 2021 (Feb.). HPS Website - Rapid Review of the literature: Assessing the infection prevention and control measures for the prevention and management of COVID-19 in healthcare settings.

Hill, J. A., Cohen, M. B., Kou, W. H., Mancini, G. B., Mansour, M., Fountaine, H., & Brinker, J. A. 1994. Iodixanol, a new isosmotic nonionic contrast agent compared with iohexol in cardiac angiography. The American Journal of Cardiology, **74**(1), 57–63.

Hirst, Jack C., & Hutchinson, Edward C. 2019. Single-particle measurements of filamentous influenza virions reveal damage induced by freezing. The Journal of general virology, **100**(12), 1631–1640.

Horne, R. W., Waterson, A. P., Wildy, P., & Farnham, A. E. 1960. The structure and composition of the myxoviruses. I. Electron microscope studies of the structure of myxovirus particles by negative staining techniques. Virology, **11**(May), 79–98.

Houser, Katherine, & Subbarao, Kanta. 2015. Influenza Vaccines: Challenges and Solutions. Cell host & microbe, **17**(3), 295–300.

Huang, I.-Chueh, Li, Wenhui, Sui, Jianhua, Marasco, Wayne, Choe, Hyeryun, & Farzan, Michael. 2008. Influenza A virus neuraminidase limits viral superinfection. Journal of Virology, **82**(10), 4834–4843.

Huang, Shengping, Chen, Jingjing, Chen, Quanjiao, Wang, Huadong, Yao, Yanfeng, Chen, Jianjun, & Chen, Ze. 2013. A second CRM1-dependent nuclear export signal in the influenza A virus NS2 protein contributes to the nuclear export of viral ribonucleoproteins. Journal of Virology, **87**(2), 767–778.

Hutchinson, E. C., & Fodor, E. 2012. Nuclear import of the influenza A virus transcriptional machinery. Vaccine, **30**(51), 7353–7358.

Hutchinson, Edward C., & Fodor, Ervin. 2013. Transport of the Influenza Virus Genome from Nucleus to Nucleus. Viruses, **5**(10), 2424–2446.

Hutchinson, Edward C., & Yamauchi, Yohei. 2018. Understanding Influenza. Methods in Molecular Biology (Clifton, N.J.), **1836**, 1–21.

Hutchinson, Edward C., Curran, Martin D., Read, Eliot K., Gog, Julia R., & Digard, Paul. 2008. Mutational Analysis of cis-Acting RNA Signals in Segment 7 of Influenza A Virus. Journal of Virology, **82**(23), 11869–11879. Publisher: American Society for Microbiology.

Hutchinson, Edward C., von Kirchbach, Johann C., Gog, Julia R., & Digard, Paul. 2010. Genome packaging in influenza A virus. The Journal of General Virology, **91**(Pt 2), 313–328.

Hutchinson, Edward C., Charles, Philip D., Hester, Svenja S., Thomas, Benjamin, Trudgian, David, Martínez-Alonso, Mónica, & Fodor, Ervin. 2014. Conserved and host-specific features of influenza virion architecture. Nature Communications, **5**(Sept.), 4816.

Iacobucci, Gareth. 2020. Covid lockdown: England sees fewer cases of colds, flu, and bronchitis. BMJ, **370**(Aug.), m3182. Publisher: British Medical Journal Publishing Group Section: News.

IMF. 2020 (Oct.). World Economic Outlook, October 2020: A Long and Difficult Ascent.

Iwatsuki-Horimoto, Kiyoko, Horimoto, Taisuke, Noda, Takeshi, Kiso, Maki, Maeda, Junko, Watanabe, Shinji, Muramoto, Yukiko, Fujii, Ken, & Kawaoka, Yoshihiro. 2006. The cytoplasmic tail of the influenza A virus M2 protein plays a role in viral assembly. Journal of Virology, **80**(11), 5233–5240.

Jackson, G. G., Muldoon, R. L., & Akers, L. W. 1963. Serological Evidence For Prevention Of Influenzal Infection In Volunteers By An Anti-Influenzal Drug Adamantanamine Hydrochloride. Antimicrobial Agents and Chemotherapy, **161**, 703–707.

Janeway, Charles A Jr, Travers, Paul, Walport, Mark, & Schlomchik, Mark J. 2001. Principles of innate and adaptive immunity - Immunobiology - NCBI Bookshelf. Garland Science.

Jin, H., Leser, G. P., & Lamb, R. A. 1994. The influenza virus hemagglutinin cytoplasmic tail is not essential for virus assembly or infectivity. The EMBO journal, **13**(22), 5504–5515.

Jones, Jennifer E., Le Sage, Valerie, & Lakdawala, Seema S. 2020. Viral and host heterogeneity and their effects on the viral life cycle. Nature Reviews Microbiology, Oct., 1–11. Publisher: Nature Publishing Group.

Kataoka, Michiyo, Ishida, Kinji, Ogasawara, Katsutoshi, Nozaki, Takayuki, Satoh, Yoh-Ichi, Sata, Tetsutaro, Sato, Yuko, Hasegawa, Hideki, & Nakajima, Noriko. 2019. Serial Section Array Scanning Electron Microscopy Analysis of Cells from Lung Autopsy Specimens Following Fatal A/H1N1 2009 Pandemic Influenza Virus Infection. Journal of Virology, July.

Kheradvar, Arash, & Pedrizzetti, Gianni. 2012. Vortex Dynamics. Pages 17–44 of: Kheradvar, Arash, & Pedrizzetti, Gianni (eds), Vortex Formation in the Cardiovascular System. London: Springer.

Kilbourne, Edwin D., & Murphy, James S. 1960. Genetic Studies Of Influenza Viruses. The Journal of Experimental Medicine, **111**(3), 387–406.

Klimenko, S. M., Orlova, N. N., Gushchin, B. V., Bukrinskaia, A. G., Smirnov, Iu A., & Glagolev, A. A. 1968. [Mechanism of fragmentation of the thread-like form of the influenza virus]. Vestnik Akademii meditsinskikh nauk SSSR, **23**(9), 60–64.

Klug, A. 1999. The tobacco mosaic virus particle: structure and assembly. Philosophical Transactions of the Royal Society B: Biological Sciences, **354**(1383), 531–535.

Kolesnikova, Larissa, Heck, Sonja, Matrosovich, Tatyana, Klenk, Hans-Dieter, Becker, Stephan, & Matrosovich, Mikhail. 2013. Influenza virus budding from the tips of cellular microvilli in differentiated human airway epithelial cells. The Journal of General Virology, **94**(Pt 5), 971–976.

Kolpe, Annasaheb, Arista-Romero, Maria, Schepens, Bert, Pujals, Silvia, Saelens, Xavier, & Albertazzi, Lorenzo. 2019. Super-resolution microscopy reveals significant impact of M2e-specific monoclonal antibodies on influenza A virus filament formation at the host cell surface. Scientific Reports, **9**(1), 4450.

Kon, Theone C., Onu, Adrian, Berbecila, Laurentiu, Lupulescu, Emilia, Ghiorgisor, Alina, Kersten, Gideon F., Cui, Yi-Qing, Amorij, Jean-Pierre, & Van der Pol, Leo. 2016. Influenza Vaccine Manufacturing: Effect of Inactivation, Splitting and Site of Manufacturing. Comparison of Influenza Vaccine Production Processes. PLoS ONE, **11**(3).

Kordyukova, Larisa V., Mintaev, Ramil R., Rtishchev, Artyom A., Kunda, Marina S., Ryzhova, Natalia N., Abramchuk, Sergei S., Serebryakova, Marina V., Khrustalev, Vladislav V., Khrustaleva, Tatyana A., Poboinev, Victor V., Markushin, Stanislav G., & Voronina, Olga L. 2020. Filamentous versus Spherical Morphology: A Case Study of the Recombinant A/WSN/33 (H1N1) Virus. Microscopy and Microanalysis: The Official Journal of Microscopy Society of America, Microbeam Analysis Society, Microscopical Society of Canada, **26**(2), 297–309.

Krammer, Florian, Smith, Gavin J. D., Fouchier, Ron A. M., Peiris, Malik, Kedzierska, Katherine, Doherty, Peter C., Palese, Peter, Shaw, Megan L., Treanor, John, Webster, Robert G., & García-Sastre, Adolfo. 2018. Influenza. Nature Reviews Disease Primers, **4**(1), 1–21. Number: 1 Publisher: Nature Publishing Group.

Kumar, Amrita, Kim, Jin Hyang, Ranjan, Priya, Metcalfe, Maureen G., Cao, Weiping, Mishina, Margarita, Gangappa, Shivaprakash, Guo, Zhu, Boyden, Edward S., Zaki, Sherif, York, Ian, García-Sastre, Adolfo, Shaw, Michael, & Sambhara, Suryaprakash. 2017. Influenza virus exploits tunneling nanotubes for cell-to-cell spread. Scientific Reports, **7**(1), 40360. Number: 1 Publisher: Nature Publishing Group.

Kuznetsova, M. A., Smirnov, Iu A., Makhov, A. M., & Kaverin, N. V. 1990. [Comparative characteristics of spherical and filamentous virions of influenza virus type A]. Voprosy Virusologii, **35**(1), 20–23.

Lai, Jimmy C. C., Chan, Wallace W. L., Kien, François, Nicholls, John M., Peiris, J. S. Malik, & Garcia, Jean-Michel. 2010. Formation of virus-like particles from human cell lines exclusively expressing influenza neuraminidase. The Journal of General Virology, **91**(Pt 9), 2322–2330.

Lakdawala, Seema S., Lamirande, Elaine W., Suguitan, Amorsolo L., Wang, Weijia, Santos, Celia P., Vogel, Leatrice, Matsuoka, Yumiko, Lindsley, William G., Jin, Hong, & Subbarao, Kanta. 2011. Eurasian-origin gene segments contribute to the transmissibility, aerosol release, and morphology of the 2009 pandemic H1N1 influenza virus. PLoS pathogens, **7**(12), e1002443.

Li, Tian, Li, Zhenyu, Deans, Erin E., Mittler, Eva, Liu, Meisui, Chandran, Kartik, & Ivanovic, Tijana. 2021. The shape of pleomorphic virions determines resistance to cell-entry pressure. Nature Microbiology, Mar.

Liu, Hsuan, Grantham, Michael L., & Pekosz, Andrew. 2017. Mutations in the Influenza A virus M1 protein enhance virus budding to complement lethal mutations in the M2 cytoplasmic tail. Journal of Virology, Oct.

Liu, Teresa, Muller, Jacqueline, & Ye, Zhiping. 2002. Association of Influenza Virus Matrix Protein with Ribonucleoproteins May Control Viral Growth and Morphology. Virology, **304**(1), 89–96.

Mahmoudabadi, Gita, Milo, Ron, & Phillips, Rob. 2017. Energetic cost of building a virus. Proceedings of the National Academy of Sciences, May, 201701670.

Makhov, A. M., Smirnov, Iu A., Kuznetsova, S. M., & Klimenko, S. M. 1989. [The phenomenon of transition of filamentous virions of influenza viruses into spherical virions]. Voprosy Virusologii, **34**(3), 274–279.

Marsh, Glenn A., Rabadán, Raúl, Levine, Arnold J., & Palese, Peter. 2008. Highly conserved regions of influenza a virus polymerase gene segments are critical for efficient viral RNA packaging. Journal of Virology, **82**(5), 2295–2304.

Martin, Isabel Fernández de Castro, Fournier, Guillaume, Sachse, Martin, Pizarro-Cerda, Javier, Risco, Cristina, & Naffakh, Nadia. 2017. Influenza virus genome reaches the plasma membrane via a modified endoplasmic reticulum and Rab11-dependent vesicles. Nature Communications, **8**(1), 1396.

Martin, K., & Helenius, A. 1991. Transport of incoming influenza virus nucleocapsids into the nucleus. Journal of Virology, **65**(1), 232–244.

McGann, Locksley E., & Walterson, Michele L. 1987. Cryoprotection by dimethyl sulfoxide and dimethyl sulfone. Cryobiology, **24**(1), 11–16.

Mitnaul, L J, Castrucci, M R, Murti, K G, & Kawaoka, Y. 1996. The cytoplasmic tail of influenza A virus neuraminidase (NA) affects NA incorporation into virions, virion morphology, and virulence in mice but is not essential for virus replication. Journal of Virology, **70**(2), 873–879.

Müller, G. 1976. Disaggregation of vaccinia virus with ultrasonic cleaners. Archives of Virology, **51**(4), 365–367.

Morgan, Councilman, Rose, Harry M., & Moore, Dan H. 1956. Structure And Development Of Viruses Observed In The Electron Microscope. The Journal of Experimental Medicine, **104**(2), 171–182.

Mosley, V. M., & Wyckoff, Ralph W. G. 1946. Electron Micrography of the Virus of Influenza. Nature, **157**(3983), 263.

Muraki, Yasushi, Washioka, Hiroshi, Sugawara, Kanetsu, Matsuzaki, Yoko, Takashita, Emi, & Hongo, Seiji. 2004. Identification of an amino acid residue on influenza C virus M1 protein responsible for formation of the cord-like structures of the virus. The Journal of General Virology, **85**(Pt 7), 1885–1893.

Murphy, J. S., Karzon, D. T., & Bang, F. B. 1950. Studies of Influenza A (PR8) Infected Tissue Cultures by Electron Microscopy. Proceedings of the Society for Experimental Biology and Medicine, **73**(4), 596–599. Publisher: SAGE Publications.

Nakajima, K., & Sugiura, A. 1977. Three-factor cross of influenza virus. Virology, **81**(2), 486–489.

Nakajima, Noriko, Hata, Satoru, Sato, Yuko, Tobiume, Minoru, Katano, Harutaka, Kaneko, Keiko, Nagata, Noriyo, Kataoka, Michiyo, Ainai, Akira, Hasegawa, Hideki, Tashiro, Masato, Kuroda, Makoto, Odai, Tamami, Urasawa, Nobuyuki, Ogino, Tomoyoshi, Hanaoka, Hiroaki, Watanabe, Masahide, & Sata, Tetsutaro. 2010. The first autopsy case of pandemic influenza (A/H1N1pdm) virus infection in Japan: detection of a high copy number of the virus in type II alveolar epithelial cells by pathological and virological examination. Japanese Journal of Infectious Diseases, **63**(1), 67–71.

Okoli, George N., Otete, Harmony E., Beck, Charles R., & Nguyen-Van-Tam, Jonathan S. 2014. Use of neuraminidase inhibitors for rapid containment of influenza: a systematic review and meta-analysis of individual and household transmission studies. PloS One, **9**(12), e113633.

Omoto, Shinya, Speranzini, Valentina, Hashimoto, Takashi, Noshi, Takeshi, Yamaguchi, Hiroto, Kawai, Makoto, Kawaguchi, Keiko, Uehara, Takeki, Shishido, Takao, Naito, Akira, & Cusack, Stephen. 2018. Characterization of influenza virus variants induced by treatment with the endonuclease inhibitor baloxavir marboxil. Scientific Reports, **8**(1), 9633.

ONS. 2020 (July). Direct and Indirect Impacts of COVID-19 on Excess Deaths and Morbidity: Executive Summary.

Organisation, World Health. 2021. WHO | WHO recommendations on the composition of influenza virus vaccines. Publisher: World Health Organization.

Ozawa, Makoto, Fujii, Ken, Muramoto, Yukiko, Yamada, Shinya, Yamayoshi, Seiya, Takada, Ayato, Goto, Hideo, Horimoto, Taisuke, & Kawaoka, Yoshihiro. 2007. Contributions of Two Nuclear Localization Signals of Influenza A Virus Nucleoprotein to Viral Replication. Journal of Virology, **81**(1), 30–41. Publisher: American Society for Microbiology.

Ozawa, Makoto, Maeda, Junko, Iwatsuki-Horimoto, Kiyoko, Watanabe, Shinji, Goto, Hideo, Horimoto, Taisuke, & Kawaoka, Yoshihiro. 2009. Nucleotide sequence requirements at the 5' end of the influenza A virus M RNA segment for efficient virus replication. Journal of Virology, **83**(7), 3384–3388.

Peukes, Julia, Xiong, Xiaoli, Erlendsson, Simon, Qu, Kun, Wan, William, Calder, Leslie J., Schraidt, Oliver, Kummer, Susann, Freund, Stefan M. V., Kräusslich, Hans-Georg, & Briggs, John A. G. 2020. The native structure of the assembled matrix protein 1 of influenza A virus. Nature, **587**(7834), 495–498.

Pinto, Rute Maria. 2019. Identification Of Novel Accessory Proteins Encoded By Influenza A Virus Segment 2 That Prevent Interferon Induction. Ph.D. thesis, University of Edinburgh.

Putri, Wayan C. W. S., Muscatello, David J., Stockwell, Melissa S., & Newall, Anthony T. 2018. Economic burden of seasonal influenza in the United States. Vaccine, **36**(27), 3960–3966.

Rakonjac, Jasna, Bennett, Nicholas J., Spagnuolo, Julian, Gagic, Dragana, & Russel, Marjorie. 2011. Filamentous bacteriophage: biology, phage display and nanotechnology applications. Current Issues in Molecular Biology, **13**(2), 51–76.

Randall, Richard E., & Goodbourn, Stephen. 2008. Interferons and viruses: an interplay between induction, signalling, antiviral responses and virus countermeasures. The Journal of General Virology, **89**(Pt 1), 1–47.

Rickwood, D. 1984. Centrifugation: a practical approach. IRL Press.

Roberts, Kari L., Leser, George P., Ma, Chunlong, & Lamb, Robert A. 2013. The amphipathic helix of influenza A virus M2 protein is required for filamentous bud formation and scission of filamentous and spherical particles. Journal of Virology, **87**(18), 9973–9982.

Roberts, Paul C., & Compans, Richard W. 1998. Host cell dependence of viral morphology. Proceedings of the National Academy of Sciences of the United States of America, **95**(10), 5746–5751.

Roberts, Paul C., Lamb, Robert A., & Compans, Richard W. 1998. The M1 and M2 Proteins of Influenza A Virus Are Important Determinants in Filamentous Particle Formation. Virology, **240**(1), 127–137.

Rodrigues, Joao V, & Shakhnovich, Eugene I. 2019. Adaptation to mutational inactivation of an essential gene converges to an accessible suboptimal fitness peak. eLife, **8**(Oct.), e50509. Publisher: eLife Sciences Publications, Ltd.

Rossman, Jeremy S., & Lamb, Robert A. 2011. Influenza Virus Assembly and Budding. Virology, **411**(2), 229–236.

Rossman, Jeremy S., Jing, Xianghong, Leser, George P., Balannik, Victoria, Pinto, Lawrence H., & Lamb, Robert A. 2010. Influenza Virus M2 Ion Channel Protein Is Necessary for Filamentous Virion Formation. Journal of Virology, **84**(10), 5078–5088.

Rossman, Jeremy S., Leser, George P., & Lamb, Robert A. 2012. Filamentous Influenza Virus Enters Cells via Macropinocytosis. Journal of Virology, **86**(20), 10950–10960.

Sakai, Tatsuya, Takagi, Hiroaki, Muraki, Yasushi, & Saito, Mineki. 2017. Unique directional motility of influenza C virus controlled by its filamentous morphology and short-range motions. Journal of Virology, Nov., JVI.01522–17.

Saletti, David, Radzimanowski, Jens, Effantin, Gregory, Midtvedt, Daniel, Mangenot, Stéphanie, Weissenhorn, Winfried, Bassereau, Patricia, & Bally, Marta. 2017. The Matrix protein M1 from influenza C virus induces tubular membrane invaginations in an in vitro cell membrane model. Scientific Reports, **7**(Jan.).

Sato, Ryota, Okura, Takashi, Kawahara, Madoka, Takizawa, Naoki, Momose, Fumitaka, & Morikawa, Yuko. 2019. Apical Trafficking Pathways of Influenza A Virus HA and NA via Rab17- and Rab23-Positive Compartments. Frontiers in Microbiology, **10**(Aug.).

Schindelin, Johannes, Arganda-Carreras, Ignacio, Frise, Erwin, Kaynig, Verena, Longair, Mark, Pietzsch, Tobias, Preibisch, Stephan, Rueden, Curtis, Saalfeld, Stephan, Schmid, Benjamin, Tinevez, Jean-Yves, White, Daniel James, Hartenstein, Volker, Eliceiri, Kevin, Tomancak, Pavel, & Cardona, Albert. 2012. Fiji: an open-source platform for biological-image analysis. Nature Methods, **9**(7), 676–682.

Seladi-Schulman, Jill, Steel, John, & Lowen, Anice C. 2013. Spherical Influenza Viruses Have a Fitness Advantage in Embryonated Eggs, while Filament-Producing Strains Are Selected In Vivo. Journal of Virology, **87**(24), 13343–13353.

Seladi-Schulman, Jill, Campbell, Patricia J., Suppiah, Suganthi, Steel, John, & Lowen, Anice C. 2014. Filament-producing mutants of influenza A/Puerto Rico/8/1934 (H1N1) virus have higher neuraminidase activities than the spherical wild-type. PloS One, **9**(11), e112462.

Sharp, D. G. 1965. Quantitative use of the electron microscope in virus research. Methods and recent results of particle counting. Laboratory Investigation; a Journal of Technical Methods and Pathology, **14**(June), 831–863.

Sieben, Christian, Sezgin, Erdinc, Eggeling, Christian, & Manley, Suliana. 2020. Influenza A viruses use multivalent sialic acid clusters for cell binding and receptor activation. PLOS Pathogens, **16**(7), e1008656. Publisher: Public Library of Science.

Sieczkarski, S. B., & Whittaker, G. R. 2005. Characterization of the host cell entry of filamentous influenza virus. Archives of Virology, **150**(9), 1783–1796.

Simpson-Holley, Martha, Ellis, Darren, Fisher, Dawn, Elton, Debra, McCauley, John, & Digard, Paul. 2002. A Functional Link between the Actin Cytoskeleton and Lipid Rafts during Budding of Filamentous Influenza Virions. Virology, **301**(2), 212–225.

Singanayagam, Anika, Zambon, Maria, & Barclay, Wendy S. 2019. Influenza Virus with Increased pH of Hemagglutinin Activation Has Improved Replication in Cell Culture but at the Cost of Infectivity in Human Airway Epithelium. Journal of Virology, **93**(17).

Skehel, John J., & Wiley, Don C. 2000. Receptor Binding and Membrane Fusion in Virus Entry: The Influenza Hemagglutinin. Annual Review of Biochemistry, **69**(1), 531–569.

Smirnov, Yu. A., Kuznetsova, M. A., & Kaverin, N. V. 1991. The genetic aspects of influenza virus filamentous particle formation. Archives of Virology, **118**(3-4), 279–284.

Speshock, Janice L., Doyon-Reale, Nicole, Rabah, R., Neely, Melody N., & Roberts, Paul C. 2007. Filamentous influenza A virus infection predisposes mice to fatal septicemia following superinfection with Streptococcus pneumoniae serotype 3. Infection and Immunity, **75**(6), 3102–3111.

Spinney, Laura. 2017. Pale Rider: The Spanish Flu Of 1918 And How It Changed The World. Penguin Books.

Sugita, Yukihiko, Noda, Takeshi, Sagara, Hiroshi, & Kawaoka, Yoshihiro. 2011. Ultracentrifugation deforms unfixed influenza A virions. The Journal of General Virology, **92**(Pt 11), 2485–2493.

Taylor, A. R., Sharp, D. G., Beard, Dorothy, Beard, J. W., Dingle, John H., & Feller, A. E. 1943. Isolation and Characterization of Influenza A Virus (PR8 Strain). The Journal of Immunology, **47**(3), 261–282. Publisher: American Association of Immunologists.

te Velthuis, Aartjan J. W., & Fodor, Ervin. 2016. Influenza virus RNA polymerase: insights into the mechanisms of viral RNA synthesis. Nature Reviews Microbiology, **14**(8), 479–493. Number: 8 Publisher: Nature Publishing Group.

Tsfasman, Tatyana, Kost, Vladimir, Markushin, Stanislav, Lotte, Vera, Koptiaeva, Irina, Bogacheva, Elena, Baratova, Ludmila, & Radyukhin, Victor. 2015. Amphipathic alpha-helices and putative cholesterol binding domains of the influenza virus matrix M1 protein are crucial for virion structure organisation. Virus Research, **210**(Dec.), 114–118.

Vahey, Michael D, & Fletcher, Daniel A. 2019a. Influenza A virus surface proteins are organized to help penetrate host mucus. eLife, **8**(May), e43764.

Vahey, Michael D., & Fletcher, Daniel A. 2019b. Low-Fidelity Assembly of Influenza A Virus Promotes Escape from Host Cells. Cell, **176**(1-2), 281–294.e19.

Valentine, R. C., & Isaacs, A. 1957. The Structure of Viruses of the Newcastle Disease-Mumps-Influenza (Myxovirus) Group. Microbiology, **16**(3), 680–685.

Van Den Berg, L. 1966. pH changes in buffers and foods during freezing and subsequent storage. Cryobiology, **3**(3), 236–242.

Verdaasdonk, Jolien Suzanne, Lawrimore, Josh, & Bloom, Kerry. 2014. Determining absolute protein numbers by quantitative fluorescence microscopy. Methods in cell biology, **123**, 347–365.

Vijayakrishnan, Swetha, Loney, Colin, Jackson, David, Suphamungmee, Worawit, Rixon, Frazer J., & Bhella, David. 2013. Cryotomography of Budding Influenza A Virus Reveals Filaments with Diverse Morphologies that Mostly Do Not Bear a Genome at Their Distal End. PLOS Pathog, **9**(6), e1003413.

Wagner, Thorsten, Hiner, Mark, & xraynaud. 2017 (Aug.). thorstenwagner/ij-ridgedetection: Ridge Detection 1.4.0.

Werner, Georges H., & Schlesinger, R. Walter. 1954. Morphological And Quantitative Comparison Between Infectious And Non-Infectious Forms Of Influenza Virus. The Journal of Experimental Medicine, **100**(2), 203–216.

Wiegmann, Lena, de Zélicourt, Diane A., Speer, Oliver, Muller, Alissa, Goede, Jeroen S., Seifert, Burkhardt, & Kurtcuoglu, Vartan. 2017. Influence of Standard Laboratory Procedures on Measures of Erythrocyte Damage. Frontiers in Physiology, **8**(Sept.).

Wilson, Martin. 2016 (Dec.). Microscope Resolution: Concepts, Factors and Calculation.

Wong, Jessica Y., Kelly, Heath, Ip, Dennis K. M., Wu, Joseph T., Leung, Gabriel M., & Cowling, Benjamin J. 2013. Case fatality risk of influenza A(H1N1pdm09): a systematic review. Epidemiology (Cambridge, Mass.), **24**(6).

Xie, Y., Wang, F., Puscheck, E. E., & Rappolee, D. A. 2007. Pipetting causes shear stress and elevation of phosphorylated stress-activated protein kinase/jun kinase in preimplantation embryos. Molecular Reproduction and Development, **74**(10), 1287–1294.

Yao, Qizhi, & Compans, Richard W. 2000. Filamentous particle formation by human parainfluenza virus type 2. Journal of General Virology, **81**(5), 1305–1312.

Ye, Jianqiang, Sorrell, Erin M., Cai, Yibin, Shao, Hongxia, Xu, Kemin, Pena, Lindomar, Hickman, Danielle, Song, Haichen, Angel, Matthew, Medina, Rafael A., Manicassamy, Balaji, Garcia-Sastre, Adolfo, & Perez, Daniel R. 2010. Variations in the Hemagglutinin of the 2009 H1N1 Pandemic Virus: Potential for Strains with Altered Virulence Phenotype? PLOS Pathogens, **6**(10), e1001145.

Ye, Qiaozhen, Guu, Tom S. Y., Mata, Douglas A., Kuo, Rei-Lin, Smith, Bartram, Krug, Robert M., & Tao, Yizhi J. 2012. Biochemical and structural evidence in support of a coherent model for the formation of the double-helical influenza A virus ribonucleoprotein. mBio, **4**(1), e00467–00412.

Zanin, Mark, Marathe, Bindumadhav, Wong, Sook-San, Yoon, Sun-Woo, Collin, Emily, Oshansky, Christine, Jones, Jeremy, Hause, Benjamin, & Webby, Richard. 2015. Pandemic Swine H1N1 Influenza Viruses with Almost Undetectable Neuraminidase Activity Are Not Transmitted via Aerosols in Ferrets and Are Inhibited by Human Mucus but Not Swine Mucus. Journal of Virology, **89**(11), 5935–5948.

Zhu, Junda, Jiang, Zhimin, & Liu, Jinhua. 2021. The matrix gene of pdm/09 H1N1 contributes to the pathogenicity and transmissibility of SIV in mammals. Veterinary Microbiology, **255**(Mar.), 109039.

Appendix A

Scripts

A.1 Image J Macros

BatchFilamentAnalysis.ijm

```
//BatchFilamentAnalysis.ijm
//Iterates through a folder containing micrographs, measures the lengths of
    the filaments in each and saves the list of lengths as a csv file for
    each micrograph

//Allows selection of the appropriate folder and selects which file type to
    analysis
@ File (label = "Input directory", style = "directory") input
output = input
#@ String (label = "File suffix", value = ".czi") suffix
e.

processFolder(input);

// function to scan folders/subfolders/files to find files with correct
    suffix
function processFolder(input) {
   list = getFileList(input);
   for (i = 0; i < list.length; i++) {
      if(File.isDirectory(input + File.separator + list[i]))
         processFolder(input + File.separator + list[i]);
      if(endsWith(list[i], suffix))
         processFile(input, list[i]);
   }
}
```

```
function processFile(input, file) {
   print("Processing: " + input + File.separator + file);
   open(input + File.separator + file);

   //Converts to a binary image, which is required by particle remover
   setAutoThreshold("Default dark");
   run("Convert to Mask");

   //Removes all circular particles to prevent ring shaped debris being
      classes as filaments
   run("Colors...", "foreground=black background=black selection=yellow");
   run("Particle Remover", " circularity=0.50-1.00 include");

   //For unclear reasons, this line is necessary on my work pc and not my
      home pc
   //run("Invert LUT");

   //Detects all filamentous particles using Ridge Detection
   run("Set Scale...", "distance=4.6267 known=0.45 pixel=1 unit=micron");
   run("Ridge Detection", "line_width=5 high_contrast=230 low_contrast=87
      extend_line displayresults method_for_overlap_resolution=NONE sigma=2
      lower_threshold=3.06 upper_threshold=7.99 minimum_line_length=15
      maximum=0");

   //Saves output and closes windows before the next iteration
   selectWindow("Summary");
   saveAs("Results", input + File.separator + getCleanTitle(file) + ".csv");
   run("Close");
   run("Close All");
   close("Results");
   close("Junctions");
}

function getCleanTitle(aString)
//Extracts the czi file name from the file path so it can be used to name
    the csv file
{
   last = lastIndexOf(aString, ".");
   cleanTitle = substring(aString, 0, last);
   return cleanTitle;
}
```

A.1.1 BatchSphereAnalysis.ijm

```
//BatchSphereAnalysis.ijm
//Iterates through a folder containing micrographs, and counts the
    spherical objects that could be non-filamentous virions. Currently lacks
    a save function, so output has to be copied from the results window

//Allows selection of the appropriate folder and selects which file type to
    analysis
#@ File (label = "Input directory", style = "directory") input
output = input
#@ String (label = "File suffix", value = ".czi") suffix

processFolder(input);

// function to scan folders/subfolders/files to find files with correct
    suffix
function processFolder(input) {
   run("Set Measurements...", "area display redirect=None decimal=3");
   list = getFileList(input);
   //list = Array.sort(list);
   for (i = 0; i < list.length; i++) {
      if(File.isDirectory(input + File.separator + list[i]))
         processFolder(input + File.separator + list[i]);
      if(endsWith(list[i], suffix))
         processFile(input, list[i]);
   }
}

function processFile(input, file) {
   print("Processing: " + input + File.separator + file);
   open(input + File.separator + file);

   //thresholds the image to allow Analyze Particles
   setAutoThreshold("Default dark");
   run("Convert to Mask");

   //Detects all the highly circular particles in a reasonable size range
       for non-filamentous virions
   run("Set Scale...", "distance=4.6267 known=0.45 pixel=1 unit=micron");
   run("Analyze Particles...", "size=0.03-0.10 circularity=0.90-1.00 display
       include");
   run("Close All");
}
```

A.1.2 Eccentricity Analysis.ijm

```
//Eccentricity Analysis.ijm
//Takes micrographs, detects the filamentous particles in each, fits an
    ellipse to the particles, and saves the major and minor axis for each
    ellipse in a csv file. Assumes the lowest level folders each represent
    one coverslip, and groups the data from each micrograph in that folder

//Specify input and output directories, and an arbitrary experiment code to
    name the output csv files
#@ File (label = "Input directory", style = "directory") input
#@ File (label = "Output directory", style = "directory") output
#@ String (label = "File suffix", value = ".czi") suffix
#@ String (label = "Experiment Code", value = "") exptCode

//Sets FIJI parameters to fit ellipses and measure the axes
run("Set Measurements...", "area fit redirect=None decimal=2");
processFolder(input);

// function to scan folders/subfolders/files to find the lowest level
    folders, and then to find files with correct suffix in that folder.
    Process each file in the folder, then saves the results as a csv file
function processFolder(input)
{
   list = getFileList(input);
   for (i = 0; i < list.length; i++) {
      if(File.isDirectory(input + File.separator + list[i]))
      {
         processFolder(input + File.separator + list[i]);
      }
      if(endsWith(list[i], suffix))
      {
         processFile(input, list[i]);
      }
      if(i == list.length-1)
         {
         currentLocation = input + File.separator + list[i];
         title = getFolderTitle(currentLocation);

         print("Saving as " + output + File.separator + exptCode + " " +
             title + ".csv");
```

```
        saveAs("Results", output + File.separator + exptCode + " " + title +
            ".csv");
        close("Results");
        }
   }
}

function processFile(input, file) {
   print("Processing: " + input + File.separator + file);
   open(input + File.separator + file);

   //Thresholds the image to allow Analyze Particles
   setAutoThreshold("Default dark");
   run("Convert to Mask");

   //Measures major and minor axes of fitted ellipses using Analyze
      Particles. Assumes all particles with circularities below 0.5 are
      filamentous.
   run("Analyze Particles...", " circularity=0.00-0.50 display include");
   run("Close All");
   selectWindow("Summary");
   saveAs("Results", input + File.separator + getCleanTitle(file) +
      "distortions" + ".csv");
}

function getCleanTitle(aString)
//extracts the name of the file being processed from the file path
{
   last = lastIndexOf(aString, ".");
   cleanTitle = substring(aString, 0, last);
   return cleanTitle;
}
function getFolderTitle(aString)
//extracts the name of the folder being processed from the file path
{
   last = lastIndexOf(aString, File.separator);
   newString = substring(aString, 0, last);
   penultimate = lastIndexOf(newString, File.separator);
   folderTitle = substring(aString, penultimate + 1, last - 1);
   return folderTitle;
}
```

A.2 Python scripts

A.2.1 FilamentAnalysisFunctions.py

```
"""
Created on Tue Jun 18 14:37:40 2019
@author: Jack Hirst
FilamentAnalysisFunctions.py
Contains several useful functions for plotting graphs when analysing
    filamentous virions - all are called by other functions within this file
    or in FilamentAnalysisPlots.py
"""

import pandas as pd
import numpy as np
from scipy import stats
import scipy.stats as st
import math
import itertools
import matplotlib.pyplot as plt
from scipy.optimize import curve_fit

def calculate_eccentricity(major, minor):
    '''takes the major and minor axes of an ellipse and returns the
       eccentricity'''
    return(np.sqrt(1-np.square((minor/2))/np.square(major/2)))

def mean_eccentricity_of_frame(frame):
   ''' calculates the eccentricity of every pair of major and minor axes in
      a data frame and returns the mean'''
    eccentricities = [calculate_eccentricity(major,minor) for major,minor
                      in zip(frame["Major"], frame["Minor"])]
    return(np.mean(eccentricities))

def strip_nans(a_list):
    ''' takes a list and returns all values that aren't na'''
    return([x for x in a_list if str(x) != "nan"])

def get_data_frames(list_of_file_names):
    '''takes a list of csv file names and imports the files as data frames'''
    frames = []
    for name in list_of_file_names:
        frames += [pd.read_csv(name + ".csv", delimiter = ",")]
```

```
    return(frames)

def get_counts(some_frames):
    ''' takes a list of data frames and returns a list of the counts for
    each column'''
    counts_list = []
    for frame in some_frames:
        counts_list += [frame.count()]
    return(counts_list)

def normalise_to_first(counts_list):
    '''normalises each value relative to the first column'''
    normalised_count = [x/counts_list[0] for x in counts_list]
    return(normalised_count)

def get_param_for_column(list_of_counts_lists, col_index, param_function):
    '''if a list of lists of values were arranged as a dataframe, this
    returns the outcome of a function applied to a given column in that
        frame'''
    targets = []
    try:
        for counts_list in list_of_counts_lists:
            targets += [counts_list[col_index]]
    except IndexError:
        print("")
    return(param_function(targets))

def get_all_params(list_of_counts, param_function):
    '''if a list of lists of values were arranged as a dataframe, this
    returns the outcome of a function applied to every column in that
        frame'''
    stdevs = []
    for i in range(0, len(list_of_counts[0])):
        stdevs += [get_param_for_column(list_of_counts, i, param_function)]
    return(stdevs)

def ss_ttests(list_of_counts_by_column):
    '''returns single sample two-tailed ttest for each list in a list of
        lists,
    with a comparison mean of 1'''
    return([stats.ttest_1samp(x,1)[1] for x in list_of_counts_by_column])

def p_to_asterisks(p_values, normalised_to_first = True):
    ''' takes a list of p_values and returns a list of strings containing
```

```
    asterisks corresponding with those values'''
    output = []
    if normalise_to_first:
        p_values = p_values[1:len(p_values)]
    for p in p_values:
        if p >= 0.05:
            output += ["n.s"]
        elif 0.01 <= p <= 0.05:
            output += ["*"]
        else:
            magnitude = math.floor(math.log10(p))
            output += ["*" * (abs(magnitude)-1)]
    if normalised_to_first:
        output = [""] + output
    return(output)

def get_centre_x(rectangle):
    '''returns the x position of the centre of a bar on the bar chart'''
    return(rectangle.get_x() + rectangle.get_width()/2)

def combine_lists(list_of_lists):
    '''takes a list of list and returns one combined list of all the
        values'''
    return(list(itertools.chain.from_iterable(list_of_lists)))

def transpose_list_of_lists(list_of_lists):
    '''if the list of lists were a dataframe, this returns a transposed data
    frame in the form of list of lists'''
    transposed_frame = pd.DataFrame(list_of_lists).transpose()
    transposed_list = pd.Series.tolist(transposed_frame)
    return([strip_nans(x) for x in transposed_list])

def get_lengths(list_of_lists):
    '''returns the length of each list in a list of lists'''
    return([len(x) for x in list_of_lists])

def get_maxes(list_of_lists):
    '''returns the maximum value for each list in a list of lists'''
    return([max(x) for x in list_of_lists])

def duplicate_x_labs(xlabs, list_of_lengths):
    '''duplicates each value in a list to allow it to be plotted as a scatter
    plot'''
    final_xlabs = []
```

```
    for index, value in enumerate(list_of_lengths):
        final_xlabs += [list(itertools.repeat(xlabs[index], value))]
    return(final_xlabs)

def get_max(list_of_frames, col_index):
    ''' returns the maximum value from a given column in multiple data
        frames'''
    subframes = [frame for frame in list_of_frames if
                len(frame.iloc[0]) >= col_index+1]
    # subframes accounts for unequal n numbers
    columns = [strip_nans(frame.iloc[:,col_index]) for frame in subframes]
    each_max = [max(column) for column in columns]
    return(max(each_max))

def make_intervals(start, stop, step):
    ''' basically just makes a range, but I think it will be easier to
    read the code this way'''
    return(np.arange(start, stop, step))

def get_kde(a_list):
    ''' takes a list and returns the kernel density estimation'''
    stripped_list = strip_nans(a_list)
    return(st.gaussian_kde(stripped_list))

def get_kdes_from_frames(list_of_frames, col_index):
    ''' takes a list of frames and column index and returns the density
    estimation for each'''
    output = []
    subframes = [frame for frame in list_of_frames if
                len(frame.iloc[0]) >= col_index+1]
    # subframes accounts for unequal n numbers
    for frame in subframes:
        column = frame.iloc[:,col_index]
        output += [get_kde(column)]
    return(output)

def kde_to_values(kde, intervals):
    ''' takes a density estimation and a list of intervals and returns
    the value for each interval'''
    return([float(kde(interval)) for interval in intervals])

def get_estimations_for_column(list_of_frames, col_index):
    ''' takes a list of frames, a column index and a list of intervals,
    and returns the estimated value of each interval in a data frame
```

```
    based on the kde of the inputs'''
    intervals = make_intervals(0, get_max(list_of_frames, col_index), 0.1)
    kdes = get_kdes_from_frames(list_of_frames, col_index)
    values = [kde_to_values(kde, intervals) for kde in kdes]
    return(pd.DataFrame(values).transpose())

def get_y_values(means):
    '''returns the y_values to plot the curve, going from 0 to the maximum
       in increments of 0.1'''
    return(np.arange(0, len(means)/10, 0.1))

def get_95CI(a_list):
    '''Takes a list of values and returns the 95% confidence interval for
    the mean'''
    return(st.t.interval(0.95, len(a_list)-1, loc=np.mean(a_list),
                         scale=st.sem(a_list)))

def get_CIs(estimates_list):
    ''' Takes a list of lists and returns the 95% confidence interval for the
       mean in each'''
    return([get_95CI(estimate) for estimate in estimates_list])

def get_CI_curves(estimates):
    '''takes the curve for the mean distribution and returns the curves for
    either end of the 95% confidence interval at each point along the mean
    curve'''
    CIs = estimates.apply(get_95CI, 1)
    lower = [CI[0] for CI in CIs]
    upper = [CI[1] for CI in CIs]
    return(lower, upper)

def get_curves_for_column(frames_list, col_index):
    ''' returns a dictionary containing the mean curve, upper CI curve,
    lower CI curve and y_values for a given column in a set of frames'''
    estimates = get_estimations_for_column(frames_list, col_index)
    means = np.mean(estimates, 1)
    lengths = get_y_values(means)
    CI_curves = get_CI_curves(estimates)
    lower_curves = CI_curves[0]
    upper_curves = CI_curves[1]
    return{"lengths":lengths, "means":means, "lowers":lower_curves,
           "uppers":upper_curves}

def get_all_curves(frames_list):
```

```
    ''' returns a dictionary containing the mean curve, upper CI curve,
    lower CI curve and y_values for every column in a set of frames'''
    all_curves = []
    for index, value in enumerate(frames_list[0]):
        all_curves += [get_curves_for_column(frames_list, index)]
    return(all_curves)

def flip_set(curveset, x_lim):
    ''' takes a curveset (upper, lower CIs and means) and returns the same
    set but reflected in the vertical axis'''
    new_curveset = {}
    new_curveset["lengths"] = curveset["lengths"]
    for name, values in curveset.items():
        if name != "lengths":
            new_curveset[name] = [x_lim - x for x in values]
    return(new_curveset)

def get_reflected_curves(list_of_curves, x_lim):
    ''' takes curvesets (upper, lower CIs and means) and returns the same
    sets but reflected in the vertical axis'''
    newcurves = []
    for curve_set in list_of_curves:
        newcurves += [flip_set(curve_set, x_lim)]
        newcurves += [curve_set]
    return(newcurves)

def get_medians_and_stdevs(frames):
    ''' returns the median and standard deviation for every column in every
    frame in a list of data frames'''
    medians = []
    medians += [list(frame.median()) for frame in frames]
    median_frame = pd.DataFrame(medians)
    mean_medians = median_frame.mean()
    stdevs = median_frame.std()
    return(mean_medians, stdevs)

def length_ttests(frames):
    ''' performs a one sample, two-tailed t test comparing the median value
    of every column in a data frame with the first column, and does this over
    every frame in the input list'''
    medians = []
    medians += [list(frame.median()) for frame in frames]
    median_frame = pd.DataFrame(medians)
    p_values = []
```

```
    for i in range(1, len(median_frame.iloc[0])):
        column = median_frame.iloc[:,i]
        column = strip_nans(column)
        p_values += [st.ttest_ind(median_frame.iloc[:,0], column)[1]]
    return(p_values)

def exp_func(x, a, b, c):
    return a * np.exp(-b * x) + c

def duplicate_values(values, list_of_lengths):
    '''duplicates each value in a list to allow it to be plotted as a scatter
    plot'''
    final_values = []
    for index, value in enumerate(list_of_lengths):
        final_values += [list(itertools.repeat(values[index], value))]
    return(final_values)

def get_asterisk_positions(subplots, frames, y_lim):
    '''Returns the x and y positions above the centre of each violin so the
    asterisks can be plotted.'''
    xs = []
    ys = []
    for value, subplot in enumerate(subplots):
        if value %2 != 0:
            continue
        else:
            xs += [subplot.get_position().get_points()[1,0]]
            ys += [subplot.get_position().get_points()[1,1]]
            #ys will be the same across the entire plot,so this isn't
            #necessarily that helpful...
    return(xs, ys)

def set_violin_params():
    '''aesthetics for the violin plot'''
    rc = {"axes.spines.left" : False,
          "axes.spines.right" : False,
          "axes.spines.bottom" : True,
          "axes.spines.top" : False,
          "xtick.bottom" : False,
          "xtick.labelbottom" : False,
          "ytick.labelleft" : True,
          "ytick.left" : False}
    plt.rc('ytick', labelsize=14)
    plt.rcParams.update(rc)
```

```
def set_bar_params():
    '''aesthetics for the bar and scatter plots and histograms'''
    rc = {"axes.spines.left" : True,
      "axes.spines.right" : False,
      "axes.spines.bottom" : True,
      "axes.spines.top" : False,
      "xtick.bottom" : False,
      "xtick.labelbottom" : True,
      "ytick.labelleft" : True,
      "ytick.left" : True}
    plt.rc('ytick', labelsize=14)
    plt.rcParams.update(rc)


def plot_violins(files, x_lim, y_lim, x_title, y_title, x_labs, ast_height,
                 figheight = 5, axis_fontsize = 16, tick_fontsize = 14,
                 axis_weight = 2, dpi = 300, make_stats = True):
    # takes a group of csv files containing lengths of filamentous virions
        and plots a violin plot showing the distribution of virion lengths
        for each condition. Assumes each column in the csv files is a unique
        condition, and each of the files has the columns in the same order.

    #imports the data
    frames = get_data_frames(files)

    #calculates the density distributions for all the samples
    curves = get_all_curves(frames)

   #reflects the curves in the vertical axis to make violins
    newcurves = get_reflected_curves(curves, x_lim)

    #calculates and plots the mean and standard deviation of the median
        filament lengths. If make_stats is True, compares each condition to
        the first condition with a two sample t-test and plots asterisks
        corresponding to statistical significance
    medians, stdevs = get_medians_and_stdevs(frames)
    if make_stats:
        p_values = [1] + length_ttests(frames)
        asterisks = p_to_asterisks(p_values)


    set_violin_params() #Hide all the boxes around the plots
```

```
    fig, axs = plt.subplots(1, len(newcurves), sharex=True, sharey=True, dpi
        = dpi)
    fig.set_figheight(figheight)
    fig.set_figwidth(len(x_labs)*2) # keeps the widths of the violins
        consistent between plots
    plt.ylim(0, y_lim)
    plt.xlim(0, x_lim)
    #plot all the curves
    for index, curve_set in enumerate(newcurves):
        axs[index].plot(curve_set["means"], curve_set["lengths"], color =
            "black",
           linewidth = 0.8)
        axs[index].fill_betweenx(curve_set["lengths"], curve_set["lowers"],
                         curve_set["uppers"], alpha = 0.2, color = "gray")
        axs[index].spines['bottom'].set_linewidth(axis_weight)
        axs[index].tick_params(axis='both', which='major',
            labelsize=tick_fontsize)
        #each violin plot is 2 plots back-to-back. Therefore only the even
            numbered plots need the labels
        if index % 2 == 0:
            axs[index].errorbar(x_lim, medians[index//2], yerr =
                stdevs[index//2],
               capsize = 6, color = "black", marker = '_')
            axs[index].set_xlabel(x_labs[index//2], fontsize = tick_fontsize)
            axs[index].xaxis.set_label_coords(1, -0.025)
        else:
            axs[index].errorbar(0, medians[index//2], yerr = stdevs[index//2],
               capsize = 6, color = "black", marker = '_')
    #label the x axis
    fig.text(0.5, -0.05, x_title, ha='center', fontsize = axis_fontsize)
    #label up the y axis on the first plot
    axs[0].spines['left'].set_visible(True)
    axs[0].spines['left'].set_linewidth(axis_weight)
    axs[0].set_ylabel(y_title, fontsize = axis_fontsize)
    fig.subplots_adjust(hspace=0, wspace=0) #remove gaps between subplots
    asterisk_coords = get_asterisk_positions(axs, frames, y_lim)
    if make_stats:
        for i, asterisk in enumerate(asterisks):
            fig.text(asterisk_coords[0][i], ast_height, asterisk, ha =
                "center",
                    fontsize = 12)

def calculate_parameters(df, multiple_values = True):
```

```
    ''' Takes a series of data frames and calculates various summary
        statistics for plotting'''
    df["means"] = [np.mean(x) for x in df["values"]]
    df["stdevs"] = [np.std(x) for x in df["values"]]
    df["max"] = [max(x) for x in df["values"]]
    if multiple_values:
        df["p_values"] = [st.ttest_1samp(x,1)[1] for x in df["values"]]
        df["asterisks"] = p_to_asterisks(df["p_values"])
    lengths = [len(x) for x in df["values"]]
    df["scatter_values"] = duplicate_values(df["conditions"], lengths)
    df["medians"] = [np.median(x) for x in df["values"]]
    return(df)

def transpose_nested_list(nested_list):
    '''if the nested+list were a dataframe, this returns a transposed data
    frame in the form of a nested_list'''
    transposed_frame = pd.DataFrame(nested_list).transpose()
    transposed_list = pd.Series.tolist(transposed_frame)
    return([strip_nans(x) for x in transposed_list])

def normalised_counts_from_file_names(file_names):
    '''import files of length data, return a nested list of the number of
    filaments in each condition normalised to the first column'''
    frames = get_data_frames(file_names)
    counts = get_counts(frames)
    normalised_counts = [normalise_to_first(x) for x in counts]
    transposed_counts = transpose_nested_list(normalised_counts)
    return(transposed_counts)

def counts_from_file_names(file_names):
    '''import files of length data, return a nested list of the number of
    filaments in each condition'''
    frames = get_data_frames(file_names)
    counts = get_counts(frames)
    print(counts)
    transposed_counts = transpose_nested_list(counts)
    return(transposed_counts)



def plot_bar(df, show_points = True, y_lim = 1.2, y_min = 0,
    make_stats=True,
            dpi = 600, figheight =5, figwidth = 12,
            x_title = "X", y_title = "Y", axis_fontsize = 12,
```

```
            tick_fontsize = 10, axis_weight = 2, edgecolor = "black",
            x_min = 0):
    '''Takes a data frame and plots the values as a bar chart. Can also
       compare each condition to the first condition with a t-test and plot
       asterisks to indicate the significance'''
    set_bar_params()
    fig, ax = plt.subplots(nrows = 1, dpi = dpi)
    fig.set_figheight(figheight)
    ax.set_ylabel(y_title,
               fontsize = axis_fontsize)
    fig.text(0.5, -0.05, x_title, ha='center', fontsize = axis_fontsize)
    plt.setp(ax.spines.values(), linewidth=axis_weight)
    plt.tick_params(axis='both', which='major', labelsize=tick_fontsize)
    plt.ylim(y_min, y_lim)
    fig.set_figwidth(len(df["means"])*2)
    plt.xlim(x_min, len(df["means"]) - 0.5)
    ax.bar(df["conditions"], df["means"], yerr = df["stdevs"], capsize = 10,
               color = "none", edgecolor = edgecolor, linewidth = 2)
    asterisk_xs = range(0, len(df["conditions"]))
    #plot individual points
    if show_points:
      ax.scatter(combine_lists(df["scatter_values"]),
                 combine_lists(df["values"]), color = "none",
                    edgecolor='black')
    #plot significance asterisks
    if make_stats:
        for i, asterisk in enumerate(df["asterisks"]):
            ax.text(asterisk_xs[i], max(df["max"][1:len(df["max"])]) + 0.1,
                   asterisk, ha = "center", fontsize = 12)

def plot_scatter(df, show_points = True, y_lim = 1.2,make_stats=True,
            dpi = 600, figheight =5, figwidth = 12,
            x_title = "X", y_title = "Y", axis_fontsize = 12,
            tick_fontsize = 10, axis_weight = 2, extra_x_space = 1,
            line_type = "Linear", y_min = 0, x_min = 0):
        '''Takes a data frame and plots the values as a scatter chart. Can
           also compare each condition to the first condition with a t-test
           and plot asterisks to indicate the significance. Fits a linear or
           a polynomial regression line by least squares'''
    set_bar_params()
    df["conditions"] = [float(x) for x in df["conditions"]]
    df["scatter_values"] = [[float(x) for x in z] for z in
        df["scatter_values"]]
    fig, ax = plt.subplots(nrows = 1, dpi = dpi)
```

```
    fig.set_figheight(figheight)
    ax.set_ylabel(y_title,
                fontsize = axis_fontsize)
    #ax.set_xlabel(x_title, fontsize = axis_fontsize)
    fig.text(0.5, -0.05, x_title, ha='center', fontsize = axis_fontsize)
    plt.setp(ax.spines.values(), linewidth=axis_weight)
    plt.tick_params(axis='both', which='major', labelsize=tick_fontsize)
    plt.tick_params(axis = "x", length = 1)
    plt.ylim(y_min, y_lim)
    fig.set_figwidth(figwidth)
    plt.xlim(x_min, max(df["conditions"]) + extra_x_space) # keeps width
        proportional to the number of conditions
    ax.errorbar(df["conditions"], df["means"], yerr = df["stdevs"], marker =
        "_",
                        markersize='15', capsize = 10, linewidth = 2,
                        color = "black", linestyle='None')
    if line_type == "linear":
        z = np.polyfit(df["conditions"], df["means"], 1)
        p = np.poly1d(z)
        plt.plot(df["conditions"], p(df["conditions"]),"--", color = "black")
    elif line_type == "exponential":
        popt, pcov = curve_fit(exp_func, list(df["conditions"]),
            list(df["means"]), maxfev = 1600)
        print("a = %s , b = %s, c = %s" % (popt[0], popt[1], popt[2])) #
            prints the equation of the line in case you want to use it for
            something
        many_xs = np.arange(0, max(df["conditions"]), 0.01) # create the
            points to plot the curve with
        plt.plot(many_xs, exp_func(many_xs, *popt), "--", color = "black")
    asterisk_xs = df["conditions"]
    if make_stats:
        for i, asterisk in enumerate(df["asterisks"]):
            ax.text(asterisk_xs[i], max(df["max"][1:len(df["max"])]) + 0.1,
                   asterisk, ha = "center", fontsize = 12)
    if show_points:
       ax.scatter(combine_lists(df["scatter_values"]),
                combine_lists(df["values"]), color = "none",
                    edgecolor='black')

def plot_hist(counts, minimum, maximum, interval, xlab, ylab,
              dpi = 600, axis_fontsize = 12, tick_fontsize = 10,
              figheight = 8, figwidth = 10, y_lim = 12):
    '''Plots a histogram from a list of values, with maximum, minimum, and
        interval values specified by the user'''
```

```
set_bar_params()
fig, ax = plt.subplots(nrows = 1, dpi = dpi)
fig.set_figheight(figheight)
fig.set_figwidth(figwidth)
ax.hist(counts, bins = np.arange(minimum, maximum, interval), #arange to
    align xticks with bins
     edgecolor = "black", color = "white",
     linewidth = 2)
ax.set_xlabel(xlab, fontsize = axis_fontsize)
ax.set_ylabel(ylab, fontsize = axis_fontsize)
ax.tick_params(axis='both', which='major', labelsize=tick_fontsize)
plt.setp(ax.spines.values(), linewidth=2)
plt.ylim(0, y_lim)
ax.spines["top"].set_color("none")
ax.spines["right"].set_color("none")
```

AllFilamentAnalysisPlots.py

```
"""
Created on Fri Jun 21 14:59:32 2019
@author: Jack Hirst

Imports csv files from the ImageJ macros and CSVCombiner and generates the
    summary graphs at the end of the confocal analysis pipeline. Also can
    generate bar charts or histograms from manually entered data
"""
import pandas as pd
import os
import numpy as np
import FilamentAnalysisFunctions as iff
import scipy.stats as st

#os.chdir("")

'''1: plot concentration of filaments and violin plots of their length
    distribution'''

#not strictly necessary, but presets let you change between conditions
    faster
presets = {
       #key :[file_list, x_label, xlabels, continuous x axis?]
       #egs here, these will need to be altered depending on the experiment
       "pip": [["pipette1", "pipette2", "pipette3"], "Pipette actions",
           ["0", "5", "10", "30"], True],
       "cla": [["clarification1", "clarification2", "clarification3"], " ",
           ["Unclarified", "Clarified"], False]
       }

'''csv files should be formatted as a column of filament lengths for each
    condition, with the title of the condition as the very first value in the
column'''

#select the conditions
condition = "pip"
preset = presets[condition]
files = preset[0]
x_title = preset[1]
conditions = preset[2]
continuous_x = preset[3]
```

```
#set the plot aesthetics
dpi = 600
axis_fontsize = 20
tick_fontsize = 18
plot_height = 5
bar_y_lim = 1
axis_weight = 1.5
extra_bar_x = 0.5
extra_scatter_x = 0.1

mf = pd.DataFrame()
mf["conditions"] = conditions
mf["values"] = iff.normalised_counts_from_file_names(files)
mf = iff.calculate_parameters(mf, multiple_values=True)

#plot the graphs
iff.plot_violins(files, x_lim = 1.1, y_lim = 40, x_title = x_title,
    make_stats=True,
                y_title = "Length of filament  (m)", x_labs =
                    mf["conditions"],
                ast_height = 0.9, dpi = dpi, axis_fontsize= axis_fontsize,
                tick_fontsize= tick_fontsize, figheight = plot_height,
                    axis_weight = axis_weight)

if continuous_x:
    iff.plot_scatter(mf, x_title=x_title, y_title = "Observed filament
        concentration\n(normalised to untreated)", dpi = dpi, axis_fontsize=
        axis_fontsize,
                tick_fontsize= tick_fontsize, figheight = plot_height,
                    y_lim=bar_y_lim,
                extra_x_space=extra_scatter_x, line_type="linear")
else:
    iff.plot_bar(mf, x_title=x_title, y_title = "Observed filament
        concentration\n(normalised to untreated)",
                dpi = dpi, axis_fontsize= axis_fontsize, make_stats=True,
                tick_fontsize= tick_fontsize, figheight = plot_height,
                    y_lim=bar_y_lim,
                axis_weight = axis_weight)

'''2: plot infectious titres'''

titre_data = [ #normalised data for plaque assays
       [1,1,1,1,1],
       [0.95, 0.71, 0.83, 0.57, 0.69],
```

```
        [0.66, 1.14, 0.55, 0.78],
        [2.2, 1.03, 0.97, 0.36, 0.98],
        [1, 0.33, 1.05],
        ]

mf = pd.DataFrame()
mf["conditions"] = conditions
mf["values"] = titre_data
mf = iff.calculate_parameters(mf)

iff.plot_bar(mf,x_title=x_title, dpi = dpi, axis_fontsize= axis_fontsize,
               tick_fontsize= tick_fontsize, figheight = plot_height,
                   y_lim=2,
               y_title = "Infectious titre (pfu)\n(normalised to untreated)"
               )

print(mf["p_values"])


'''3: Plot the eccentricities of fitted ellipse to the filaments. These
require csv files with columns "Condition", "Major", "Minor" which can be
partially generated using the imageJ macro "Eccentricity Analysis" (also in
the Github repository)'''

os.chdir("")
#using freezing as an example, takes repeats from each repeat and pools the
    same
#conditions from each
frozen_files = ["frozen1", "frozen2", "frozen3"]
unfrozen_files = ["unfrozen1", "unfrozen2", "unfrozen3"]
conditions = ["Unfrozen", "Frozen"]
frozen_frames = iff.get_data_frames(frozen_files)
unfrozen_frames = iff.get_data_frames(unfrozen_files)

def get_all_eccentricities(frames):
    eccs = []
    for frame in frames:
        eccentricities = [iff.calculate_eccentricity(major,minor) for
            major,minor
                    in zip(frame["Major"], frame["Minor"])]
        eccs += eccentricities
    return(eccs)

frozen_eccs = get_all_eccentricities(frozen_frames)
```

```
unfrozen_eccs = get_all_eccentricities(unfrozen_frames)

kinky_data = [unfrozen_eccs, frozen_eccs]

kinky_data = [[iff.mean_eccentricity_of_frame(x) for x in unfrozen_frames],
            [iff.mean_eccentricity_of_frame(x) for x in frozen_frames]]

mf = pd.DataFrame()
mf["conditions"] = conditions
mf["values"] = kinky_data
mf = iff.calculate_parameters(mf)

iff.plot_bar(mf,x_title=x_title, dpi = dpi, axis_fontsize= axis_fontsize,
               tick_fontsize= tick_fontsize, figheight = plot_height,
                  y_lim=1,
               y_min = 0.75, y_title = "Mean eccentricity of fitted
                  ellipses",
               edgecolor = "none")

p_values = []
for i in range(1, len(mf["values"])):
   p_values += [st.ttest_ind(mf["values"][0], mf["values"][i])]
print(p_values)
print("")


''' 4: Plot histograms of how length and concentrations vary across several
samples'''
#raw mean values for each condition, drawn from the same population (n = 3)
val_medians = [3.430500, 3.425833, 3.722500, 3.392167, 3.686833, 3.448833,
   3.538667, 3.541333, 3.768833, 3.604667, 3.285167, 3.839333, 3.608333,
   3.706500, 3.174167, 3.683667, 3.430667, 3.634667, 3.324000, 3.609167,
   3.563333, 3.569000, 3.246167, 3.673000]

val_counts = [244.00,252.00,270.67, 278.67, 283.00, 298.67, 277.00, 275.33,
   291.50, 283.33, 258.00, 270.50, 271.67, 329.00, 259.33, 229.00, 220.00,
   268.67, 288.00, 227.33, 325.33, 309.00, 266.50, 242.00]

#normalise the values to the plate mean
val_counts = val_counts/np.mean(val_counts)
val_medians = val_medians/np.mean(val_medians)


iff.plot_hist(val_medians, 0.75, 1.4, 0.05, y_lim = 12,
```

```
            xlab = "Median filament length\n(normalised to plate mean)",
            ylab = "Frequency", figheight = plot_height, axis_fontsize =
                axis_fontsize,
            tick_fontsize = tick_fontsize)

iff.plot_hist(val_counts, 0.75, 1.4, 0.05, y_lim = 12,
            xlab = "Filament concentration\n(normalised to plate mean)",
            ylab = "Frequency", figheight = plot_height, axis_fontsize =
                axis_fontsize,
            tick_fontsize = tick_fontsize)
```

A.2.2 CSVCombiner.py

```
"""
Created on Thu Apr 18 11:28:49 2019
@author: Jack Hirst

Allows the user to navigate to a folder and combine every column with a
    specific title of every csv file in that folder into a new single csv
    file.
"""
import os
import glob
import csv

currentDirectory = "C:/"
outputDirectory = "C:/"

target = "Length" #Means every column entitled "Length" will be added to
    the new file

def findPenultimate(text, pattern):
   '''Returns the penultimate instance of some text from a string'''
    return text.rfind(pattern, 0, text.rfind(pattern))

def findnth(haystack, needle, n):
   '''Returns the nth instance of some text from a string'''
    parts= haystack.split(needle, n+1)
    if len(parts)<=n+1:
        return -1
    return len(haystack)-len(parts[-1])-len(needle)

def goUp():
   '''Moves the current working directory up one level'''
    directory = os.getcwd()
    newDirectory = directory[0:directory.rfind("\\")+1]
    os.chdir(newDirectory)
    print(newDirectory)

def listContents(contents):
   '''Prints the contents of the current directory'''
    for index, content in enumerate(contents):
        print(index, content)

def goDown():
```

```
    '''Moves the current working directory down one level, allowing the user
       to select which directory'''
    contents = next(os.walk('.'))[1]
    listContents(contents)
    newFolderIndex = input("Enter the number of the folder you like to go
        to: ")
    newDirectory = os.getcwd() + "\\" + contents[int(newFolderIndex)] + "\\"
    os.chdir(newDirectory)
    print(newDirectory)

def goSideways():
    goUp()
    goDown()

def getRegularCSVTitle(directory):
    '''extracts the title of the current directory'''
    final = directory.rfind("\\")
    title = directory[final+1:len(directory)] + ".csv"
    return(title)

def equilibrateLengths(listOfLists):
    '''Takes a list of lengths and adds blank values to each until all lists
       are the same length'''
    maxLength = len(max(listOfLists, key=len))
    newList = []
    for iList in listOfLists:
        newList = newList + [iList + [None] * (maxLength - len(iList))]
    return(newList)

def CSVColumnToList(columnOfInterest):
    '''Moves through every csv file in a folder, and stores every value from
       every column with a particular title in a list'''
    lengthList = []
    fileList = glob.glob("*csv")
    for file in fileList:
        print("processing " + file)
        if os.stat(file).st_size > 2: #avoid empty files
            with open (file, "r") as csvfile:
                myReader = csv.reader(csvfile, delimiter=',')
                headers = next(myReader)
                columnIndex = headers.index(columnOfInterest)
                for row in myReader:
                    if len(row) > 0:
                        lengthList = lengthList + [row[columnIndex]]
```

```
    return(lengthList)

def combineCSVs(columnOfInterest):
     '''Moves through every csv file in a folder and stores every value
        from every column with a particular title in a new csv file with
        the title of the folder'''
    lengths = CSVColumnToList(columnOfInterest)
    currentDirectory = os.getcwd()
    title = "tidied " + getRegularCSVTitle(currentDirectory)
    print("Creating " + os.getcwd() + "\\" + title)
    with open (title, "w", newline = "") as outputFile:
        myWriter = csv.writer(outputFile, delimiter = ',')
        myWriter.writerow([columnOfInterest])
        for length in lengths:
            myWriter.writerow([length])

def getCompiledCSVTitle(directory):
   '''extracts the name of the folder being processed, which should be one
      complete experiment'''
    final = directory.rfind("\\")
    pen = findPenultimate(directory, "\\")
    pretitle = directory[pen:final] + ".csv"
    newpen = findnth(pretitle, " ", 2) + 1
    title = pretitle[newpen:len(pretitle)]
    return(title)

def combineConditions(keyword, outputDirectory):
   '''Moves through every csv file in a folder and stores every value from
      every column with a particular title in a new csv file with the title
      of the folder. Combines these new csv files into another new csv
      file, where each file is included as one column'''
    combinedLengths = []
    filesUsed =[]
    startDirectory = os.getcwd() + "\\"
    myDirectories = next(os.walk('.'))[1]
    outputTitle = getCompiledCSVTitle(startDirectory)
    for i in myDirectories:
        filesUsed += [i]
        lengths = []
        os.chdir(startDirectory + i)
        tidyFile = glob.glob("*" + keyword + "*")
        with open(tidyFile[0], "r") as csvfile:
            myReader = csv.reader(csvfile, delimiter = ',')
            next(myReader) #Skip the header row...
```

```
            for row in myReader:
                lengths += row
        combinedLengths += [lengths]
    extendedLengths = equilibrateLengths(combinedLengths)
    os.chdir(outputDirectory)
    print("Saving final compilation as " + os.getcwd() + "\\" + outputTitle)
    with open(outputTitle, 'w', newline='') as outputFile:
        myWriter = csv.writer(outputFile, delimiter = ',')
        myWriter.writerow(filesUsed)
        for i in range(0, len(extendedLengths[0])):
            myRow = []
            for j in extendedLengths:
                myRow = myRow + [j[i]]
            myWriter.writerow(myRow)
    os.chdir(startDirectory) #return to start directory

def processFolder(columnOfInterest, keyword, outputDirectory):
    '''Starts with an experiment directory, that contains subdirectories for
       each experiment condition, and each subdirectory contains a series of
       csv files containing length data for the filaments in a micrograph.
       Returns a single csv file, with each experimental condition as a
       column and each column populated with lengths from the relevant
       micrographs'''
    myDirectories = next(os.walk('.'))[1]
    startDirectory = os.getcwd() + "\\"
    for i in myDirectories:
        os.chdir(startDirectory + i)
        combineCSVs(columnOfInterest)
    os.chdir(startDirectory)
    combineConditions(keyword, outputDirectory)

os.chdir(currentDirectory)
print("Current directory: " + currentDirectory)

#Simple user interface to navigate through files and process folders
while True:
    print("q to quit. up to move the directory up a level. down to move the
        directory down a level. side to move up then down. p to process a
        folder")
    myInput = input()
    if myInput == "q":
        break
    if myInput == "up":
        goUp()
```

```
    if myInput == "down":
        goDown()
    if myInput == "side":
        goSideways()
    if myInput == 'p':
        processFolder(target, "tidied", outputDirectory)
```

A.2.3 PTMAnalyser.py

```
# -*- coding: utf-8 -*-
"""
Created on Thu Jul 16 15:21:30 2020

@author: Jack Hirst

Imports a csv containing a list of proteins, modification sites, and the
    abundance of modified and unmodified residues at those sites. Returns a
    graph for each protein showing the proportion of modified residues in
    user specified groups
"""

import csv
import os
import pandas as ps
import matplotlib.pyplot as plt
from Bio import SeqIO
import numpy as np

#specific to the sample - here are my groups of sample types
mock_f3 = ["Sample 1"]
mock_f7 = ["Sample 2"]
mock_f10 = ["Sample 3"]
virus_f3 = ["Sample 4", "Sample 5", "Sample 6"]
virus_f7 = ["Sample 7", "Sample 8", "Sample 9"]
virus_f10 = ["Sample 10", "Sample 11", "Sample 12"]

all_samples = []
for i in range(0,12):
    all_samples += ["Sample " + str(i+1)]

def titles_to_mod_unmod(a_list):
    '''takes a list of column titles and returns a list with "modified" and
    "unmodified" appended to each:'''
    new_list = []
    for i in a_list:
        new_list += [i + " modified", i + " unmodified"]
    return(new_list)

#this is currently blunt - need to check residue AND modification
mod_filters = ["Oxidation (M)", "Carbamidomethylation", "Deamidation (NQ)"]
inclusion_filter = ["Ubiquitin"]
```

```
#import initial, unfiltered data
os.chdir("C:/Users/jackh/OneDrive - University of Glasgow/Data/"
        "FP Filament Purification/FP Proteomics/PEAKS PTM Analysis")
raw_frame = ps.read_csv("2020 07 15 all proteins ptm.csv")

#remove common ms mutations
#mod_frame = raw_frame[raw_frame["Modifications"].isin(mod_filters)==False]
mod_frame =
    raw_frame[raw_frame["Modifications"].isin(inclusion_filter)==True]

#remove anything not detected twice in virus_f3 AND virus_f10
#(Because this is PTMs, the protein needs to be present in both to compare)
f3_filter = titles_to_mod_unmod(virus_f3)
f10_filter= titles_to_mod_unmod(virus_f10)

def combine_mod_unmod(a_list):
    new_list = []
    for i in range(0, len(a_list), 2):
        new_list += [a_list[i] + a_list[i+1]]
    return(new_list)

indices_to_keep = []
for index, row in mod_frame.iterrows():
    f3 = row[f3_filter]
    combined_f3 = combine_mod_unmod(f3)
    if np.count_nonzero(combined_f3)<2:
        continue
    else:
        f10 = row[f10_filter]
        combined_f10 = combine_mod_unmod(f10)
        if np.count_nonzero(combined_f10)<2:
            continue
        else:
            indices_to_keep += [index]

vir_frame = mod_frame.ix[indices_to_keep]

#convert the separate modified and unmodified columns to % modified
for sample in all_samples:
    vir_frame[sample + " % modified"] = (vir_frame[sample + "
        modified"]*100)/(vir_frame[sample + " unmodified"]+vir_frame[sample
        + " modified"])
    #vir_frame = vir_frame.drop(titles_to_mod_unmod([sample]), 1)
```

```
#get the list of viral proteins
viral_proteins = []
for sequence in SeqIO.parse("udorn_proteome_3.fasta", "fasta"):
    viral_proteins += [sequence.name]

#replace infinities with 100%
vir_frame = vir_frame.replace(np.inf, 100)

#get a better label for the modifications for the graphs
vir_frame["Labels"] = vir_frame["Protein Position"] +
    vir_frame["Modifications"]


cutoff = 1 #at least one set of samples must have higher than this %, and
    so filters out all nearly unmodified results which aren't that
    interesting

#take means of the repeats
vir_frame["Fraction 3 Mean"] = vir_frame.loc[: , "Sample 4 %
    modified":"Sample 6 % modified"].mean(axis = 1)
vir_frame["Fraction 7 Mean"] = vir_frame.loc[: , "Sample 7 %
    modified":"Sample 9 % modified"].mean(axis = 1)
vir_frame["Fraction 10 Mean"] = vir_frame.loc[: , "Sample 10 %
    modified":"Sample 12 % modified"].mean(axis = 1)
vir_frame = vir_frame[(vir_frame.loc[: , "Fraction 3 Mean":"Fraction 10
    Mean"] > cutoff).any(axis=1)]

vir_frame = vir_frame[(vir_frame.loc[: , "Fraction 3 Mean":"Fraction 10
    Mean"] > cutoff).any(axis=1)]

vir_frame["Fraction 3 std"] = vir_frame.loc[: , "Sample 4 %
    modified":"Sample 6 % modified"].std(axis = 1)
vir_frame["Fraction 7 std"] = vir_frame.loc[: , "Sample 7 %
    modified":"Sample 9 % modified"].std(axis = 1)
vir_frame["Fraction 10 std"] = vir_frame.loc[: , "Sample 10 %
    modified":"Sample 12 % modified"].std(axis = 1)

#split the frames up into distinct proteins
unique_proteins = set(vir_frame["Protein Description"])
unique_frames = []

for protein in unique_proteins:
```

```
    unique_frames += [vir_frame.loc[vir_frame["Protein Description"] ==
        protein]]

#plot graphs
for frame in unique_frames:
    if len(frame) > 0:
        title = list(frame["Protein Description"])[0]
        errors = frame.loc[: , "Fraction 3 std":"Fraction 10 std"]
        means = frame.loc[: , "Fraction 3 Mean":"Fraction 10 Mean"]
        labels = frame["Labels"]
        bar_width = 15
        r1 = np.arange(len(labels))*bar_width*3.5
        r2 = [x + bar_width for x in r1]
        r3 = [x + bar_width for x in r2]
        fig, ax = plt.subplots()
        #means.plot.bar(yerr = errors, capsize = 4, ax = ax, rot = 0)
        ax.bar(r1, means.iloc[:,0], yerr = errors.iloc[:,0], color =
            "lightcoral", width = bar_width)
        ax.bar(r2, means.iloc[:,1], yerr = errors.iloc[:,1], color =
            "orange", width = bar_width)
        ax.bar(r3, means.iloc[:,2], yerr = errors.iloc[:,2], color =
            "olive", width = bar_width)
        ax.set_xticks(r2)
        ax.set_xticklabels(labels, rotation = 45)
        ax.set_ylim(0, 100)
        ax.set_title(title, loc="left")
        fig.set_figwidth(len(labels))
        #break
'''
#separate the viral and host proteins
virus_frame = vir_frame[vir_frame["Protein"].isin(viral_proteins)]
host_frame = vir_frame[vir_frame["Protein"].isin(viral_proteins)==False]

virus_frame.to_csv("virus_ptms.csv", index = False)
host_frame.to_csv("host_ptms.csv", index = False)
'''
```

A.3 R Scripts

A.3.1 Major-minor axis plot.R

```
rm(list = ls())
library(ggplot2)
library(reshape2)

theme_set(
  theme_light() + theme(legend.position = "top")
)

#setwd("")
myFile <- read.csv("YOURFILENAME.csv")
head(myFile)

gg <- ggplot(myFile, aes(x=Major, y = Minor))
gg +
  facet_wrap(~ Condition, nrow = 3) +
  geom_point(size = 1, alpha = 0.2) +
  coord_cartesian(xlim = c(0, 30), ylim = c(0, 10), expand = (0.5)) +
  labs(x="Major axis (µm)", y="Minor axis (µm)", expand = FALSE) +
  theme(
    strip.text.x = element_text(size = 12, color = "black", face = "bold"),
    axis.text=element_text(size=14),
    axis.title=element_text(size = 14),
    panel.grid.minor = element_blank()
  )
```